OLLSCOIL NA GAILLIMHE
UNIVERSITY OF GALWAY

Modelling human brain circuitry in patients with *KCNQ2*-Developmental Epileptic Encephalopathy using induced pluripotent stem cells

Rachel Stewart

A thesis submitted to the *University of Galway*, for a Degree of Doctor of Philosophy

July 2023

Supervisors: Professor Nicholas Allen &

Professor Sanbing Shen

University of Galway

Table of Contents

List of Figures

List of Tables

Acknowledgement

Firstly, I would like to thank my primary supervisor Prof. Nicholas Allen for the great opportunity to work on this *KCNQ2* project, which has been so fulfilling and interesting to work on. Thank you for all your guidance and support throughout the past 4 years. Also, I would like to thank my secondary supervisor, Prof. Sanbing Shen for teaching me invaluable skills in the lab and introducing me to the wonderful world of iPSCs.

I would also like to thank my GRC members Prof. David Finn, Leo Quinlan, and Una Fitzgerald for your advice and support throughout the course of my PhD. I would like to thank both Prof. Leo Quinlan and Dr. Katarzyna Whysall for their contributions to the project in electrophysiology and miRNA experiments, respectively. I would like to thank everyone in our group, especially Alessia Arbini who I worked closely with on this project. I would also like to thank everyone in REMEDI for all their support in both experiments and friendships over the past years.

Thanks to all my friends in Galway for all their encouraging words and support making my PhD life so exciting. I would like to thank my family for all their love and support. Finally, I would like to thank my partner, Stephen, for listening (selectively) to me endlessly talking about my project and keeping me calm during the stressful moments.

Declaration

This thesis describes work that I undertook between 2019 and 2023 at the Regenerative Medicine Institute, University of Galway, Ireland. This work was supervised and mentored by Professor Nicholas Allen & Professor Sanbing Shen.

I declare that the results in this thesis are from original experimental work carried out by me for the purpose of this PhD thesis. The results generated for this thesis has not been submitted for a degree, diploma, or any other qualification at any other institution.

Abstract

Mutations (pathogenic variants) in *KCNQ2*, which encode the voltage-dependent K^+ channel Kv7.2 (responsible for neuronal M-current) can cause developmental epileptic encephalopathy (DEE), a disorder presenting with severe early-onset seizures and impaired neurodevelopment. Treatment of this disorder is very difficult because the effect of *KCNQ2* mutations on neurodevelopment is still largely unknown. In this study, we generated patient-specific iPSCs from 4 patients harbouring different *KCNQ2*-DEE loss-of-function, mutations: R213Q, F261L, A265T and A294V, and 4 sibling controls which were subsequently differentiated into excitatory cortical neurons to model the disease *in vitro*. We performed multi-electrode array (MEA) recordings of cortical neurons with the *KCNQ2*-DEE pathogenic variants F261L, A265T and A294V and found that for each mutation, neurons were hyperexcitable and displayed a burst-suppression firing pattern that is reminiscent of the interictal electroencephalography pattern seen in patients (burst suppression). We chose to focus on the pathogenic variant A265T for further functional analysis and found that A265T neurons displayed functional enhancement of Na^+ channels and Ca^{2+} activated K^+ channels while also exhibited altered spontaneous Ca^{2+} transients via Ca^{2+} imaging experiments. We showed that the Na^+ channel blocker carbamazepine, and the K^+ channel opener retigabine, were capable of reducing the phenotype in patient neurons, albeit not to the level of controls. Our data shows for the first time that patient-specific iPSC-derived cortical neurons harbouring the pathogenic variants F261L, A265T and A294V are hyperexcitable and display an irregular firing pattern compared to sibling controls. Moreover, we have generated a patient-specific disease model which is invaluable for drug testing and discovery with great potential for precision medicine.

Chapter 1. Introduction

This thesis describes the generation of human induced pluripotent stem cells (iPSCs) and iPSC-derived neurons from human patients (children) suffering from a severe rare genetic epilepsy known as *KCNQ2*-developmetnal and epileptic encephalopathy (*KCNQ2*-DEE), a potassium ion channelopathy. This introductory Chapter provides a brief overview of the epilepsies (in humans), their classification and causes. The Chapter also discusses the potassium ion channel disorders, with a focus on *KCNQ2*-epilepsies, patho-mechanisms, treatments, and challenges. I then describe the pertinent literature (in brief) of the models used to investigate this disorder and provide an overview of iPSC-literature in general in brain developmental ion-channel and epilepsy disorders and where relevant, to *KCNQ2*-DEE. Some of the discussion points, will be brought out in greater detail in various other experimental, and the final Discussion Chapters.

1.1 Definition and prevalence of epilepsy

Epilepsy is a brain disorder involving unprovoked recurrent seizures (Moshé et al., 2015). An epileptic seizure can be defined as a period of symptoms that occur as a result of abnormal neuronal activity in the brain (Huff et al., 2023). Epilepsy affects approx. 50 million people worldwide and over 45,000 people in Ireland (Thijs et al., 2019). Of this 45,000 people, over 10,000 of these are children. The prevalence of epilepsy is largely dependent on a number of factors such as socio-economic background, age, and gender (Beghi, 2020). The incidence of epilepsy is higher (139 per 100,000) in low to middle income countries compared to higher income countries (48.9 per 100,000) (Fiest et al., 2017) and also slightly higher in males than females (Hu et al., 2021).

1.2 Classification of seizures and the epilepsies

Classification is critical as it provides a common language for clinical care, families, and for clinical research. Classification systems should adapt alongside advances in our understanding of disease, like we have seen in the numerous classification systems proposed since 1985 (Scheffer et al., 2017). In 2017, the International League Against Epilepsy (ILAE) published papers on new classification of seizures and the epilepsies (Scheffer et al., 2017). This new system uses clearer language/wording, removes imprecise terminology, and is translatable into many languages

As a result of more recent research, the ILAE introduced new terms such as *developmental and epileptic encephalopathies (DEE's)*, showing that an epilepsy can occur as part of a wider (e.g genetic) brain disorder, affecting neurodevelopment, which is independent of seizures. The new classification system has included many decades of advances in the understanding of the epilepsies, creating an up-to-date system that allows for more accurate diagnosis and treatment for epilepsy patients.

1.3 Seizure classification

During a seizure event, seizure onset or semiology, can either be a focal onset, generalised onset, or have an unknown onset (Scheffer et al., 2017). During focal onset seizures, the seizure arises in a specific part of the brain in one hemisphere. In generalised onset seizures, the seizure arises from both hemispheres at the same time (Falco-Walter et al., 2018). Unknown onset seizures may occur if the seizure happens while the patient is asleep at home or if it is not witnessed by anyone (Chang et al., 2017). This information, combined with previous knowledge of the various seizure types, either motor or non-motor, provide a clear and concise pathway for making an informed decision on an epilepsy diagnosis **(Figure 1.1)**. The latest seizure classification system from the ILAE is outline below in **Figure 1.1**.

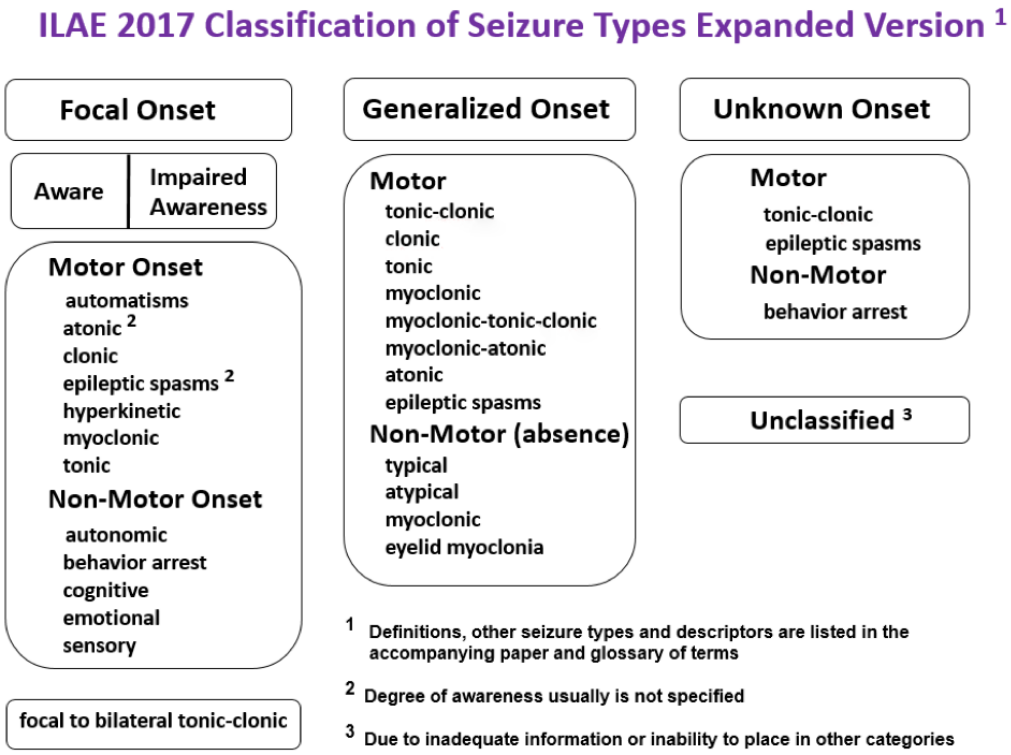

Figure 1.1: Classification of seizure types by the ILAE.

Motor seizures (involve many different types of movements -see under this category above) which can be further characterised depending on their exact nature. Non-motor seizures involve behaviour arrest, meaning movement stops which can be further categorised depending on seizure onset, and other seizure types (e.g., sensory for focal or absence for generalised – see under this category above). This seizure classification system is widely applied in clinical practice (Falco-Walter et al., 2018).

1.4 Epilepsy classification

Epilepsy type is determined by seizure type i.e., patients with focal seizures have focal epilepsy and patients with generalised seizures have generalised epilepsy. For many patients, it's possible to determine a specific *epilepsy syndrome*. Epilepsy syndromes usually have common characteristics such as types of seizure(s), EEG features, co-morbidities and age of onset (Katyayan et al., 2021). Epilepsy type/syndrome then guides the relevant treatments, investigation, and prognosis for patients. Evaluation of co-morbidities and aetiology is critical for optimal treatment and has now also been included in the epilepsy classification systems (Falco-Walter et al., 2018). The inclusion of aetiology has been facilitated by advancements in next generation sequencing (NGS) technologies and a greater understanding of the aetiology of epilepsies in the field.

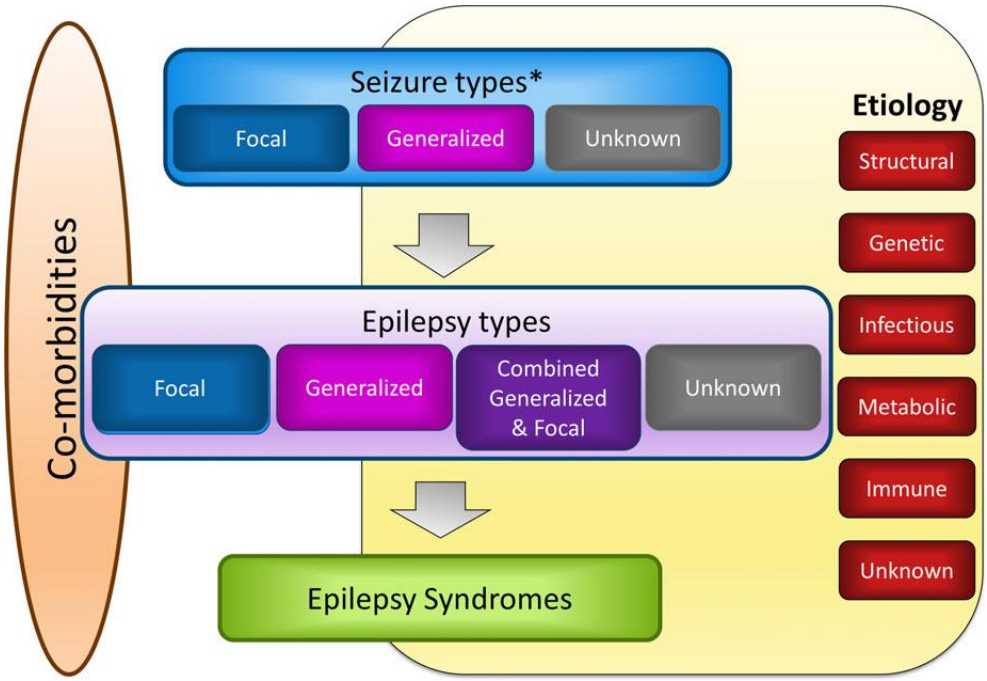

Figure 1.2 : Structure of the 2017 ILAE classification of epilepsies.

This classification is clinical (i.e., not a scientific classification system). Seizure type informs epilepsy type which enables the diagnosis of specific *epilepsy syndromes* in 50% of patients e.g., West syndrome. Co-morbidities are an essential part of the epilepsy classification. Determining possible aetiologies are also critical for understanding why the epilepsy has occurred and for devising investigations and treatment plans for patients (Scheffer et al., 2017).

1.5 Epilepsy syndromes

In 2022, the ILAE classified the *epilepsy syndromes* in a number of position papers (Zuberi et al., 2022). They formally defined an epilepsy syndrome as "*a characteristic cluster of clinical and EEG features, often supported by specific etiological findings (structural, genetic, metabolic, immune, and infectious*)". To date, there are 40 distinct epilepsy syndromes, with each syndrome often having age-dependent presentations, specific EEG patterns, specific seizure types, and a range of specific co-morbidities. In the new classification of epilepsy syndromes, syndromes are organised in numerous ways, such as age of onset. However, they may also be divided into epilepsy syndromes which have a) focal seizures, b) those with generalised seizures, and c) those with *developmental and epileptic encephalopathy (DEE)*, which can arise in various age groups. The *DEE* group often presents in young children, seizures are often drug resistant and comorbidities include a range of learning, behavioural and physical disabilities (Specchio et al., 2021). A noteworthy sub-group of the *DEE*s includes the *aetiology-specific syndromes.* In these syndromes, there is a specific known aetiology for the epilepsy, which is associated with a clearly distinct clinical phenotype in the majority of affected individuals. The aetiology may be any of those discussed above such as a genetic

mutation, a structural brain lesion, a defined metabolic alteration, a specific neuronal autoantibody, or an infectious agent (Scheffer & Liao, 2020a). For example, *KCNQ2*-DEE is a relatively newly accepted aetiology-specific epilepsy syndrome).

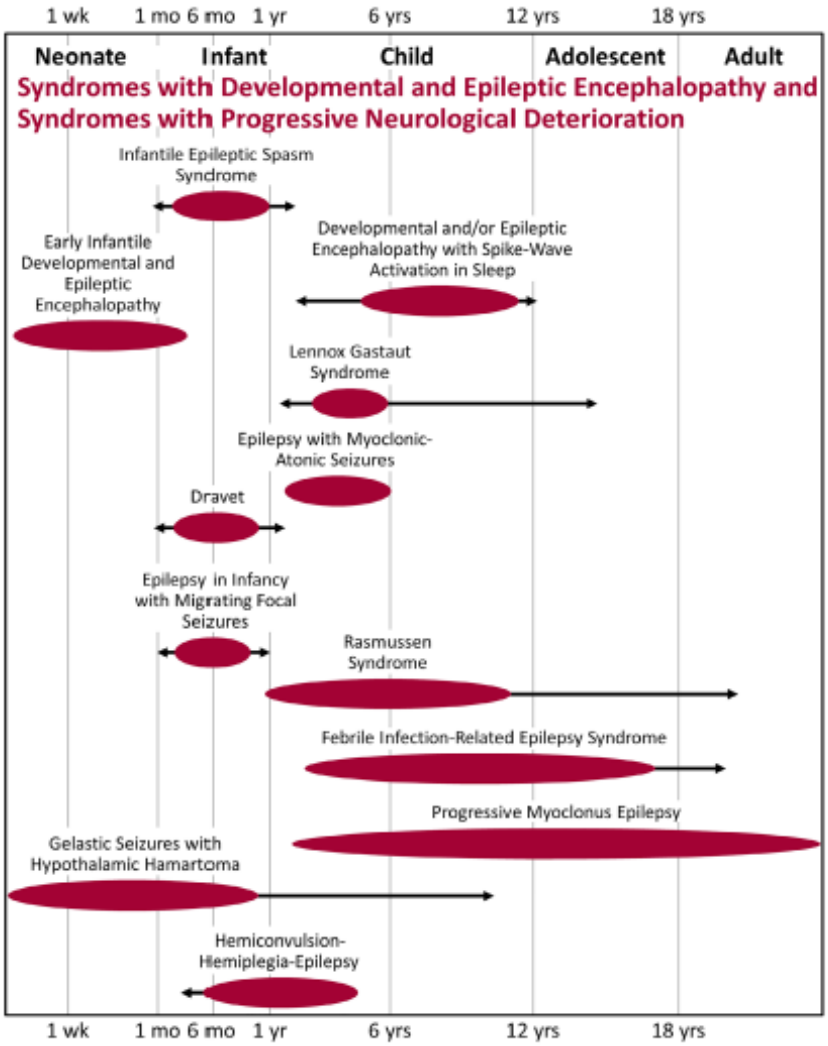

Figure 1.3. Classification of the 2022 ILAE Epilepsy syndromes by age of onset.

An epilepsy syndrome generally refers to a range of parameters including seizure types, EEG, age of onset, imaging features, seizure triggers, and sometimes prognosis. It may also be associated with comorbidities such as intellectual and psychiatric dysfunction. There are several well recognized syndromes, for example, childhood absence epilepsy, West syndrome, and Dravet syndrome. Shown here are syndromes with developmental and/or epileptic encephalopathy or with progressive neurological deterioration the typical ages of presentation, with ranges indicated by arrows.

1.5.1 Epilepsy Diagnosis

Seizure and epilepsy diagnoses are often based on clinical symptoms and signs (the history/story or witnessed seizure events). However, an electroencephalogram (EEG) is the primary tool used for also aiding diagnosis of seizure types and epilepsy classification. An EEG records the electrical activity in the brain and can detect a multitude of irregular epileptiform discharge patterns and brain states, in epilepsy patients (Paszkiel, 2020). Brain imaging (magnetic resonance imaging) is the radiological imaging tool of first choice, which may uncover a structural lesion in some patients with epilepsy. Other investigations depending on the context (seizure type, age, epilepsy type) may also inform the type of epilepsy, and the underlying cause (or aetiology). E.g., genetic investigations, metabolic testing, etc.

1.6 Aetiology of Epilepsy

In the most recent classification of the epilepsies by the ILAE, the new framework outlines the importance of considering aetiology at each level: seizure type, epilepsy type, and epilepsy syndrome (Fisher et al., 2014). The different categories of aetiologies include (i) structural, (ii) genetic, (iii) infectious, (iv) metabolic, (v) immune, or (vi) unknown **(Figure 1.2)**. More than one aetiology may be present for a patient with epilepsy, for example, a metabolic disorder may also have a genetic underpinning e.g., GLUT1 deficiency syndrome. The unknown category, which account for a substantial percentage of patients, is due to a combination of both gaps in our knowledge and a lack of diagnostic tools (Syvertsen et al., 2015).

1.6.1 Structural Aetiology

A structural aetiology is whereby visible abnormalities can be seen using structural neuroimaging techniques such as brain MRI. An electroclinical assessment combined with the neuroimaging findings has led to a reasonable inference that the structural abnormality seen from the imaging is the likely cause of the seizures (Berg et al., 2010). Structural abnormalities may be acquired, for example after a brain injury such as a stroke due to glial scarring that occurs in response to the injury (Steinhäuser et al., 2016). Other common causes of structural abnormalities that are associated with focal seizures include hippocampal sclerosis, malformations of cortical development, vascular malformations, brain tumours and inflammation in the brain (Blumcke et al., 2017). However, the cause of a structural abnormality may also be genetic, or both acquired and genetic (Whelan et al., 2018). For example, polymicrogyria, an epileptogenic malformation of cortical development, may occur

due to mutations in genes such as *GPR56*, or may be acquired, due to an intrauterine cytomegalovirus infection (Guerrini & Dobyns, 2014).

1.6.2 Genetic Aetiology

A genetic aetiology is when epilepsy results directly from a known genetic mutation (Steinlein, 2008). Many patients with early-onset epilepsy who are also developmentally delayed and possibly drug-resistant are likely candidates for a genetic cause of epilepsy. The most common example is Dravet syndrome, whereby over 80% of patients have a pathogenic variant in the *SCN1A* gene (brunklaus et al., 2013). In these genetic epilepsies, a large amount are caused by de novo mutations e.g., *KCNQ2*-related epilepsies (Weckhuysen et al., 2012).

1.6.3 Infectious Aetiology

Infectious aetiology is where epilepsy occurs as a direct result of an infection, whereby seizures are a core symptom of the disorder (Vezzani et al., 2016). The type of disease may be specific to certain regions of the world such as HIV, cerebral malaria, cerebral toxoplasmosis, and congenital infections such as cytomegalovirus and Zika Virus (Ngugi et al., 2013). These infections may also have a structural component (Falco-Walter et al., 2018).

1.6.4 Metabolic Aetiology

A wide range of either acquired or genetic metabolic disorders are associated with epilepsy. Acquired metabolic causes of epilepsy can occur due to nutritional deficiencies, liver failure or exogenous toxins (Angel et al., 2011). Metabolic causes can result in metabolic defects with biochemical changes seen throughout the body such as uraemia, porphyria, aminoacidopathies, or pyridoxine-dependent seizures (Almannai et al., 2021). In certain cases, metabolic disorders will also have a genetic defect. Inborn errors of metabolism, while rare, can lead to epilepsy (Rahman et al., 2013; Wolf et al., 2005). Identifying specific metabolic causes of epilepsy is critical due to implications for specific therapies such as substrate replacement therapy, without which symptoms may worsen the patient's encephalopathy or developmental outcome (Tan et al., 2015). Examples of metabolic aetiologies include pyridoxine-dependent epilepsy, Glut-1 deficiency, and vitamin dependency (Stockler et al., 2011; Gras et al., 2014).

1.6.5 Immune Aetiology

Immune aetiology refers to epilepsy that results directly from an immune disorder (Granata et al., 2011). Immune epilepsies present in both adults and to a lesser extent, children (Husari et al., 2019). Greater access to antibody testing has resulted in an increased diagnosis in autoimmune epilepsies (Geis et al., 2019). Examples of auto-immune epilepsies include anti-NMDA (*N*-methyl-d-aspartate) receptor encephalitis, mGlur5, GlyR and anti-LGI1 encephalitis (Balestrini et al., 2021). These types of epilepsy respond well to immunotherapy e.g., immunoglobulins and steroids (Jang et al., 2020).

1.6.6 Unknown Aetiology

Unknown aetiology means that the cause of the epilepsy is not yet known. The number of unknown aetiologies is decreasing due to advances in diagnostic tools and increased knowledge. An example of these advancements can be seen in the 3T MRI which has significantly increased the detection rate of epileptogenic lesions compared to the previously used 1.5T MRI (Fitsiori et al., 2019).

1.7 Genetic Aetiology in Paediatric Epilepsies

1.7.1 Monogenic Epilepsies and DEEs

Genomics technologies have enabled the discovery of numerous monogenic epilepsies and DEEs (Dunn et al., 2018). Due to the complexity of the human brain, it's not surprising that many gene discoveries have occurred in the field of epilepsy. The majority of monogenic discoveries occurred in the *DEEs* (Stenshorne et al., 2022). There are hundreds of known distinct monogenic neurodevelopmental disorders, though some are more frequently linked to frequent seizures and epilepsy e.g., *SCN1A, SCN2A, SCN8A, KCNQ2/3, etc* **(Figure 1.4)** (Tărlungeanu et al., 2018). In monogenic epilepsies, genotype-phenotype heterogeneity is common, whereby one genetic disorder can give rise to different phenotypes of varying severity (Nappi et al., 2020). Similarly, an epilepsy type can also be caused by separate genetic mutations. For many DEEs, inheritance is often *de novo* (no other family members affected) although recessive, X-linked inheritance, and mosaicism also occurs (Bartolini, 2021). Finally, copy number variants (CNVs), or chromosomal alterations in patients with severe epilepsies also contribute to these epilepsies, accounting for approx. 5-10% of this group (Coppola et al., 2019).

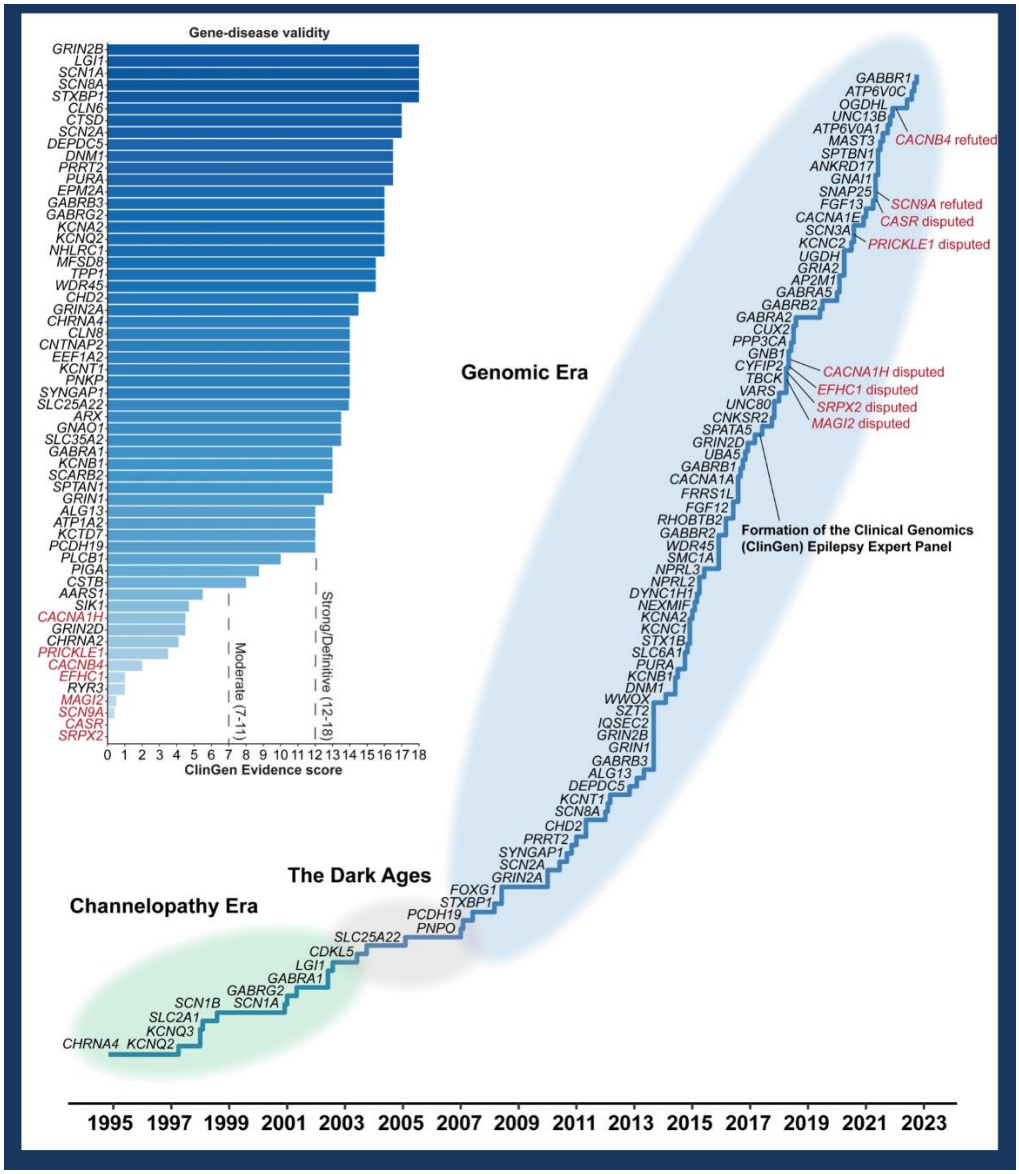

Figure 1.4. Timeline of gene discoveries in the epilepsies.

The timeline of gene discovery in the epilepsies, including 126 manually reviewed genes across the three main eras of epilepsy gene discovery, namely, the Channelopathy era, the Dark Ages, and the Genomic Era. The inset on the left highlights genes officially reviewed by a ClinGen Epilepsy Gene Curation Expert Panel (GCEP) to validate the genes. From Xiang and Helbing 2023 (http://epilepsygenetics.net/2023/01/18/the-history-of-epilepsy-genetics/).

1.8 Potassium channel Epilepsies

1.8.1 Potassium ion channels

Channelopathies are a group of epileptic disorders which occur due to pathogenic variants in ion-channel genes i.e., Na^+, K^+, $Ca^{2+}$and Cl^- channels (Allen et al., 2020). Recent estimates believe that ~25% of genes identified in epilepsy encode ion channels (Oyrer et al., 2018). The voltage-gated K^+ channel superfamily (Kv) makes up the largest component of these

channelopathies, representing a diverse group of approx. 80 primary genes (Allen et al., 2020). K^+ channels have a wide array of functions including controlling the resting membrane potential (RMP), shaping action potentials (APs) and control excitability in neurons (Humphries & Dart, 2015). Different types of K^+ channels have different roles in neurophysiology. These K^+ channels are categorised into 4 larger groups: a) K_v family (voltage-gated) b) K_{Ca} family (calcium-activated), c) K_{ir} family (inward rectifier), and d) K_{2P} (two-pore) (Noh et al., 2019). Within these families, there are K^+ channel sub-families, based on amino-acid sequence similarities of the protein core (Allen et al., 2020). The K_v family is divided into 12 subfamilies (K_v1-12), composed of approximately 40 individual α-subunits (genes)**(Table 1)**. *KCNQ*-related (K_v7) epilepsies represent the longest studied disorders of this group to date since 1998 **(Figure 1.4)** (Singh et al., 1998).

Table 1.1: Voltage-gated ion-channel Kv family and sub-families marking the Kv7 family (KCNQ) in red

Channels (α subunits)	Genes
Kv1.1-Kv1.8	*KCNA1-7, 10*
Kv2.1-Kv2.2	*KCNB1-2*
Kv3.1-Kv3.4	*KCNC1-4*
Kv4.1-Kv4.3	*KCND1-3*
Kv5.1	*KCNF1*
Kv6.1,Kv6.4	*KCNG1,4*
Kv7.1-Kv7.5	***KCNQ1-5***
Kv8.2-Kv6.2	*KCNV2,3*
Kv9.1-Kv9.3	*KCNS1-3*
Kv10.1-Kv10.2	*KCNH1,5*
Kv11.1-Kv11.3	*KCNH2,6,7*
Kv12.1-Kv12.3	*KCNH8,3,4*

1.8.2 Structure of K_v potassium channels

K^+ channels are transmembrane (TM) proteins that span the lipid bilayer. Each K^+ channel is made up of α-subunits **(Figure 1.5)** (Sansom et al., 2002). Within each α-subunit exists a homologous pore segment which is selective for K^+ ions and possesses other gating mechanisms and domains that allow responsiveness to diverse stimuli such as the voltage-sensing domain and the C-terminus (Yi et al., 2001). The α-subunit structure of the *K_v family* contains 6 TM segments and can assemble into tetramers when 4 α-subunits localise together (tetramerisation) resulting in a pore-forming K^+ channel (Ranjan et al., 2019). α-subunits may combine to be composed of either identical (homomeric) or different (heteromeric) α-subunits to form either homo-tetramers or hetero-tetramers. Further

molecular diversity is seen as each K_v channel has specific neuronal types, subcellular distributions and expression patterns, and membrane signalling interactions (Trimmer, 2015). Our particular gene of interest, *KCNQ2,* is expressed throughout the CNS, with particular enrichment seen at the axon initial segment (AIS) (Cavaretta et al., 2014). Kv7.2 channels most commonly form hetero-tetramers with Kv7.3 channels and less frequently form hetero-tetramers with Kv7.5 channels (Dirkx et al., 2020). Kv7 channel's main function is regulating the M current, a slow-activating, non-inactivating potassium current that controls membrane excitability (Wang, 1998).

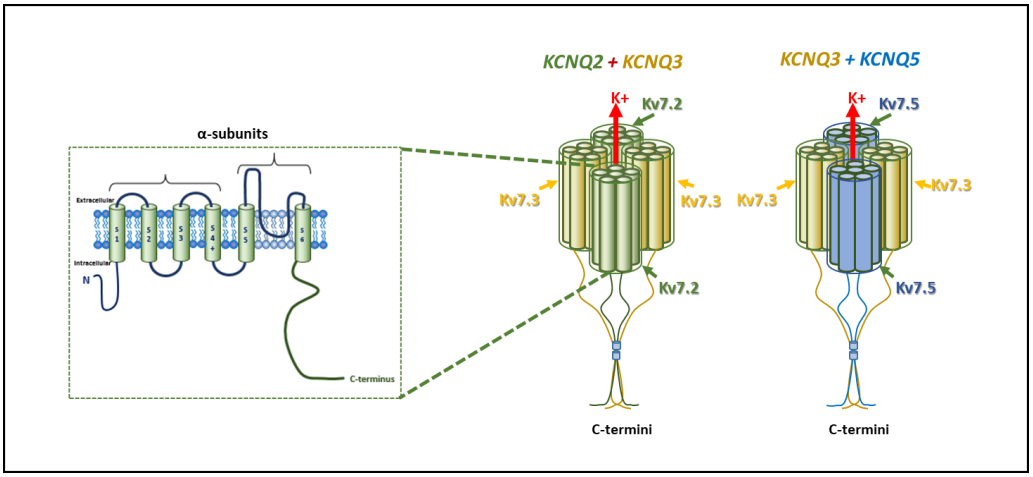

Figure 1.5. Structure of a *KCNQ2* α-subunit and formation of hetero-tetramers.

α-subunit structure shows 6 transmembrane spanning regions across the lipid bilayer, the S4 voltage sensing domain, the pore-forming region, and the N- and C- termini. Kv7.2 α-subunits (green) form hetero-tetramers with Kv7.3 α-subunits (yellow) or with Kv7.5 α-subunits (blue) to form a pore-forming K^+ channels (Figure generated with permission, by Prof. Nicholas Allen adapted from (Allen et al., 2020)).

1.8.3 Effects of *KCNQ2* functional defects

Pathogenic gene variants commonly affect highly conserved regions within the channel subunits e.g., the voltage-sensor in a voltage-gated channel (Sun et al., 2019). Numerous *in silico* analysis tools can be used to estimate the likelihood of the pathogenic effects of a particular variant in a particular gene (Pérez-Palma et al., 2020). However, modelling the effect of the mutation experimentally, is the most useful criterion for pathogenicity (Richards et al., 2015). In *Kv* channels, including *KCNQ2,* this can be determined by comparing the effect of mutant versus wildtype (WT), commonly using *in vitro* electrophysiological technologies in non-neuronal heterologous expression systems (e.g. Voltage-clamping in *Xenopus* Oocytes or patch-clamping in CHO or HEK cells) (Kang *et al.*, 2019). A pathogenic variant can affect different properties of the channel such as channel

assembly, physiology, or biophysical properties such as channel gating kinetics (Laddach et al., 2021). These pathogenic effects ultimately result in either a loss-of-function (LOF) or gain-of-function (GOF) effects (Miceli et al., 1993). Additionally, a dominant-negative effect (DNE)/mutation may also exist, whereby a mutant protein (subunit) can significantly impair WT co-assembled channels (Allen *et al.*, 2020). LOF in Kv7.2 channels is more common than GOF, and results in reduced *KCNQ2* protein, potentially due to defects in gating/expression of the Kv7.2 channels at the AIS (Millichap et al., 2016). GOF can also occur in *KCNQ2*-related disorders whereby there is an increase in K^+ conductance, thought to be attributable to a large increase in single channel open probability (Nappi et al., 2022). *KCNQ2* pathogenic variants are clustered within mutational 'hotspots', within the critical, functional domains of the protein **(Figure 1.6)** (Millichap et al., 2016).

1.8.4 Genotype-phenotype correlation in *KCNQ2*-related epilepsies

Determining a genotype-phenotype correlation can provide information on disease pathogenicity, future disease progression and disease severity (Frew et al., 2019). Pathogenic variants in *KCNQ2* typically causes one of two phenotypes; (i) *benign familial neonatal epilepsy (BFNE)*(also known as Self-limited (familial) neonatal epilepsy) or (ii) *developmental epileptic encephalopathy (DEE)* (Allen et al., 2020). It has been shown that pathogenic variants located close together in a specific location within the protein i.e., the pore-forming domain may cause similar phenotypes in patients. A study looked at 216 different pathogenic *KCNQ2* variants and found that *BFNE* variants are more likely to be located in the intracellular domain between S2 and S3, while *DEE* variants are more likely to be situated in the pore region, S6 segment and the intracellular domain between S6 and helix A (Goto et al., 2019). In a study with 10 different *KCNQ2* pathogenic variants located in or nearby the pore-domain, tonic seizures were present in 9/10 patients, and all had a burst-suppression (EEG pattern) phenotype by 1.5 months of age (Olson et al., 2017). However, there was no clear pattern of medication response seen in these patients. A more recent study examined the effects of 28 *de novo* pathogenic *KCNQ2* variants clustered in a conserved region of the protein and could not identify a relationship between variant location and seizure offset or cognitive outcome (Malerba et al., 2020). This study highlights the complexity of using variant location to interpret the impact of a *de novo* mutation.

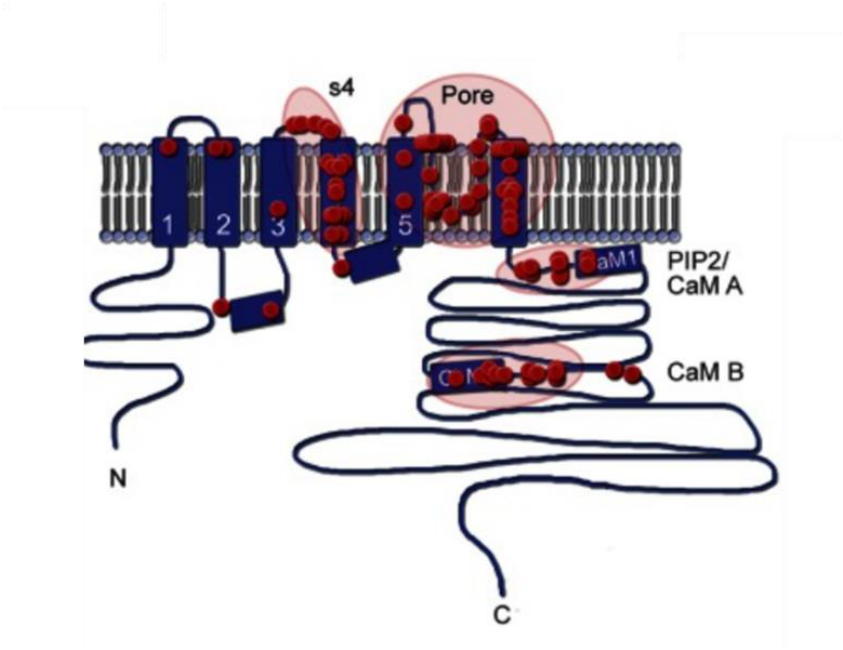

Figure 1.6: Schematic illustrating the location of pathogenic *KCNQ2* variants within the transmembrane protein.

Pathogenic variants (red circles) are marked along the transmembrane protein. Clustered areas of mutations/variants located within the critical, functional domains (S4 voltage sensor, Pore, and Cam A and Cam B region of the C terminus) are highlighted in large pink circles. (Millichap et al., 2016)

1.8.5 Effects of *KCNQ2* functional defects

A GOF mutation is characterised by an increase in the mean K^+ current amplitude and a negative shift in RMP (Dirkx et al., 2020). Various *KCNQ2* GOF mutations have been reported in patients, though less commonly than LOF mutations. Patients carrying *KCNQ2* R144 GOF variants, located within the S2 segment, experience developmental delay with prominent language impairment, autistic features, often accompanied by infantile- to childhood-onset epilepsy and EEG sleep-activated epileptiform activity. A study used patch-clamping to analyse the functional defects of the variant in CHO cells and found an increased K^+ conductance, and significant changes in activation gating, likely due to PIP-2 binding (Miceli et al., 2022). They showed that the Kv7.2/7.3 channel blocker amitriptyline could successfully block the K^+ current in the diseased model. The absence of neonatal seizures is an important clinical differentiator between *KCNQ2* GOF and LOF variants.

A LOF mutation is characterised by a decrease in the mean K^+ current amplitude. A study analysed the phenotype of 7 patients carrying the recurrent A294V mutation (a *KCNQ2* mutation which is subject of this thesis) located within the S6 segment of the pore-forming domain (Abidi et al., 2015). In this study they simultaneously analysed the functional and subcellular consequences of this mutation and another mutation located on the same

residue which causes *BFNE*, A294G. In CHO cells, the total expression of Kv7.2 (A294V) alone, assessed by western blotting, was only 20% compared to wild-type, however, this could be rescued to wild-type levels in cells co-expressing the Kv7.3 subunit. In contrast to A294V, the current density of homomeric A294G was not significantly changed compared to wild-type Kv7.2 (Abidi et al., 2015). Furthermore, in neurons, they showed that the A294V mutation induced a mis-localization of heteromeric mutant channels to the AIS, while the A294G mutation had no effect on the localization of the heteromeric channels to the AIS. These results show that a mutation at this residue can cause either a severe or a benign epilepsy depending on the amino acid change. This study revealed that the functional effect of the A294V mutation is not due to a dominant-negative effect of loss of K^+ current, but rather is due to the alteration in the preferential axonal targeting of heteromeric Kv7 channels. This data also suggests that disease severity may not necessarily be a consequence of strong M current inhibition and that other mechanisms such as abnormal subcellular distribution of Kv7 channels could be determinant. **Table 2** summarises the functional effects and correlation to severity and known approach to treatments, specific to *KCNQ2*-related disorders.

Table 1.2: *KCNQ2* (Kv7.2) function, clinical phenotypes, functional defects, and approach to specific treatments. Adapted from (Allen et al., 2020)

Kv gene (channel subunit)	Epilepsy (and related) phenotypes	Examples of key functional defects and variants	Individual therapeutic considerations
KCNQ2 (Kv7.2)	BFNE	LOF (usually haplo-insufficiency). Less severe loss of M current.	Na^+ channel blockers.
	DEE	LOF (many missense mutations along 'hotspot' zones). Severe loss of M current (Often dominant negative).	Na^+ channel blockers Retigabine (K^+ opener).
	PNH	LOF (Dominant negative).	Na^+ channel blockers.
	Profound new-born encephalopathy without seizures	GOF R201C/R201H.	Consider avoiding K^+ channel openers.
KCNQ3 (Kv7.3)	Infantile Spasms 4-6 mo BFNE (rare)	GOF e.g., R198Q.(S4). LOF missense majority.	Consider avoiding K^+ channel openers. Na^+ channel blockers.
	Severe DEE (neonatal onset) Developmental disability with few seizures	LOF: bi-allelic (rare) homozygous F534lfs*15. GOF: missense 4227Q (S4).	Consider K^+ channel openers. Na^+ channel blockers.
	Neurodevelopmental disability: non-verbal with ASD.	GOF: R230C, R230H, R230S.	Consider checking for ESES (Electrical status epilepticus).
Abb: BFNE, benign familial neonatal epilepsy; DEE, developmental and epileptic encephalopathy; PNH, peripheral nerve hyperexcitability disorder; ASD, autism spectrum disorder; LOF, loss of function; GOF, gain of function.			

1.9 Pharmacological therapies in Epilepsy and *KCNQ2*-related disorders

1.9.1 Anti-seizure therapies

Of the approximately 28 routinely used anti-seizure medications (ASMs), with various mechanisms of action (**Figure 1.7**), none treat the underlying molecular basis of the disease for individual patients. Despite the number of ASM's, 30% of people still continue to experience seizures (Ventola, 2014). In a study examining the effects of common ASM's on *KCNQ2*-DEE, only 65% of patients responded to routinely used sodium-channel blockers (Kuersten et al., 2020), however patients continue to often have seizures, and the underlying developmental brain disorder has not been shown to improve using these anti-seizure therapies. Therefor there is still a large cohort of patients who do not benefit from these treatments, resulting in a large treatment gap in epilepsy therapy, principally to tackle the underlying cause of the disease.

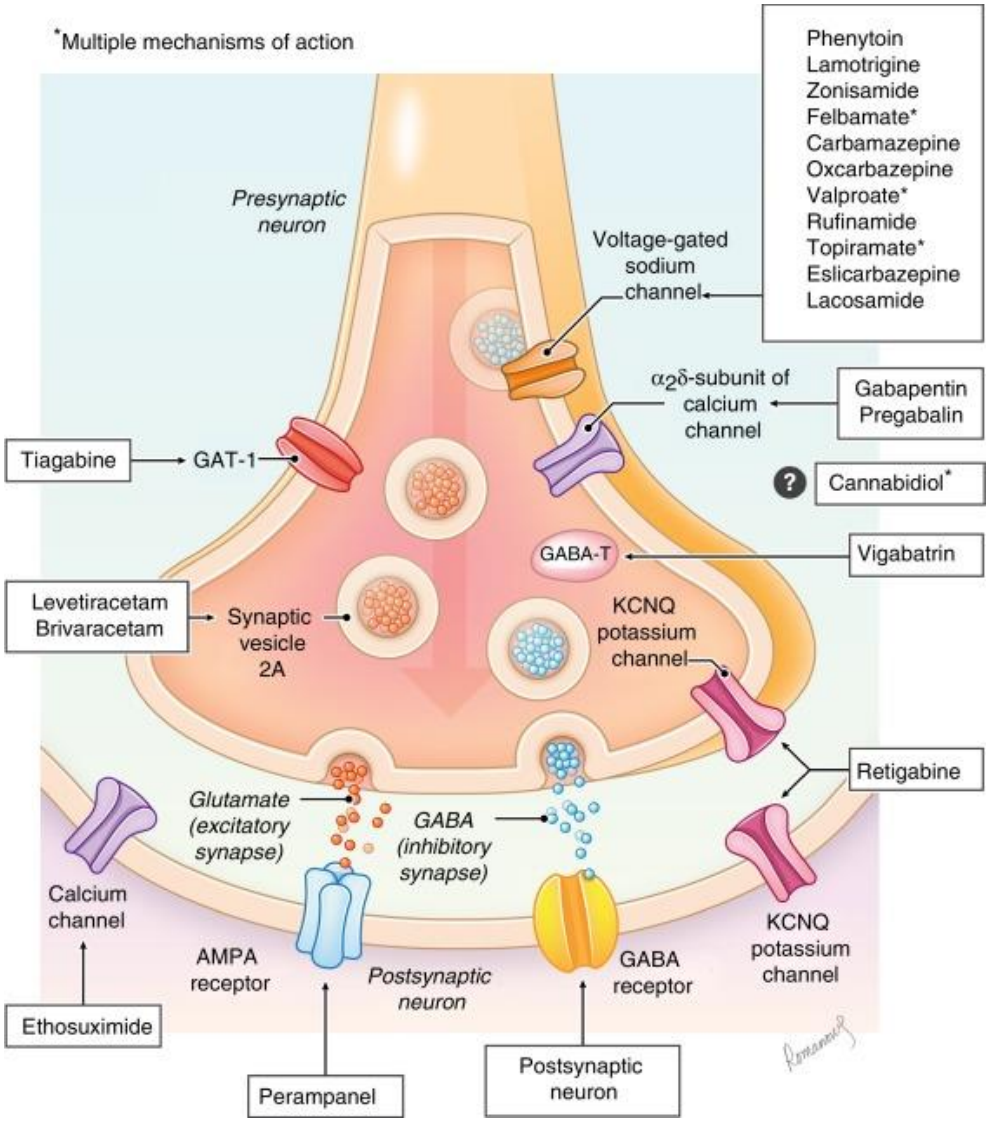

Figure 1.7: A simplified illustration of the mechanism of action of the main ASM's in the synapses.

For many patients, the choice of antiseizure medications are based on clinical presentation, experience, known efficacy in specific seizure types, epilepsy types and epilepsy syndromes. e.g., carbamazepine is used to treat focal seizures while ethosuximide is used as a first line in absence seizures (Málaga et al., 2019).

1.9.2 Precision therapies in Epilepsies

Precision therapy or personalised medicine is where the treatment is targeted to the individual needs of patients based on genetic and phenotypic characteristics. As a large percentage of epilepsies in children have a genetic component, individual considerations are required, often based on simple seizure and epilepsy classification. However, in some cases, the cause of the epilepsy may also be the cause of the underlying developmental, cognitive, physical, and social problems and co-morbidities experienced by the patients. Therefore, even when seizures are well managed by ASM's, many patients, particularly those with DEE,

remain to be severely neurologically impaired affecting their quality of life. Precision therapies which directly target the underlying disease, rather than the symptoms, will greatly improve the outcome for these patients.

Precision medicine in epilepsy is not only targeted to genetic epilepsies (molecular pathways) but is also targeted to molecular aetiology/pathophysiology of a disease (McGinn et al., 2022). To date, in practice, good evidence based *effective* precision therapies targeting the molecular basis of disease exists for only a few rare genetic disorders (e.g., tuberous sclerosis), and metabolic epilepsies (e.g., pyridoxine-dependent epilepsies or GLUT1 deficiency syndrome) (Schubert-Bast et al., 2021).

1.9.3 Treatment and precision therapy in *KCNQ2*-related Epilepsy

In *KCNQ2*-DEE with a LOF mutation, a potassium channel opener retigabine, was shown to effectively open K^+ channels, presenting a potential precision therapy for patients based on the genetic mutation. This drug was subsequently withdrawn due to safety concerns but is being re-examined for re-purpose in severe *KCNQ2*-DEE, given the severity and lack of available specific ASMs in this disorder. In addition, sulfide analogues that function as potassium openers could theoretically avoid the negative side effects associated with retigabine and serve as a potential precision therapy for certain patients (Bock et al., 2019). Benefits of gabapentin have also been published but only in one case of *KCNQ2*-DEE pathogenic variant, G310S, due to LOF mutation (Soldovieri et al., 2020). A recent study evaluated the efficacy of the Kv7 openers, retigabine, HN37 and XEN1101 on 6 mutations all located within the pore region. They found that for each drug, the restoration of the loss of potassium current varied between each mutation, illustrating the potential of these drugs for personalised medicine (Yang et al., 2023).

1.10 *In vivo* and *In vitro* models of *KCNQ2* mutations

1.10.1 Introduction to *in vivo* model systems

Animal models for epilepsy and seizures have played a crucial role in advancing our understanding of basic mechanisms underlying epileptogenesis and have been critical in the discovery of novel antiepileptic drugs (AEDs)(Löscher, 2011). Animal models offer many benefits as model systems e.g., detection of anti-convulsant activity, adverse side effects and estimation of effective plasma concentrations of new drugs (White et al., 2006). The majority of animal models used in epilepsy research are seizure models rather than models of epilepsy,

as seizures are induced in a normal, non-epileptic animals. More accurate animal models of epilepsy are transgenic models with spontaneous recurrent seizures, which more accurately represent human models. Mice are commonly used *in vivo* epilepsy models. A recent study using a mouse model of *KCNQ2*-BFNE (with a heterozygous deletion of *KCNQ2*) revealed for the first time, the efficacy of the sodium channel blocker eslicarbazepine acetate (ESL) and eslicarbazepine metabolite (S-Lic) in reducing seizure threshold in the mice. Another study examined the pathophysiology of a *KCNQ2*-DEE pathogenic variant T274M in a knock-in mouse model. They revealed that the mutation caused generalised spontaneous seizures and that the brains had no major structural defects, similar to that seen in humans (Milh et al., 2020). Animal models of epilepsy have dominated the field with regard to research and development, however in recent years they have failed to deliver new agents that can provide seizure control in patients with drug refractory epilepsy. Moreover, these models also have substantial issues with regard to validity and animal welfare considerations (Morris, 2021).

1.10.2 Introduction to *in vitro* model systems

Chinese hamster ovary (CHO) cells are a commonly used cell line as they are easily modified, making them ideal for recombinant protein production and cloning (Rahimpour et al., 2016). CHO cells have been used extensively as an *in vitro* model of epilepsy for drug discovery and testing (Bandaranayake et al., 2014). Retigabine, the Kv7.2 channel opener, was discovered using a CHO cell line transfected with *KCNQ2/KCNQ3* constructs. In this study they showed that retigabine was capable of opening the Kv7.2/Kv7.3 channels that were expressed in the CHO cell line expression system, thus discovering the first M current activator (Rundfeldt et al., 2000). Aside from drug discovery, CHO cell lines have also been used to model disease phenotypes *in vitro*. One study recruited 4 unrelated, seizure-free, patients all with the same *KCNQ2* pathogenic variant, R198Q, and expressed these variants in CHO cells by transient transfection. They showed that the K_v7.2 R198Q subunit, expressed alone or in combination with K_v7.2 and/or K_v7.3 subunits, increased potassium current activated by partial membrane depolarization. They saw no significant changes in the pore properties, heteromerization or neuronal subcellular localization. This study led to the discovery of a new subclass of *KCNQ2* variants causing infantile spasms and encephalopathy, without preceding neonatal seizures (Millichap et al., 2017). Other heterologous expression systems in non-neuronal cell lines (such as HEK293 or *Xenopus laevis* oocytes) are also used to analyse protein dysfunction caused by a genetic variant or a DNE that the mutant protein may exert on the WT counterparts. However, proteins may function differently outside their non-native

environment as a result of disparities in splicing patterns, posttranslational regulation, interactions with different proteins, cellular and protein trafficking, and various other neuronal factors (Simkin et al., 2018).

1.11 Use of induced pluripotent stem cells (iPSCs) in modelling epilepsy

Despite the many advantages the aforementioned models offer, considerable differences in gene expression, protein function, and network participation exist between humans and mice with roughly 20% of CNS genes showing distinct expression patterns in the cortex (Xu et al., 2007). These discrepancies may explain the disparate efficiencies of ASMs in clinical trials and why refractory epilepsy still remains at 30%. Therefore, there is an obvious requirement to generate a model that more closely resembles human conditions. This had previously been hampered by the inability to isolate human neuronal tissue until the discovery of induced pluripotent stem cells (iPSCs) in 2006. The discovery of iPSCs, which can be readily generated by reprogramming adult somatic cell types such as skin-derived fibroblasts, have allowed us to elucidate human pathogenic mechanisms of genetic diseases such as *KCNQ2*-DEE, which will be the focus of this PhD.

1.11.1 Definition of iPSCs

The discovery of iPSC technology occurred in 2006 by the Yamanaka group with mouse embryonic and adult fibroblasts (Takahashi et al., 2006), which was soon after replicated in human adult fibroblasts in 2007 (Takahashi et al., 2007). Three previous scientific studies contributed to the discovery of iPSC technology. The first of these studies occurred in 1962 by Gurdon's laboratory (Yamanaka, 2012). Gurdon discovered somatic cell nuclear transfer (SCNT) by isolating the nucleus of a terminally differentiated adult cell from a Xenopus laevis which was subsequently transplanted into an oocyte, generating a cloned frog that carried DNA identical to the transplanted nucleus (Gurdon, 1962). Over 30 years later, Wilmut et al utilised SCNT to create the first mammalian clone, the famous 'Dolly' the sheep (Wilmut et al., 1997). These critical experiments indicated that all nuclei, whether immature or terminally differentiated, contain the genetic information necessary to form a whole organism. The second important milestone was the revelation of 'master' transcription factors. Master transcription factors are critical genes that coordinate the pathways governing cell fate (Mattick, 2010). The third and final revelation was the development of ESC culture conditions that allowed ESCs to maintain their pluripotent state *in vitro* (Yamanaka, 2012).

Taken together, these scientific milestones led to the hypothesis that key factors in maintaining pluripotency in ESCs, could be used to directly reprogramme adult somatic cells to an embryonic state. In 2007, Takahashi et al. (Takahashi et al., 2007) generated a list of 24 candidate genes associated with pluripotency in ESCs which was narrowed down to 4 factors, known as the Yamanaka factors [Octamer-binding transcription factor 4 (Oct4), c-Myc, Krüppel-like factor 4 (Klf4) and SRY-box 2 (Sox2)] . The Thompson group also established a similar set of transcription factors capable of reprogramming somatic cells (Oct4, Sox2, Nanog and Lin28) (Yu et al., 2007). The introduction of these transcription factors into human somatic cells, most commonly dermal fibroblasts or mononuclear blood cells, results in the formation of embryonic stem-like cells capable of self-renewal and the ability to differentiate into the three germ layers.

1.11.2 Application of iPSCs

The applications of iPSCs can be divided into three major groups: regenerative medicine, drug discovery and disease modelling (Stadtfeld et al., 2010). In each of these applications, iPSCs are required to be differentiated into a specific cell type e.g., neurons, related to the disorder of interest e.g., epilepsy (Nishihara et al., 2019). iPSCs have a major advantage in the field of regenerative medicine compared to ESCs, as they are autologous so are less likely to provoke an immune reaction in the patient (Scheiner et al., 2014). iPSCs as a method of cellular therapy/repair have an array of therapeutic applications for genetic disorders such as epilepsy, neurodegenerative disorders including Alzheimer's or Parkinson's disease and accidental injuries such as spinal cord injuries (Nagoshi et al., 2019).

Patient-derived iPSC models are an ideal method for high throughput screening of pharmaceutical compounds which may lead to the identification of new drugs. They also have the potential for personalised therapy, which as discussed previously may be very advantageous for monogenic epilepsies (Chun et al., 2011). iPSC models more accurately represent human conditions, providing more accurate data on safety and efficacy in drug screening than animal models. Lack of efficacy and toxicity concerns are some of the reasons associated with product failure in clinical trials (Sun et al., 2022).Patient-derived iPSC models can reduce the cost and the time associated with clinical trial failure due to a product that may prove to be cytotoxic due to inaccurate data obtained from inaccurate/inappropriate *in vitro* and *in vivo* models (Thanaskody et al., 2022). However, animal models and iPSC models are used synergically to model human disorders as they both offer unique advantages.

In many cases, the pathophysiology of certain diseases are not fully understood. Due to an increase in the discovery of genes associated with epilepsy due to NGS advances, there is an even greater need to model these mutations in appropriate disease models to elucidate disease mechanisms (Hmeljak et al., 2019). As iPSCs can proliferate indefinitely and can differentiate into all cell types, excluding extra-embryonic tissue such as the placenta, these cells are excellent for studying a wide range of diseases (Sato et al., 2021). To date, numerous 2D and 3D protocols have been developed for differentiating iPSCs into various cell types and organoids respectively (Centeno et al., 2018). These iPSC-derived models have and will continue to enable the discovery of novel pathways involved in pathogenesis and identification of new therapeutic targets.

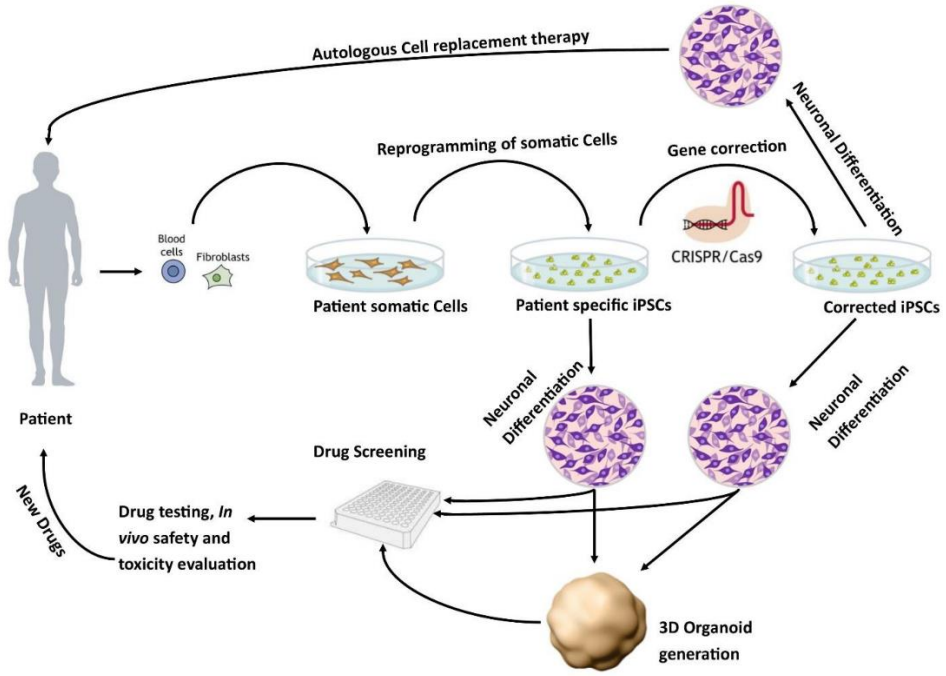

Figure 1.8: Schematic illustrating the applications of iPSC-derived neurons.

Patient-specific stem cell lines for cell replacement therapy, drug discovery and disease modelling. Somatic cells, usually taken from the patient's skin or blood cells, can be isolated and reprogrammed into iPSCs. These cells can be differentiated into different neuronal populations and can be used to further study the pathophysiology of the disease or as a drug screening model to test novel therapies. Additionally, these lines can undergo gene editing using CRISPR/Cas9 to generate isogenic iPSCs (Javaid et al., 2022).

1.11.3 iPSC-derived neuronal 2D and 3D protocols

Patients with different mutations in the same gene can have vastly different clinical presentations, as we have seen in the milder phenotype of *KCNQ2*-BFNE versus *KCNQ2*-DEE. Additionally, patients can have different clinical responses to pharmacological treatments (Roden et al., 2011). The profound advantage of iPSCs is that they enable the study of human

disease in the context of each person's unique genetic makeup, in disease-relevant cells, while also providing a platform for modelling the effects of genetic variants in early developmental stages of the disease (Simkin et al., 2018). Neuronal sub-types derived from patient iPSCs have been used to effectively model many neurodevelopmental diseases associated with epilepsy, including Dravet Syndrome due to *SCN1A* mutations (Liu et al., 2013), Timothy Syndrome (Krey et al., 2013), Angelman Syndrome (Stanurova et al., 2016) and *STXBP1*-associated EE (Yamashita et al., 2016).

Traditional iPSC protocols are based on the differentiation of adherent 2D cultures using either a combination of small molecules or expression of key regulatory transcription factors. In more recent years, the development of 3D cerebral organoids has facilitated the differentiation of multi-cellular models that recapitulate specific spatial and temporal aspects seen in human brain development (Lancaster et al., 2014). **Table 1.3** include a list of various 2D and 3D differentiation protocols relevant for studying EEs (Simkin et al., 2022). There are many benefits to both 2D and 3D neuronal differentiation protocols, and careful consideration should be taken to choose the protocol most relevant to the research question. 2D protocols have been used more extensively and there now exists numerous well-established protocols with sufficient reproducibility. On the other hand, 3D protocols may more accurately resemble the spatial and temporal aspects in the human brain, but these protocols are more costly, technically challenging, and still in their infancy (Centeno et al., 2018).

Table 1.3 Literature related to iPSC 2D and 3D neuronal differentiation protocols (Simkin et al., 2022)

Protocol type	Cell type	Protocol details	Reference
Small molecule-mediated	Cortical neurons	WNT/dual-SMAD inhibition	(Chambers *et al.*, 2009)
	Glutamatergic neurons		(Shi *et al.*, 2012a; Shi *et al.*, 2012b)
	GABAergic neurons		(Liu *et al.*, 2013a; Maroof *et al.*, 2013)
	Dopaminergic neurons		(Kriks *et al.*, 2011; Zhang *et al.*, 2014)
	Serotonergic neurons		(Lu *et al.*, 2016)
	Hippocampal neurons		(Yu *et al.*, 2014; Sarkar *et al.*, 2018)
	Sensory peripheral neurons		(Guimaraes *et al.*, 2018)
	Astrocytes		(Krencik and Zhang, 2011; Gupta *et al.*, 2012; Santos *et al.*, 2017; Tcw *et al.*, 2017)
	Oligodendrocytes		(Hu *et al.*, 2009; Wang *et al.*, 2013; Douvaras *et al.*, 2014; Douvaras and Fossati, 2015; Piao *et al.*, 2015)
	Microglia		(Muffat *et al.*, 2016; Abud *et al.*, 2017)
Transcription factor-mediated	Glutamatergic neurons	NGN2, WNT/dual-SMAD inhibition	(Zhang *et al.*, 2013; Nehme *et al.*, 2018)
	GABAergic neurons	ASCL1 and DLX2	(Sun *et al.*, 2016a; Yang *et al.*, 2017)
	Dopaminergic neurons	ASCL1, NURR1, LMX1A or PITX3	(Caiazzo *et al.*, 2011; Theka *et al.*, 2013; Mahajani *et al.*, 2019)

	Serotonergic neurons	NKX2.2, FEV, GATA2, LMX1B, ASCL1, NGN2	(Vadodaria *et al.*, 2016)
	Motor neurons	LHX3, NGN2, ISL1	(Goto *et al.*, 2017)
	Astrocytes	SOX9, NFIB	(Canals *et al.*, 2018)
	Oligodendrocytes	SOX10, OLIG2, NKX60.2	(Ehrlich *et al.*, 2017; Pawlowski *et al.*, 2017)
Organoids	Cerebral whole brain organoids		(Lancaster *et al.*, 2013; Lancaster *et al.*, 2017)
	Cerebral whole brain organoids		(Li *et al.*, 2017)
	Cerebral whole brain organoids		(Quadrato *et al.*, 2017)
	Cortical organoids		(Eiraku *et al.*, 2008)
	Cortical organoids		(Kadoshima *et al.*, 2013, 2014)
	Cortical organoids		(Bershteyn *et al.*, 2017)
	Forebrain organoids		(Rigamonti *et al.*, 2016)
	Forebrain organoids		(Qian *et al.*, 2016)
	MGE		(Xiang *et al.*, 2017)
	Dorsal, ventral forebrain assembloids		(Bagley *et al.*, 2017)
	Pallial–subpallial assembloids		(Birey *et al.*, 2017)
	Cortical spheroids		(Pasca *et al.*, 2015; Sloan *et al.*, 2017; Pasca, 2019)
	Cortico-striatal assembloids		(Miura *et al.*, 2020)
	Oligodendrocytes containing neurocortical spheroids		(Madhavan *et al.*, 2018)
	Microglia containing neurocortical spheroids		(Song *et al.*, 2019)
	Midbrain organoids		(Jo *et al.*, 2016)
	Midbrain organoids		(Qian *et al.*, 2016)
	Hypothalamus		(Qian *et al.*, 2016)
	Cerebellum		(Muguruma *et al.*, 2015)
	Hippocampus and choroid plexus		(Sakaguchi *et al.*, 2015)
	Blood brain barrier organoids		(Bergmann *et al.*, 2018; Wimmer *et al.*, 2019)

1.11.4 iPSC modelling in epilepsy related ion-channelopathies

Channelopathy accounts for a significant bulk of genetic mutations associated with epilepsy (Oyrer et al., 2018). iPSC modelling has greatly accelerated research in ion-channelopathies, particularly in Na^+ and K^+ channelopathies as these are the most abundant. Voltage-gated sodium channels (NaV) play a fundamental role in the depolarizing phase of an AP, by promoting spike firings (Yu et al., 2003). In the mature CNS, NaV1.1, NaV1.2, and NaV1.6 (encoded by *SCN1A, SCN2A*, and *SCN8A*, respectively) are the most abundant sodium channels and are all closely linked to epilepsy (Wang et al., 2017). NaV1.1 has been the most extensively studied NaV in the human *in vitro* system. NaV1.1 is located at the AIS of neurons and contributes to the initiation and propagation of action potentials as well as their excitability (Child et al., 2014). Using iPSCs-derived inhibitory neurons from a patient harbouring a *SCN1A* mutation (S1328P), it has been shown that neurons carrying this LOF

mutation, displayed a reduced Na^+ current amplitude (Sun et al., 2016). Further studies showed that *SCN1A* (c.4261G>T/c.3576_3580del TCAAA) mutated neurons displayed decreased Na^+ current density (Kim et al., 2018), with *SCN1A* (c. 4261G > T) showing a greater reduction in Na^+ current compared to *SCN1A* (c.3576_3580del TCAAA). The differences seen in biophysical properties from these mutations correlated with the severity of symptoms in the patients whose iPSCs were generated from. Interestingly, these disparities in Na^+ current amplitude were primarily observed in inhibitory neurons but not excitatory neurons.

Voltage-gated potassium ion-channels (Kv's) make-up the largest group of ion channels in the nervous system. Kv's allow the selective efflux of K^+ ions and are responsible for repolarizing and hyperpolarizing membrane potentials to prevent hyperexcitability (Kim & Nimigean, 2016). Only a few Kv mutations have been modelled using iPSC-derived models **(Table 1.4)**. A study investigated the *KCNQ2* LOF mutation R581Q and revealed that the mutation led to faster AP repolarization and shorter spike width (Simkin et al., 2018). Either as a consequence of the loss of Kv7.2 activity, or as a consequence of the genetic mutation itself, the mutant neurons exhibited a higher spontaneous firing frequency and burst activity compared to the control using a multi-electrode array (MEA) assay. This revealed for the first time *in vitro*, that the *KCNQ2* LOF mutation R581Q in excitatory neurons led to an increased excitability. A complete list of channelopathy-associated epilepsy iPSC lines is provided in **Table 1.4**.

Table 1.4. Available channelopathy-associated epilepsy iPSC lines (from Simkin et al, 2022)

Gene	Mutation	Patient or Control iPSC line	Clinical diagnosis	Source	Phenotype
CACNA1C	c.1216G>A; p.G406R	Patient mutant (plus isogenic control)	Timothy Syndrome	(Birey *et al.*, 2017)	Abnormal migration of interneurons in neural spheroids
				(Pasca *et al.*, 2011)	Defects in calcium signaling and activity-dependent gene expression; abnormal expression of tyrosine hydroxylase; increased production of dopamine and norepinephrine in cortical neurons
				(Krey *et al.*, 2013)	Dendritic retraction in cortical neurons
				(Yazawa *et al.*, 2011)	Irregular contraction, calcium handling, and prolonged APs in cardiomyocytes
CACNA1C	c.1216G>A; p.G406R	engineered mutant (homozygous)	Timothy Syndrome associated mutation	(Martinez *et al.*, 2015)	No phenotype reported
CACNA1C	Gene knockout	engineered mutant (homozygous)	*CACNA1C* knockout	(Deneault *et al.*, 2018)	Reduced frequency of spontaneous excitatory postsynaptic currents (non-significant) in excitatory neurons
CACNA1S	c.4060A>T; p.T1354S	patient mutant	Ataxia; cerebral palsy, hand tremors, developmental delay	Coriell institute	No phenotype reported
KCNA2	c.869T>G; p.L290R	patient mutant	DEE	(Arbini *et al.*, 2020)	No phenotype reported
KCNA2	c.890G>A; p.R297Q	patient mutant	DEE	(Schwarz *et al.*, 2019)	No phenotype reported

KCNA2	c.982G>C; p.L328V	patient mutant	DEE	(Schwarz *et al.*, 2018)	No phenotype reported
KCNA2	c.1120A>G; p.T374A	patient mutant	DEE	(Uysal *et al.*, 2019)	No phenotype reported
KCNA2	c.1214C>T; p.P405L	patient mutant	DEE	(Gong *et al.*, 2020)	No phenotype reported
KCNB1	c.990G>T; p.E330D	patient mutant	DEE	(Guo *et al.*, 2021)	No phenotype reported
KCNC1	c.959G>A; p.R320H	patient mutant	Myoclonus Epilepsy and Ataxia	(Nengqing *et al.*, 2020)	No phenotype reported
KCNC1	c.959G>A; p.R320H	patient mutant	Myoclonus Epilepsy and Ataxia	European Bank for iPSCs (EBiSC)	No phenotype reported
KCNQ2	**c.619C>T; p.R207W**	**Patient mutant (plus isogenic control)**	***KCNQ2*-related DEE**	**(Simkin *et al.*, 2022b)**	**No phenotype reported**
KCNQ2	**c.683A>G; p.H228R**	**Patient mutant (plus isogenic control)**	***KCNQ2*-related DEE**	**(Simkin *et al.*, 2022b)**	**No phenotype reported**
KCNQ2	**c.821C>T; p.T274M**	**Patient mutant (plus isogenic control)**	***KCNQ2*-related DEE**	**(Simkin *et al.*, 2022b)**	**No phenotype reported**
KCNQ2	**c.1004C>T; p.P335L**	**Patient mutant (plus isogenic control)**	***KCNQ2*-related DEE**	**(Simkin *et al.*, 2022b)**	**No phenotype reported**
KCNQ2	**c.1742G>A; p.R581Q**	**Patient mutant (plus isogenic control)**	***KCNQ2*-related DEE**	**(Simkin *et al.*, 2021)**	**Faster AP repolarization; larger post-burst after-hyperpolarization; enhancement of calcium-activated potassium channels; overall increased bursting in cortical excitatory neurons**
KCNQ2	**Gene knockout**	**engineered mutant (homozygous)**	***KCNQ2* knockout**	**(Deneault *et al.*, 2018)**	**Reduced spontaneous excitatory postsynaptic current frequencies; reduced AP firing in cortical excitatory neurons**
KCNQ3	**c.1599dup; p.F534I fsTer15**	**patient mutant (homozygous)**	**Neonatal-onset epilepsy and non-syndromic intellectual disability**	**(Longobardi *et al.*, 2021)**	**No phenotype reported**
KCNT1	c.2771C>T; p.P924L	engineered mutant (homozygous)	*KCNT1*-related epilepsy associated mutation	(Quraishi *et al.*, 2019)	Increased sodium-activated potassium current; faster AP repolarization; increased numbers of evoked APs and firing rates; increased bursting in iCell Neurons (Cellular Dynamics)
LGI1	c.1418C>T; p.S473L	patient mutant	Autosomal dominant temporal lobe epilepsy (ADTLE)	(Tan *et al.*, 2017)	No phenotype reported
SCN1A	c.23del; p.P8H fsTer91	engineered mutant	Dravet syndrome associated mutation	(Frasier *et al.*, 2018)	Increased sodium current and rates of spontaneous contraction in cardiomyocytes
SCN1A	c.314C>T; p.T105I	patient mutant	Dravet syndrome	European Bank for iPSCs (EBiSC)	No phenotype reported
SCN1A	c.323_326dupTGTA; p.I110V fsTer10	patient mutant	Dravet syndrome	European Bank for iPSCs (EBiSC)	No phenotype reported
SCN1A	c.434T>C; p.M145T	patient mutant	Febrile seizures (FS), temporal lobe epilepsy (TLE)	(Scalise *et al.*, 2020)	No phenotype reported
SCN1A	c.650C>G; p.T217R	patient mutant	Dravet syndrome	(Schuster *et al.*, 2019a; Schuster *et al.*, 2019b)	Reduced sodium current, impaired response to oxidative stress and dysregulated transcriptomic pathways for chromatin remodeling and neurodevelopment in GABAergic neurons
SCN1A	c.664C>T; p.R222Ter	patient mutant (plus isogenic control)	Dravet syndrome	(Frasier *et al.*, 2018)	Increased sodium current and rates of spontaneous contraction in cardiomyocytes
SCN1A	c.730G>T; 735G>T; 736A>T; p.V244L; p.K245Ter	patient mutant (plus isogenic control)	Dravet syndrome	(Maeda *et al.*, 2016)	Increased levels of tyrosine hydroxylase transcript; higher concentrations of secreted dopamine in excitatory neurons
SCN1A	c.965G>T; p.R322I	patient mutant (plus isogenic control)	Dravet syndrome	(Frasier *et al.*, 2018)	Increased sodium current and rates of spontaneous contraction in cardiomyocytes
SCN1A	c.975T>A; p.Y325Ter	patient mutant	Dravet syndrome	(Liu *et al.*, 2013b)	Increased sodium currents; spontaneous bursting; general hyperexcitability in forebrain-like pyramidal- and bipolar-shaped neurons

SCN1A	c.975T>A; p.Y325Ter	patient mutant (plus isogenic control)	Dravet syndrome	(Frasier *et al.*, 2018)	Increased sodium current and rates of spontaneous contraction in cardiomyocytes
SCN1A	c.1112C>T; p.A371V	patient mutant (plus isogenic control)	Dravet syndrome	European Bank for iPSCs (EBiSC)	No phenotype reported
SCN1A	c.1649_1650del; p.550fs *	patient mutant	Dravet syndrome	European Bank for iPSCs (EBiSC)	No phenotype reported
SCN1A	c.2593C>T; p.R865Ter	patient mutant	Epilepsy	hPSC Registry, INSERM, France	No phenotype reported
SCN1A	c.2672delG; p.G891EfsTer3	patient mutant	Dravet syndrome	(Simkin *et al.*, 2022b)	No phenotype reported
SCN1A	c.2965G>C; p.A989P	patient mutant	Dravet syndrome with developmental delay	(Schuster *et al.*, 2019a; Schuster *et al.*, 2019b)	Reduced sodium current, impaired response to oxidative stress and dysregulated transcriptomic pathways for chromatin remodeling and neurodevelopment in GABAergic neurons
SCN1A	c.3306C>A; p.Y1102Ter	patient mutant	Dravet syndrome	(Kimura *et al.*, 2020)	No phenotype reported
SCN1A	c.3576_3580del; p.I1194CfsTer21	patient mutant	Dravet syndrome	(Kim *et al.*, 2018)	Reduced sodium current density and reduced AP firing in GABAergic neurons
SCN1A	c.3733C>T; p.R1245Ter	patient mutant (plus isogenic control)	Dravet syndrome	European Bank for iPSCs (EBiSC)	No phenotype reported
SCN1A	c.3809A>C; p.K1270T	patient mutant (plus isogenic control) and engineered mutant (homozygous)	Dravet syndrome	(Xie *et al.*, 2020)	Reduced sodium current and AP firing in inhibitory neurons; reduced sodium current in excitatory neurons
SCN1A	c.3982T>C; p.S1328P	patient mutant (plus isogenic control)	Dravet syndrome	(Frasier *et al.*, 2018)	Increased sodium current and rates of spontaneous contraction in cardiomyocytes
SCN1A	c.3982T>C; p.S1328P	patient mutant	Dravet syndrome	(Sun *et al.*, 2016b)	Reduced sodium currents and AP firing in medial ganglionic eminence-like inhibitory neurons; no phenotype detected in telecephalic excitatory neurons
SCN1A	p.V1352CfsTer5 *	patient mutant	Dravet syndrome with developmental delay	European Bank for iPSCs (EBiSC)	No phenotype reported
SCN1A	c.4243T>A; p.F1415I	patient mutant	Dravet syndrome	(Jiao *et al.*, 2013)	Increased persistent sodium current; increased spontaneous and evoked activity in glutamatergic excitatory neurons
SCN1A	c.4261G>T; p.G1421W	patient mutant	Dravet syndrome	(Kim *et al.*, 2018)	Reduced sodium current density and reduced AP firing in GABAergic neurons
SCN1A	c.4522TdelT; p.Y1508fsTer4	patient mutant	Dravet syndrome	European Bank for iPSCs (EBiSC)	No phenotype reported
SCN1A	c.4573C>T; p.R1525Ter	patient mutant	Dravet syndrome	(Tanaka *et al.*, 2018a)	No phenotype reported
SCN1A	c.4933C>T; p.R1645Ter	patient mutant (plus isogenic control)	Dravet syndrome	(Higurashi *et al.*, 2013; Tanaka *et al.*, 2018b)	Reduced AP firing in GABAergic neurons
SCN1A	c.5162C>A; p.T1721K	patient mutant	Dravet syndrome	European Bank for iPSCs (EBiSC)	No phenotype reported
SCN1A	c.5222G>C; p.C1741S	patient mutant	Dravet syndrome	European Bank for iPSCs (EBiSC)	No phenotype reported
SCN1A	c.5502_5509dupGCTTGAAC; p.P1837RfsTer24	patient mutant	Dravet syndrome with developmental delay and ataxia	(Schuster *et al.*, 2019a; Schuster *et al.*, 2019b)	Reduced sodium current, impaired response to oxidative stress and dysregulated transcriptomic pathways for chromatin remodeling and neurodevelopment in GABAergic neurons
SCN1A	c.5768A>G; p.Q1923R	patient mutant (plus isogenic control) and engineered mutant	Partial epilepsy with febrile seizures (PEFS+)	(Liu *et al.*, 2016; Zhao *et al.*, 2020a; Zhao *et al.*, 2020b; Zhao *et al.*, 2020c)	Reduced sodium current and reduced AP firing in GABAergic neurons, altered postsynaptic currents
SCN1A	c.5768A>G; p.Q1923R	patient mutant	Mild febrile seizures	(Jiao *et al.*, 2013)	Increased persistent sodium current; increased spontaneous and evoked activity in glutamatergic excitatory neurons
SCN1A	c.5768A>G; p.Q1923R	engineered mutant	Dravet syndrome associated mutation	(Chen *et al.*, 2014)	No phenotype reported
SCN1A	Gene knockout	engineered mutant	*SCN1A* knockout	(Shan *et al.*, 2021)	No phenotype reported

SCN1A	c.IVS14+3A>T	patient mutant	Dravet syndrome	(Liu *et al.*, 2013b)	Increased sodium currents; spontaneous bursting; general hyperexcitability in forebrain-like pyramidal- and bipolar-shaped neurons
SCN1B	Gene knockout	engineered mutant	*SCN1B* knockout	hPSC Registry: Beijing Tiantan Hospital (BJTTH)	No phenotype reported
SCN1B	Gene knockout	engineered mutant (heterozygous and homozygous)	*SCN1B* knockout	(Tidball *et al.*, 2017)	No phenotype reported
SCN2A	c.386+2T>C; IVS3+2T>C	patient mutant	ASD, Epilepsy	Simon's Foundation	No phenotype reported
SCN2A	c.584A>G; p.D195G	patient mutant	ASD, Epilepsy	Simon's Foundation	No phenotype reported
SCN2A	c.605+1G>T; IVS5+1G>T	patient mutant	ASD, Epilepsy	Simon's Foundation	No phenotype reported
SCN2A	c.788C>T; p.A263V	patient mutant	ASD, Epilepsy	Simon's Foundation	No phenotype reported
SCN2A	c.1283A>T; p.Y428F	patient mutant	ASD, Epilepsy	Simon's Foundation	No phenotype reported
SCN2A	c.2566C>T; p.R856Ter	patient mutant	ASD, Epilepsy	(Sampaio *et al.*, 2019)	No phenotype reported
SCN2A	c.2877C>A; p.C959Ter	patient mutant	ASD, Epilepsy	Simon's Foundation	No phenotype reported
SCN2A	c.3464_3468delAACAG ; p.E1155A fsTer2	patient mutant	ASD, Epilepsy	Simon's Foundation	No phenotype reported
SCN2A	c.4025T>C; p.L1342P	engineered mutant (heterozygous)	SCN2A-related epilepsy associated mutation	(Que *et al.*, 2021)	Increased sodium currents, faster AP repolarization, increased spike and bursting frequency
SCN2A	c.4264A>G; p.K1422E	patient mutant	Epileptic encephalopathy	European Bank for iPSCs (EBiSC)	No phenotype reported
SCN2A	c.4308+1G>A; IVS23+1G>A	patient mutant	ASD, Epilepsy	Simon's Foundation	No phenotype reported
SCN2A	c.4801G>T; p.V1601L	patient mutant	ASD, Epilepsy	Simon's Foundation	No phenotype reported
SCN2A	c.4832T>C; p.L1611P	patient mutant	ASD, Epilepsy	Simon's Foundation	No phenotype reported
SCN2A	c.4904G>A; p.R1635Q	patient mutant	ASD, Epilepsy	Simon's Foundation	No phenotype reported
SCN2A	c.4996C>T; p.L1666F	patient mutant	ASD, Epilepsy	Simon's Foundation	No phenotype reported
SCN2A	Gene knockout	engineered mutant	*SCN2A* knockout	(Lu *et al.*, 2019)	Reduced network activity in mixed excitatory/inhibitory cultures
SCN2A	Gene knockout	engineered mutant (homozygous)	*SCN2A* knockout	(Deneault *et al.*, 2018)	Reduced spontaneous excitatory postsynaptic current frequencies; reduced AP firing in cortical excitatory neurons
SCN8A	c.4774G>C; p.V1592L	patient mutant	*SCN8A*-related epileptic encephalopathy	(Tidball *et al.*, 2020)	Elevated persistent sodium current; shorter axon initial segment in cortical excitatory neurons
SCN8A	c.5269G>A; p.V1757I	patient mutant	*SCN8A*-related epileptic encephalopathy	(Tidball *et al.*, 2020)	No phenotype reported
SCN8A	c.5276A>G; p.N1759S	patient mutant	*SCN8A*-related epileptic encephalopathy	(Tidball *et al.*, 2020)	Increased resurgent sodium current; shorter axon initial segment; prolonged AP repolarization; increased bursting in cortical excitatory neurons
SCN8A	c.5615G>T; p.R1872L	patient mutant	*SCN8A*-related epileptic encephalopathy	(Tidball *et al.*, 2020)	Elevated persistent sodium current; shorter axon initial segment; prolonged AP repolarization; increased bursting in cortical excitatory neurons
SCN8A	Gene knockout	engineered mutant (heterozygous and homozygous)	*SCN8A* knockout	(Tidball *et al.*, 2017)	No phenotype reported

1.12 Applications of gene-editing and iPSCs

The discovery of gene editing has introduced the ability to alter the genome of cells, thus enabling the correction of genetic mutations in patients with monogenic diseases such as

KCNQ2 (Chuang et al., 2017). In drug screening experiments, gene editing that specifically targets the mutated gene locus can correct the mutation, generating isogenic controls from patient cells, thus reducing genetic variation and other variables that may influence phenotypic differences (Brookhouser et al., 2017). The development of the CRISPR (clustered regularly interspaced short palindromic repeats) -Cas9 system for genome-editing in 2012, has made gene-editing more efficient, accessible, and cost-effective than previous gene-editing techniques (Jinek et al., 2012). Gene-editing techniques, particularly CRISPR/CAS9 have been used extensively in disease modelling experiments for monogenic disorders and will be discussed further in **Chapter 3**.

1.13 Conclusion

Advances in NGS and other technologies, has enabled an increased understanding of the disease aetiology particularly in the early-onset epilepsies. Obtaining a genetic diagnosis is advantageous and diagnostic strategies are constantly evolving. Improved epilepsy experimental models, drug discovery/design, data sharing and collaboration, are changing the way we practice more individualised, precision therapies for patients. With further advances in gene editing tools, and improved drug delivery systems, there is great potential for translation of new gene therapies. Combining collaborative genotype-phenotype data, micro-RNA approaches, the many -omics approaches, and new experimental models including iPSCs-derived models, it is likely that more relevant precision medicines will be the future in epilepsy research. However, given the underlying mechanisms of many of the newly discovered genetic disorders including *KCNQ2*-related DEE, and the large number of different types of mutations, combined with the current lack of understanding and therapies, poses a massive challenge, and no specific gene-modifying and disease modifying therapies have to date been used in routine clinical practice.

1.14 Aim of the study

The aim of this study is to model the phenotype of 3 pathogenic *KCNQ2* variants from human patients suffering from severe early onset developmental and epileptic encephalopathy. This study examines the mutations of these patients (F261L, A265T, and A294V) in an iPSC-derived 2D cortical neuronal model for the first time, to provide a platform for drug screening and investigation of other therapeutic approaches. To achieve this aim, the recruited *KCNQ2*-DEE patients will have their skin cells reprogrammed into patient-specific iPSC lines and then differentiated into patient-specific neuronal models by differentiating iPSCs into 2D cortical

neurons. To assess the phenotype, we will evaluate the electrophysiological and biochemical properties of the disease neurons. Finally, I aim to provide preliminary data/proof-of-principle to try to modify or 'rescue' the phenotype using several basic antiseizure medications and examine feasibility to deliver miRNA molecules to generated mature cortical neurons.

Chapter 2 of this thesis will now discuss the generation of patient-specific iPSCs from *KCNQ2*-DEE patients and sibling controls. **Chapter 3** will outline the gene-editing techniques employed. **Chapter 4** will describe the differentiation of excitatory cortical neurons from iPSCs. **Chapters 5** and **6** will outline the phenotypic analysis of *KCNQ2*-DEE neurons using MEA analysis and calcium imagining respectively.

Chapter 2: Reprogramming of patient-specific fibroblasts into induced pluripotent stem cells.

2.1 Introduction

2.1.1 Limitations of Use of Embryonic Stem Cells

Embryonic Stem Cells (ESCs) are self-replicating cells which are capable of differentiating into cells from each of the three germ layers (Martin, 1981). These cells are derived from the inner cell mass of mammalian blastocysts, meaning human embryos are the main source of obtaining human ES cells (Rippon et al., 2004). This pluripotency capability of ES cells makes them an extremely attractive therapy for a host of diseases. In particular, neurological diseases where cell sourcing is a huge limitation. However, due to the ethical issues regarding the use of human embryos, coupled with host tissue rejection after transplantation in patients (Swijnenburg et al., 2008), ES cell use has its limitations. In several countries the use of ES cells in scientific research is illegal. In Ireland, there is currently no regulation for the use of ES cells. One way to overcome these ethical issues is to generate a patient's own pluripotent stem cells (PSCs) from somatic cells in their body. Perhaps the most important advantage of induced PSCs (iPSCs) over ES cells is the possibility to use somatic cells from patients who suffer from genetic disorders, and thus patient-specific disease models (Eggenschwiler et al., 2013; Maetzel et al., 2014).

2.1.2 Induced Pluripotent Stem Cells

In 2006, Yamanaka and colleagues showed that they were capable of generating PSCs from mouse somatic cells by expressing four transcription factors known to play a role in maintaining pluripotency in ES cells (Takahashi et al., 2006). They combined the transcription factors oct3/4, sox2, c-Myc and Klf-4 with mouse embryonic fibroblasts to generate what are now commonly known as induced pluripotent stem cells (iPSCs). In the study they investigated 24 candidate genes using an assay which measured the induction of pluripotency based on the level of resistance to G418, as the mouse fibroblasts carried a βgeo fusion transgene which was knocked into the *Fbx15*, a stem cell expressing gene. They narrowed down the selection of genes to four transcription factors of oct3/4, sox2, c-Myc and Klf-4, based on which genes were critical for generating pluripotent cells based on the following criteria: colony number, cell morphology, the expression of ES cell marker genes and their ability to form teratomas. One year later in 2007, the same group of researchers showed they could generate iPSCs from adult human somatic cells via retroviral transduction

of the same four transcription factors of OCT3/4, SOX2, c-Myc and Klf-4 (Takahashi et al., 2007). This discovery opened the door for the field of human iPSC research.

2.1.3 Sources of Induced Pluripotent Stem Cells

Selecting a cell source for generating iPSCs is an important consideration when planning a study. The most commonly used sources are fibroblasts, keratinocytes, and blood cells (Raab et al., 2014). One of the main concerns around selecting the correct source cell is due to the concept of 'Epigenetic Memory'. Several studies have shown that cells are capable of retaining their initial epigenomes and transcriptomes. This means that any genetic abnormalities, altered gene copy number or unique DNA methylation signatures present in the origin cell will be passed onto the iPSCs (Hussein et al., 2011). It has also been shown that certain cell sources favour the differentiation towards one specific lineage of origin over another, for example, blood cell-derived iPSCs prefer to differentiate into a hematopoietic lineage, while fibroblast-derived iPSCs can be more effectively differentiated into cells of an osteogenic lineage than blood cell-derived iPSCs (Kim et al., 2010). However, this concept has been disputed in the literature with many researchers showing that if iPSCs are cultured for long enough, they lose this epigenetic memory, however, somatic mutations may arise from extensive culture, and iPSCs with <50 passages are recommended for research.

Keratinocytes offer many advantages as a cell source for generating iPSCs. They can be cultured from hair follicles from both vellus and terminal hair which can be taken from the scalp, facial hair, eyebrows, and the nose. The non-invasive process of removing hair makes keratinocytes a very attractive cell source compared to other more invasive sources like blood withdrawal or a skin biopsy. However, this procedure is not completely without limitations as there is a certain level of expertise needed to remove the hair correctly. The hair must be removed with the root still attached and the outer root sheath fully intact in order to obtain a sufficient number of cells, and children may resist to repeat hair sampling. Another advantage of keratinocytes is the faster reprogramming protocol (Raab et al., 2014). It only takes 1-2 weeks to generate iPSCs compared to the 3-4 week protocol necessary for skin fibroblasts. In recent years there has been a steady increase in the number of studies using keratinocytes over fibroblasts (Re et al., 2018).

Since their initial use in 2007, adult fibroblasts are still the most commonly used cells for reprogramming. A key reason for their popularity is that they are affordable and easy to culture, having been used extensively in many research fields. However, one major drawback is the invasive procedure required to obtain dermal fibroblasts from the donor. This is done

by taking a small skin (punch) biopsy usually around 3.5-mm to 4-mm from the donor (Raab et al., 2014). This may be painful for the patient and usually requires clinically trained professional to perform the biopsy. Once cultivated, fibroblasts are extremely easy to grow as they require low serum/medium and proliferate quickly resulting in efficient reprogramming (Streckfuss-Bömeke et al., 2013). One drawback compared to other cell sources is that it can take approximately 3 to 5 weeks for stem cell colonies to appear after reprogramming and reprogramming efficiency is reported to be as low as 0.01% to 0.5% using the four original retroviral vectors (Takahashi et al., 2007).

In this study we used fibroblasts as our cell source and achieved sufficient reprogramming efficiency using Sendai viral vectors, with stem cell colonies appearing 3 weeks after reprogramming was initiated. Therefore, there seems to be quite a high level of variability between studies which could depend on the donor, the medium/serum used, reprograming method, operator technique, and other factors (Volpato & Webber, 2020; Beekhuis-Hoekstra et al., 2021).

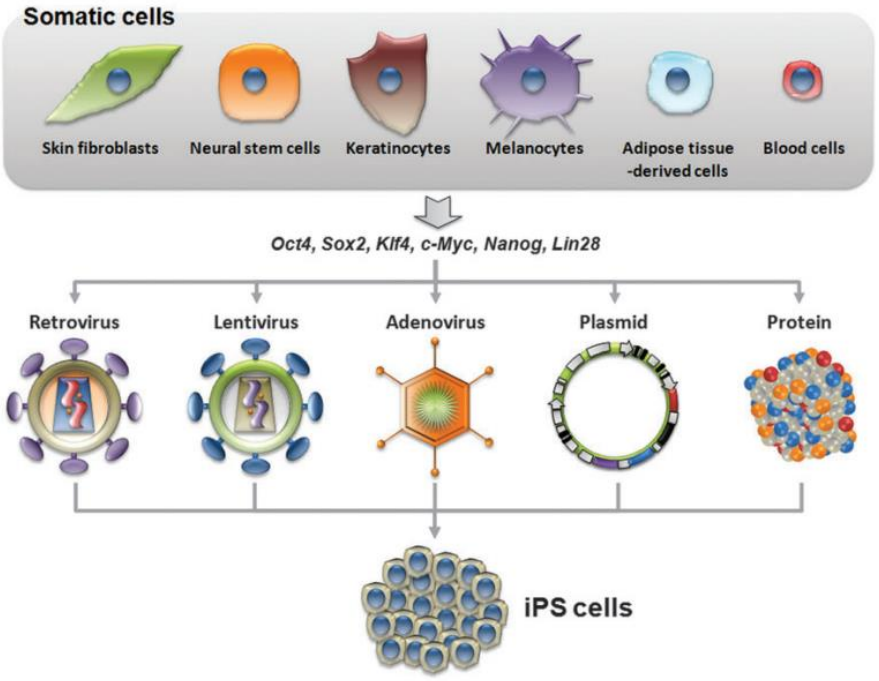

Figure 2.1. A summary of somatic cell sources, reprogramming factors and delivery methods used to generate induced Pluripotent Stem Cells.

These cell types are reprogrammed into iPSCs by delivering reprogramming factors such as Oct4, Sox2, Klf4, c-Myc, Nanog and Lin28 using different vectors such as Retrovirus, Lentivirus, Adenovirus, Sendai virus, plasmids, and purified proteins (Han et al., 2011).

2.1.4 Reprogramming methods

The earliest methods of reprogramming involved the use of retroviruses and lentiviruses, both of which were capable of achieving good reprogramming efficiency (Park et al., 2008; Takahashi et al., 2007). However, both of these methods resulted in random integration of the transgenes into the host genome which could lead to an increase in tumour formation and mortality in mouse studies (Wu et al., 2014), raising concerns about safety and clinical translation. To combat these safety concerns, a research group tried to reprogramme mouse fibroblasts with a non-integrating adenovirus for the first time in 2008 (Stadtfeld et al., 2008). This resulted in an extremely low efficiency rate and the researchers speculated that this was a result of the short expression window of the reprogramming factors, which may have been insufficient to induce somatic cells into a pluripotent state (Stadtfeld et al., 2008). This has led to the use of a Sendai Virus, an RNA virus that does not integrate into the host genome but is still capable of producing protein at high levels and for a long duration. This means that iPSCs generated using a Sendai Virus can be easily translated into the clinic as there's no presence of any transgenes after several passages (Fusaki et al., 2009). For this reason, we chose to reprogramme our dermal fibroblasts with a commercially available Sendai Virus kit.

In 2015, a study compared the reprogramming efficiency of several non-integrating methods. Using dermal fibroblasts, they compared the reprogramming efficiency of a Sendai Virus, Nucleofector, the Neon transfection system and Lipofectamine 3000 in 3 patient lines. They found that the Sendai Virus was the most efficient method resulting in an average of 0.019% efficiency among the 3 lines. Nucleofector was the second most effective method resulting in 0.012% efficiency followed by the Neon transfection system with less than 0.001% efficiency. Finally, Lipofectamine 3000 was only capable of reprogramming 1 out of the 3 patient lines with an efficiency of 0.001%. Despite the difference in efficiency between the reprogramming methods, it is worth noting that the researchers found no significant difference in iPSC morphology, gene expression of the pluripotency markers, karyotyping and embryoid body (EB) formation (Manzini et al., 2015).

2.1.5 Characterisation of iPSCs

The methods of characterising iPSCs varies greatly between labs, making the availability of reliable, quality controlled, well-characterised iPSCs difficult (Stacey et al., 2013). In an effort to standardise protocols and characterisation methods, the European Bank for induced Pluripotent Stem Cells (EBiSC) was generated in 2014. The EBiSC is a central repository whereby they receive iPSCs generated in various laboratories, fully characterise them using

standardised quality control and quality assurance measures and then re-distribute them internationally (O'Shea et al., 2020). This is currently only done for research use, however standardising iPSC production and characterisation methods in research will help generate more reliable, reproducible results which in turn will facilitate the translation of iPSC studies into the clinic.

Firstly, they looked at Mycoplasma screening as the need for Mycoplasma-free iPSC culture is essential. For this they used a highly sensitive qPCR method to detect Mycoplasma contamination and found that 5 out of 467 lines were positive for Mycoplasma. This number was present despite the pre-requirement for iPSCs to be sent to the repository already confirmed to be Mycoplasma free. In the initial 'hot start' phase of the study, they found that 8 out of 47 lines had the incorrect cell line identity (De Sousa et al., 2017). This was linked to the accidental mixing of cell lines, incorrect labelling, and poor data traceability. Following these results, the centre provided workshops and training to combat this issue and found this resulted in a significant reduction in incorrect cell line identification for the remainder of the study.

To analyse differentiation potential, the researchers developed an EB assay, whereby the iPSCs underwent spontaneous EB differentiation and then expression levels of markers from each of the 3 germ layers were measured. However, they found that multiple iPSC lines failed this assay on repeated attempts, so opted to use a commercially available kit (StemDiff Trilineage Differentiation Kit, Stem Cell Technologies, cat #05230) for the remainder of the study. All lines successfully passed QC controls including lines which had failed in the previous tests (O'Shea et al., 2020). This was a fundamental finding from the study, as spontaneous EB differentiation assays still remain common practice for measuring differentiation potential in research.

Another important aspect in standardising iPSC characterisation is assessment of the cell lines for genomic stability. It has been shown that iPSCs are particularly susceptible to changes in the genome overtime with chromosomes 12, 17, 20 and X known as 'hotspots' for such duplications or deletions (Weissbein et al., 2014). G-banding has been considered the gold standard for karyotyping, however it has many drawbacks for research laboratories, such as the need for outsourcing to specialist labs, high cost and slow turnaround time due to the skilled requirements of the procedure, as well as limited best resolution of 3^{10} Mb, therefore only gross chromosomal abnormality can be detected by G banding with close examination.

Single Nucleotide Polymorphism (SNP) arrays offer a more affordable and accessible alternative while also yielding higher resolution data, when a large number of iPSC lines are in need of characterisation. Another method of karyotyping which is used is the KaryoLite BoBs Kit (PerkinElmer cat# 4501-0010) which can detect gains or losses in all chromosomes in a single assay. When comparing methods, they found there is significant differences in sensitivity, resolution, turnaround time, sample requirements and cost between each method. They tested 13 iPSC lines against all methods and only 4 lines yielded consistent results in all methods. They found the SNP array to be the most effective at detecting abnormalities, while the KaryoLite was the least sensitive. However, they noted that G-banding was more effective at determining genomic stability through the detection of inversions and translocations. The SNP array has its own limitations: it is oversensitive and normal population often have copy number variations (CNVs) from the raw data. It is therefore essential to filter out small CNVs which are commonly present in most samples of the assay, to avoid false alarm. The second issue with the SNP array is that it can't detect balanced translocations or inversions, as rearrangements do not alter DNA abundance in the genome or signal intensity on chips. While combining both G-banding and SNP array would lead to optimal results, the detection method should be chosen based on the main goal of detection, often due to resource limitations.

If each of the critical release criteria of viability, mycoplasma, STR analysis, gene expression, are not strictly adhered to, studies using iPSCs can become unreliable, and may lead to reproducibility issues. These findings highlight extreme importance when planning a study to carefully consider the characterisation methods.

The **aim** of the research in this **Chapter** is to generate and characterise iPSCs from patients with *KCNQ2*-Developmental and Epileptic Encephalopathy (DEE) and healthy sibling controls. In this study we measured pluripotent gene expression using quantitative RT-PCR and immunocytochemistry. Differentiation potential was examined by spontaneous differentiation of EBs. Cell line identity was analysed using STR, while karyotyping was performed using SNP array. Finally, we used a Mycoplasma PCR kit for the detection and exclusion of any Mycoplasma in our cultures.

2.2 Materials and Methods

2.2.1. Fibroblast culture

Skin biopsies were collected from Irish patients with a *KCNQ2*-encephalopathy (due to pathogenic variants) and healthy sibling controls. Sample procedures were performed as per clinical practice in the Clinical Research Facility Galway. This study was ethically approved by the University of Galway Research Ethics Committee (C.A. 750). Skin biopsies were washed in Dulbecco's Phosphate Buffered Saline (PBS)(Thermo Fisher Scientific, 14190250) containing 5% Penicillin/Streptomycin (Thermo Fisher Scientific 10,000 U/ml, 15140122). Each 3-mm skin biopsies were cut into smaller pieces using a scalpel and placed into several wells of a 6-well plate. The biopsies were then firmly scored into the plastic dish using the scalpel and left to dry for 2 min to enhance the attachment.

Biopsy-derived tissues (skin fibroblasts) were cultured in media containing DMEM High Glucose GlutaMAX™ (Thermo Fisher Scientific, 31966-021), 10% Fetal Bovine Serum (FBS)(Sigma-Aldrich, 12106C), 1% Penicillin/Streptomycin and 1% non-essential amino-acids (Invitrogen, 15140-122) at 37 ˚C at 5% CO_2. Media was changed every 2-3 days and fibroblasts were passaged with Trypsin-EDTA (0.25%) (Thermo Fisher Scientific, 25200056) every 5-6 days. Fibroblasts were frozen in 90% FBS and 10% Dimethyl sulfoxide (DMSO) (Sigma-Aldrich, D1435).

Table 2.1 Source Information of patient and control fibroblasts

Patient ID	Age	Affected	Gene, Inheritance	Gender	cDNA change	Protein change, location in KCNQ2 subunit	Clinical Phenotype
EP2001	5	Proband only	*KCNQ2*, de novo	Male	c.881C>T	p.Ala294Val (A294V) in S6	*KCNQ2*-DEE
EP2C001	15	Brother	Control	Male	N/A	N/A	N/A
EP2002	4	Proband only	*KCNQ2*, de novo	Female	c.783A>C	p.Phe261Leu (F261L) in pore-forming region between S5 and S6	*KCNQ2*-DEE
EP2C002	4	Brother	Control	Male	N/A	N/A	N/A
EP2003	5	Proband only	*KCNQ2*, de novo	Female	c.638C>T	p.Arg213Gln (R213Q) in S4	*KCNQ2*-DEE
EP2C003	21	Brother	Control	Male	N/A	N/A	N/A
EP2004	7	Proband only	*KCNQ2*, de novo	Female	c.793G>A	p.Ala265Thr (A265T) in pore-forming region between S5 and S6	*KCNQ2*-DEE
EP2C004	12	Sister	Control	Female	N/A	N/A	N/A

Abbreviations: EP represents "epilepsy project" and C for control sample cell lines; DEE, developmental and epileptic encephalopathy; N/A, not applicable

2.2.2 Derivation of iPSCs using a Sendai Virus Reprogramming kit

The iPSCs were generated using the CytoTune™-iPS 2.0 Sendai Reprogramming kit (Thermo Fisher Scientific, A16517). **Figure 2.2** shows a summary of the reprogramming protocol.

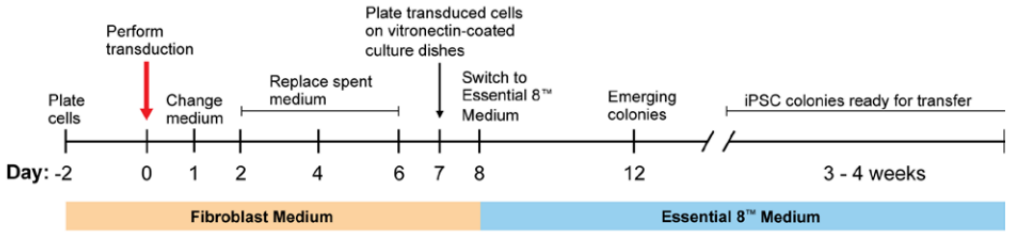

Figure 2.2. A brief schematic illustrating the Sendai virus reprogramming protocol used to generate iPSCs from fibroblasts.

Details expanded in below text.

2.2.2.1 Reprogramming protocol

Step 1: Day -2 (Plating fibroblasts)

Fibroblasts were plated into 2 wells on a 6-well plate containing fibroblast medium, so that cells are approximately 60-70% confluent at day 0.

Step 2: Day 0 (Perform Transduction)

Fibroblasts were transduced using the CytoTune™ reprogramming vectors at their appropriate multiplicity of infection (MOI). One well of fibroblasts were detached using 0.05% Trypsin-EDTA and incubated at room temperature. The cells were counted on a haemocytometer using Trypan blue (Thermo Fisher Scientific, 15250061) to determine live/dead ratio. The volume of each virus to be added was calculated using the following calculation:

$$\text{Volume of virus (µL)} = \frac{\text{MOI (CIU/cell)} \times \text{number of cells}}{\text{titer of virus (CIU/mL)} \times 10^{-3}\ \text{(mL/µL)}}$$

The recommended MOI for KOS, hc-Myc and hKlf4 –containing virus was 5, 5 and 3, respectively. The appropriate volume of each virus was added to 1ml of warm fibroblast medium in the second well on the 6-well plate. The cells were incubated overnight at 37 ˚C at 5% CO_2.

Step 3: Day 1 (Replace medium and culture cells)

24 hours after transduction, the medium was replaced with fresh fibroblast medium. The cells were cultured for 6 more days, and the medium was changed every other day.

Step 4: Day 7 (Plate transduced cells on Geltrex™-coated dishes)

Tissue culture dishes were coated using Geltrex™ LDEV-Free, hESC-Qualified, Reduced Growth Factor Basement Membrane Matrix (Thermo Fisher Scientific, A1413302) by adding 1ml of 1% Geltrex ™ into each well of a 6 well plate and incubating at 37 ˚C for at least 1 hour. The transduced cells were dissociated using 0.05% Trypsin-EDTA. Cells were passaged into the Geltrex™ coated plates at varying quantities ($2.5X10^4$, $5x10^4$, $7.5x10^4$, $1x10^5$) and incubated overnight.

Step 5: Day 8 to 28 (Feed and monitor the cells)

Fibroblast medium was replaced with Essential 8™ Medium (Thermo Fisher Scientific, A1517001) and E8 medium was refreshed every other day. Between three and four weeks after transduction, colonies emerged from the culture and were large enough to select for transfer. Individual round and compact colonies were passaged by scraping them from the culture dish using a 200µl pipette and transferred into a new Geltrex™-coated well of a 6 well plate. Colonies were cultured in Essential 8™ Medium for up to 8 days and were then expanded and cryopreserved as required. iPSCs were frozen in 90% KnockOut™ Serum Replacement (KOSR) (Thermo Fisher Scientific, 10828028) and 10% DMSO.

2.2.3 iPSC culture

2.2.3.1 Geltrex™ Coating protocol

A 5-mL bottle of Geltrex™ LDEV-Free hESC-Qualified Reduced Growth Factor Basement Membrane Matrix (Thermo Fisher Scientific, A1413302) was thawed overnight at 2–8°C. The thawed Geltrex™ solution was then diluted in a 1:1 ratio with cold Knockout™ DMEM/F-12 (Thermo Fisher Scientific, 12660012). The solution was then aliquoted into 1ml vials on ice and was stored in the –20°C freezer. To generate a working solution used for coating, 1ml aliquots were thawed and diluted in 50ml of Knockout™ DMEM/F-12, making a total 1:100 dilution. 1ml of 1% Geltrex™ solution was added to each well of a 6 well plate and incubated at 37 ˚C for at least 1 hour.

2.2.3.2 Passaging iPSCs

iPSCs are passaged every 3-5 days, or once the cells reach approximately 80% confluency. Before passaging, any differentiated cells are removed by scraping with a 1ml pipette. iPSC colonies are then passaged using Gentle Cell Dissociation Reagent (GCDR) (Stem Cell Technologies, 100-0485). 1ml of GCDR was added to each well of a 6 well plate and cells were incubated at room temperature under an inverted microscope. Colonies were monitored and once holes began to form, GCDR was removed from the cells and replaced with Essential 8™ Medium. The plate was then tapped harshly to detach cells from the surface of the plate, and cells were then transferred into a new Geltrex™-coated plate.

2.2.4 Immunocytochemistry

Cells for staining were seeded in 8 well glass chamber slides (Ibidi, 80807). Cells were washed using PBS and fixed with 4% Paraformaldehyde (Santa Cruz, 30525- 89-4) for 15 to 20 minutes at room temperature. Cells were washed 3 times with PBS. Then, cells were permeabilized with 0.3% Triton X-100 (Sigma) in PBS for 15 min. Cells were washed 3 times with PBS. Next, the cells were blocked with 1% Bovine Serum Albumin (BSA)(Sigma, A3608) and 0.1% Triton X-100 in PBS for 1 hour. Primary antibodies outlined in **Table 2.2** were diluted in blocking buffer and added to the cells. Cells were incubated overnight at 4˚C. The next day, cells were washed 3 times with PBS. Secondary antibodies and Hoechst nuclear dye were diluted in blocking buffer and added in the appropriate dilutions as outlined in **Table 2.3**. Cells were incubated for 45 minutes at room temperature. Cells were washed 3 times with PBS. Chambers were stored in the dark at 4˚C for microscopic analysis.

Table 2.2. List of primary antibodies used

Name	Manufacturer	Species	Dilution	Cat no.
Oct4	Cell Signalling Technology	Rabbit	1:500	2840
Sox2	Cell Signalling Technology	Rabbit	1:500	3579
Nanog	Cell Signalling Technology	Rabbit	1:500	4903
SSEA4	Cell Signalling Technology	Mouse	1:500	4755
Tra1-81	Cell Signalling Technology	Mouse	1:500	4745
Tra1-60	Cell Signalling Technology	Mouse	1:500	4746
Tuj1	Abcam	Mouse	1:500	ab78078
SMA	Cell Marque Corp	Mouse	1:500	202 M-96
AFP	Sigma Aldrich	Mouse	1:200	A8452

Table 2.3. List of secondary antibodies used

Name	Manufacturer	Species	Dilution	Cat no.
AF488 Anti-Rabbit IgG	Cell Signalling Technology	Goat	1:1000	4412
AF555 Anti-Mouse IgG	Cell Signalling Technology	Goat	1:1000	4409
Hoechst Nuclear stain	Cell Signalling Technology	N/A	1:2000	4082

2.2.5. Quantitative Reverse Transcription Polymerase Chain Reaction (RT-qPCR)

RNA was extracted from cells using the RNeasy Mini Kit (Qiagen, 74104) following the manufacturer's instructions. RNA purity and concentration was measured using the NanoDrop 2000 UV. 1µg of RNA was transcribed into complementary DNA (cDNA) using the SensiFAST™ cDNA synthesis kit (Bioline, BIO-65054) according to manufacturer's instructions. Samples were run using the StepOne Plus Real Time PCR System with Fast SYBR™ Green Master Mix (Applied Biosystems, 43-091-55). Primers used are listed in **Table 2.4.** The resulting cycle threshold (ct) values were normalised to GAPDH expression. The relative quantities of mRNA expression were calculated as being 2^{-ddct} using the average dCt value of a fibroblast line.

Table 2.4. List of RT-qPCR and PCR primers used

Target	Forward (5'-3')	Reverse (5'-3')
SeV	GGATCACTAGGTGATATCGAGC	ACCAGACAAGAGTTTAAGAGATATGTATC
KOS	ATGCACCGCTACGACGTGAGCGC	ACCTTGACAATCCTGATGTGG
KLF4	TTCCTGCATGCCAGAGGAGCCC	AATGTATCGAAGGTGCTCAA
GAPDH	AGGGCTGCTTTTAACTCTGGT	CCCCACTTGATTTTGGAGGGA
OCT4	AACTTCACTGCACTGTACTCCTC	CACCCTTTGTGTTCCCAATTCC
SOX2	AGACTTCACATGTCCCAGCACT	CGGGTTTTCTCCATGCTGTTTC
NANOG	ATAACCTTGGCTGCCGTCTC	AGCCTCCCAATCCCAAACAA
KCNQ2 variant c.881C>T	GCTCACTCGCTGATACTTCC	GTCATCAGGACACGTAGCTA
KCNQ2 variant c.783A>C	GGTCACTGCCTGGTACATCG	ATAATCGGGACACGGAGCAG
KCNQ2 variant c.638C>T	GACATCATGGTGCTCATCGC	GAGGCTCGTTCACACCTGAT

KCNQ2 variant c.793G>A	GGTCACTGCCTGGTACATCG	ATAATCGGGACACGGAGCAG

2.2.6. In vitro differentiation into each of three germ layers

iPSCs were plated onto a low-adherence 6 well plate which was rinsed with anti-adherence solution (Stem Cell, cat # 07010) and were incubated at 37°C/5% CO_2. The resulting embryoid bodies (EBs) were cultured for 5 to 7 days in DMEM high glucose (Gibco, cat#11965092) supplemented with 20% Knockout-out Serum Replacement (Gibco, cat# 10828028), 1% L-Glutamine (Gibco, cat # 25030081), 1% MEM-NEAA Solution (Gibco, cat# 11140050), 1% Antibiotic-Antimycotic (Gibco, cat# 15240062) and 0.2% β-Mercaptoethanol (Gibco, cat# M6250). EBs were transferred to Geltrex™-coated 8-well glass chambers (Ibidi) to allow spontaneous differentiation. Media was changed every other day for 3 to 4 weeks. EBs were stained with antibodies against AFP (endoderm), α-SMA (mesoderm) and TUJ1 (ectoderm) to identify tissues from each germ layer.

2.2.7. Single Nucleotide Polymorphism (SNP) analysis

Genomic DNA was extracted from iPSCs using the DNeasy Blood and Tissue kit (Qiagen, cat #69506). DNA was then loaded on a 1.5% agarose gel for DNA purity and measured on NanoDrop to determine quantity. The 990 k SNP array for karyotyping was performed at Beijing Hyslar Biotech (Beijing, China). Data was analysed with Axiom Analysis Suite (Thermo Fisher, USA), and log2 ratio was generated to detect copy number variations (CNVs).

2.2.8. Mycoplasma PCR

iPSCs were kept in culture until at least 80% confluency was reached. 1 ml of supernatant was transferred to a microcentrifuge tube. The supernatant was centrifuged at 500 x g for 5 min to remove cellular debris. The supernatant was transferred to a new tube which was centrifuged again at 14,000 x g for 15 min. The supernatant was discarded, and the pellet was resuspended in 100ul of DNA free water. Once samples were prepared, the PCR was performed using Promokine's PCR mycoplasma test kit (Promocell, PK-CA91-1024) according to manufacturer's instructions. Once the PCR was complete, samples underwent agarose gel electrophoresis, and the gel was imaged.

2.2.9. Fingerprinting

Genomic DNA was extracted using DNeasy Blood and Tissue Kit (Qiagen) and analysed using Cell Line authentication service by Eurofins Genomics (Germany). This cell line authentication service tests 16 different Short Tandem Repeat (STR) markers on different chromosome (TPOX, D2S1338, D3S1358, FGA, D5S818, CSF1PO, D7S820, D8S1179, TH01, vWA, D13S317, D16S539, D18S51, D19S433, D21S11, AMEL).

2.3 Results

2.3.1 Generation of fibroblasts from *KCNQ2*-DEE patients and healthy sibling controls

Four patients with *KCNQ2*-DEE and four healthy control donors were recruited for the study. The pathogenic *KCNQ2* variants of each patient can be found in **Table 2.1**. Skin biopsies from each donor were plated into 6 well culture dishes and fibroblasts were allowed to expand from the biopsy over the following 1-2 weeks. As early as 6 days after plating, fibroblasts can be seen emerging from the biopsy **(Figure 2.3)**. Approximately 2 weeks after plating, fibroblasts were passaged using 0.25%Trypsin and expanded in T-25 flasks up until passage 8 **(Figure 2.3)**. Fibroblasts were cryopreserved in 90% FBS and 10% DMSO.

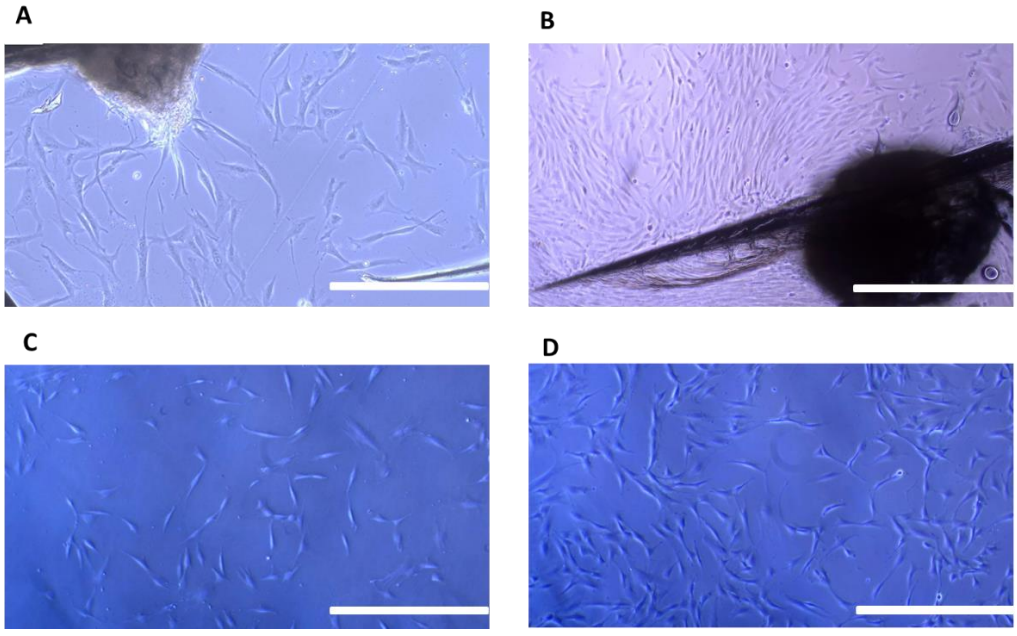

Figure 2.3. Images of fibroblasts emerging from skin biopsy.

(A) Image taken 6 days after biopsy was plated. **(B)** Image taken 12 days after biopsy was plated. **(C)** Fibroblasts after Passage one and **(D)** Fibroblasts after passage two. Magnification 5X. Scale bar is 100 µM.

All Fibroblast lines underwent a PCR for the detection of Mycoplasma. PCR products were then loaded onto a 1.5% Agarose gel to visualise results. In **Figure 2.4**, all fibroblast lines were negative for the presence of mycoplasma. The internal control band of 479bp was present in each of four fibroblast lines, confirming the success of the PCR reaction.

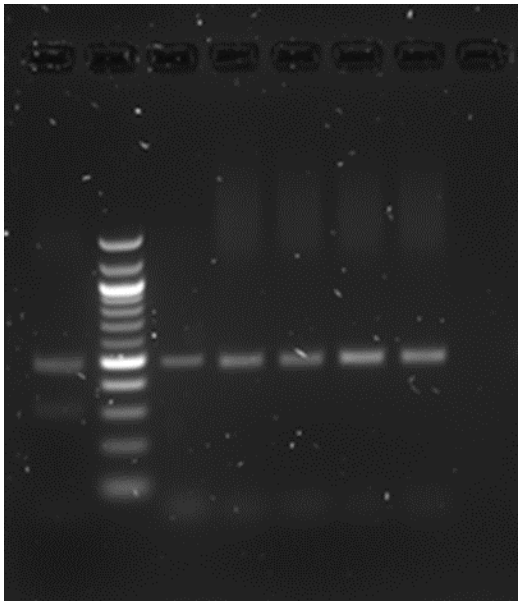

Figure 2.4. Representative Gel Electrophoresis result of Mycoplasma PCR test.

From left to right; positive control for mycoplasma (288 bp) and for PCR reaction (479bp), 100bp DNA ladder, negative control and four separate fibroblast samples from 4 patient donors. The PCR internal control band is 479bp and positive mycoplasma control band is 288bp. Positive controls were provided by the kit and the negative control was RNase free water. The DNA templates were extracted from fibroblast culture media taken from each fibroblast cell line. All samples were negative for mycoplasma contamination.

2.3.2 Generation of induced pluripotent stem cells

A Sendai Virus containing the four Yamanaka transcription factors *OCT4, SOX2, KLF4* and *c-MYC* was used to reprogramme fibroblasts into iPSCs. At approximately 10 days post-transduction, small colonies could be seen forming **(Figure 2.5)**. These colonies were allowed to expand until they were large enough to be passaged from the plate. To allow the colonies to grow, surrounding fibroblasts were scraped from the plate using a 2µl tip. Care was taken to ensure that no colonies merged during this stage so only single colonies were chosen for passaging. The colonies were passaged using the cut and paste method at about 3 to 4 weeks

after transduction. Selected colonies had a distinct ES-like morphology of defined edges, round borders, a large nuclei/cytoplasm ratio, and tightly packed colonies **(Figure 2.5)**. iPSC lines were expanded and frozen in 90% Knock-out Serum Replacement and 10% DMSO.

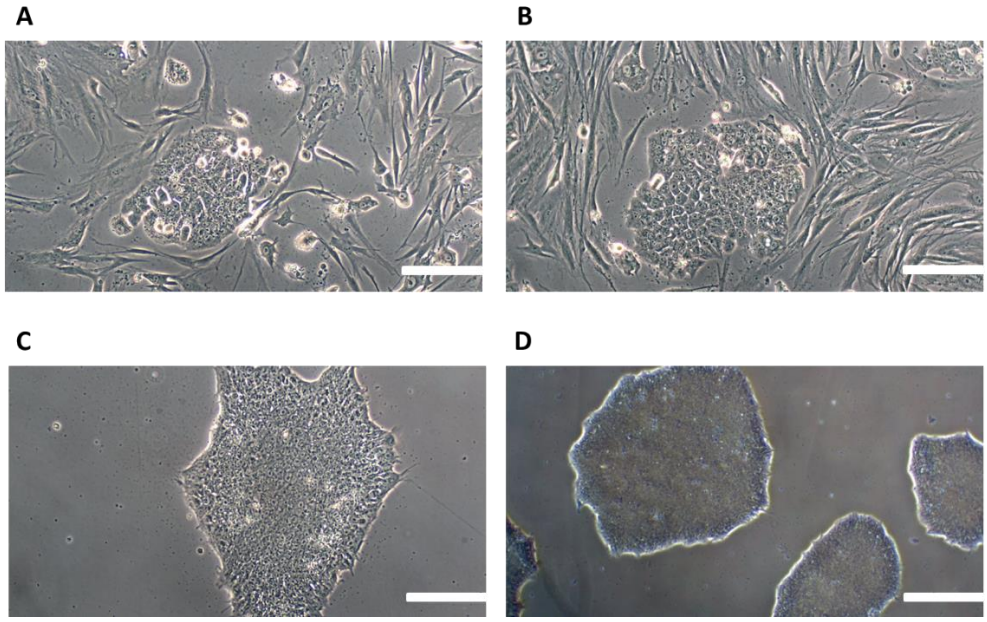

Figure 2.5. Representative images of induced pluripotent stem cell generation from fibroblasts using a Sendai virus.

(A) Image of iPSC colony emerging from fibroblasts 10 days post transduction. **(B)** Image of iPSC colony 15 days post transduction. **(C)** Image of iPSC colony after first passage from the reprogramming plate. **(D)** Image of iPSCs after second passage. Magnification is 10X. Scale bar is 100µM.

Three stable iPSC lines were generated from each donor fibroblast line. Information regarding iPSC lines can be found in **Table 2.5**. All generated iPSC lines were fully characterised in detail as required for the registration of iPSC lines.

Table 2.5. IPSC lines generated from *KCNQ2* patients and healthy controls

Family	ID	Mutation	Cell lines
Family 1	EP2001	c.881C>T; p.A294V	C4, C5, C8
	EP2C001	Sibling Control	C1, C2, C4
Family 2	EP2002	c.783A>C; p.F261L	C1, C2, C3
	EP2C002	Sibling Control	C5, C6, C7
Family 3	EP2003	c.638C>T; p.R213Q	C2, C3, C4
	EP2C003	Sibling Control	C1, C2, C4
Family 4	EP2004	c.793G>A; p.A265T	C1, C7, C8

	EP2C004	Sibling Control	C2, C4, C5

2.3.3 Characterisation of iPSC lines

2.3.3.1 Alkaline Phosphatase Staining

Alkaline Phosphatase (AP) is a hydrolase enzyme responsible for dephosphorylating molecules such as nucleotides, proteins, and alkaloids under alkaline conditions, and is highly expressed in undifferentiated pluripotent ESCs, iPSCs as well as tumour cells. AP staining, a very simple and quick method, is used to confirm the undifferentiated status of cells in a red/purple colour, whereas negative cells remain white. All iPSC colonies were positively stained for AP which was indicated by the red/purple colour seen in **Figure 2.6**. A negative result for AP staining in differentiated cells would be colourless.

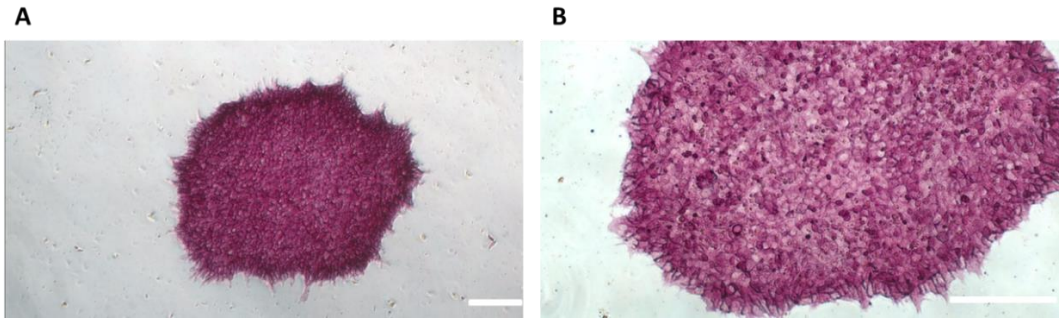

Figure 2.6. Representative images of Alkaline Phosphatase staining of iPSC colonies.

Images were taken of alkaline phosphatase staining of EP2001 C4 (A) and EP2C001 C1 (B). Both cell lines were positive for Alkaline phosphatase staining. Magnification of (A) 5X and (B) 10X. Scale bar = 100µM.

2.3.3.2 Confirmation of transgene-free status of iPSC lines

Although the Sendai Virus used to reprogramme the iPSCs is a non-integrating virus, transgenes may persist in the cells for several passages after reprogramming. To ensure all iPSC lines were negative for any transgenes which were introduced during reprogramming, we performed a RT-PCR using cDNA from the iPSC lines and checked for the presence of the transgenes *KOS, C-MYC, KLF4* and *SeV.* PCR products were then analysed on an agarose gel to visualise results. At passage 15, each cell line was negative for the presence of all transgenes used during reprogramming **(Figure 2.7)**.

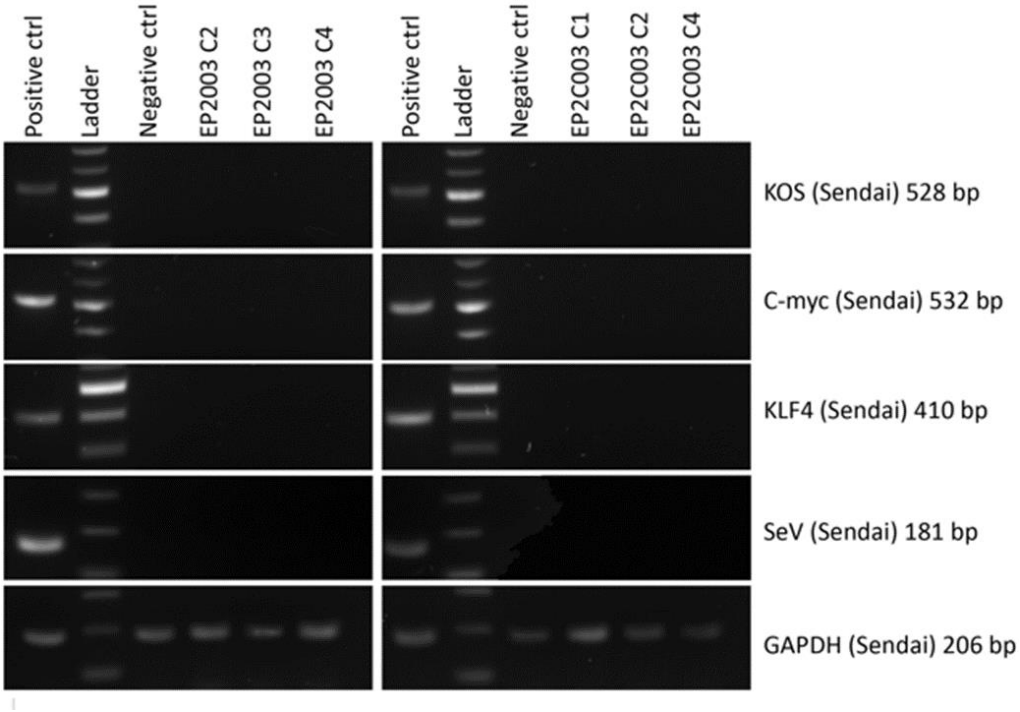

Figure 2.7 Representative result of gel electrophoresis of transgene free- PCR.

DNA was extracted from the cells at passage 15 and underwent PCR to test for the presence of transgenes KOS, c-MYC, KLF4 and SeV. GAPDH was used as a positive control. DNA taken from cells immediately after reprogramming was used as a positive control. Normal fibroblasts were used as a negative control. All cell lines at passage 15 were negative for the presence of all transgenes used in the transduction process. Results shown are from EP2003 (R213Q) and EP2C003.

2.3.3.3 Single Nucleotide Polymorphism (SNP) analysis revealed that no major chromosomal abnormalities were introduced to the cell lines during reprogramming

All iPSC lines were analysed on a 990k SNP array using genomic DNA extracted from each line at passage 15. Data was then analysed using Axion Analysis Suite (ThermoFisher, USA) and standardised with an internal control of 95 samples. Data is presented as Log2 ratios which can detect CNVs specific to individual samples. For each iPSC line, the log2 ratios of the SNP analysis revealed that no major chromosomal abnormalities were found to be introduced during reprogramming and cells have a normal karyotype **(Figure 2.8)**.

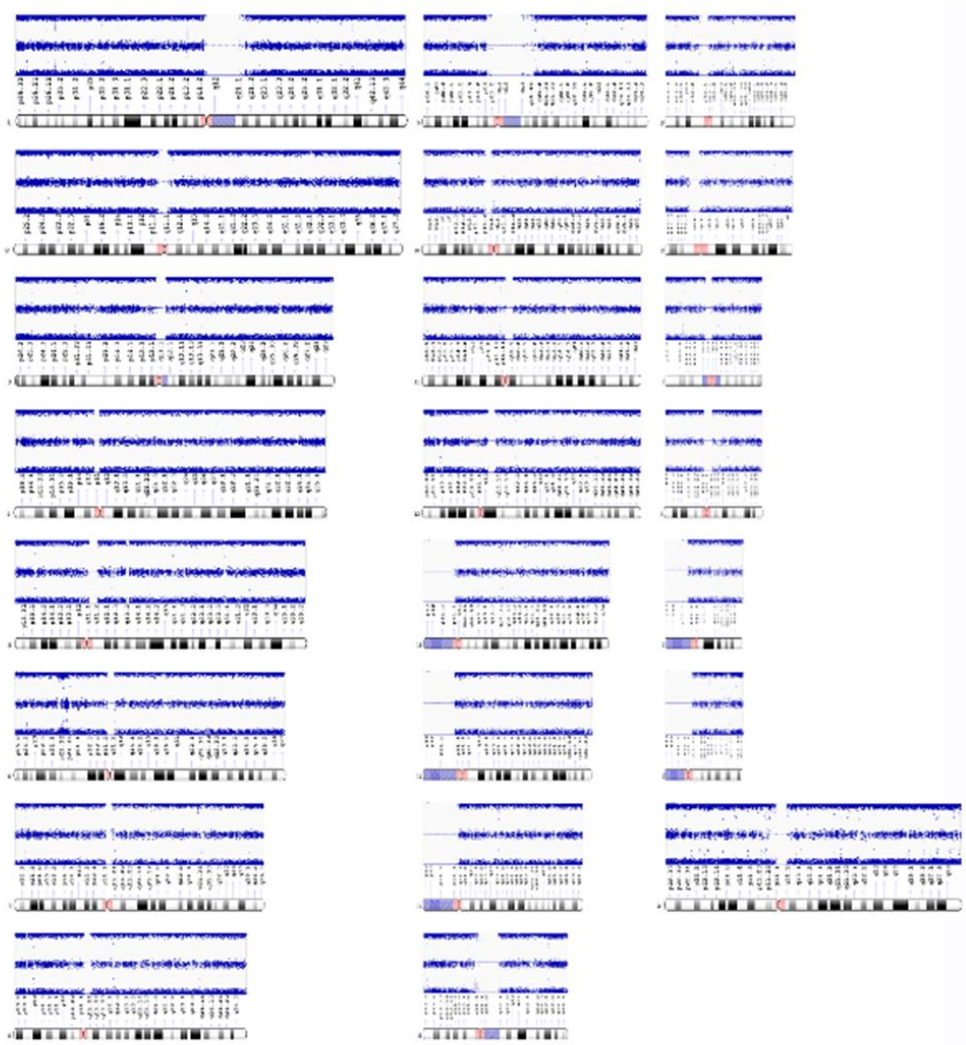

Figure 2.8. Representative image of result for Single Nucleotide Polymorphism karyotyping.

Log 2 ratio results of SNP analysis for the iPSC line EP2003 (R213Q) C1. No karyotypic abnormalities were found in any of the cell lines. The gaps are the regions which have no SNP present in the chips.

2.3.3.4 Cell Line Authentication of iPSC lines confirms their identical identity to parent fibroblast line

To confirm the parental identity of fibroblast lines to the generated iPSC lines, genomic DNA was extracted from the iPSCs at passage 10, and cells underwent cell line authentication tests by Eurofins Genomics. Sixteen different STR genomic loci were amplified and compared between the parent fibroblast line and the three generated iPSC lines from each donor. As shown in **Figure 2.9**, all sixteen loci were identical between original fibroblasts and derived iPSC lines confirming their genomic identity.

Client Sample Name	EP2003 C1	EP2003 C3	EP2003 C4	F.EP2003
Sample Code	CL00001536	CL00001537	CL00001538	CL00002216
D8S1179	15,17	15,17	15,17	15,17
D21S11	30,30	30,30	30,30	30,30
D7S820	8,9	8,9	8,9	8,9
CSF1PO	10,11	10,11	10,11	10,11
D3S1358	16,17	16,17	16,17	16,17
TH01	7,7	7,7	7,7	7,7
D13S317	11,11	11,11	11,11	11,11
D16S539	11,12	11,12	11,12	11,12
D2S1338	23,24	23,24	23,24	23,24
D19S433	13,13	13,13	13,13	13,13
vWA	16,18	16,18	16,18	16,18
TPOX	8,11	8,11	8,11	8,11
D18S51	12,15	12,15	12,15	12,15
AMEL	X,X	X,X	X,X	X,X
D5S818	11,11	11,11	11,11	11,11
FGA	22,24	22,24	22,24	22,24

Figure 2.9 Representative image of Short Tandem Repeat Analysis.

16 different STR loci were analysed by Eurofins genomics for the number of repeats in each STR. All iPSC lines from EP2003 (R213Q) (EP2003 C1, EP2003 C3, EP2003 C4) contain the same numbers of repeats in 16 STR loci as the fibroblast line F.EP2003.

2.3.3.5 iPSC lines contain high levels of pluripotency markers OCT4, SOX2 and NANOG

To measure the expression of the pluripotency markers OCT4, SOX2 and NANOG, we performed qRT-PCR using RNA extracted from the iPSC lines at passage 12. There is a significant increase in the expression of the pluripotency markers OCT4, SOX2, and NANOG in iPSCs compared to fibroblast lines. **(Figure 2.10)**. Data is presented as relative mRNA expression of iPSCs normalised to the level of gene expression in the parent fibroblast line using the delta delta CT method. GAPDH was used as the housekeeping gene. Experiments were performed in biological and technical triplicates.

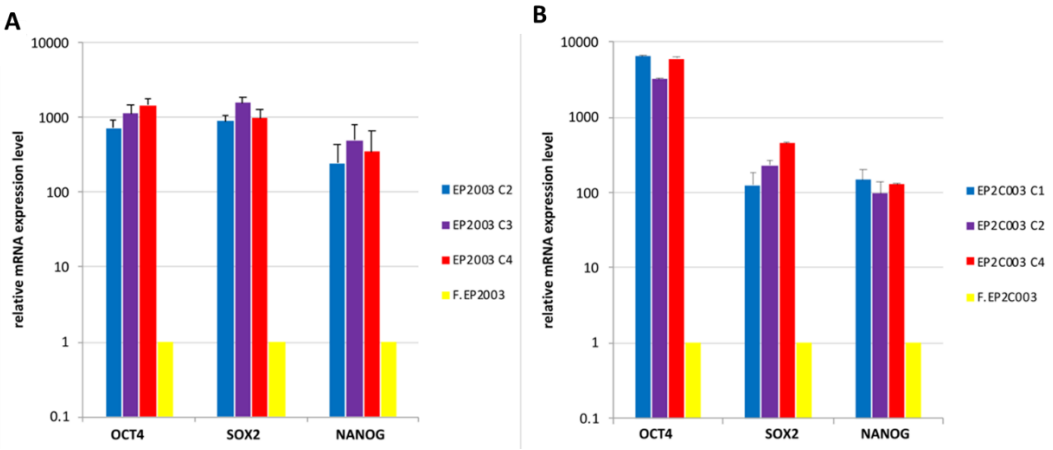

Figure 2.10: Representative image of RT-qPCR results of relative mRNA expression levels of pluripotent genes in patient and control iPSCs.

(A) Relative mRNA expression of the pluripotent genes *OCT4*, *SOX2* and *NANOG* in the *KCNQ2*-DEE lines EP2003 C2, EP2003 C3, EP2003 C4 compared to parental fibroblast line F.EP2003. **(B)** Relative mRNA expression of the pluripotent genes *OCT4*, *SOX2* and *NANOG* in the healthy control lines EP2C003 C1, EP2C003 C2, EP2C003 C4 compared to parental fibroblast line F.EP2C003. GAPDH was used as the house-keeping gene. The fold change of gene expression in iPSCs was presented in Log10 in relation to that of the parental fibroblast line. The data are from three repeated experiments and presented as Mean ± SEM.

2.3.3.6 iPSCs are positive for undifferentiated stem cell markers by immunocytochemistry

iPSCs were stained for the nuclear pluripotency markers SOX2, OCT4 and NANOG and the cell surface markers TRA-1-81, TRA-1-60 and SSEA4 by immunocytochemistry at passage 10. All cell lines were positive for each of these markers as seen in **Figure 2.11**. As iPSC colonies grow outwards from their edges, staining is often higher in these areas as seen in OCT4, NANOG and SSEA4.

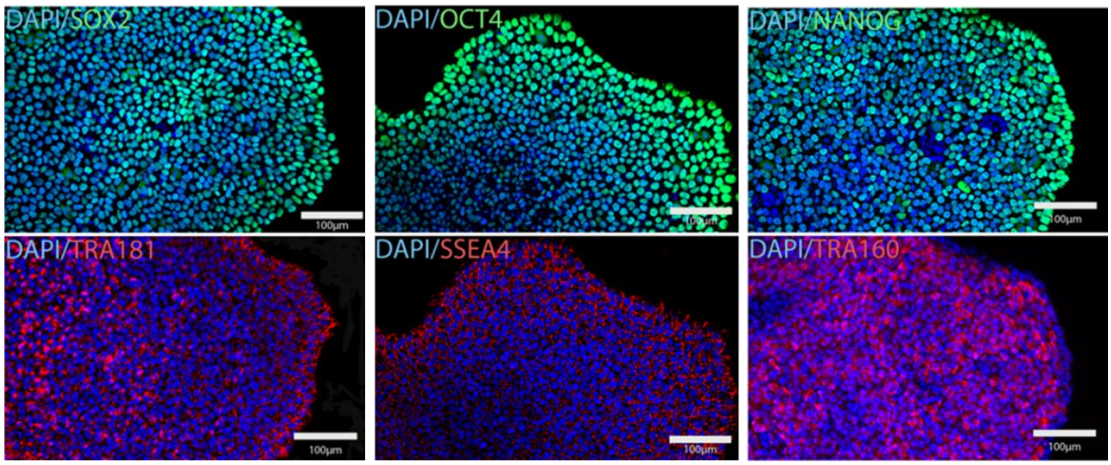

Figure 2.11 Representative image of immunocytochemistry staining of iPSC lines for pluripotency markers.

EP2002 C1 colonies were positively stained for the pluripotent markers SOX2, OCT4, NANOG, TRA1-81, TRA1-60 and SSEA4. Magnification is 10X. Scale bar = 100µM.

2.3.3.7 iPSCs are capable of spontaneously forming cells from three germ layers through Embryoid Body formation

An important characteristic of iPSCs is their ability to differentiate into any of three germ layers. To determine whether our iPSCs were capable of differentiating into cells from each of the three germ layers, Embryoid Bodies (EBs) were generated from the iPSCs in suspension

culture, and they were allowed to attach and spontaneously differentiate in a culture dish for 3 to 4 weeks. Cells were then fixed and stained using immunocytochemistry for a marker from each of the three germ layers: alpha-fetoprotein (AFP) for Endoderm; Beta III Tubulin (TUJ1) for Ectoderm and smooth muscle actin (SMA) for Mesoderm. As can be seen in **Figure 2.12**, cells were capable of forming each of these germ layers in different parts of the EB cultures.

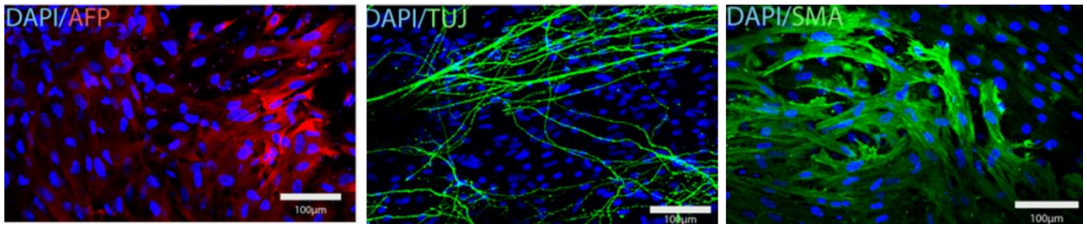

Figure 2.12 Representative image of immunocytochemistry staining of iPSC lines for the three germ layer markers after spontaneous differentiation.

EBs were allowed to spontaneously differentiate for 4 weeks. Cells were then fixed and stained. Above our representative images of cells from EP2004 C1 from the three germ layers; the endoderm, ectoderm and mesoderm stained with alpha-fetoprotein (AFP), Beta III Tubulin (TUJ1) and smooth muscle actin (SMA), respectively. All lines were positive for markers for each germ layer. Magnification is 10X. Scale bar = 100µM.

2.3.3.8 All iPSCs were negative for the presence of Mycoplasma

A common problem that is encountered when culturing iPSCs is the presence of Mycoplasma contamination in cultures. As Mycoplasma cannot be seen with the naked eye, all cell lines were tested for Mycoplasma contamination after thawing cells from LN_2 or prior to cryopreservation. For testing, the culture medium was collected from the cells when they reached at least 80% confluency to ensure any potential contamination would be detected. DNA were extracted from particles in the culture medium, PCR was carried out with a commercial mycoplasma amplification kit under standard conditions and PCR products were subsequently electrophoresed on a 1.5% agarose gel. All cell lines were found to be negative for the presence of Mycoplasma **(Figure 2.13)**. The positive control was provided with the Mycoplasma detection kit (Promokine) and water was used as a negative control.

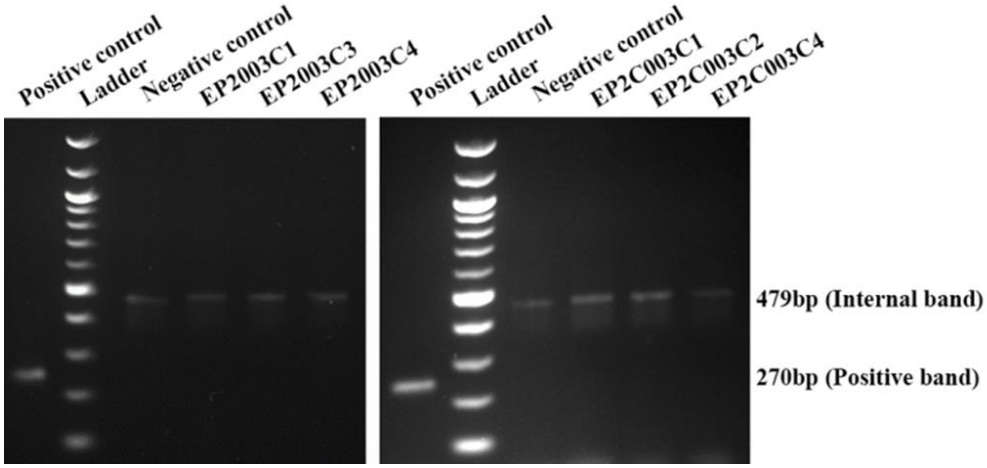

Figure 2.13 Representative image of Mycoplasma PCR result after gel electrophoresis.

From left to right; mycoplasma positive control, 100bp DNA ladder, negative control and four separate samples of fibroblast and derived iPSC lines. PCR internal control band is 479bp and positive control band is 270bp. Positive control was provided by the kit and negative control was RNase free water. The samples were culture media taken from each iPSC cell line. All samples were negative for mycoplasma contamination.

2.3.3.9 Sanger sequencing confirms mutations in *KCNQ2*-DEE patient-derived iPSCs

To ensure the *KCNQ2*-DEE related variants/mutations were present in the patient fibroblasts and generated iPSCs, DNA was extracted from the cells and underwent PCR with primers designed specifically to flank the target regions (Primer information is provided in **Table 2.4**). The PCR product was then purified and sent for Sanger sequencing by Eurofins Genomics. **Figure 2.14** shows the presence of the mutation marked 'R' (for A and G) in the patient fibroblast line F.EP2003 and the iPSCs EP2003 C1, EP2003 C3 and EP2003 C4. The presence of the double peaks (A in green and G in black) indicates it is a heterozygous mutation with a wild type G and a mutant A. Conversely, there is an absence of a mutation seen in the healthy control fibroblast line F.EP2C003 and the iPSCs EP2C003 C1, EP2C003 C2 and EP2C003 C4, which are homozygous for G on the respective nucleotide c.638. The PCR products were sequenced with a reverse primer, so the confirmed mutation was c.638C>T.

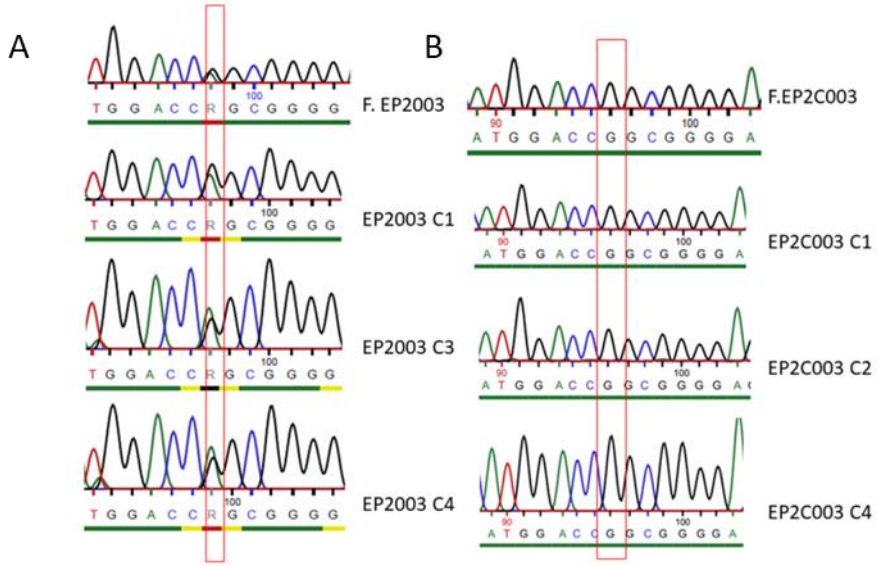

Figure 2.14 Representative image of Sanger Sequencing results to confirm the presence of mutation (*KCNQ2*-DEE lines) and the absence of mutation (healthy control lines).

(A) The presence of the mutation is confirmed in the Fibroblast line F.EP2003 and all derived iPSC lines, which is heterozygous for A (green) and G (black). **(B)** The absence of the mutation is confirmed in the healthy control fibroblast line F.EP2C003 and all derived iPSC lines which is homozygous for G (black). R represents nucleotides for A and G. The sequencing was carried out with a reverse primer, and the *KCNQ2* mutation in this patient was confirmed to be c.638C>T.

2.4 Discussion

Since the discovery of iPSCs from human somatic cells by Yamanaka' group (Takahashi et al., 2007), the field of stem cell technology has progressed rapidly. iPSCs are of particular interest for neuronal disorders. Their applications can be divided into 2 main groups: cell replacement therapy, which is very important in disorders such as Alzheimer's or Parkinson's disease and secondly, disease modelling of monogenic disorders including those which give rise to epilepsy and the developmental and epileptic encephalopathies (DEEs) including those due to pathogenic variants in *KCNQ2* (*KCNQ2*-DEE) the commonest cause of genetic neonatal epilepsy (Yang et al., 2016). This in turn allows the exploration of novel drug screening approaches for patients in human cell-based models.

In this study, we have generated and characterised 24 human iPSC lines, including 12 lines from healthy controls and 12 lines from epilepsy patients carrying KCNQ2 pathogenic variants including c.638C>T (p.R213Q), c.783A>C (p.F261L); c.793G>A (p.A265T) and c.881C>T (p.A294V), respectively. In patients with *KCNQ2*-DEE, the genotype-phenotype correlation is not fully understood but disease severity largely correlates to key hotspots

(location) of the pathogenic variant/mutation within the gene (and corresponding KCNQ2-protein). Below is a table generated on the UniProt website which shows which regions are located within each functional domain in the protein **(Table 2.6)**.

Table 2.6: Functional domains with *KCNQ2* transmembrane protein

Domain	Region	Function
Topological domain	1-91	Cytoplasmic
Transmembrane	92-112	Helical; Segment S1
Topological domain	113-122	Extracellular
Transmembrane	123-143	Helical; Segment S2
Topological domain	144-166	Cytoplasmic
Transmembrane	167-187	Helical; Segment S3
Topological domain	188-195	Extracellular
Transmembrane	196-218	Helical; Voltage-sensor; Segment S4
Topological domain	219-231	Cytoplasmic
Transmembrane	232-252	Helical; Segment S5
Topological domain	253-264	Extracellular
Intramembrane	265-285	Pore-forming; Segment H5
Topological domain	286-291	Extracellular
Transmembrane	292-312	Helical; Segment S6
Topological domain	313-872	Cytoplasmic
Modified residue	5	Phosphoserine
Modified residue	11	Phosphotyrosine
Modified residue	15	Phosphoserine
Modified residue	52	Phosphoserine; by PKA1 Publication
Modified residue	217	Phosphothreonine1 Publication
Modified residue	466	Phosphoserine
Modified residue	466	Phosphoserine
Modified residue	468	Phosphoserine
Modified residue	472	Phosphoserine
Modified residue	476	Phosphoserine
Modified residue	476	Phosphoserine
Modified residue	478	Phosphoserine
Modified residue	507	Phosphoserine
Modified residue	672	Phosphoserine
Modified residue	801	Phosphoserine
Modified residue	803	Phosphoserine

In **Figure 2.15**, known *KCNQ2* variants are marked next to their corresponding functional domain. Mutations marked in red are associated with *KCNQ2*-benign familial neonatal convulsions (a milder epilepsy phenotype now also known as self-limited familial neonatal epilepsy) and variant markers in black are associated with the severe seizures and brain developmental disorder *KCNQ2*-Developmental and Epileptic encephalopathy (DEE)(Lee et

al., 2022). Three out of four of the variants used in this study are recorded here (R213Q, A265T, A294V). The fourth variant F261L has not been previously recorded in the literature. In this chapter, we generated iPSCs from four *KCNQ2*-DEE patients. To date, there has been only one study published using *KCNQ2* patient-derived iPSCs to generate a neuronal model of the disease **(Table 2.7)**.

Table 2.7 Summary of iPSC-derived neuronal models in *KCNQ2*-DEE

***KCNQ2* variant**	**Domain**	**Somatic cell**	**Reprogramming method**	**Reference**
(Q2-04) R581Q	C helix	Patient peripheral blood mononuclear cells	CytoTune-iPS 2.0 Sendai	(Simkin et al., 2021)
iso- Q2-04	-	Isogenic by CRISPR/CAS9	-	(Simkin et al., 2021)

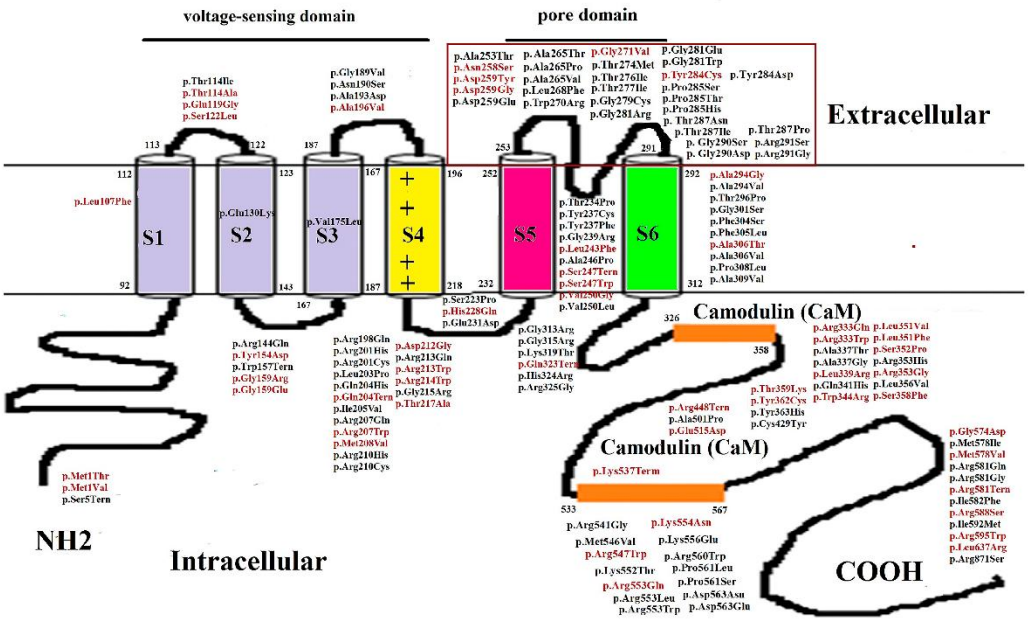

Figure 2.15. Mutations in KCNQ2 are grouped according to their functional domain.

Mutations marked in red are associated with *KCNQ2-benign familial neonatal convulsions* and mutations in black are associated with *KCNQ2*-DEE (I.-C. Lee et al., 2022).

iPSCs can now be generated from a variety of different somatic cell sources including dermal fibroblasts (Yu et al., 2007), keratinocytes (Piao et al., 2014), blood cells (Kim et al., 2016),

and other cell types (Zhou et al., 2012). As previously mentioned, it has been debated in the literature how much of an impact somatic cell source has on iPSC generation. Here, we report the use of dermal fibroblasts as a somatic cell source for the generation of iPSCs. We achieved a 100% success rate of isolating fibroblasts from skin biopsies and no repeat biopsies were required. Fibroblasts began to emerge from the biopsies after 1 week in culture and were ready for passaging after approximately 2 weeks in culture. All fibroblasts were confirmed to be negative for Mycoplasma by PCR.

In this study we chose to reprogramme our Fibroblasts using a Sendai Virus. The main reason for this decision was because the Sendai Virus is a non-integrating virus, meaning it cannot integrate into the host genome (Fusaki et al., 2009). It's only capable of expressing the exogenous transgenes, resulting in no random insertional mutagenesis which substantially decreases the risk of tumorigenicity or genomic disruption (MacArthur et al., 2012). Sendai Virus is a respiratory virus of mouse and rat. It was first isolated in the 1950's in Japan. It is an enveloped virus of 150-250nm in diameter made up of a single RNA chain (15,384 bases) in the minus sense. It's capable of infecting a broad range of cell types by attaching to sialic acid receptors on the cell surface (Chan et al., 2009). Since SeV vectors are in the form of a single chain RNA, it's not possible to integrate with the host genome and disrupt the function of any important genes as mammals including human do not have reverse transcriptase gene. Importantly, the gene encoding the Fusion protein is removed from the Sendai Virus reprogramming kit, rendering the virus incapable of producing any infectious particles. The pluripotency transgenes are transcribed using RNA polymerase which is encoded by the 'L' gene which works by splitting the viral RNA into daughter cells during proliferation. To allow the vector to be removed from the cells after passaging, functional variants such as temperature sensitivity have been inserted into the SeV vector.

For these reasons, SeV has become a very popular choice of reprogramming method used to generate iPSCs. In this study we used the CytoTune 2.0 Sendai Virus Reprogramming Kit. We found that the efficiency of transduction was sufficient for ample colony selection. Colonies were ready to be passaged 3-4 weeks post viral transduction. However, we did find some variability in the number of passages required to achieve complete removal of all transgenes (*KOS*, *c-MYC, KLF4* and *SeV*). In 50% of donors (4/8), all lines were transgene free after passage 10. For two of the donors, they were transgene free after passage 12 while for the remaining 2 donors they achieved a transgene free status at passage 15. These results appear consistent with other reports (Kudva et al., 2012).

In this study, 24 iPSC lines were generated and fully characterised. To confirm the pluripotency of the iPSCs, cells were stained for Alkaline Phosphatase (AP), immunocytochemistry staining of pluripotency markers and finally quantitative RT-PCR of pluripotency markers. All cells stained for AP were positive, which is indicative of a pluripotent state **(Figure 2.6)**. However, the importance of AP activity for pluripotent cells still remains generally unclear (Štefková et al., 2015). For this reason, we did not perform AP staining on all iPSC lines, as it was not deemed to provide any additional information.

To effectively demonstrate that our iPSCs were pluripotent, we measured the expression of 3 known pluripotency markers; *NANOG, OCT4* and *SOX2* by RT-qPCR, stained for pluripotency markers by immunocytochemistry and showed their capacity to differentiate into cells from each of the three germ layers **(Figure 2.12)**. We showed that there was over a 100-fold increase in the expression of each pluripotency marker relative to the parent fibroblasts **(Figure 2.10)**. There was some variability between lines from the same donor which was expected as iPSCs are known to have heterogeneity (Kyttälä et al., 2016). Also, there was less expression of *NANOG* compared to *OCT4* and *SOX2* which has been reported in other iPSC lines (Navarro et al., 2012).

Simultaneously, we demonstrated that our iPSCs expressed the cell surface markers SSEA4, TRA-1-81 and TRA-1-60 and nuclear markers OCT4, SOX2 and NANOG **(Figure 2.11)**. These markers are all commonly used markers to confirm pluripotency in embryonic/induced pluripotent stem cells (Rodda et al., 2005). The borders of the iPSC colonies often had higher expression of these markers which may be due to the iPSC colonies growing outward from their edges, meaning proliferative cells would be on the border of the colonies (Warmflash et al., 2014).

For a cell to be truly pluripotent, it must be able to differentiate into cells from each of the 3 germ layers ectoderm, mesoderm, and endoderm (Hadjantonakis, 2014). In this study, we showed that through the formation of Embryoid Bodies (EBs), our iPSCs were capable of forming cells from each of these germ layers. EBs are multicellular aggregates that were spontaneously generated from iPSCs when grown in suspension. These suspensions contain cells from each of the germ layers and it is thought that they somewhat recapitulate development in the early embryo (Guo et al., 2020). Here, we showed that our EBs formed cells of the ectoderm, mesoderm, and endoderm by staining with β-III Tubulin (TUJ1), smooth muscle actin (SMA) and alpha fetoprotein (AFP) respectively **(Figure 2.12)**. This approach offers many advantages over the teratoma assay, which was traditionally used to

demonstrate pluripotency by injecting iPSCs into an immuno-compromised mouse and testing for their ability to form a teratoma containing cells from each of the germ layers. The tri-lineage differentiation assay used here is less costly, time-consuming, and labour intensive (Nelakanti et al., 2015).

Genomic integrity of iPSCs is crucial for both research and clinical applications (Bhutani et al., 2016). There is multiple opportunities to introduce genetic alterations i.e., during the reprogramming of somatic cells, during cell culture or during gene editing. Therefore, it's imperative to assess the genomic integrity of iPSCs to ensure that cells are an exact copy of parent cells. In this study we chose to analyse our cell genomes using SNP arrays due to its higher resolution and computational accessibility. Compared to G-banding, which is still the most commonly used technique for assessing genomic stability, SNP analysis has a significantly higher resolution, covering every 3kb of the genome on average (Peterson & Loring, 2014). Several studies in recent years have shown that when compared with SNP arrays, G-banding was unable to detect as many genetic abnormalities (D'Antonio et al., 2017). However, one downside of the SNP array is its inability to detect translocations or inversions (Monzon et al., 2008). On the other hand, SNP arrays also cause challenges because of their high degree of sensitivity. This can make analysing the data tedious as it's essential to sieve through the data for any artifacts which may have been introduced by technical errors. Some regions such as GC-rich telomeres or centromeres, may have little or no SNPs. To combat this, an internal control is generated with most of the samples analysed on the same chip, which can be applied to remove some of the common CNVs on the majority of the samples, which may have been caused by small differences in DNA contents during processing. As a positive control we used the SNP array to confirm chromosomal deletions in other disease models in our laboratory i.e., *NRXN1* deletions patients with autism spectrum disorder. In this study, the SNP array found no gross chromosomal abnormalities in *KCNQ2*-DEE and control lines.

To confirm the identity of our iPSCs, we performed short tandem repeat (STR) analysis **(Figure 2.9)**. STRs are short, simple repeats of sequences that involve a repetitive unit that can be used to identify if cell lines are closely related. This type of genetic fingerprinting is commonly used in forensics to identify missing persons (Wyner et al., 2020). If a cell is derived from another cell, both cells should have identical STR profiles. The next closest match will be a sibling, but since they only share half their DNA from 2 parents with extensive recombination during gamete formation, the amount of matches they will have on STR analysis can vary (Zaken et al., 2013). Here, we confirmed that all generated iPSCs have

identical STR profiles to their parental fibroblast line, but they differ between different donors.

Genetic or presumed genetic epilepsies represent the cause of epilepsy in over 50% of cases (Mullen et al., 2018). Within this group are hundreds of monogenic disorders, the genes of which encode important cellular processes and functions, mostly the sodium and potassium ion channel epilepsies, which play a pivotal role action potential generation, conduction, and repolarisation (Khamdiyeva et al., 2021). Some common ion channel genes (when dysfunctional) causing epilepsy are *SCN1A, SCN2A, SCN8A, KCNQ2, KCNQ3, KCNA2, KCNT1, CLCN1*) (Weckhuysen et al., 2012;Poryo et al., 2017; Wang et al., 2017; Stewart et al., 2023; Arbini et al., 2020). In this study we recruited 4 patients with missense pathogenic variants in the *KCNQ2* gene. To confirm this, we sequenced DNA from the patient's iPSCs using Sanger Sequencing. We designed primers specific to each patient which flanked the mutation site and sequenced approx. 400bp region. Our results confirmed the presence of the mutation in each patient cell line and the absence of the mutation in the paired sibling control line.

Contamination of cells by pathogens is a huge problem in cell culture. Unlike bacteria, fungi or viruses, mycoplasma can easily go undetected in cell culture if not routinely monitored. Larger pathogens like fungi or bacteria cause changes to the cell culture medium which are visible to the naked eye including media turbidity, visible pathogens, and cell death (Mirjalili et al., 2005). Due to their small size (0.1µM – 0.8µM), and the ability of cells to survive during infection, mycoplasma is a silent yet detrimental form of contamination in cell culture (Sugita et al., 2021). iPSCs infected with mycoplasma may have altered gene expression, growth factors, and ion channels among other things (Olarerin-George et al., 2015). Prior to freezing and after thawing our iPSCs, we performed a routine PCR-based mycoplasma test to ensure cells were free of any mycoplasma contamination. All cell lines used in the experimentation of this project were confirmed to be mycoplasma free for the entirety of the project **(Figure 2.13)**. However, other cells in our laboratory that tested positive for mycoplasma were destroyed immediately as mycoplasma treatment options were shown to be unsuccessful in our laboratory in the past.

In summary, we have generated and characterised fully 24 iPSC lines from 4 patient donors who have pathogenic variants in *KCNQ2* (c.881C>T,c.783A>C, c.638C>T, c.793G>A) and 4 sibling controls. These cell lines were novel and invaluable resources for researching not only epilepsy but also the role of *KCNQ2* in early brain development. We used a proportion of these cell lines to model disease in vitro by differentiation into excitatory cortical neurons in

Chapter 4. Due to time constraints, we chose to study 3 out of the 4 pathogenic variants based on their prevalence and severity.

2.5 Supplementary data to Chapter 2

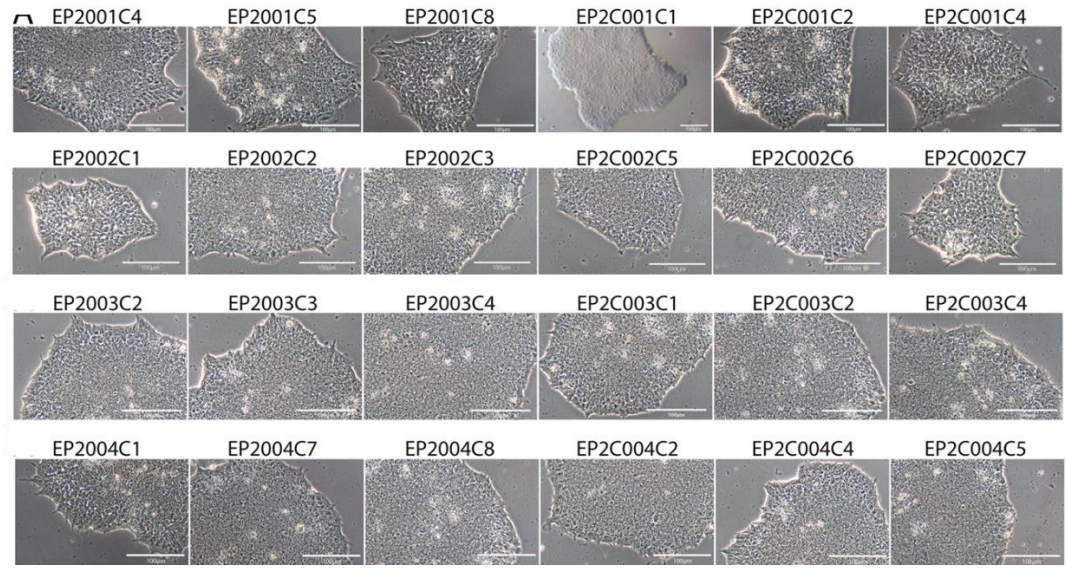

Figure S2.1. Morphology of iPSC lines.

Images were taken under light microscope at passage 4. All iPSC lines showed normal ESC-like colonies with tightly packed colonies, defined edges, and round borders. Total magnification is 10x. Scale bar is 100 µM.

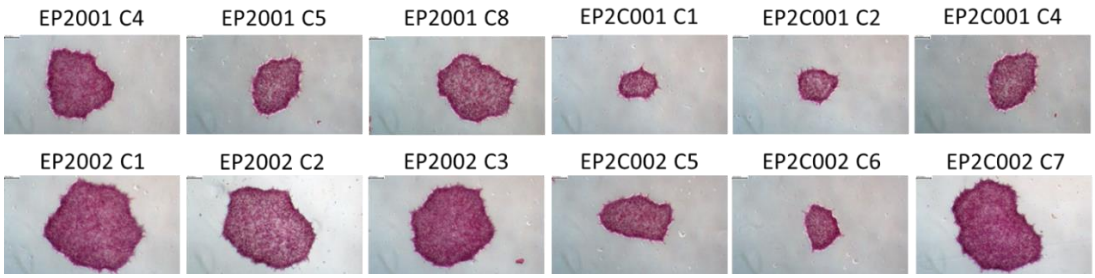

Figure S2.2. Alkaline Phosphatase staining of iPSC lines.

IPSC lines from donors EP2001, EP2C001, EP2002 and EP2C002 were positive for Alkaline phosphatase staining. Alkaline Phosphatase staining was not performed for the remaining donors as it is no longer required as a technique in characterising iPSC lines. Total Magnification is 5x. Scale bar is 100 µM.

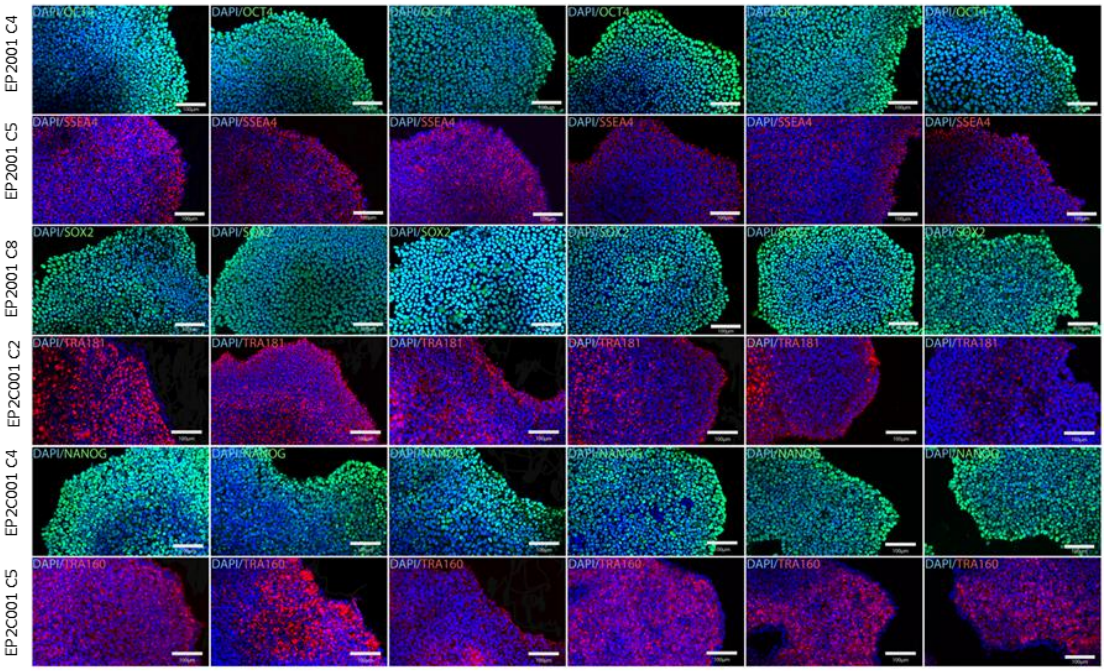
EP2001 C4
DAPI/OCT4
EP2001 C5
DAPI/SSEA4
EP2001 C8
DAPI/SOX2
EP2C001 C2
DAPI/TRA181
EP2C001 C4
DAPI/NANOG
EP2C001 C5
DAPI/TRA160

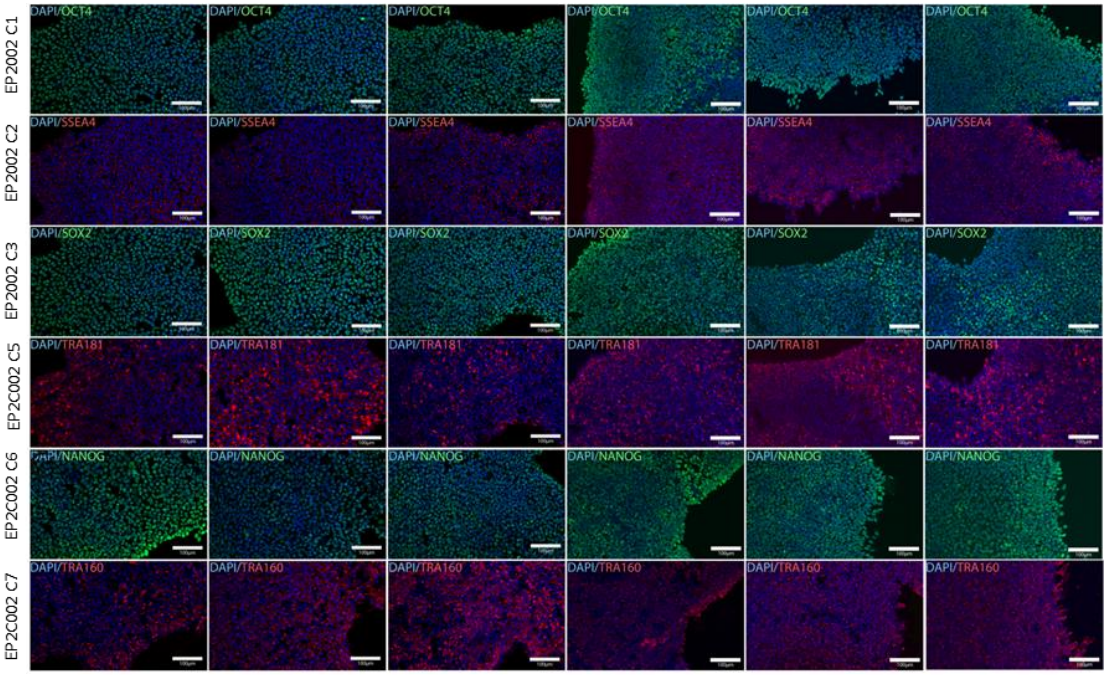
EP2002 C1
DAPI/OCT4
EP2002 C2
DAPI/SSEA4
EP2002 C3
DAPI/SOX2
EP2C002 C5
DAPI/TRA181
EP2C002 C6
DAPI/NANOG
EP2C002 C7
DAPI/TRA160

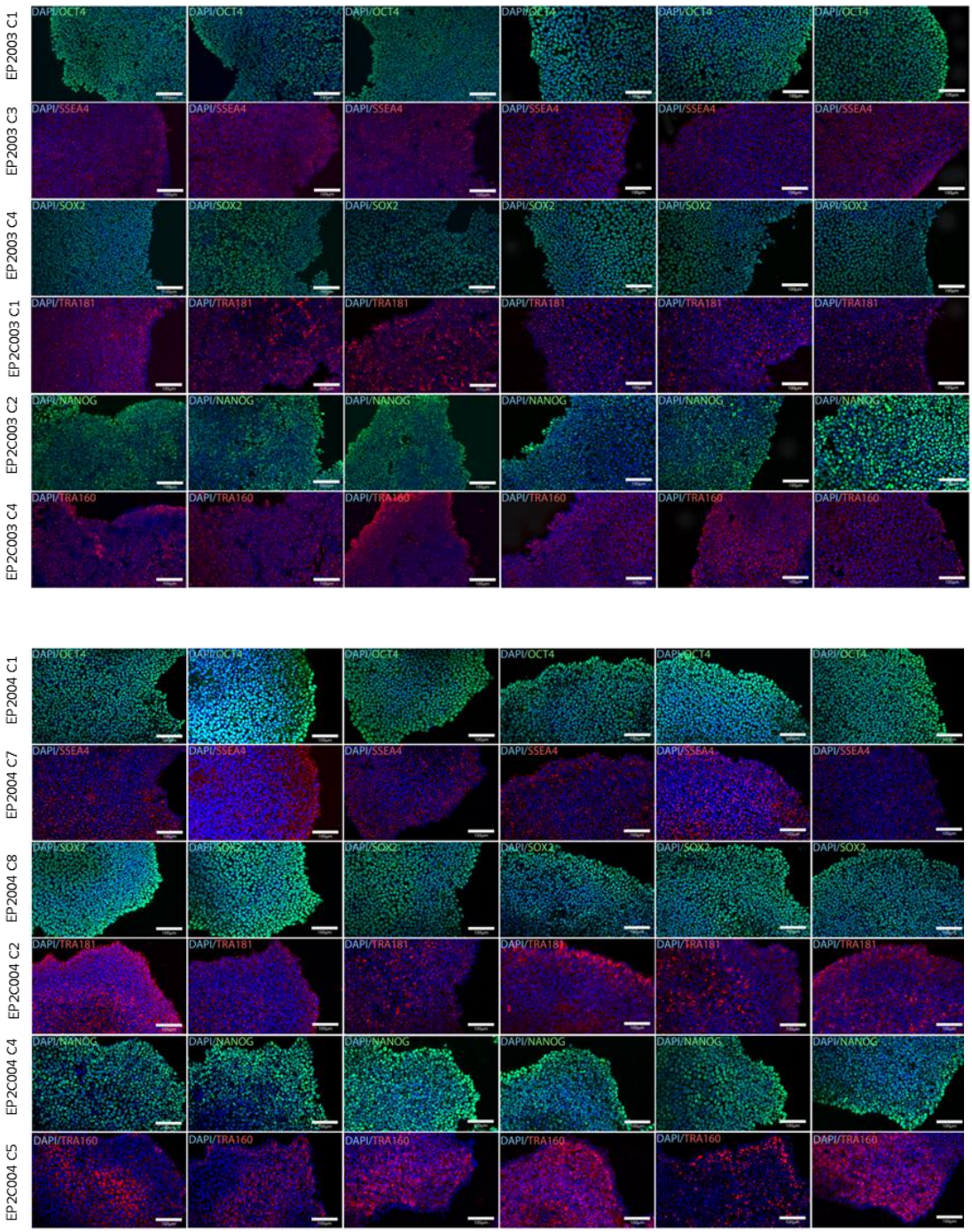

Figure S2.3. Immunocytochemistry analysis of undifferentiated stem cell markers OCT4, SOX2, NANOG, SSEA4, TRA-1-81 and TRA-1-60.

All Cell lines from EP2001, EP2C001, EP2002, EP2C002, EP2003, EP2C003, EP2004 and EP2C004 were positive for all markers. Total magnification is 20X. Scale bar = 100 µM.

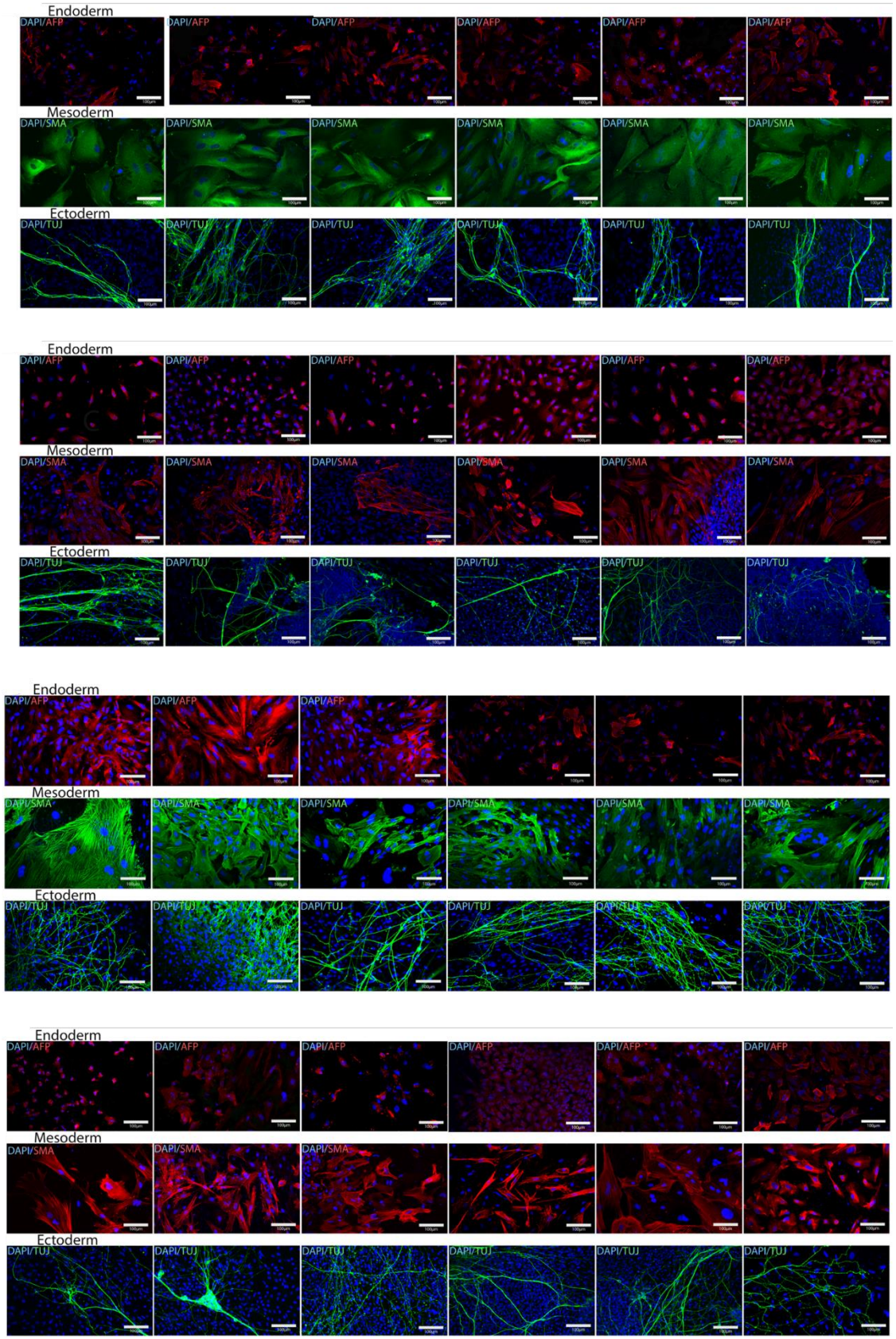

Figure S2.4. Immunocytochemistry analysis of markers from the 3 germ layers.

All iPSC lines were positive for the markers AFP, SMA and TUJ-1. Total magnification is 20x. Scale bar = 100 µM.

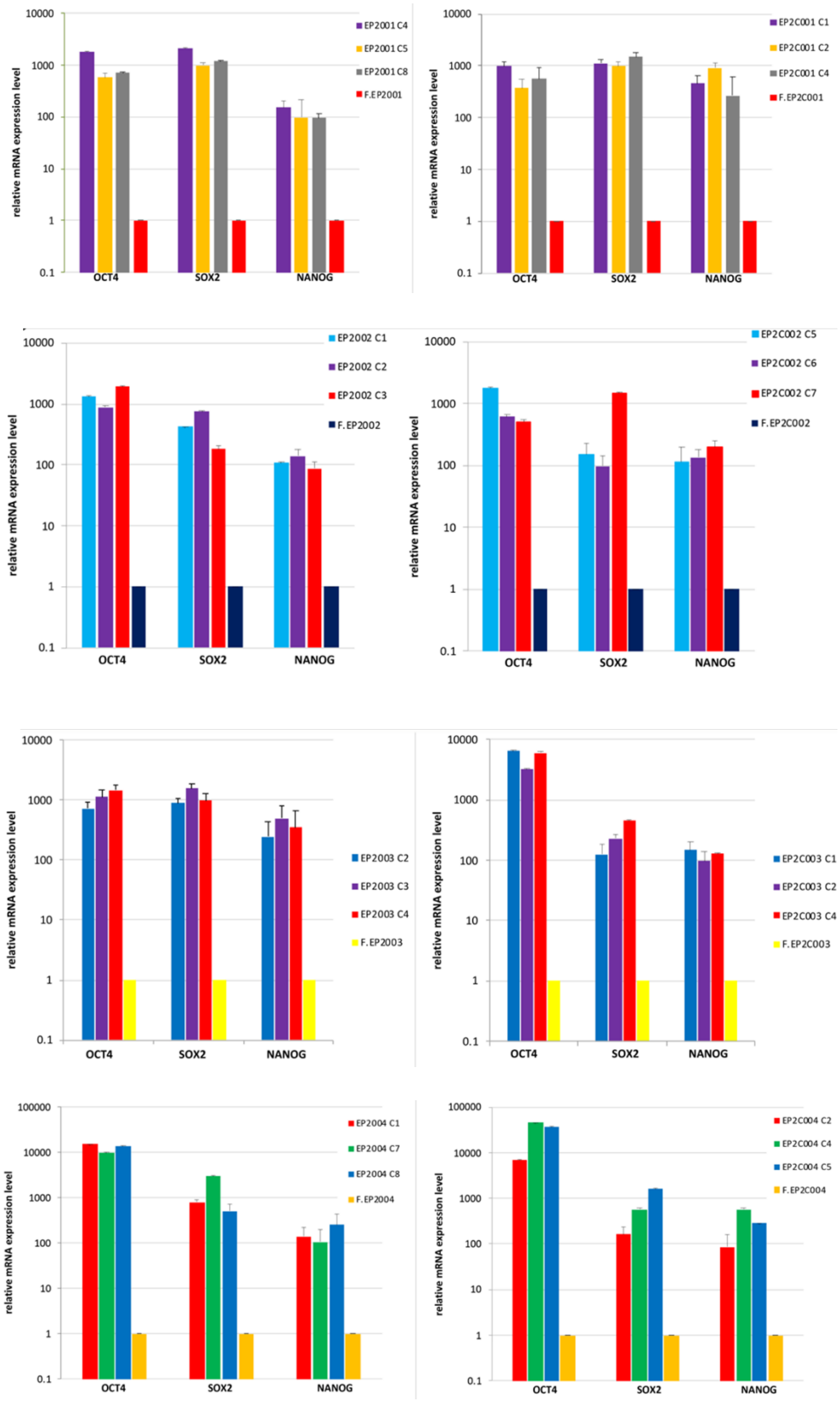

Figure S2.5. RT-qPCR results showing expression of pluripotency markers OCT4, SOX2 and NANOG in iPSC lines.

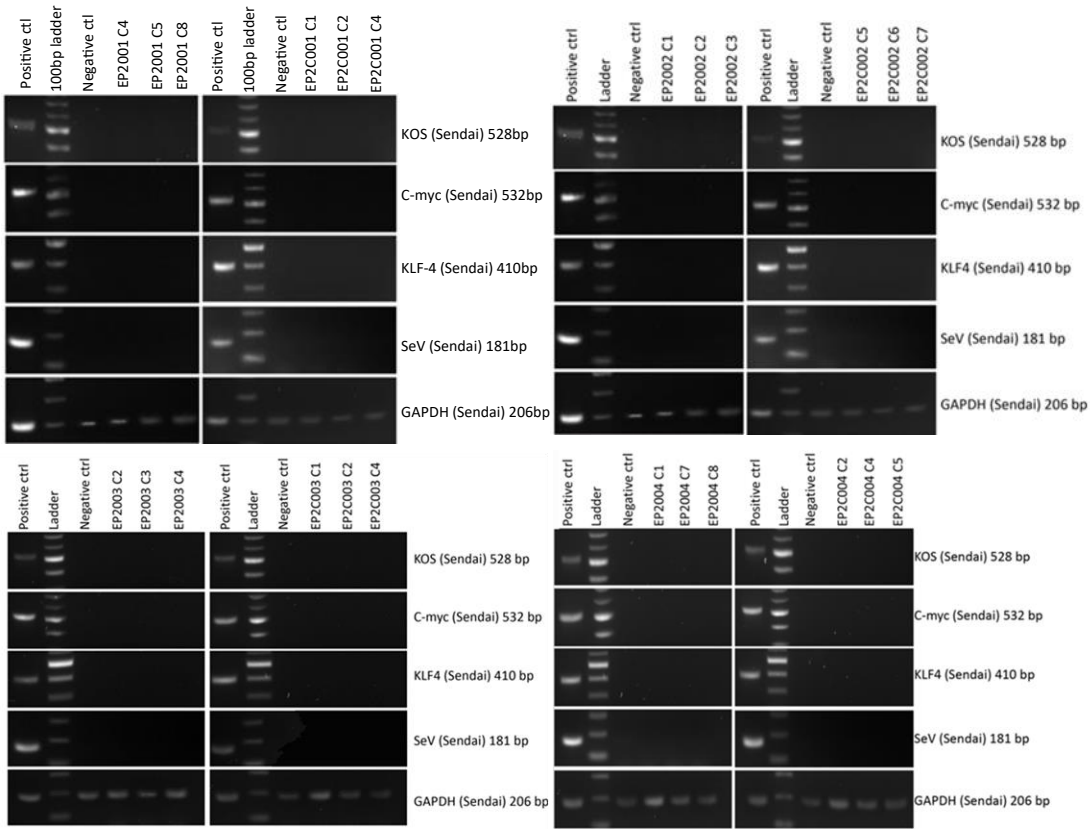

Figure S2.6. RT-PCR results show the absence of any transgenes in the iPSC lines.

All cell lines were negative for the presence of the transgenes *KOS, C-MYC, KLF4* and *SeV.* cDNA taken from cells 24 hour after transduction was used as a positive control. cDNA from fibroblasts were used as a negative control. GAPDH was the house-keeping gene used as an internal control.

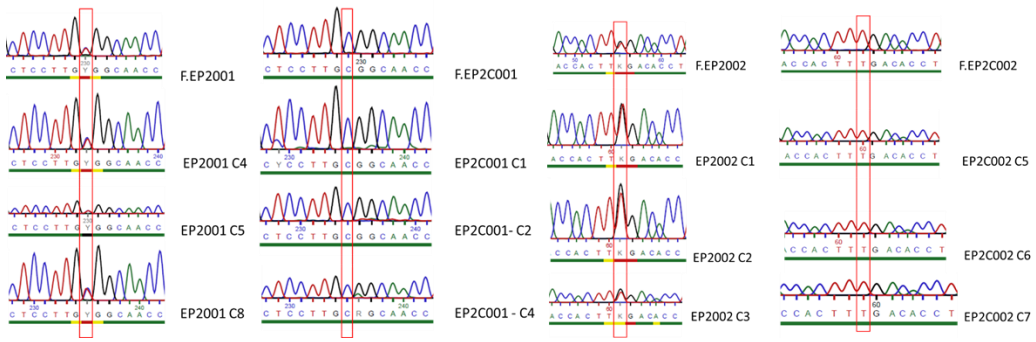

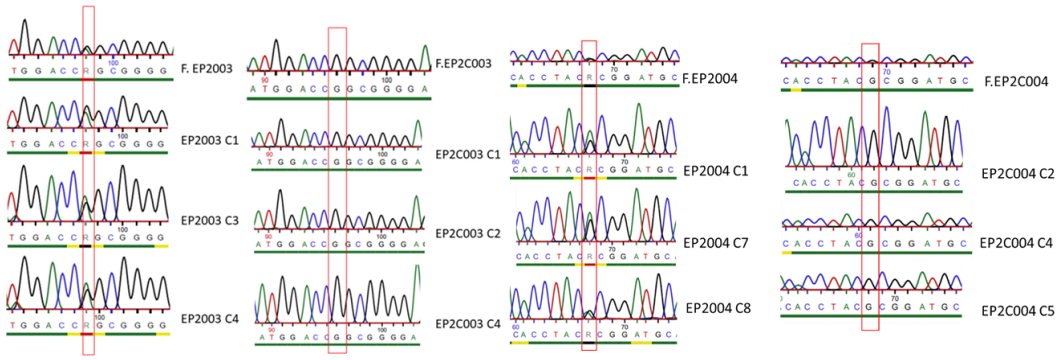

Figure S2.7. Sanger Sequencing Chromatograms from all iPSC lines.

The mutation of each patient fibroblast line was confirmed as well as in all the derived iPSC lines. The absence of the mutation in the healthy control fibroblast line was confirmed as well as in all the derived iPSC lines. The Red boxes highlight the nucleotides of interest.

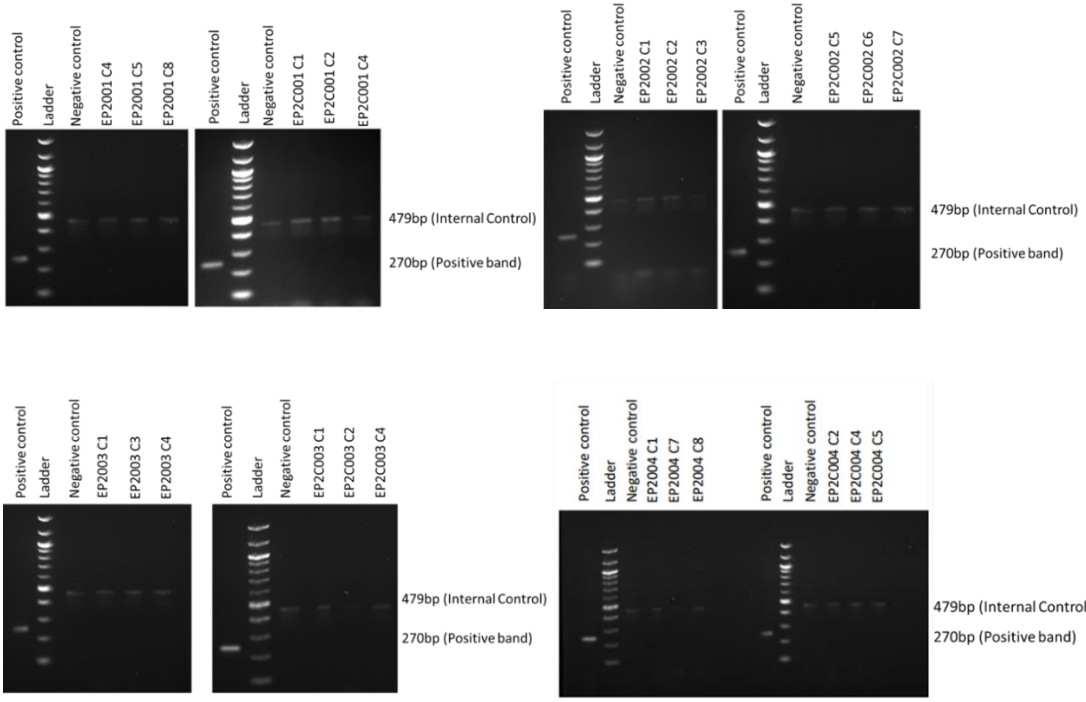

Figure S2.8. Mycoplasma PCR results for all iPSC lines.

Cell culture supernatant was collected from each IPSC line and underwent PCR for the detection of Mycoplasma. PCR products were electrophoresed on an agarose gel. All cell lines were negative for the presence of mycoplasma. Positive control is lyophilised mycoplasma product provided by the kit, ladder is 100bp DNA ladder, negative control is water.

Client Sample Name	EP2001 C4	EP2001 C5	EP2001 C8	F.EP2001
Sample Code	CL00002188	CL00002189	CL00002190	CL00002185
D8S1179	11,14	11,14	11,14	11,14
D21S11	30,30.2	30,30.2	30,30.2	30,30.2
D7S820	10,13	10,13	10,13	10,13
CSF1PO	10,12	10,12	10,12	10,12
D3S1358	17,18	17,18	17,18	17,18
TH01	7,9.3	7,9.3	7,9.3	7,9.3
D13S317	12,12	12,12	12,12	12,12
D16S539	10,11	10,11	10,11	10,11
D2S1338	16,24	16,24	16,24	16,24
D19S433	14,15	14,15	14,15	14,15
vWA	16,17	16,17	16,17	16,17
TPOX	8,8	8,8	8,8	8,8
D18S51	13,15	13,15	13,15	13,15
AMEL	X,Y	X,Y	X,Y	X,Y
D5S818	11,12	11,12	11,12	11,12
FGA	21,21	21,21	21,21	21,21

Client Sample Name	EP2C001 C1	EP2C001 C2	EP2C001 C4	F.EP2C001
Sample Code	CL00002186	CL00002187	CL00002182	CL00002183
D8S1179	12,14	12,14	12,14	12,14
D21S11	30,30.2	30,30.2	30,30.2	30,30.2
D7S820	9,13	9,13	9,13	9,13
CSF1PO	12,12	12,12	12,12	12,12
D3S1358	14,15	14,15	14,15	14,15
TH01	7,8	7,8	7,8	7,8
D13S317	11,12,13	11,12	11,12	11,12
D16S539	10,12	10,12	10,12	10,12
D2S1338	16,26	16,26	16,26	16,26
D19S433	14,17	14,17	14,17	14,17
vWA	16,17	16,17	16,17	16,17
TPOX	8,8	8,8	8,8	8,8
D18S51	14,20	14,20	14,20	14,20
AMEL	X,Y	X,Y	X,Y	X,Y
D5S818	11,12	11,12	11,12	11,12
FGA	21,21	21,21	21,21	21,21

Client Sample Name	EP2002 C1	EP2002 C2	EP2002 C3	F.EP2002
Sample Code	CL00001533	CL00001534	CL00001535	CL00002215
D8S1179	13,13	13,13	13,13	13,13
D21S11	29,31	29,31	29,31	29,31
D7S820	8,10	8,10	8,10	8,10
CSF1PO	9,12	9,12	9,12	9,12
D3S1358	15,17	15,17	15,17	15,17
TH01	6,10	6,10	6,10	6,10
D13S317	8,12	8,12	8,12	8,12
D16S539	9,13	9,13	9,13	9,13
D2S1338	17,19	17,19	17,19	17,19
D19S433	15,17	15,17	15,17	15,17
vWA	16,18	16,18	16,18	16,18
TPOX	8,8	8,8	8,8	8,8
D18S51	14,16	14,16	14,16	14,16
AMEL	X,X	X,X	X,X	X,X
D5S818	12,13	12,13	12,13	12,13
FGA	22,24	22,24	22,24	22,24

Client Sample Name	EP2C002 C5	EP2C002 C6	EP2C002 C7	F.EP2C002
Sample Code	CL00002196	CL00002191	CL00002192	CL00002193
D8S1179	13,14	13,14	13,14	13,14
D21S11	28,28	28,28	28,28	28,28
D7S820	10,11	10,11	10,11	10,11
CSF1PO	9,12	9,12	9,12	9,12
D3S1358	15,17	15,17	15,17	15,17
TH01	9.3,9.3	9.3,9.3	9.3,9.3	9.3,9.3
D13S317	13,13	13,13	13,13	13,13
D16S539	13,13	13,13	13,13	13,13
D2S1338	17,24	17,24	17,24	17,24
D19S433	14,15	14,15	14,15	14,15
vWA	18,18	18,18	18,18	18,18
TPOX	8,11	8,11	8,11	8,11
D18S51	14,16	14,16	14,16	14,16
AMEL	X,Y	X,Y	X,Y	X,Y
D5S818	12,13	12,13	12,13	12,13
FGA	22,24	22,24	22,24	22,24

Client Sample Name	EP2003 C1	EP2003 C3	EP2003 C4	F.EP2003
Sample Code	CL00001536	CL00001537	CL00001538	CL00002216
D8S1179	15,17	15,17	15,17	15,17
D21S11	30,30	30,30	30,30	30,30
D7S820	8,9	8,9	8,9	8,9
CSF1PO	10,11	10,11	10,11	10,11
D3S1358	16,17	16,17	16,17	16,17
TH01	7,7	7,7	7,7	7,7
D13S317	11,11	11,11	11,11	11,11
D16S539	11,12	11,12	11,12	11,12
D2S1338	23,24	23,24	23,24	23,24
D19S433	13,13	13,13	13,13	13,13
vWA	16,18	16,18	16,18	16,18
TPOX	8,11	8,11	8,11	8,11
D18S51	12,15	12,15	12,15	12,15
AMEL	X,X	X,X	X,X	X,X
D5S818	11,11	11,11	11,11	11,11
FGA	22,24	22,24	22,24	22,24

Client Sample Name	EP2C003 C1	EP2C003 C2	F.EP2C003	EP2C003 C4
Sample Code	CL00002207	CL00002208	CL00005479	CL00005476
D8S1179	11,15	11,15	11,15	11,15
D21S11	30,30	30,30	30,30	30,30
D7S820	8,10	8,10	8,10	8,10
CSF1PO	10,11	10,11	10,11	10,11
D3S1358	15,16	15,16	15,16	15,16
TH01	7,9.3	7,9.3	7,9.3	7,9.3
D13S317	13,14	13,14	13,14	13,14
D16S539	11,12	11,12	11,12	11,12
D2S1338	20,24	20,24	20,24	20,24
D19S433	14,15	14,15	14,15	14,15
vWA	16,18	16,18	16,18	16,18
TPOX	8,11	8,11	8,11	8,11
D18S51	12,16	12,16	12,16	12,16
AMEL	X,Y	X,Y	X,Y	X,Y
D5S818	11,12	11,12	11,12	11,12
FGA	22,24	22,24	22,24	22,24

Client Sample Name	EP2004 C7	EP2004 C8	F.EP2004	EP2004 C1
Sample Code	CL00002200	CL00002201	CL00002204	CL00002205
D8S1179	11,14	11,14	11,14	11,14
D21S11	29,30	29,30	29,30	29,30
D7S820	9,12	9,11,12	9,12	9,12
CSF1PO	10,10	10,11	10,10	10,10
D3S1358	17,17	15,17	17,17	17,17
TH01	6,9.3	6,9.3	6,9.3	6,9.3
D13S317	10,12	10,12	10,12	10,12
D16S539	12,12	11,12	12,12	12,12
D2S1338	19,25	19,25	19,25	19,25
D19S433	14,14	14,14	14,14	14,14
vWA	17,18	14,17,18	17,18	17,18
TPOX	8,8	8,8	8,8	8,8
D18S51	12,13	12,13,17	12,13	12,13
AMEL	X,X	X,X	X,X	X,X
D5S818	11,12	11,12	11,12	11,12
FGA	21,21	21,25	21,21	21,21

Client Sample Name	EP2C004 C2	EP2C004 C4	EP2C004 C5	F.EP2C004
Sample Code	CL00002197	CL00002198	CL00002199	CL00002202
D8S1179	11,14	11,14	11,14	11,14
D21S11	29,30	29,30	29,30	29,30
D7S820	11,12	11,12	11,12	11,12
CSF1PO	11,11	11,11	11,11	11,11
D3S1358	15,15	15,15	15,15	15,15
TH01	6,9.3	6,9.3	6,9.3	6,9.3
D13S317	12,12	12,12	12,12	12,12
D16S539	11,11	11,11	11,11	11,11
D2S1338	18,25	18,25	18,25	18,25
D19S433	14,14	14,14	14,14	14,14
vWA	14,17	14,17	14,17	14,17
TPOX	8,8	8,8	8,8	8,8
D18S51	12,17	12,17	12,17	12,17
AMEL	X,X	X,X	X,X	X,X
D5S818	11,12	11,12	11,12	11,12
FGA	21,25	21,25	21,25	21,25

Figure S2.9. Cell Line Authentication results of the parent fibroblasts and the generated iPSC lines.

16 different STR genomic Loci were tested in both parental fibroblast lines and derived iPSC lines to validate the origin of each iPSC line.

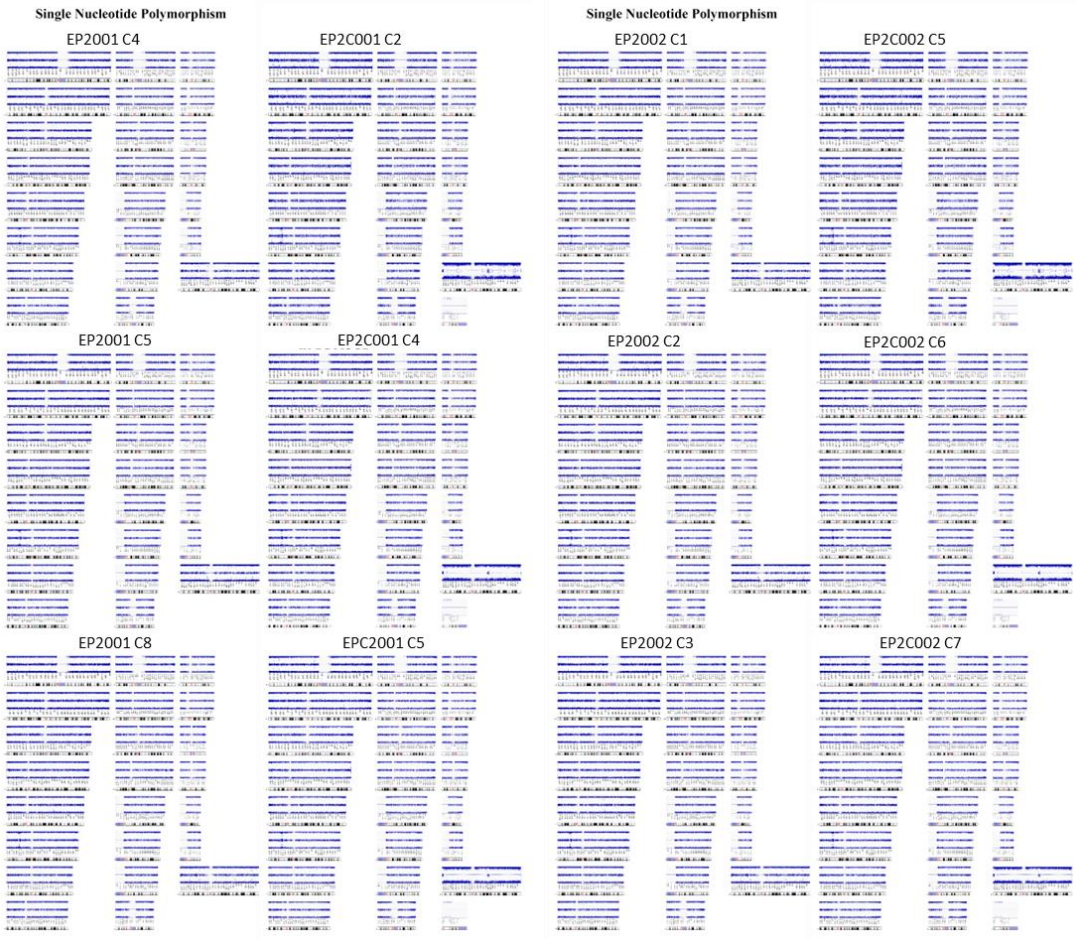

Figure S2.10. Log2 ratio results showing no gross chromosomal abnormalities were introduced during reprogramming.

The SNP data (Log2 ratio) of all generated IPSC lines. No major chromosomal abnormalities were found.

Chapter 3: Genome-Editing of iPSCs Using CRISPR/Cas9 technology and iPSC-Derived Cortical Neurons Using the microRNA mir-34a

3.1 Introduction

The editing of disease-causing genetic mutations has the potential to revolutionise disease modelling, save lives and improve the outcome of genetic diseases for many patients. The earliest methods of gene editing included gene targeting via homologous recombination, zinc Finger Nuclease (ZFNs) and Transcription Activator-like Effector Nucleases (TALENS) (Urnov et al., 2010). The ZFNs and TALENS methods utilised engineered DNA-cleaving enzymes and were successful tools used for the development of therapeutics for mutations in the *HBB* gene as well as the editing of immune cells in childhood cancer (Qasim et al., 2017). However, these tools lacked sufficient accuracy and specificity and were time-consuming due to the amount of design, synthesis and validation required (Doudna, 2020). Since then, the development of the CRISPR (clustered regularly interspaced short palindromic repeats)-Cas9 system for genome-editing has made gene-editing more efficient, accessible, and cost-effective (Jinek et al., 2012). In this **Chapter**, I will discuss our attempts at using CRISPR-Cas9 technology to generate isogenic mutant and control lines and outline the benefits of genome-editing in therapeutics and disease modelling.

3.1.1 CRISPR-Cas9 background principles

In the CRISPR-Cas9 system, a protospacer adjacent motif (PAM) sequence, usually 2-5bp in length, is needed for Cas9 to identify the target DNA sequence. Cas9 is the protein which assembles with the guide RNA (gRNA), either as two separate CRISPR targeting RNA (crRNA) and tracrRNA components or as a combined single guide RNA (sgRNA) (Jinek et al., 2012). The role of Cas9 is to bind and cut the DNA at the target site. This RNA-DNA binding occurs at approx. a 20bp DNA sequence, which is designed by the researcher, complementary to that of the nucleotide sequence in the gRNA (Gasiunas et al., 2012). The PAM sequence acts as a switch next to the DNA recognition site, causing the Cas9 protein to perform a double-stranded DNA break at the target site. This DNA break induces DNA repair by either Non-Homologous End Joining (NHEJ), or Homology Directed Repair (HDR) **(Figure 3.1)** (Szostak et al., 1983). HDR can take place by using homologous chromosomal DNA or a DNA template. The HDR mechanism is considered to be more accurate but less efficient than NHEJ (Stark et al., 2004).

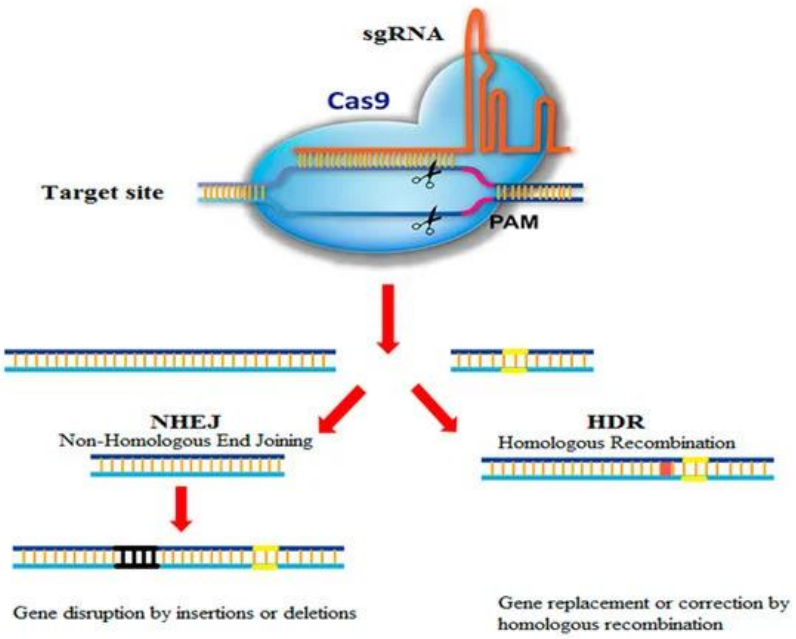

Figure 3.1: Schematic illustration of CRISPR-Cas9 genome-editing system.

A single guide RNA (sgRNA) molecule can be synthesized by joining the target sequence (without PAM) with crRNA and TracrRNA. The Cas9/sgRNA complex can find the target genomic DNA sequence and Cas9 cleaves DNA at 3-4bp 5' of the PAM sequence. Cells can repair the double DNA break via efficient NHEJ which may introduce small deletion or insertion, or by efficient mechanism of HDR with high fidelity (Tavakoli et al., 2021).

The Cas9 of *streptococcus pyogenes* is the most used enzyme in CRISPR-Cas9 experiments in the recent decade (Knott et al., 2018), whereas, a wide range of Cas9 homologues are constantly being explored as alternatives (Liu et al., 2019). For CRISPR-Cas9 technology to be effective and safe, editing needs to be extremely accurate. As previously mentioned, when a double stranded DNA break occurs, HDR or NHEJ repair occurs in the cell. HDR is typically not used as frequently as NHEJ in cells. Additionally, a cell can use both forms of repair at the same time, generating different alleles of an edited gene (Chatterjee et al., 2017). Two double-stranded breaks occurring in parallel may also leads to chromosomal translocations (Gómez-Herreros, 2019). Therefore, there is great desire to strictly control the form of DNA repair that occurs after a double-stranded DNA break. Alternatively, researchers have developed methods to perform CRISPR-Cas9 mediated genome editing without the DNA cleavage step. This has been achieved by directly altering the chemical sequence and by creating RNA templates for gene alteration (prime editing)(Qi et al., 2013).

The most commonly used strategy for the delivery of CRISPR-Cas9 components *in vitro* is electroporation. Electroporation involves pulsing the cells with a high-voltage current that

generates temporary pores in the cell membranes of approx. 1nM in size (Remy et al., 2017). This enables CRISPR-Cas9 ribonucleoprotein (RNP) complex to effectively enter the cells. Optimisation of electroporation parameters is necessary to balance transfection efficiency with the level of stress to the cells. While a percentage of cell death after electroporation is expected, if parameters such as voltage, time and number of pulses are not optimised, excessive cell death may occur (Batista Napotnik et al., 2021).

3.1.2. CRISPR-Cas9 and iPSC modelling

One of the main advantages of the CRISPR-Cas9 system in disease modelling is the ability to rescue the mutation in iPSCs from patients, thus allowing creation of isogenic iPSC lines to minimise heterogeneity, to elucidate the effects of the mutation and to provide a proof of principle for gene therapy (De Masi et al., 2020). Genome edited iPSC-derived cells such as neurons have various other uses such as drug development and screening **(Figure 3.2)**. Additionally, introducing the mutation in a control cell line can allow us to examine the disease effects *in vitro* with minimal influence from genetic background (Torres-Ruiz at al., 2017). In an optimal experiment, a patient line, a closely related control line, a mutation-corrected patient isogenic line and an isogenic mutant line of control iPSCs should be included. In this study, we aimed to perform a two-pronged approach to (1) rescue the human *KCNQ2*-DEE mutation (A294V) in the patient line EP2001 C4 and (2) introduce the mutation (A294V) in the control line EP2C001 C2 to generate an isogenic control and isogenic patient line, respectively. We chose this mutation as this is a recurrent mutation in *KCNQ2*-DEE with a severe phenotype.

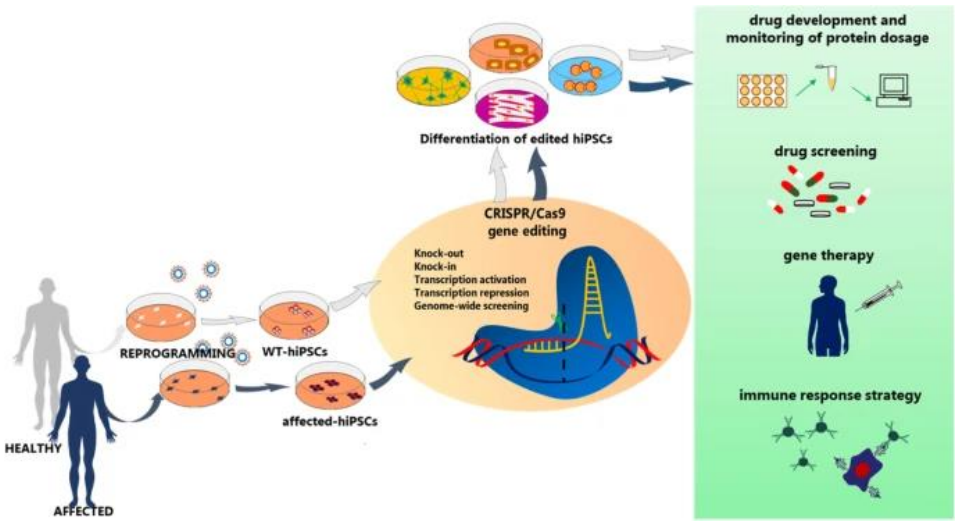

Figure 3.2: Schematic illustrating the various uses of gene-edited iPSCs.

Somatic tissues taken from either healthy controls or patients can be reprogrammed into iPSCs which can then undergo CRISPR/Cas9 gene editing to either introduce a mutation or correct the mutation. These edited cells can then be differentiated into different cell types such as neurons or muscle cells which can then be used for disease modelling, drug development and gene therapy (De Masi et al., 2020).

3.1.3 miRNAs and gene regulation

An alternative method of controlling gene expression is the use of microRNAs (miRNAs). miRNAs are short, non-coding RNA sequences that control gene expression post-transcriptionally. They can be used to silence gene expression by binding to the 3' untranslated region of their mRNA targets causing the mRNA to degrade, resulting in reduced protein production and translational silencing (Ha et al., 2014). However, miRNAs have also been reported to bind with 5' untranslated regions and gene promoters (Broughton et al., 2016) and activate gene expression (Vasudevan, 2012). Thus, the roles of miRNAs are very diverse. In monogenetic diseases such as *KCNQ2*-DEE, the use of miRNAs known to interact with mutant *KCNQ2* mRNA can be an attractive therapeutic approach. Mir-34a is a miRNA that has been shown to be enriched in the brain and is upregulated during neuronal differentiation and maturation (Jauhari et al., 2018). Using TargetScan (targetscan.org), we found that mir-34a targets our gene of interest, *KCNQ2*. A third aim of the work presented in this Chapter, is proof of principle approach to transfect cells with mir-34a to analyse its effects on *KCNQ2* expression.

3.2 Materials and Methods

3.2.1 Design of single-stranded guide RNA and single-stranded donor oligonucleotide

Based on the variant information for EP2001, single-stranded guide RNAs (sgRNA) and single-stranded donor oligonucleotides (ssODN) were designed for introducing the *KCNQ2* variant (c.881C>T, A294V) into a sibling control line and rescuing the mutation in a patient line, respectively. This was done using a publicly available design tool (https://zlab.bio/guide-design-resources) from Integrated DNA Technologies (IDT, USA). Briefly, a 200bp length of wild-type (WT) genomic DNA sequence (Human Gene *KCNQ2*) surrounding the pathogenic variant of interest ("C" coloured in red) (5'-CGGATGCACTCTGGTGGGGCCTGATCACGCTGACCACCATTGGCTACGGGGACAAGTACCCCCAGACCTGGAACGGCAGGCTCCTTGCGGCAACCTTCACCCTCAT**CGG**TGTCTCCTTCTTCGCGCTGCCTGCAGGCATCTTGGGGTCTGGGTTTGCCCTGAAGGTTCAGGAGCAGCACAGGCAGAAGCACTTTGAGAAG-3') was uploaded onto the IDT website (https://sg.idtdna.com/site/order/designtool/index/CRISPR_CUSTOM) to identify the most suitable 20-nucleotides (nt) sgRNA sequence, with a PAM sequence. We designed the two ssODNs to be 100-nt oligo in length with the variant located in the middle, with ~40-50-nt flanking either side of the mutation to mediate homologous recombination **(Table 3.1).** Based on the predicted on-target and off-target scores, we chose the most optimal sgRNA which had a minimal distance between the variant to be edited and the cut site **(Figure 3.3)**. We then designed primers for sgRNA DNA template synthesis, and the ssODN templates for both the introduction of the *KCNQ2* pathogenic variant in the healthy control iPSC line and the rescue of the phenotype in the patient iPSC lines via HDR. These are listed in **Table 3.1**. All the oligonucleotides were ordered from IDT.

Table 3.1 Primers for sgRNA synthesis and ssODN templates

KCNQ2 (MI) ssODN	ACCACCATTGGCTACGGGGACAAGTACCCCCAGA CCTGGAACGGCAGGCTCCTTGTGGCTACATTTACATTA ATCGGTGTCTCCTTCTTCGCGCTGCCTGCAgtaagtccagctgcccct
KCNQ2 (rescue) ssODN	ACCACCATTGGCTACGGGGACAAGTACCCCCAGACCT GGAACGGCAGGCTCCTTGCGGCTACATTTACATTAAT CGGTGTCTCCTTCTTCGCGCTGCCTGCAgtaagtccagctgcccct
KCNQ2 (MI) For	5'TAATACGACTCACTATAGGTGGCAACCTTCACCCTCAT 3'
KCNQ2 (MI) Rev	5' TTCTAGCTCTAAAACATGAGGGTGAAGGTTGCCAC 3'
KCNQ2 (rescue) For	5'TAATACGACTCACTATAGGCGGCAACCTTCACCCTCAT 3'

KCNQ2 (rescue) Rev	5’ TTCTAGCTCTAAAACATGAGGGTGAAGGTTGCC**G**C 3’

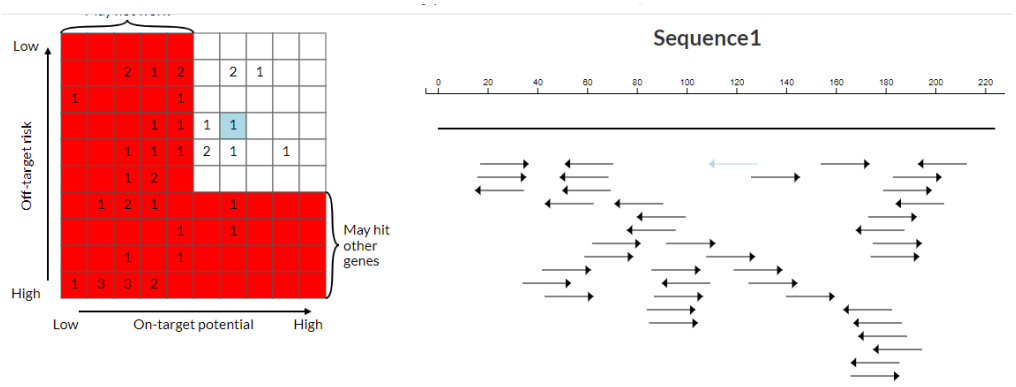

Position	Strand	Sequence	PAM	On-target score	Off-target score
109	-	G**C**GGCAACCTTCACCCTCAT	CGG	62	63

Position	Strand	Sequence	PAM	On-target score	Off-target score
51	-	GCTGACCACCATTGGCTACG too far 5’	GGG	68	83
Position	Strand	Sequence	PAM	On-target score	Off-target score
63	-	GCGGCAACCTTCACCCTCAT	CGG	62	63

Figure 3.3: Information of candidate sgRNAs provided by IDT software.

A 200-nt sequence flanking the variant was uploaded onto the IDT program. All 20-nt sequences 5’ of any NGG or 3’ of any CCN were aligned to the whole human genome. Candidate sgRNA designs were competed for on-target specificity and off-target unintended nuclease activity. The target and off-target were scored by the program based on the number and position of mismatches of chromosomal regions to the 20-mer sequence and shown on the left. A high on-target score suggests a high efficacy of the sgRNA binding to the pre-selected target, with a low number of other non-specific chromosomal loci which have sufficient length of matches for pairing. A high off-target score means there are fewer chromosomal regions which can bind the 20-mer RNA with sufficient match at 3’ end and followed by NGG. An ideal sgRNA would appear in the top right corner of white boxes and physically locate in a close vicinity of the variant. On the right, the line represents the input 200bp *KCNQ2* sequence on the top, and all putative sgRNA are shown below with forward arrows to right to indicate putative gRNA from the + strand of DNA, and or arrows to left for (-) strand DNA sequence.

3.2.2. sgRNA synthesis

Step 1

The *KCNQ2*(MI)-sgRNA and *KCNQ2*(Rescue)-sgRNA were selected as the optimal sgRNAs and were synthesized using the GeneArtTM Precision gRNA Synthesis Kit (Invitrogen, Cat.A29377). Briefly, a 120bp short sgRNA template DNA was synthesized by PCR assembly using the following: three complementary DNA fragments of designed sgRNA Forward oligo, sgRNA reverse oligo and the commercial cr/Tracr Fragment, Universal Forward primer, Universal Reverse primer and T7 Primer Mix were set up in a test tube together with other PCR reagents from the kit **(Table 3.2)**. PCR assembly of the gRNA DNA template included the following:

Table 3.2: Step 1 of protocol for *in vitro* sgRNA synthesis

Component	**Volume**
Phusion™ High-Fidelity PCR Master Mix (2×)	12.5µl
Commercial mix of Tracer Fragment +Universal Forward primer, Universal Reverse primer +PCR Mix	1µl
0.3µM Forward and Reverse oligonucleotide mix	1µl
Nuclease-free water	10.5µl
Total	25µl

Step 2

PCR was performed under the following reaction conditions: [98°C for 10s (initial denaturation) for one cycle; Denaturation at 98°C 5s, Annealing and extension at 55°C 15s for 32 cycles; extension at 72°C 1min for 1 cycle; and finally, 4°C (Hold)]. 5µl of the PCR product (gRNA DNA template) was used for gel electrophoresis on 1.5% Agarose gel, and 6µl of the PCR product was used directly in the following in vitro transcription (IVT) reaction. The IVT reaction was set up as described in **Table 3.3**. The sgRNA synthesis was carried at 37°C for 3 hours. DNase I (1U/µl) was added to the reaction mix for digesting DNA templates and primers at 37°C for 15min.

Table 3.3: Step 2 of protocol for *in vitro* sgRNA synthesis

Component	**Volume**
NTP mix (100mM each of ATP, GTP, CTP, UTP)	8µl

gRNA DNA template (taken from step 1)	6µl
5× TranscriptAid™ Reaction Buffer	4µl
TranscriptAid™ Enzyme Mix	2µl
Total	20µl

Step 3

Then sgRNA was purified using the gRNA Clean Up Kit (included in GeneArtTM Precision gRNA Synthesis Kit). Briefly, the volume of IVT reaction (20µl) was adjusted to 200µl with nuclease-free water (180µl) and mixed thoroughly with 100µl of binding buffer. One volume (300µl) of 96% ethanol was added to the mix and then transferred into a GeneJET™ RNA Purification Micro Column to purify the sgRNA. The purified sgRNA was finally eluted in 20µl of nuclease-free water.

Step 4

Finally, the quality of the sgRNA was determined by mixing the sgRNA with RNA Loading Dye (2X) Solution (NEB, Cat.B0363S) and heating at 70°C for 10min and running on 2% electrophoresis with a Low Range ssRNA Ladder (NEB, Cat.N0364S). The concentration of sgRNA was measured using Nanodrop 2000 Spectrophotometer (ThermoFisher, ND2000), and then stored at -80°C until required.

3.2.3 Electroporation using the Neon transfection system

Four to five wells of iPSC colonies with approximately 70- 80% confluence in 6-well culture plates were treated with ROCK (Rho-associated protein kinase) inhibitor Y-27632 (STEMCELL, Cat.#72302) for 1h at a final concentration of 10µM. On ice, 10 µM of Cas9 protein and sgRNA in TE Buffer, was prepared. The conditioned E8 medium was removed from the cells (kept for later cell resuspension step) and cells were rinsed with DPBS. Tryple Select (1ml per well) was added, and the cells incubated at 37°C for approx. 8 mins, checking cells periodically under the microscope to examine morphology changes. Cells were resuspended in E8 medium kept from the previous stage by carefully pipetting slowly and transferred (cells) into a 15ml centrifuge tube. Cells were centrifuged at 100g for 4 min. Cells were resuspended in 1ml of E8 medium supplemented with Y-27632 and cell counting was performed using a haemocytometer. After the cell count, 1 x 10^6 cells were transferred into a new 1.5ml

centrifuge tube and were centrifuged at 200g for 3 min. Cells were then resuspended in 100µl of buffer R and incubated at 37°C. Any remaining cells were seeded into Geltrex-coated 6 well plates. Next, the RNP (ribonucleoprotein) complex was prepared as outline in **Table 3.4** and left to incubate at room temperature for 15 min.

Table 3.4: RNP complex components

Component	**Volume**
Cas9 Protein (10µM)	2µl
sgRNA (10µM)	2µl
Buffer R	6µl
Total	10µl

The ssODN was also prepared by combining 5µl of ssODN-*KCNQ2* (MI) or (Rescue) (600ng/µl) with 5µl of buffer R. The RNP complex, cell suspension and ssODN template were mixed together in a small tube as described in **Table 3.5**. 100µl of the electroporation mix was carefully transferred into a Neon 100µl tip using the Neon pipette, carefully avoiding the formation of any bubbles. The Neon pipette was placed into the Neon chamber which contained 3ml of Buffer E2, within the Neon Pipette Station, and electroporated under optimized programme (1300V, 30ms and 1pulse), according to the instructions of the manufacturer.

Table 3.5: Electroporation reaction setup

Component	**Volume**
RNP complex	10µl
Cell suspension ($1x10^6$ iPSCs in 100µl)	50µl
ssODN template (10µM)	10µl
Buffer R	70µl

3.2.4. Single cell expansion

Immediately after electroporation, cells were resuspended in 2ml Essential 8™ Flex Medium (supplemented with 1% (V/V) RevitaCell Supplement) and transferred on a noncoated 6-well plate. Cells were then seeded as single cells or onto a separate plate to form a cell pool. Single

iPSCs were manually picked and seeded directly into one well of a Geltrex-coated 48-well plate (Sarstedt, Cat.#83.3924.300) in 300µl Essential 8™ Flex Medium with 1% (V/V) RevitaCell Supplement. The remaining cells were seeded in two wells of a Geltrex-coated 6-well plate as the cell pool. Eighteen hours later, microscopic examination was carried out. The wells with a single iPSC inside were marked for expansion while any wells with multiple cells were excluded. The culture medium was changed to fresh Essential 8™ Flex Medium without RevitaCell Supplement 48h after electroporation. Once the colonies were large enough after approx. 2 weeks, each colony was passaged onto a well of a 12 well plate using Gentle Cell Dissociation Reagent. iPSCs were cultured as previously described in **Chapter 2** for cell expansion.

3.2.5. On target PCR screening

Genomic DNA was extracted from the cells as previously described in **Chapter 2** for on-target PCR sequencing. The *KCNQ2* EP2001 primer (For: GCTCACTCGCTGATACTTCC and Rev: GTCATCAGGACACGTAGCTA) was used for the screening of the *KCNQ2* genome-edited clones. Genomic DNA (100ng) was used to amplify the *KCNQ2* gene flanking the nucleotide variant by using AllTaq Master Mix (Qiagen, Cat.#203144) and was then purified by QIAquick PCR Purification Kit according to the instructions of the manufacturer. Purified PCR products were submitted to Eurofins Genomics (Germany) for Sanger sequencing with the Forward primer.

3.2.6 In vitro digestion of DNA with Cas9 Nuclease

In vitro digestion of DNA with Cas9 Nuclease was carried out to examine gRNA/Cas9 on-target cleavage activity. All components of the *in vitro* digestion reaction were combined as outlined in **Table 3.6**. The components were mixed thoroughly and pulse-spun in a micro centrifuge tube. The reaction was incubated at 37°C for 15 min. 1µl of proteinase k was added to the reaction and pulse spun. The reaction was incubated at room temperature for 10 min. The DNA was analysed on a 1.5% agarose gel.

Table 3.6: In vitro digestion of DNA template using RNP complex

Component	Volume
Nuclease-free water	20µl
NEbuffer r3.1	3µl
300nM sgRNA	3µl (30nM final)
1uM cas9 nuclease	1µl (30nM final)

Pre-incubate for 10 min at 25°C	
30nM substrate DNA	3µl (30nM final)
Total	30µl

3.2.7 mir-34 treatment on iPSC-derived cortical neurons

Mir-34 (100nM), Mir-34 antagomir (100nM) and scrambled RNA (100nM) were added to separate wells of a 12-well plate of 100 day cortical neurons in patient lines (A265T) and control lines. Cells were incubated at 37° for 48 h. After 48 h, RNA was extracted from the cells using the Qiagen RNA extraction kit as described previously in **Chapter 2**. Single strand cDNA was synthesised using the RNA and was used for downstream qRT-PCR experiments. Additionally, cortical neurons were fixed 48 h after treatment with Mir-34, Mir-34 antagomir and scrambled RNA and stained using immunocytochemistry. Mir-34 was FITC labelled, allowing for identification by fluorescent imaging.

3.3 Results

3.3.1 Sanger sequencing confirms the presence of the mutation in iPSCs prior to gene-editing

To ensure there was no mislabelling of cells or cross-contamination between patient and control lines before performing gene editing using CRISPR/Cas9, we carried out Sanger sequencing on one patient line EP2001 C4 (A294V) and one control line EP2C001 C2. The sequencing results confirmed the presence of the mutation marked 'Y' (heterozygous T/C) in EP2001 C4 **(Figure 3.4 A)** and homozygous for C of the nucleotide in the sibling control line EP2C001 C2 **(Figure 3.4 B)**.

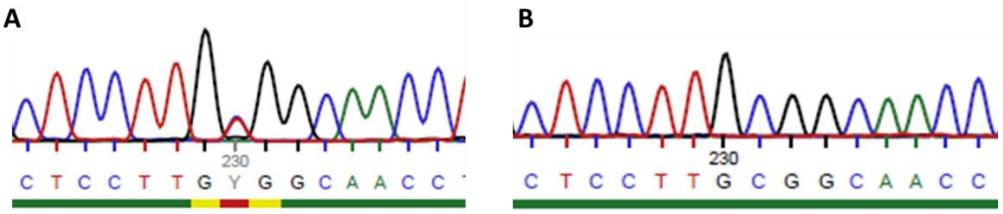

Figure 3.4: Sanger sequencing results confirming the presence of the mutation in the patient line EP2001 C4 and the absence of the mutation in the control line EP2C001 C2.

(A) Sequencing results show the heterozygous mutation marked 'Y' from the mutation change (A294V) in the patient line EP2001 C4. **(B)** Sequencing results show the unchanged nucleotide 'C' at the mutation site in the sibling control line EP2C001 C2.

3.3.2 Synthesis of *KCNQ2* (MI) and (Rescue) templates

A short 120bp template for both *KCNQ2* (MI) and *KCNQ2* (Rescue) were synthesised by PCR as previously described, using three-fragment DNA PCR. We then electrophoresed these PCR products on a 1.5% agarose gel to visualise the product size. As seen in **Figure 3.5**, a single band appeared at approx. 120bp position for each PCR product, and this confirmed the successful generation of the two DNA templates required for the sgRNA synthesis in vitro.

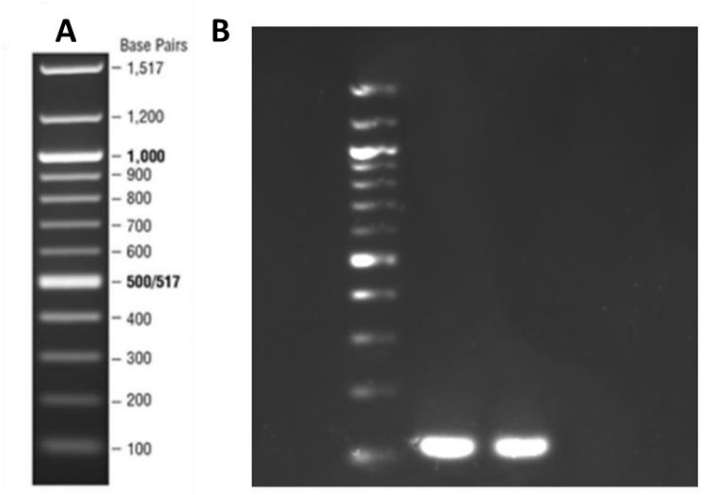

Figure 3.5: *KCNQ2* DNA templates (120bp) for mutation induction (left) and rescue (right) by three-fragment PCR.

(A) 100bp DNA ladder. (B) Double strand DNA templates for sgRNA synthesis generated by PCR for both mutation induction (left) and rescue (right).

3.3.3 Single cells attached 18 hours after electroporation

After electroporation, single cells were seeded into individual wells of a 48-well plate and were incubated for 18 hours to allow for cell attachment. After 18 hours, cells were examined under the light microscope to ensure that any cells that attached were single cells. At this point, if any double cells were found they were discarded. If two cells were located in the same well at a distance from one another, one cell could be manually removed from the well using a pipette tip. Wells with single cells were then marked and cultured for cell expansion. We found that approx. 15% of seeded single cells were capable of attachment and survival. Representative images of single cells are shown in **Figure 3.6**.

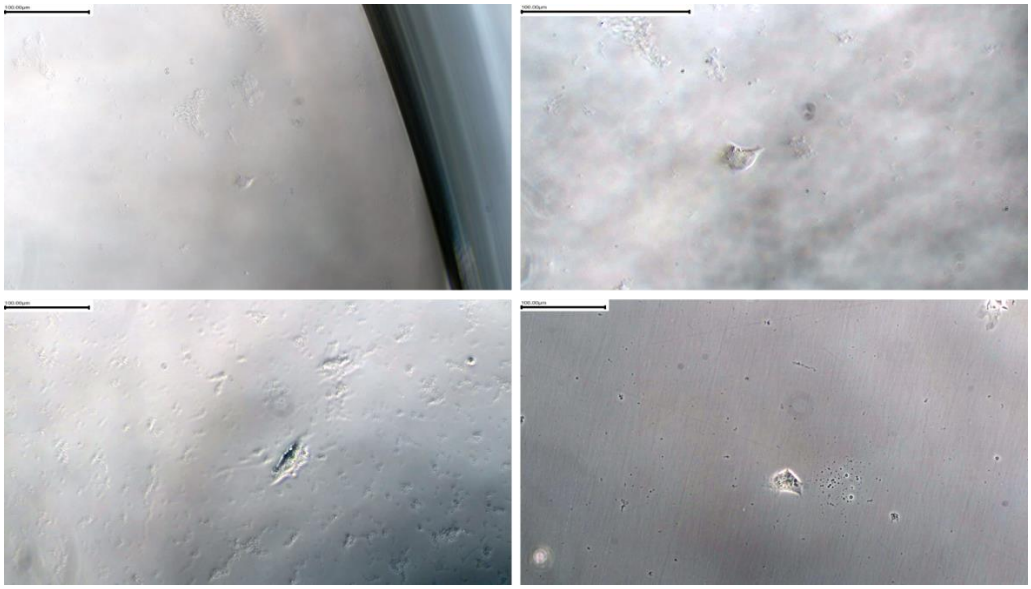

Figure 3.6: Representative images of single cells approximately 18 hours after electroporation.

Wells with single cells were expanded for sequencing analysis. Any wells with double cells were discarded. Magnification = 10X. Scale bar = 100µM.

3.3.4 Sanger sequencing results revealed no successful gene-editing at the target site

Using the *KCNQ2* (MI) sgRNA and template (Wt. DNA), we performed an electroporation to introduce the mutation in the patient cell line EP2C001 C2. We found that after electroporation there was an 80% cell survival rate. We extracted DNA from 46 single cell derived clones and sent the samples for Sanger Sequencing. We found that there was no heterozygous mutation in any of the single cell-derived cell lines after electroporation **(Figure 3.7)**. This result was unexpected, so we then decided to repeat the experiment again using the *KCNQ2* (rescue) sgRNA and template (mut DNA) in the control cell line. After electroporation, we saw a 68% cell survival rate, which was considerably lower than the previous attempt. We extracted DNA from 14 single cell-derived clones and sent the samples for Sanger sequencing. The sequencing results revealed no successful editing at the target location. As seen in **Figure 3.8**, the heterozygous mutation marked 'Y' is unchanged for each of the cell lines. Based on these results, we began to troubleshoot the experiment to identify the problem.

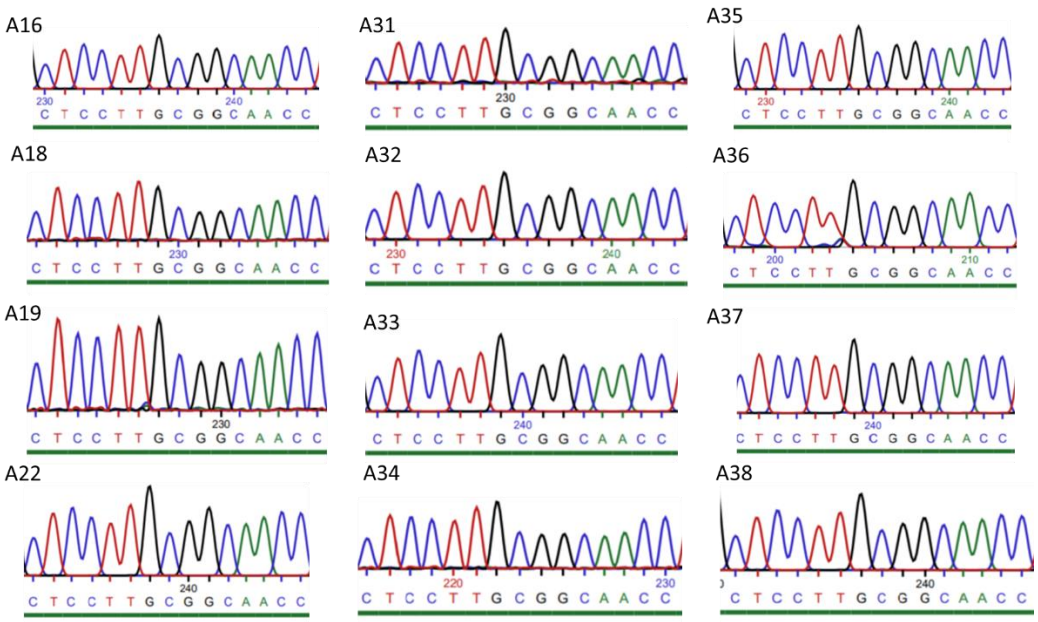

Figure 3.7: Representative images of Sanger sequencing results of EP2C001 C2 clones after electroporation showing no introduction of mutation at the target site.

Sequencing results from 12 individual single cell-derived clones reveal no successful introduction of the mutation (T) at the target site of C in the TTG**C**GG sequence.

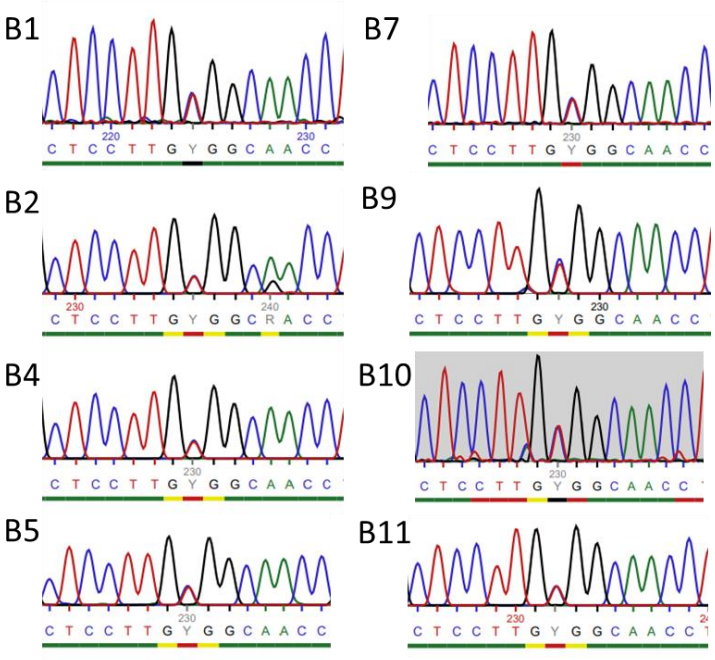

Figure 3.8: Representative images of Sanger sequencing results of EP2001 C4 clones after electroporation showing no rescue of mutation at the target site.

Sequencing results from 8 individual single cell-derived clones revealed no successful rescue of the mutation at the target site. The heterozygous mutation remains unchanged as seen marked by 'Y' rather than C as we would wish for.

3.3.5 In vitro digestion of template DNA by Cas9 nuclease showed Cas9 enzyme and sgRNA are working

The first step in troubleshooting for the lack of anticipated gene-editing in 46+14 clones after electroporation was to examine each of the individual components in the reaction. To do this, we performed an in-vitro digestion reaction using all the components in the RNP complex namely the template DNA of genomic PCR products, Cas9 enzyme and the designed sgRNA at the same concentrations they were used in the electroporation. We found that Cas9 was capable of cutting the template DNA (Wt DNA)(498bp) at the approximate correct locations resulting to two fragments of 216bp and 282bp, guided by the sgRNA **(Figure 3.9)**. These results demonstrated that the gRNA/Cas9 enzyme was working correctly, and that the sgRNA also guided Cas9 to cut at the correct location within the 498 bp target sequence. There was some DNA remaining uncut, suggesting that the Cas9 enzyme did not cut all of the DNA, which could be related to DNA:gRNA ratio, Cas9 activity and reaction conditions including reaction time.

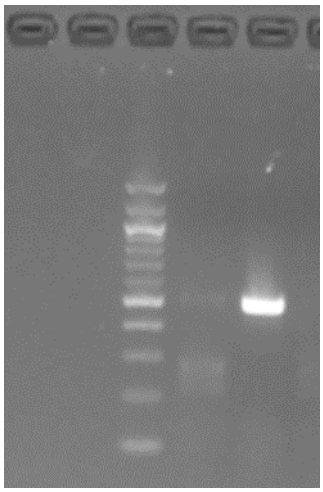

Figure 3.9: In vitro digestion of template DNA by Cas9 nuclease.

Lane 1 is 100bp DNA ladder. Lane 2 is in vitro digestion reaction (DNA template (Wt DNA) incubated with Cas9 enzyme and sgRNA). Lane 3 is template DNA alone. Wild type DNA template (498bp, lane 3) was successfully cut at the approximate correct locations resulting 216bp and 288bp by sgRNA (lane 2) guided Cas9 cleavage, A proportion (~20%) of DNA still remained at intact 498 bp position.

3.3.6 Transfection of iPSCs with fluorescently labelled mCherry plasmid revealed very low transfection efficiency

To determine whether the lack of gene-editing seen in our experiments was due to issues with delivery of the components into the cells, we transfected cells with a mCherry plasmid (pGL3-sgRab18.N-Cas9-T2A-mCherry-P2A-Puro) which was fluorescently labelled **(Figure**

3.10). 100k iPSCs were seeded into 1 well of a 6-well plate. After 24 and 48 hours, cells were examined under the fluorescent microscope to calculate the transfection rate. We found that less than 1% of iPSCs were fluorescently labelled at 24 and 48 hour **(Figure 3.10)**, suggesting a very low transfection efficiency. This plasmid was then transfected into the same iPSC line under the same or different electroporation conditions using a different electroporation system and over 50% of cells were fluorescently labelled with the mCherry plasmid. These results suggest a possible problem with the Neon transfection system we used to carry out the electroporation.

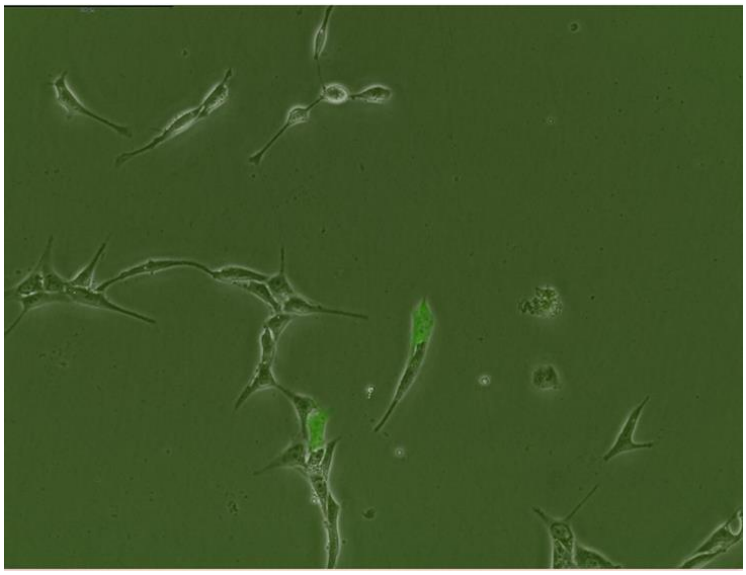

Figure 3.10: Image of iPSCs electroporated with an mCherry plasmid to analyse transfection efficiency.

Transfection efficiency using the mCherry plasmid in iPSCs was less than 1%. Image is not representative of the entire well. A total of 6 fluorescent cells were visible in the well out of 100,000 cells seeded into the well.

3.3.7 Mir-34 downregulates *KCNN2* and *KCNN3* expression in *KCNQ2*-DEE neurons

MicroRNAs are known for their ability to control gene expression, primarily be gene silencing (Duchaine et al., 2019). Mir-34-a (**5'** (Fl) mA(*)mC (*)mAmA mCmCmA mGmCmU mAmAmG mAmCmA mCmU(*) mG(*)mC (*)mC(*) mA (3'-Chl) **3'**) was found to interact with our gene of interest *KCNQ2* as well as two other genes *KCNN2* and *KCNN3* which were found to be upregulated in EP2004 (A265T) iPSC derived neurons **(see Figure 4.16 in Chapter 4)**. For this reason, we decided to treat these cortical neurons (generated in **Chapter 4**) with mir-34a in an attempt to silence the *KCNQ2* gene in our neurons. We transfected the cells with the cholesterol-linked mir-34a and extracted RNA from the cells after 48 hours of treatment. The

mir-34a was also FITC-labelled which allowed us to image the cells using a confocal microscope after 48 hours. We found that approx. 42% of cells were positive for mir-34a uptake **(Figure 3.11 A).** We then performed a qRT-PCR to measure the effects of mir-34a, the antagomir and scrambled RNA on the expression of *KCNQ2, KCNN2* and *KCNN3*. We found that mir-34a could successfully downregulate *KCNN2* and *KCNN3* expression, while the antagomir upregulated *KCNN3* expression. However, mir-34a had no effect on *KCNQ2* expression in patient neurons **(Figure 3.11 B)**.

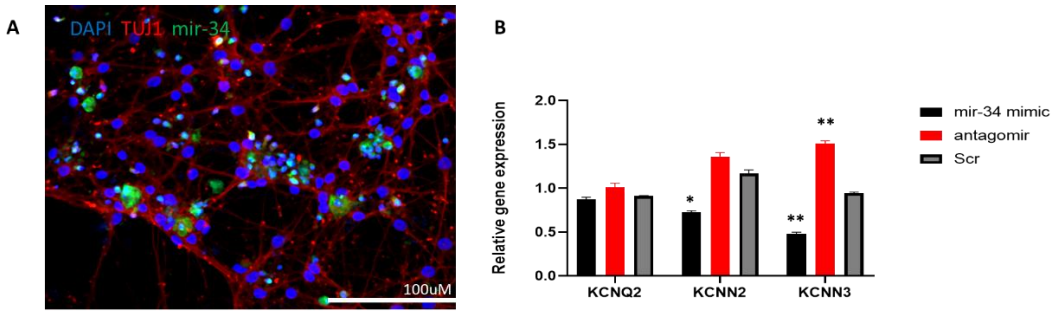

Figure 3.11: Mir-34 downregulates *KCNN2* and *KCNN3* expression in *KCNQ2*-DEE neurons.

(A) Immunocytochemistry analysis revealed a 42% uptake of mir-34 by *KCNQ2*-DEE cortical neurons (labelled in green). **(B)** qRT-PCR analysis showed mir-34a could downregulate the expression of *KCNN2* and *KCNN3* in *KCNQ2*-DEE neurons but had no significant effect on *KCNQ2* expression.

3.4 Discussion

Gene-editing using CRISPR-Cas9 has greatly improved the quality of disease modelling experiments as it enables the generation of isogenic lines to minimise genetic influence. This is of particular importance when studying monogenic diseases such as the genetic developmental encephalopathies and epilepsies, where genetic background is expected to have major influences on the disease (Gibson et al., 2017). Here, we designed two ssODN templates (wt and mutant) and corresponding sgRNA sequences to perform both the correction of the mutation in patient cells and the induction of the mutation in control cells. Attempts at both experiments were unsuccessful at introducing any changes in the genome at the target site among 60 clones screened, which was far lower than the anticipated gene targeting efficiency (~10%). To investigate the root cause of the problem, we performed several troubleshooting experiments. Furthermore, we investigated other methods of altering the gene expression of our mutated gene of interest, *KCNQ2*. Here, I will briefly discuss the results from the CRISPR-Cas9 experiments, the trouble-shooting experiments, and alternative strategies for altering gene expression.

Our results showed no effective gene-editing in either our correction or induction of mutation models **(Figure 3.7 and Figure 3.8)**. After the first electroporation (mutation induction), we saw approx. 20% cell death compared to the 32% cell death seen in the repeated experiment after the second electroporation (mutation correction). It has been reported that an expected level of cell death after electroporation is between 20% and 80% (Xu et al., 2021). However, rates of cell death seem to be higher in iPSCs than other cell types (Xu et al., 2018). Several studies suggest a correlation between high efficacy of genome-editing and high percentage of cell death, with studies reporting a cell death percentage of approx. 75% in iPSCs (Li et al., 2018). Furthermore, of the cells that do survive, cell proliferation is often poor (Jafari et al., 2017). In our experiments, the level of cell death was low compared to published results, and cells that did survive appeared to proliferate at normal rates. These results suggest that iPSCs did not undergo as much stress as expected during electroporation. This could indicate that insufficient current was applied to the cells, reducing the number of openings in the cell's membranes, which in turn could have prevented the RNP complex from efficiently entering the cells.

To determine the efficiency of the CRISPR-Cas9 RNP system in vitro, we performed a one-step cleavage or digestion of template DNA using the RNP complex. This technique is often used as a pre-validation step prior to electroporation (Mehravar et al., 2019). Our results showed

that the RNP complex was successful at cleaving DNA at the approximate correct locations according to the gel analysis **(Figure 3.9)**. This result suggests that all the components in the RNP complex i.e., the Cas9 enzyme, the ssODN template and the sgRNAs were all working effectively. This was a useful troubleshooting experiment as it had excluded the possibility that the lack of gene-editing we witnessed was as a result of poor gRNA in the RNP complex or inactive Cas9.

When we performed a literature search to investigate potential causes for the lack of gene-editing seen in our cell lines, we found that there is a huge level of variability in CRISPR-Cas9 experiments. Different studies reported the use of different instrument settings, varying concentrations of the components within the RNP complex, different optimal cell passage number and different cell sources (Sledzinski et al., 2021). For this reason, there is conflicting advice on which parameters are optimal for a specific cell type. Many groups have reported a lack of gene-editing after electroporation using the RNP complex (Modarai et al., 2018). To combat this, researchers have simply increased the amount of RNP introduced to the cells in an attempt to force gene-editing. However, this brings its own set of problems such as reduced cell viability and difficulties for translation to the clinic. In my opinion, improved standardisation for CRISPR-Cas9 experiments are necessary to enhance gene-editing efficiency to ensure experiments and reliable and reproducible.

To determine whether the lack of gene-editing seen in our cell lines was due to inefficient delivery of the RNP complex into the cells, we transfected the same cell line (EP2001 C4) with a fluorescently labelled plasmid **(Figure 3.12)** and calculated the percentage of cells containing the plasmid after 24 and 48 hours. For this experiment, we ensured to keep all other conditions the same as previous experiments used for *KCNQ2* editing. We found that less than 1% of iPSCs contained the fluorescently labelled plasmid both 24 and 48 hours after electroporation **(Figure 3.10)**. Importantly, the exact same experiment was set up using a different electroporation system soon after and the transfection efficiency was >50%. These results suggest that a lack of gene-editing seen in our cell lines was due to inefficient delivery of the RNP complex into the cells. At the rate of transfection efficiency seen using our electroporation system, we would need to screen hundreds of single cell-derived lines to capture a gene-edited line.

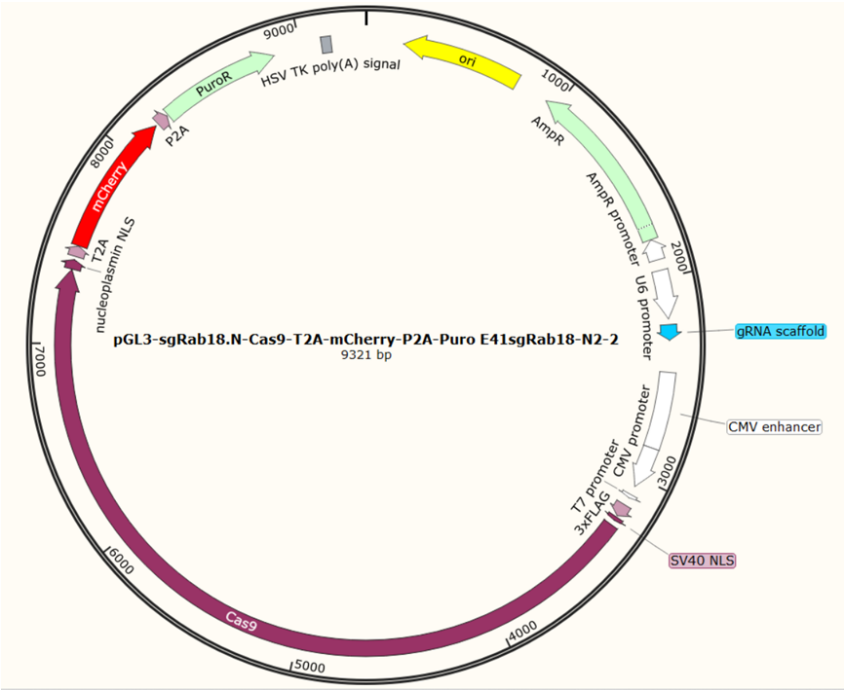

Figure 3.12 mCherry construct.

Structure of mCherry plasmid used to test delivery efficiency in electroporation experiments.

Moving on from gene editing experiments, as a proof of principle experiment, we wanted to explore the capacity of the miRNA, mir-34a-5p, to silence *KCNQ2* expression in our cell models. We chose to transfect cells after neuronal differentiation from iPSCs to cortical neurons (described in **Chapter 4**), as *KCNQ2* would be more highly expressed in neurons compared to iPSCs. Additionally, we chose mir-34a because it could target two other K^+ channel genes which were shown to be upregulated in our disease models **(Figure 4.16)**. Our mir-34a mimic was cholesterol-linked and fluorescently labelled meaning it could enter the cells and be easily visualised as shown by fluorescent imaging **(Figure 3.11)**. Furthermore, we found that mir-34a mimic could successfully downregulate the expression of *KCNN2* and *KCNN3* in our disease models **(Figure 3.11)**. However, we saw no significant effect on *KCNQ2* expression. Some interesting follow up experiments would be to perform phenotypic analysis of cortical neurons treated with mir-34a to determine whether the upregulation of *KCNN2* and *KCNN3* are contributing to the hyper-excitable phenotype in our disease models. Furthermore, the exploration of other miRNAs that may downregulate mutant *KCNQ2* expression would also be interesting. In my opinion, a mutation-specific and personalised therapy approach, holds great promise for the treatment of these rare *de novo* mutations.

Chapter 4: Differentiation of Cortical Excitatory Neurons from Human (patient)-derived iPSCs

4.1 Introduction

Developmental and Epileptic Encephalopathy (DEE) can be defined as epilepsies where patients experience severe seizures coupled with developmental delay, where often the developmental disorder is also a result of the aetiology (in this case genetic aetiology) as well as in part due to the epileptic activity (Hamdan et al., 2017). In DEEs seizures are often severe and drug resistant (Scheffer et al., 2020). In DEE, the epileptic encephalopathy component of the disease may be improved by seizure control by anti-seizure medications (ASMs) for some patients. However, a developmental component of the disease often remains as these developmental delays are intrinsically linked to the genetic cause of their epilepsy (Gardella et al., 2018). Therefore, treating patients with ASMs to control seizures do often not usually greatly impact the developmental impairment, or may only do so to a varying degree depending on the specific disorder in question.

To develop better treatment options which may directly tackle the root cause of the disease, a better understanding of the pathophysiology and phenotypical characteristics of the disease are needed. What complicates this matter is that there are hundreds of reported *KCNQ2* mutations that are linked to DEE, where the disease phenotype may vary significantly depending on the location of the mutation within the gene (Zhang et al., 2020). This also means there is likely mutation-specific (variant-specific) pathophysiology in some *KCNQ2*-DEEs, resulting in the potential need for individualised precision-therapies. Patient-specific iPSCs provide the ideal 'disease in a dish' model which will allow us to carefully examine the mutation-specific disease effects *in vitro*. Understanding the key stages of brain development involved in cortical growth and folding and how *KCNQ2* is involved in brain development and cortical excitability are critical to discovering new therapeutic targets.

In this **Chapter**, we will first give a brief background to developmental brain (cortex development), the role of KCNQ2 in brain development and a brief summary on the current progress of *in vitro* disease modelling in *KCNQ2*-DEE patients.

4.1.1 Anatomy of the cerebral cortex

The growth and organisation of the human cerebral cortex during brain development are crucial factors that affect human sensorimotor and cognitive abilities (Lee et al., 2019). Any disruption that occurs during this stage of brain development can lead to neurological

disorders with seizures, physical, cognitive, and intellectual disabilities seen in the genetic DEEs. The neocortex accounts for over 90% of the surface area of the cortex. It is folded into sulci and gyri to allow for a reduction in brain volume **(Figure 4.1)**(Klyachko et al., 2003). The neocortex is divided into 6 distinct layers (layers I to VI). There are two major cell types found in the cortex; pyramidal neurons which are excitatory neurons that comprise approximately 80% of all cells in the cortex, and interneurons which are inhibitory neurons which make up the remaining 20% of cells (Raybaud et al., 2011). Pyramidal neurons form long glutamatergic (excitatory) circuits while interneurons establish local GABAergic (inhibitory) connections between pyramidal neurons (Squier et al., 2010).

4.1.2. Normal development of the human cortex

The cerebral cortex is formed from neuroepithelial cells (NECs). During the fourth week of development, NECs proliferate in the neural plate until the neural tube closes (Bystron et al., 2008). From this point onwards, cells divide by asymmetric division whereby one neuron and one stem cell are generated. This results in differentiated neurons residing in the periphery or preplate (PP), while the stem cells are located in the deep germitive zone known as the ventricular zone (VZ)(Supèr et al., 1998). New excitatory neurons must migrate via radial migration from the VZ, where they are formed, to the surface of the cortex. This process is assisted by radial glial cells (RGCs), otherwise known as neuroepithelial progenitor cells (NPCs). Cells that migrate to the VZ during the earlier stages of development end up in the deep cortex layers, while cells that migrate later pass over the deeper layers and reside in the outer cortex layers (Nadarajah et al., 2002). Apart from their role in assisting the migration of pyramidal neurons to the surface of the cortex, RGCs are also progenitor cells which give rise to both neurons and astrocytes (Pontious et al., 2008). Interneurons migrate differently to excitatory neurons. They are made in the medial ganglionic eminence and move via tangenital migration toward the cortex. These interneurons interact with pyramidal neurons during this process to acquire positional information, thus, the complex interactions between excitatory and inhibitory neurons are crucial for normal cortex development (Kriegstein, 2005).

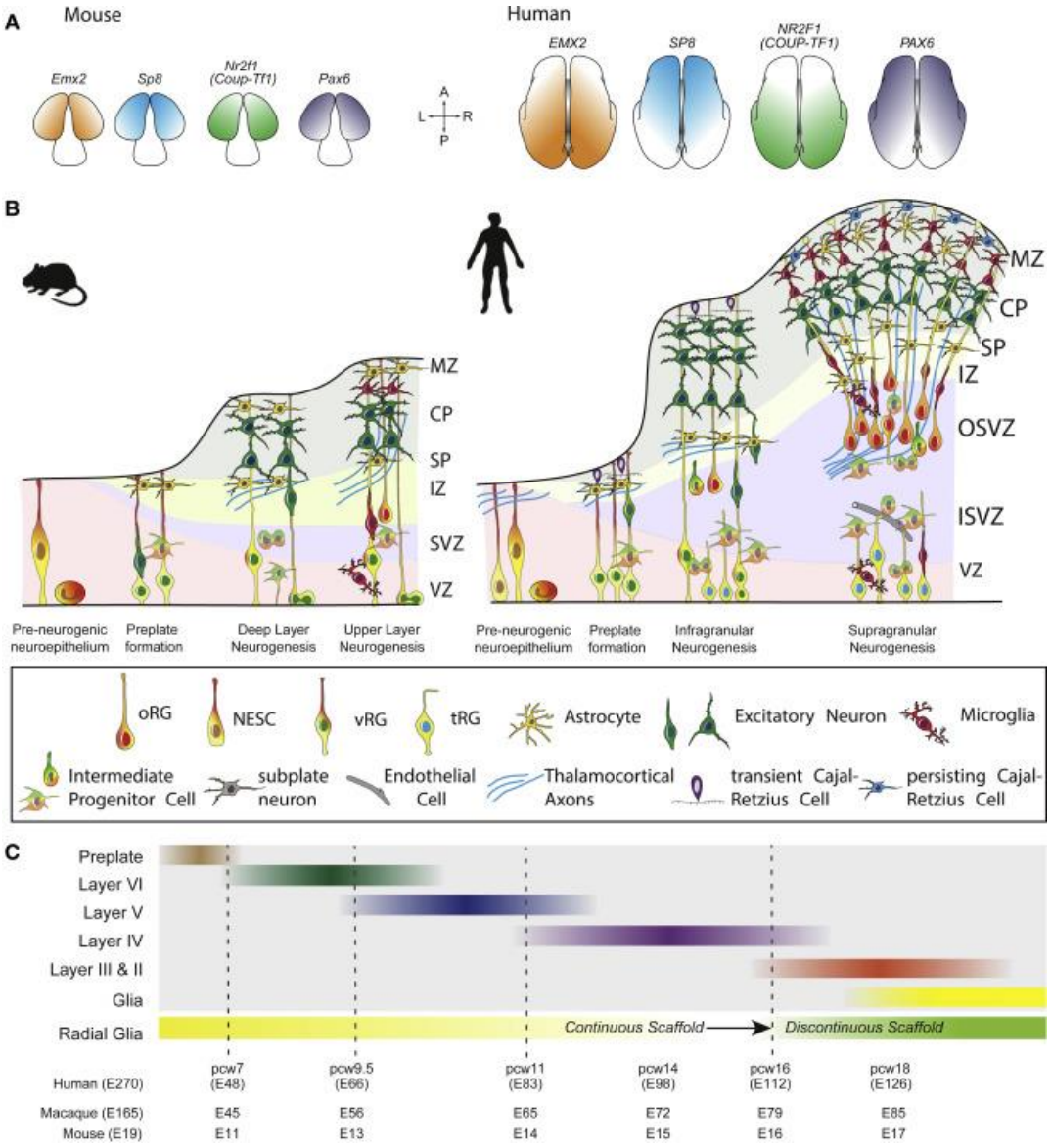

Figure 4.1. Schematic of neurodevelopment of the cerebral cortex.

(A) Patterning centres in the brain initiate important transcription factors to influence location-specific cell fates in the cortex. **(B)** Schematic of cortical development in both mouse and human. **(C)** Comparison of important neurogenesis stages across species (Cadwell et al., 2019).

4.1.3 Role of KCNQ2 in normal brain development

The importance of the M current in neurodevelopment is underscored by the observation that numerous pathogenic variants in *KCNQ2* lead to a broad spectrum of neurodevelopmental disorders as well as prior work in non-human cell and rodent models. A recent study has shown that pathogenic variants in *KCNQ2* are the most common genetic cause of DEE in neonates where 40% of patients in the study with neonatal onset DEE, had a

pathogenic variant in *KCNQ2* (Shellhaas et al., 2017). *KCNQ2* encodes Kv7.2 (the α-subunit of the ion channel), which co-assembles with Kv7.3 (encoded by *KCNQ3*) to form heterotetrametric Kv7 ion-channels, expressed in excitatory and inhibitory neurons in the human brain. They are present in high amounts in the cortex but are also present in the hippocampus (Cooper et al., 2000). These channels play various roles depending on their subcellular localisation within the neuron. For example, Kv7.2 channels are highly expressed at the axon initial segment (AIS) and nodes of Ranvier to help stabilise the resting membrane potential (RMP) (Battefeld et al., 2014). While Kv7.2 channels located in the Soma and Pre-Synaptic terminals, and a crucial role is to prevent repetitive action potential (AP) firing following depolarisation and regulate neurotransmitter release respectively (Martire et al., 2004).

KCNQ2 transcripts have been shown to be expressed from as early as the stem cell stage to throughout the entire neurodevelopment. Six transcripts can be found for *KCNQ2* on the RefSeq database. The longer *KCNQ2* transcripts are upregulated during neuronal differentiation and this expression increases as neurons mature overtime in culture (J. S. Smith et al., 2001). Interestingly, studies have shown that amongst all ion channels, *KCNQ2* expression was the highest in hiPSCs (Jiang et al., 2010; Wang et al., 2005). Kv7.2 channels have been shown to be present at the plasma membrane of immature neurons, whereby expression then increases overtime. This was shown using an antibody that targeted the long *KCNQ2* transcripts in neonatal mouse CA3 neurons. They recorded a low M current density at first which gradually increased overtime postnatally. This low M current density in neonatal neurons is crucial to allow for intrinsic bursting and neuronal synchronisation, critical for the stabilisation of hippocampal networks (Safiulina et al., 2008). Finally, hyperpolarisation of the RMP has been shown to correlate with expression of Kv7.2 channels in iPSC-derived neurons (Telezhkin et al., 2018). Three temporally distinct phases in M current density that are regulated by *KCNQ2* transcript expression are outlined in **Figure 4.2**.

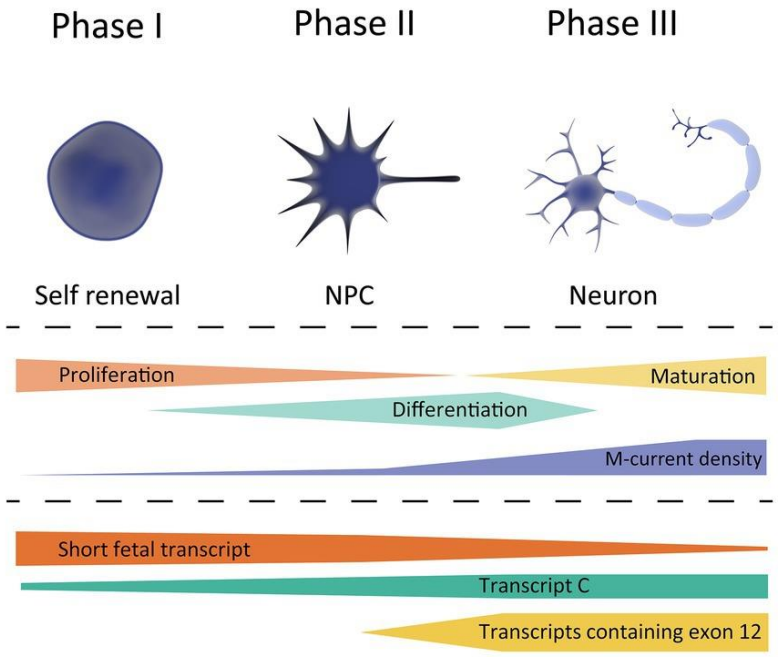

Figure 4.2. Schematic overview of *KCNQ2* transcript expression during the stages of normal neuronal development.

Top panel indicates different cell types, stem cell, NPC, and neurons. Middle panel shows the characteristics of the cells and how this correlates with M current density and the bottom panel shows transcript expression based on the data exported from the LIBD stem cell browser (Dirkx et al., 2020).

4.1.4. 2D Cortical neuronal differentiation protocols

iPSCs capacity to differentiate into neurons offers two main pathways: disease modelling and cell replacement therapy. To date, many protocols have been developed to generate cortical neurons *in vitro* using iPSCs to model neurological disorders. Here, I review various different differentiation protocols and discuss the current progress in disease modelling.

One of the initial methods used to differentiate iPSCs into cortical neurons was based upon an embryoid aggregate technique, which had previously been shown to work in ESCs (Li et al., 2006). Briefly, they grew iPSC colonies in suspension in hESC medium for 4 days, followed by culture in a neural medium (DMEM/F12, N2, Heparin (2µg/ml)). On day 8, Neuroepithelial (NE) cells could be seen adhering to the plastic dish. Cultures were induced to express anterior transcription factors *OTX2* and *LHX2* at day 24, while they were negative for any posterior *HOX* proteins. For induction of the midbrain neural cells, NE cells were treated with 50 ng/ml FGF8 and 100 ng/ml Sonic Hedgehog (SHH) on day 10 for 1 week. Finally, to induce hindbrain and motor neurons, NE cells were treated with 0.1µM Retinoic Acid at day 10 NE cells then formed rosettes which were gently removed from the culture dish and were kept

in suspension in the same trophic factors for 1 week before being plated on poly-ornithine/Laminin coated plates (Zeng et al., 2010). The Neurobasal medium supplemented with BDNF, GDNF and IGF1 was used for terminal differentiation. Since the publication of this protocol in 2010, there have been several modified versions. such as using different coating agents, co-culturing with glial cells and different neural progenitor cell isolation methods.

Another commonly used protocol is the monolayer dual SMAD inhibition protocol, which was shown to generate cortical neurons from iPSCs in 2009 (Chambers et al., 2009). This technique involves dissociating iPSCs and culturing them in a monolayer, as opposed to the cell aggregates in the previous protocol. The authors showed that neuroectoderm formation could be induced by antagonising the bone morphogenic protein (BMP) and transforming growth factor beta (TGF-B) signalling pathways by using the morphogen Noggin and small molecule SB431542 respectively. Noggin and SB431542 have been shown to induce neural progenitor cell fate after 7 days in neural induction medium consisting of DMEM/F12, Insulin, N2 and B27 (Y. Shi, Kirwan, & Livesey, 2012). By day 11, cells were passaged into a new dish and cultured in the same neural differentiation medium as described in the previous protocol. This dual SMAD Inhibition technique is more time efficient in inducing neural differentiation. Neuroectoderm can be seen at day 7 and neurons at day 12, compared to day 17 and day 25 in the EB aggregate method (Muratore et al., 2014).

A neuronal differentiation method commonly used today to generate cortical neurons is the exogenous over-expression of *Neurogenin-2 (NGN2). NGN2* is a transcription factor and overexpression of NGN2 has been used to generate excitatory neurons (Zhang et al., 2013), motor neurons (Liu et al., 2013), dopaminergic neurons (Liu et al., 2012) and sensory neurons (Hulme et al., 2020). The *NGN* family, which consists of *NGN1, NGN2* and *NGN3*, are a basic-helix-loop-helix class of transcription factors which are expressed throughout the nervous system (Ma et al., 1996). These factors play many roles throughout neural development, however in this context, we are interested in how *NGN2* can rapidly induce neuronal differentiation. This was first shown by Thoma and colleagues in 2012 (Thoma et al., 2012), who differentiated mouse PSCs into functional neurons by overexpressing NGN2. These induced neurons (iNs) were shown to express several cortical markers including NEUN, SOX1 and VGLUTI/II. Importantly, these iNs had no expression of the GABAergic marker GAD1 and had very little tyrosine hydroxylase expression, indicating that it was mostly glutamatergic neurons in our culture.

Shortly after this, Zhang et al demonstrated that glutamatergic neurons generated using the overexpression of NGN2 method could be effectively integrated into the mouse brain (Zhang et al., 2013). While these iNs did express cortical markers from the upper layers (I/II), they lacked the expression of cortical layer VI marker TBR1. Also, they expressed AMPA glutamate receptors but not NMDA receptors. Finally, most iNs were positive for VGLUT2, which is expressed by neurons in the thalamus and brainstem, while only 20% of iNs were positive for VGLUT1, which is expressed by neurons in the cerebral cortex, cerebellum and hippocampus (Balaram et al., 2011). Together these results show us that these iNs consist of a very mixed population of neurons, mainly of the thalamus and brainstem. This protocol has since been modified to include co-culture with astrocytes to promote spontaneous excitatory currents in iNs (Fernandopulle et al., 2018). Similarly, to direct differentiation to a more specific cell fate, the use of small molecules have also been incorporated into these protocols (Ho et al., 2016). NGN iNs are rapid to produce, scalable and easy to handle making them attractive for disease modelling. However, it's important to note that as NGN2 inhibits GABAergic neuronal differentiation, co-culturing iNs with inhibitory GABAergic interneurons is useful for modelling diseases, where GABAergic neurons may also play an important role in the disease phenotype such as in *KCNQ2*-DEE (Simkin et al., 2021).

4.1.5. 3D Cortical Neuronal Differentiation Protocols

The aforementioned 2D protocols have all contributed invaluable insights into the pathophysiology of neurological disorders. However, a limitation of these protocols is that they do not closely mimic the cytoarchitectural features and cell to cell interactions of *in vivo* conditions e.g., on a neuronal network level (Costamagna et al., 2019). Modelling disease so they resemble *in vivo* conditions as closely as possible is crucial to understanding the pathophysiology of the disease. To achieve this, 3D culture conditions are being used whereby cells form 3D structures known as organoids (Lancaster et al., 2013). 3D organoids can be defined as a self-organising group of various cell types derived from PSCs which can differentiate to form fully grown tissues comparable to those found *in vivo* (Mariani et al., 2012). In 2013, (Lancaster et al., 2013) demonstrated that EBs cultured in the absence of small molecules could give rise to neuroepithelial buds, which could then mature into different regions of the brain. Since then, there has been great interest in organoid generation for different areas of the CNS. Researchers have successfully developed organoids of the spinal cord, hippocampus, hypothalamus, midbrain, cerebral cortex, and the ventral forebrain (Sakaguchi et al., 2015; Qian et al., 2016; Xiang et al., 2017).

Cortical neurons have been shown to be effective at modelling some monogenic disorders, enabling the study of genotype-phenotype interactions during cortical maturation. For example, Birey et al (2017) modelled a monogenic disorder (due to variants in *CACNA1C*) Timothy Syndrome (in which patients also experience epilepsy) using ventral and dorsal forebrain organoids derived from patient iPSCs (Birey et al., 2017). This model included a complex interaction between glutamatergic neurons from the dorsal forebrain and GABAergic neurons from the ventral forebrain. As epilepsy disorders involve both glutamatergic and GABAergic neurons, this protocol overcomes the limitations associated with the overexpression of NGN2 protocol which exclusively generates glutamatergic neurons. This is particularly important in epilepsy models as during development of the fetus, interneurons migrate to the neocortex where they integrate with cortical circuits (Gelman et al., 2010). Any disruptions of migration of inhibitory neurons to early circuit formation may lead to neurological disorders including epilepsy. The researchers also showed that there was formation of functional synapses between the ventral and forebrain organoids by calcium imaging and patch clamping.

4.1.6 Importance of glial cells in neuronal development

Glial cells, the most abundant cells of the CNS, play many important roles during the development of the nervous system (Freeman, 2006). They shape development of the nervous system by regulating axon pathfinding, nerve fasciculation, promoting neuronal cell death, synapse formation and functional maturation of neurons (Lemke, 2001). Glial cells' role in promoting synaptogenesis is particularly important in modelling diseases *in vitro* to ensure neurons are functional and mature. One study showed that when cultured underneath an astrocyte feeder layer, retinal ganglion cells (RGCs) produced approximately 7 times more functionally mature synapses than RGCs cultured alone (Nägler et al., 2001). In this study there was no contact between the feeder layer and the RGCs, suggesting that soluble, trophic factors released by the astrocytes promoted the formation of more functionally mature synapses. This has also been shown for neurons in the spinal cord, where without co-culture with Schwann cells, neurons formed very few functional synapses (Ullian et al., 2004). For this reason, incorporation of glial cells in differentiation protocols, depending on the model or hypotheses in question, may be critical to promote the generation of mature neurons which can act as a physiologically relevant disease model.

In this study we used a 2D differentiation protocol based on the dual SMAD inhibition method with some minor modifications. This protocol has been used previously in our

laboratory to generate mature, functional cortical neurons (Avazzadeh, 2018). We chose this method as it is a robust, reliable method used to generate excitatory cortical neurons, that has been used extensively in the literature. As patients with *KCNQ2*-DEE experience focal seizures that arise in the cortex, we aimed to generate excitatory neurons of a cortical origin.

4.2 Materials and Methods

4.2.1 iPSC lines used for cortical neuron differentiation

The iPSCs were cultured as outlined in **Chapter 2**. The genetic information of the iPSC lines discussed in this Chapter are outlined below in **Table 4.1.**

Table 4.1. Information of iPSC lines used for cortical neuron differentiation

Status	iPSC line	Gender	Age	cDNA change and amino acid abbreviation
9 iPSC lines from 3 *KCNQ2*-pathogenic variants (patients)	EP2004 C1	Female	7	c.793G>A (p.A265T)
	EP2004 C7	Female	7	c.793G>A (p.A265T)
	EP2004 C8	Female	7	c.793G>A (p.A265T)
	EP2002 C1	Female	4	c.783A>C (p. F261L)
	EP2002 C2	Female	4	c.783A>C (p. F261L)
	EP2002 C3	Female	4	c.783A>C (p. F261L)
	EP2001 C4	Male	5	c.881C>T (p. A294V)
	EP2001 C5	Male	5	c.881C>T (p. A294V)
	EP2001 C8	Male	5	c.881C>T (p. A294V)
9 iPSC lines from 3 healthy donors	EP2C004 C2	Female	12	N/A
	EP2C004 C4	Female	12	N/A
	EP2C004 C5	Female	12	N/A
	EP2C003 C1	Male	21	N/A
	EP2C003 C2	Male	21	N/A
	EP2C002 C5	Male	4	N/A
	EP2C001 C2	Male	21	N/A
	EP2C001 C4	Male	21	N/A
	EP2C001 C5	Male	21	N/A

4.2.2 Cortical neuronal differentiation protocol

Below is a step-by-step description of the cortical differentiation protocol, depicted in **Figure 4.3.**

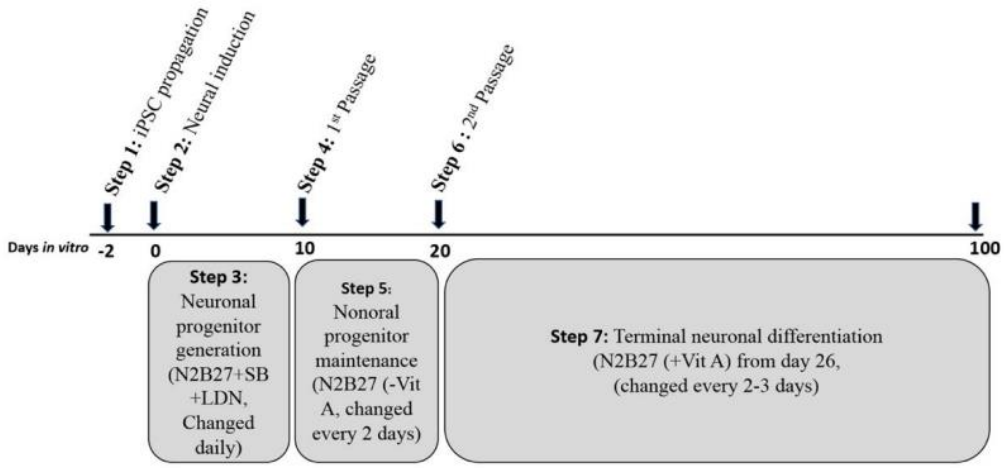

Figure 4.3 Schematic outlining the workflow of the cortical differentiation protocol.

Outline of 7 step process from iPSCs to terminally differentiated cortical neurons (Avazzadeh, 2018).

Step 1: Day -3 (iPSC Propagation): iPSCs were seeded at a density of ~50,000 cells/cm^2 on Geltrex-coated 6 well plates. Cells were passaged using 1ml of gentle cell dissociation reagent (Stem Cell Technologies) and incubated for 5 minutes at room temperature. Once cells began to detach, the gentle cell was removed, and the cells were sprayed with Essential 8 (E8) medium to detach the remaining cells from the plate. 10µM of Rock Inhibitor was added to the medium (Stem Cell Technologies, Y27632). Cells were then transferred onto new Geltrex-coated plates. Cells were fed every day for 3 days until they reached at least 80% confluency, at which point they are ready for neuronal induction.

Step 2: Day 0 (Neuronal Induction): The E8 medium was removed from the cells and cells were washed once with DPBS. 2ml of Neural Induction Medium (NIM) was added to the cells. The NIM consisted of 2/3 (v/v) DMEM F12 (Thermo Fisher Scientific), 1/3 (v/v) Neurobasal Medium (Thermo Fisher Scientific, 21103-049), N2 supplement (50X) (Thermo Fisher Scientific, 17502048), B27 supplement without Vitamin A (100X)(Thermo Fisher Scientific, 12587010) and 0.1mM β-Mercaptoethanol (Gibco, cat# M6250). Media was supplemented daily with 100nM LDN193189 (MCE, HY-12071) and 10nM SB431542 (MCE, HY-10431).

Step 3: Day 10- 12 (Neural Progenitor formation): The cells underwent a half media change every day until day 10-12. This was dependent on the formation of a thick neuroepithelial sheet and the appearance of rosettes, which can be dependent between cell lines.

Step 4: Day 10-12 (First passage of Neural Progenitors): The cells were incubated with 10µM Rock Inhibitor for 1 hour before passaging the cells. After the incubation period, the

conditioned medium was removed from the cells and transferred to a 15ml falcon tube. The cells were washed with 1ml DPBS. 1ml of 0.02% EDTA was added to the cells for approx. 2 minutes at 37 °C. The EDTA was removed from the cells and replaced with the conditioned medium from the previous step. Cells were then carefully scraped with the tip of a 5ml pipette. Scratches were made gently to detach the cells in large clumps. As much of the cells as possible were removed from the plate. The cells were transferred to a 15ml falcon tube. Cells in each well of a 6-well plate were then passaged into 4 wells of Geltrex-coated a 12-well plate and were then incubated at 37 °C until the next day.

Step 5: Day 10/12 – 20 (Neural Progenitor maintenance): After the first passage, small molecules LDN193189 and SB431542 were no longer added to the medium. Half of the medium was changed every other day until day 20. This varied slightly between lines depending on the confluency of cells. When multiple layers of cells become visible, the cells were ready to be passaged for terminal differentiation.

Step 6: Day 20 -100 (Second passage for terminal differentiation): Cells were passaged a final time for terminal differentiation. Cells were passaged onto 12-well plates with 15mm coverslips (Fisher Scientific), or 8-well chambers or 48-well MEA plates in varying passaging ratios. Passaging ratios were 1:4 from 12-well plate to 12-well plate, 1:6 from 12-well plate to 12-well plate containing coverslips and 1:8 for 8-well chambers. For passaging to 48-well MEA plates, cells were seeded in triplicate at 25 X 10^4, 50 X 10^4 and 75 X 10^4. Cells were added in a small volume of 8µl to ensure cells attached directly on top of the electrodes in the middle of each well. Culture dishes underwent a double coating step. Firstly, they were coated with Poly-D-Lysine (10µg/ml in DPBS) for 1 hour at 37 °C. Dishes were then washed three times with DPBS and then incubated with Laminin (10µg/ml) overnight at 37 °C. The next day, the dishes were rinsed once with DPBS before use. Cells were passaged as described in step 4.

Step 7: Day 20- Day 26: Cells were fed with 2ml of NIM medium every other day until day 26. Between days 20 and 26, 0.1µM Compound E (MCE, HY-14176) was added to the medium of half of the cells.

Step 8: Day 26 - Day 100 Maintenance for mature neuronal differentiation: Medium was changed to a maintenance medium by switching B27 supplement without Vitamin A to B27 supplement with Vitamin A (Thermo Fisher Scientific, 17504044). Cells underwent a half media change every day until day 100. Throughout the 100 days of the differentiation

protocol, phenotypic analysis of cells were performed at various time points outlined in **Table 4.2.**

Table 4.2. Important timepoints for characterisation of neurons

Day	Analysis performed
20	Immunocytochemistry for neuronal progenitor markers
	RNA extraction for qPCR for neuronal progenitor markers
30	Immunocytochemistry for early neuronal markers
	RNA extraction for qPCR for early neuronal markers
40	Immunocytochemistry for early neuronal markers
	RNA extraction for qPCR for early neuronal markers
	MEA analysis from Day 40 to Day 61.
60	Immunocytochemistry for neuronal markers
	RNA extraction for qPCR for neuronal markers
	Calcium Imaging time point 1
80	Immunocytochemistry for mature neuronal markers
	RNA extraction for qPCR for mature neuronal markers
100	Immunocytochemistry for mature neuronal markers
	RNA extraction for qPCR for mature neuronal markers
	Calcium Imaging time point 2
	DNA extraction for sequencing

4.2.3 RT-PCR and RT-qPCR

Total RNA was extracted from the cells on days marked in **Table 4.2** (days 20, 30, 40, 60, 80, 100) to monitor the differentiation process. Briefly, cells were lysed with 350µl of Buffer RLT by vortex. Homogenized cell lysates could then be used directly for RNA extraction with the RNeasy plus Mini Kit (Qiagen, cat# 74104) or stored at -80°C until future use. After extraction, RNA quantity and quality was measured using the NanoDrop 2000 Spectrophotometer (ThermoFisher, cat#ND-2000). RNA was then stored in the -80°C freezer. To generate cDNA, 1µg of RNA was reversely transcribed using the SensiFAST cDNA Synthesis Kit according to manufacturer's instructions (Bioline, cat# BIO-65053). The cDNA was diluted 1:10 in RNase-free water and stored at -20°C as a template for RT-PCR. RT-PCR analysis was carried out using TopTaq® Master Mix (Qiagen, cat# 200203) under standard working conditions. qPCR experiments were performed using Fast SYBR™ Green Master Mix (Applied Biosystems, cat# 4385612) on the Step One Plus Real-Time PCR System (Applied Biosystems) or on the LightCycler 480 (Roche). The following standard programme was used: Holding stage: 95°C 20s (1×); Cycling stage: 95°C 3s, 60°C 30s (40×); Melt curve stage: 95°C 15s, 60°C 1min, 95°C 15s (1×). Primers used are listed in **Table 4.3.** The resulting cycle threshold (ct) values were

normalised to GAPDH expression. The relative quantities of mRNA expression were calculated as being 2^{-ddct} using the average dCt value of an iPSC line.

Table 4.3. Primers used for Cortical Neuronal Differentiation

Application	Target	Forward (5'-3')	Reverse (5'-3')
iPSC marker	*OCT4*	ACTTCACTGCACTGTACTCCTC	CACCCTTTGTGTTCCCAATTCC
iPSC marker and Neural Stem Cell (NSC) marker	*SOX2*	AGACTTCACATGTCCCAGCACT	CGGGTTTTCTCCATGCTGTTTC
NSC markers	*PAX6*	CCGCCTATGCCCAGCTTCAC	AAGTGGTGCCCGAGGTGCCC
	NESTIN	CTGGCGCACCTCAAGATGTC	TCCAGCTTGGGGTCCTGAAAG
	FOXG1	CCTGCCCTGTGAGTCTTTAAG	GTTCACTTACAGTCTGGTCCC
NPC marker	*DCX*	TATGCGCCGAAGCAAGTCTCCA	CATCCAAGGACAGAGGCAGGTA
Pan- Neuronal marker	*TUJ1*	GGCCTTTGGACATCTCTTCA	ATACTCCTCACGCACCTTGC
Synaptic markers	*SYN1*	CCCCAATCACAAAGAAATGCTC	ATGTCCTGGAAGTCATGCTG
	PSD95	GTGACGACCCATCCATTTTC	TGACATAGAGGCGAACGATG
Mature neuronal marker	*MAP2*	CAGTTTCTGCGCCCAGATTTTA	TCCCAATCAATGCTTCCTCG
Inhibitory neuronal marker	*GABA1*	AAAAGCGTGGTTCCAGAAAA	GCTGGTTGCTGTAGGAGCAT
Glutamate transporter	*VGLUT1*	TCAATAACAGCACGACCCAC	TCCTGGAATCTGAGTGACAA
Cortical neuronal markers	*TBR1*	TCACTGGAGGTTTCAAGGAGGC	TTTCTTGGCGCATCCAGTGAGC
	BRN2	TATGGCAACGTGTTCTCGCA	CCTCCTCCAACCACTTGTTCAA
	CTIP2	CTCCCTTTGGATGCCAGTGTCA	GGCTCCAGGTAGATGCGGAAG
	SATB2	CAAGAGTGGCATTCAACCGCAC	ATCTCGCTCCACTTCTGGCAGA
Glial cell markers	*GFAP*	GTACCAGGACCTGCTCAAT	CAACTATCCTGCTTCTGCTC
	S100B	GAAGAAATCCGAACTGAAGGAGC	TCCTGGAAGTCACATTCGCCGT
BK channel (alpha and beta subunits)	*KCNMA1*	TTCTCTACTTCGGCTTGCGG	ACACAGACACAAACACGGGG
	KCNMB1	GAGCTGAAGGGCAAGAAGG	GCTGCCTGGGATGTAGGAG
	KCNMB2	GAGGACCGAGCTATTCTCCTG	TGTTTCCGTGATGGACGCATT
	KCNMB3	GGGCTTCTCAGTCCTAATGTTC	AGTGCAGGTCGATTCTTCTCTC
	KCNMB4	GATTGGTTCCCAGCCATTTAC	AATGAGAACGCCCACCAC
SK channels	*KCNN1*	TCGGGGAAACCCTCAAATGTG	CCATGACGACGATGCCAAAC
	KCNN2	TTGATTGGTAGCATCCACGC	ACCGCTCAGCATTGTAAGTGA
	KCNN3	AAGCGGAGAAGCACGTTCATA	CTGGTGGATAGCTTGGAGGAA
	KCNN4	AAGCTCCGGGAACAAGTGAAC	CGCCAGCGTGTCAATCTGT
Other channel genes	*KCND2*	GCCTCATCCCGGAAATCATCG	CCCCGTGACATAGTAGAACACC
	KCNT1	GACCCGTCCTTCCAGAACG	ACGCGCACAATGTAGAGCA
	KCNA1	CATCGTGGAAACGCTGTGTAT	CTAAAAACCCTTACCAAGCGGAT
	KCNA2	AGACCACGAGTGCTGTGAGA	AGTACCTCATTCGTTTCTTTGGG
	KCNA4	ATGAGTGTTCCTACACGGATCT	CCTGACACATTTATCACCACACG
	HCN1	AGGCAATCGCTCCCATCAAT	CCGGTGGAGATTGTGTCCTC
	HCN2	ACTACATCATCCGCGAAGGC	AGCCATCGGACAGCTTCATC
	SCN8A	CTCCTGACTGGTCGAAGAATGT	CATGGGTCCCGTAAAAAGGTAA
Reference	*GAPDH*	AGGGCTGCTTTTAACTCTGGT	CCCCACTTGATTTTGGAGGGA

4.2.4. Immunocytochemistry

Immunocytochemistry of neurons was performed as described in **Chapter 2 (2.2.4)**. Neurons were fixed with 4% Paraformaldehyde at days 20, 30, 40, 60, 80 and 100 to analyse neurons throughout the differentiation process. Fixed chambers were kept no longer than 2 weeks or used directly for subsequent staining steps. The primary and secondary antibodies used at each time point to characterise NSCs, NPCs and mature cortical neurons are listed in **Table 4.4** and **Table 4.5,** respectively. The stained cells were images using the Fluoview 1000 Confocal microscope (Olympus, FV1000) at a magnification of 20X and 60X. Image J was used to perform quantification of staining. Four images were taken for each staining at both magnifications. First nuclei were counted and marked, followed by counting of nuclear stains and cytoplasmic stains.

Table 4.4. List of antibodies used for cortical neuron characterisation

Application (marker)	Name	Manufacturer	Species	Dilution	Cat#
Pluripotency	OCT4	CST	Rabbit	1:500	2840
NSC markers	PAX6	CST	Rabbit	1:500	60433S
	SOX2	CST	Mouse	1:500	4900S
	NESTIN	Invitrogen	Mouse	1:500	2388598
	FOXG1	Abcam	Rabbit	1:200	Ab196868
Proliferation	Ki67	Abcam	Rabbit	1:500	Ab16667
NPC	DCX	Abcam	Rabbit	1:500	Ab18723
Pan-Neuronal	TUJ1 (βIII-tubulin)	CST	Rabbit	1:500	5568S
Mature neuronal	MAP2	Abcam	Mouse	1:500	Ab254143
Synaptic markers	SYN1	Abcam	Rabbit	1:500	Ab52636
	PSD-95	CST	Mouse	1:500	36233S
Layers 2/3 cortical	SATB2	Abcam	Mouse	1:500	Ab51502
Layer V cortical	CTIP2	Abcam	Mouse	1:500	Ab233713
Layer IV	TBR1	Abcam	Rabbit	1:500	Ab183032
Glial cell	S100B	Sigma	Mouse	1:500	S2632
Inhibitory neuronal	GAD67	Millipore	Mouse	1:500	MAB5406
	NMDAR1	Abcam	Rabbit	1:500	Ab109182
Excitatory neuronal	VGLUT1	Invitrogen	Rabbit	1:500	48-2400
	GLUR1	Abcam	Mouse	1:500	Ab174785
KCNQ2 marker	KCNQ2	Abcam	Rabbit	1:500	Ab22897

Table 4.5. List of secondary antibodies used for cortical neuron characterisation

Name	Manufacturer	Species	Dilution	Cat#
Anti-mouse IgG (H+L), F(ab')2 Fragment (Alexa Fluor® 555 Conjugate)	CST	Goat	1:1000	4409S
Anti-mouse IgG (H+L), F(ab')2 Fragment (Alexa Fluor® 488 Conjugate)	CST	Goat	1:1000	4408S
Anti-mouse IgG (H+L), F(ab')2 Fragment (Alexa Fluor® 647 Conjugate)	CST	Goat	1:1000	4410S
Anti-rabbit IgG (H+L), F(ab')2 Fragment (Alexa Fluor® 488 Conjugate)	CST	Goat	1:1000	4412S
Anti-rabbit IgG (H+L), F(ab')2 Fragment (Alexa Fluor® 555 Conjugate)	CST	Goat	1:1000	4413S
Donkey anti-Goat IgG (H+L) CrossAdsorbed Secondary Antibody, Alexa Fluor® 488	Life Technologies	Donkey	1:1000	A-11055

4.2.5. Statistical Analysis

Statistical analyses were performed with GraphPad Prism version 9.3.1. Statistical analysis was performed using paired or unpaired non-parametric t-test with a level of significance set at *$p<0.05$, **$p<0.01$, ***$p<0.001$. A specific method for each analysis was described under each figure or table. All data were presented as mean ± SEM.

4.3 Results

4.3.1 Generation of neural progenitor cells using dual SMAD inhibition

iPSCs were cultured in 6-well plates for 2-3 days until they reached a confluency of 80-90%. The Essential 8 medium was then removed from the cells and replaced with neural induction medium which contained two SMAD inhibitors: 100nM LDN193189 and 10nM SB431542. These molecules were freshly added daily until day 10-12 depending on the thickness of the neuroepithelium being formed. Over this time, the cell morphology changes. The large nuclei of the iPSCs are replaced with more elongated, columnar like nuclei. Between days 10-12, cells were passaged in a 1:2 ratio onto Geltrex-coated 12-well plates. From this point onwards, LDN193189 AND SB431542 were no longer added to the neural induction medium. Neural rosettes could be seen forming under the microscope which are indicative of neural progenitor cell formation **(Figure 4.4)**.

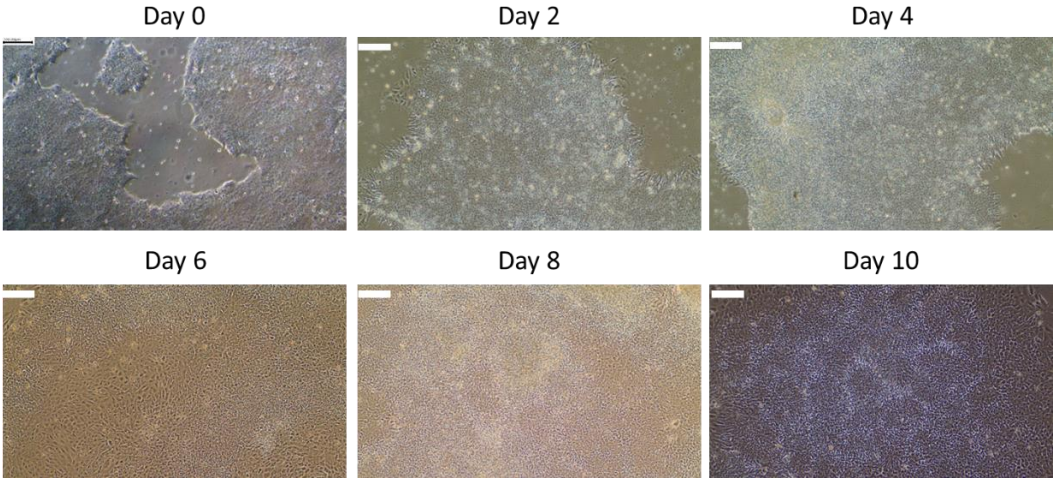

Figure 4.4: Representative images of neural progenitor cell development.

Generation of neural rosettes seen overtime from day 0 to day 12 in EP2004 C1. Cell morphology changes from small, round compact cells with large nuclei to cells with a more columnar shape, with a much larger cytoplasm of NPCs. Scale bar is 100µM. Total magnification = 10x.

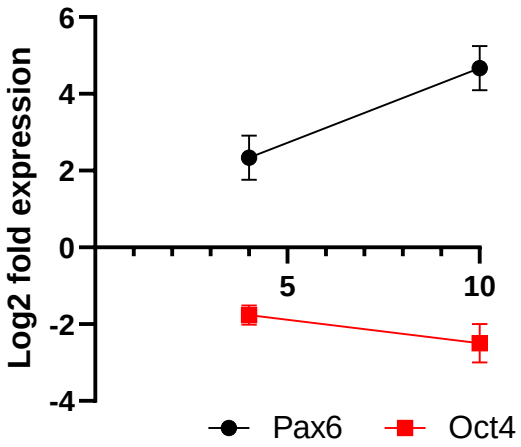

Figure 4.5 Confirmation of neural induction by upregulation of *PAX6* and downregulation of *OCT4*.

RT-qPCR data confirms the neural induction of iPSCs by upregulation of neural progenitor marker *PAX6* mRNA and downregulation of pluripotency marker *OCT4* mRNA between day 4 and day 10 in control lines (n=9).

4.3.2 Generation of cortical neurons over 100 days

Cells were cultured for an additional 8 days on Geltrex-coated plates until Day 20 of culture, changing media every other day. Cells were then passaged on day 20 for terminal differentiation onto Laminin/ Poly-D-Lysine coated plates. After passaging, the presence of neural rosettes can be seen at Day 20 **(Figure 4.6)**. Neurons matured in culture overtime until Day 100, changing media every other day. By Day 100, neurons are very confluent and appear to have a more mature morphology **(Figure 4.6)**.

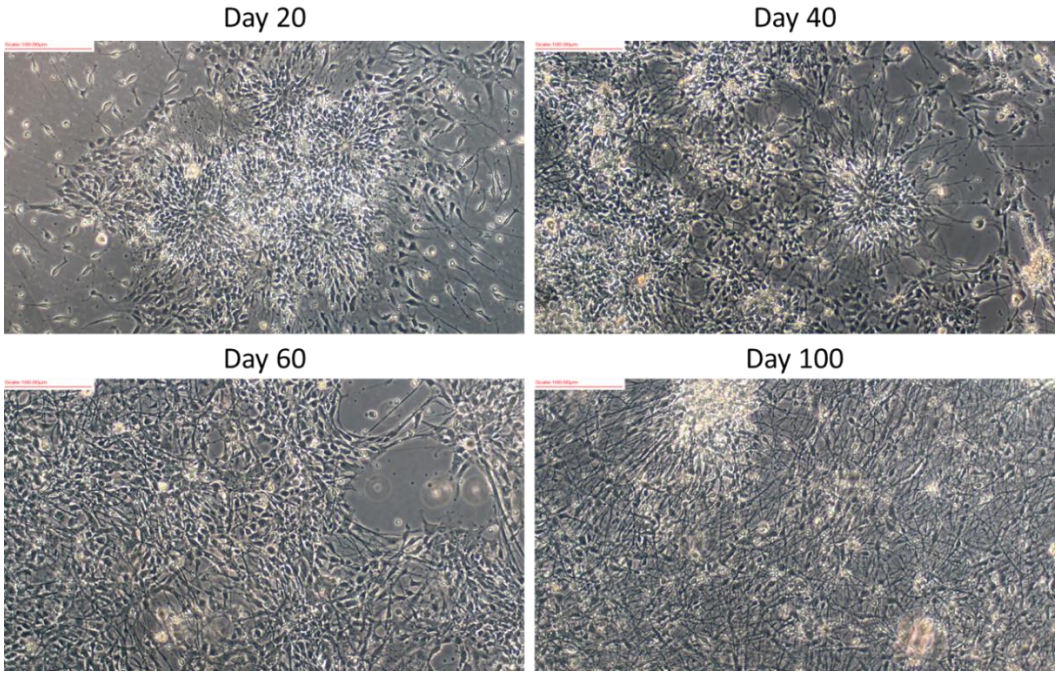

Figure 4.6. Representative images of cortical neuron generation from iPSCs using the dual SMAD inhibition protocol.

Images of EP2004 C1 (A294V) neurons at day 20, day 40, day 60 and day 100. Total magnification is 10X. Scale bar is 100µM.

4.3.3. Day 20 neurons are positive for neural progenitor cell markers as shown by immunocytochemistry and RT-qPCR

To confirm neural induction, we measured the expression of neural progenitor cell marker *PAX6* and stem cell marker *OCT4* **(Figure 4.5)**. Between day 0 and day 10, there was an increase in the expression of *PAX6* and a decrease in the expression of *OCT4*. To further characterise neurons at Day 20, immunocytochemistry was peroformed. Cells were fixed and stained for the markers SOX2, NESTIN, PAX6, FOXG1, OCT4, S100B and Ki67 to analyse neural progenitor cells, stem cells, glial cells and proliferating cells respectively. As seen in **Figure 4.7**, large proportions of cells are positive for the neural progenitor cell markers SOX2, NESTIN, PAX6 and FOXG1. The percentage of cells positive for each marker was calculated on ImageJ and presented in **Figure 4.7**. PAX6 is positive in ~61% ±2.4%, SOX2 is positive in approx. 76% ± 3.9%, Nestin is positive in approx. 77% ± 1.9% and FOXG1 is positive in approx. 79% ± 2.1% of cells. There is also some positive staining for the proliferation marker Ki67 in 63% ± 4.1%. Similarly, there is some expression of the glial cell marker S100B with positive staining in 40% ± 2.8% of cells. There is no expression of the stem cell marker OCT4. The blue cells are DAPI stained only, suggesting they could be post-mitotic newborn neurons. We then

measured the expression of the same markers at the RNA level and found there was no significant difference between patient and control lines **(Figure 4.8)**.

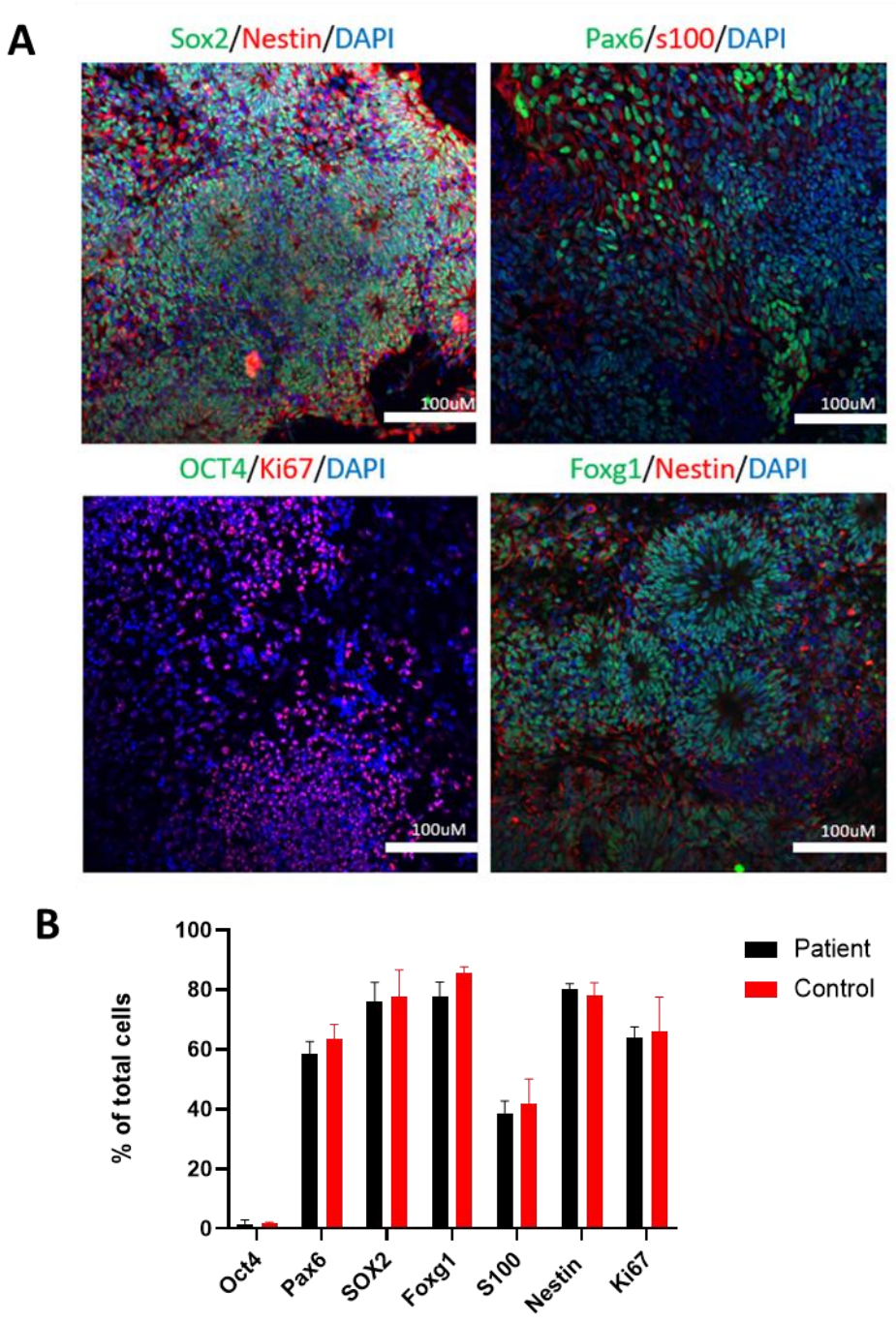

Figure 4.7. Representative images of immunocytochemistry staining and quantitative analysis of day 20 neural progenitor cells.

(A) At Day 20, cells were fixed and most cell were positively stained for neural progenitor cell markers FOXG1, NESTIN, PAX6 and SOX2, but negative for OCT4. Representative images from A294V. Total magnification 20x. Scale bar is 100µM. **(B)** The quantification of each marker was performed using ImageJ. Results are based on three biological and technical replicates. Error bars represent standard error of the mean. The cells in blue are only stained by DAPI and they are most likely the post-mitotic new (early) neurons.

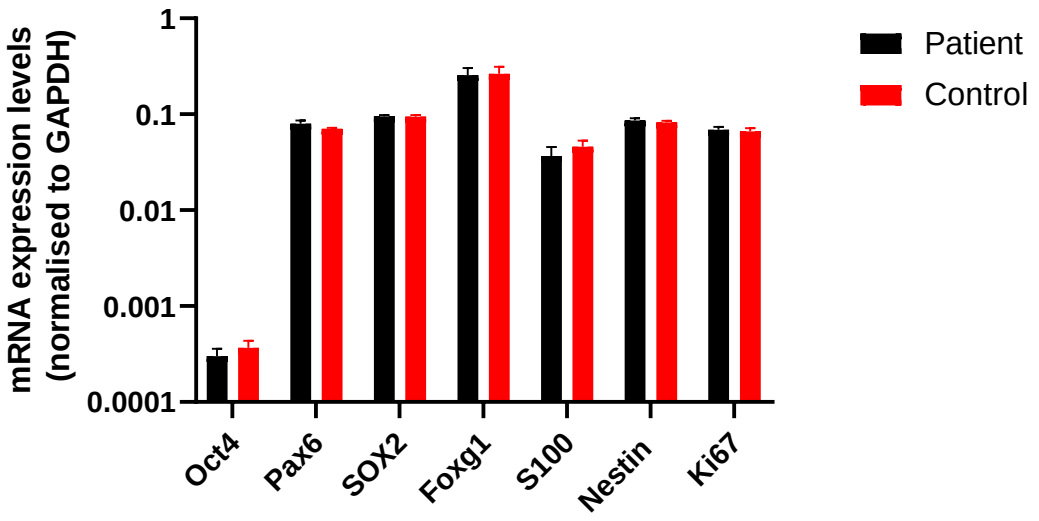

Figure 4.8. The presence of NPC markers are confirmed in Day 20 NPCs using RT-qPCR.

RT-qPCR shows the relative expression of NPC markers *PAX6, SOX2, FOXG1* and *NESTIN*. Data also shows very little expression of pluripotency marker *OCT4*. Proliferation marker *MKI67* (encoding Ki67) is confirmed to be present in large amounts as well as glial marker *S100B*. Data taken from controls (n=9) and patients (n=9). 3 lines for each mutation A265T, F261L and A294V and each sibling control were used. Error bars represent standard error of the mean.

4.3.4. Day 30 neurons begin to lose expression of neural progenitor cell markers and express mature neuronal cell markers

Cells were fixed and stained at Day 30 using immunocytochemistry to analyse the expression of neuronal markers during the differentiation process. At Day 30, approximately 56% ± 3.4% of neurons begin to express the mature neuronal marker MAP2 and approximately 71% ± 3.0% of neurons express the pan-neuronal marker TUJ1. Approximately 42% ± 1.4% of cells are positive for the astrocyte/oligodendrocyte marker S100B, essentially unchanged from that seen at Day 20. There is a significant reduction seen in the percentage of cells positive for the neural progenitor cell marker NESTIN and the proliferation marker Ki67 at Day 30 compared to Day 20 **(Figure 4.9)**, the NESTIN$^+$ cells were reduced from 77% ± 1.9% in day 20 to 59% ± 1.7% in day 30 (*p=0.028), and this was reflected by the reduction of Ki67$^+$ proliferating cells from 63% ± 4.1% in day 20 to 35% ± 2.9% in day 30 (**p=0.003) **(Figure 4.9)**. The percentage of Ki67$^+$ appeared lower than NESTIN$^+$, and this was likely caused by cell cycle specific expression Ki67 with the highest level in the M phase. However, there is no

difference seen between the expression of TUJ1, MAP2 and S100B at the RNA level between patient and control lines at day 30 **(Figure 4.10)**.

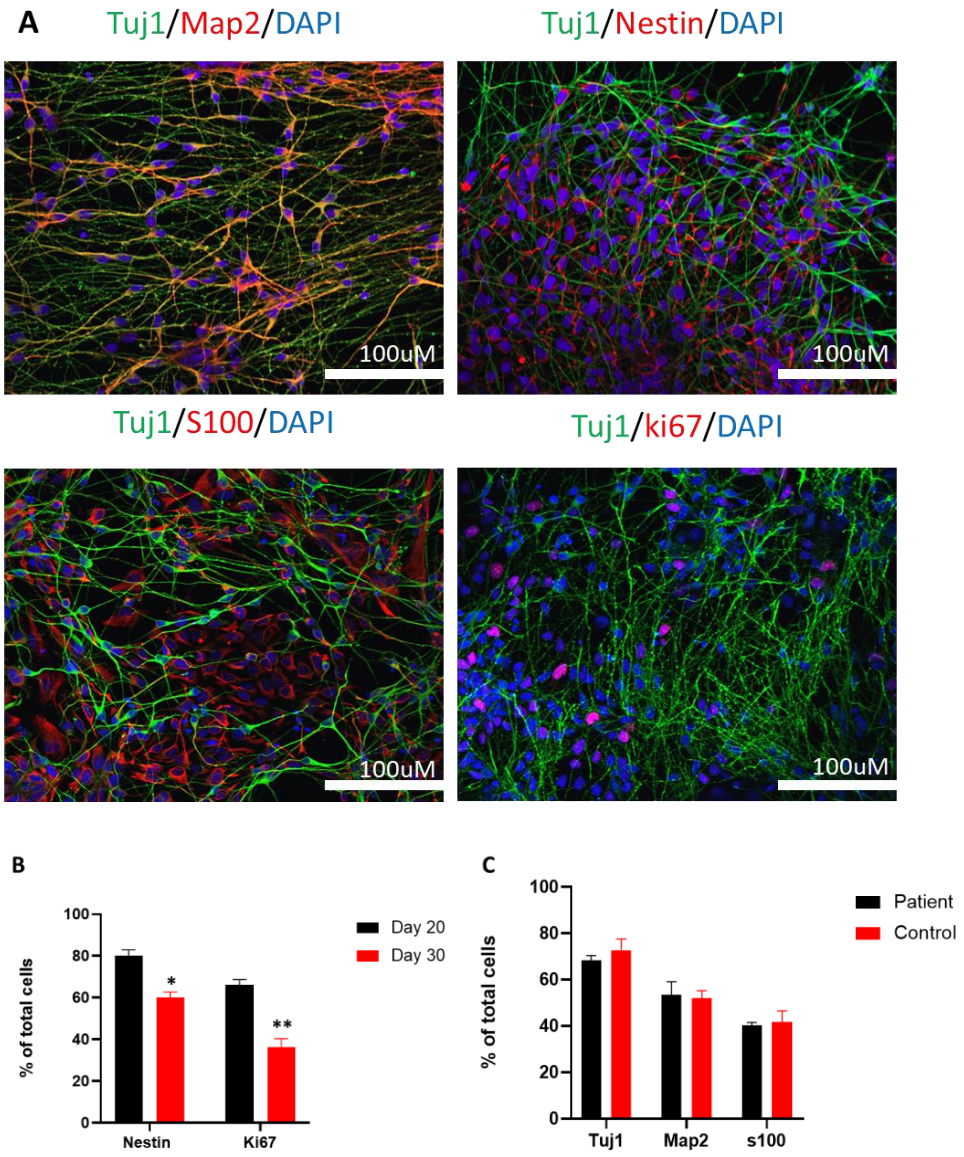

Figure 4.9. Immunocytochemistry and quantitative analysis of Day 30 neurons.

(A) Day 30 neurons are positive for the mature neuronal marker MAP2, TUJ1, NESTIN, S100B and Ki67. Representative images from A265T. **(B)** Quantitative analysis reveals Day 30 cultures contain significantly less NESTIN^{+} and Ki67^{+} than Day 20 cultures. **(C)** Quantitative analysis of TUJ1, MAP2 and S100B in Day 30. The quantification of each marker was performed using ImageJ. Results are based on three biological and technical replicates for A265T. Error bars and standard error of the mean.

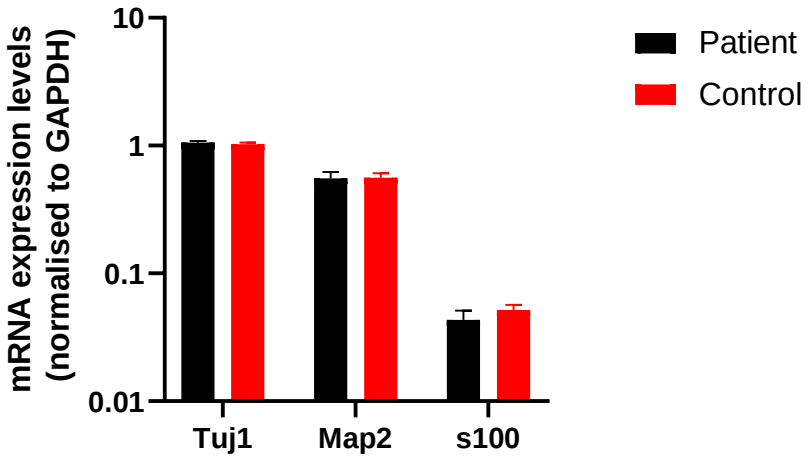

Figure 4.10. The presence of neuronal markers *TUJ1* and *MAP2* and glial cell marker *S100B* are confirmed in Day 30 neurons using RT-qPCR.

RT-qPCR shows the relative expression of *TUJ1, MAP2* and *S100B transcripts*. Data taken from controls (n=9) and patient (n=9). 3 lines for each mutation A265T, F261L and A294V and each sibling control were used. Error bars represent standard error of the mean.

We then measured the expression levels of *PAX6* and *DCX* between days 20 and 30. There was a reduction in the expression of *PAX6* in day 30 cells compared to day 20 **(Figure 4.11)**. Conversely, there was an increase in the expression of *DCX*, a post-mitotic marker **(Figure 4.11)**. These data are consistent with immunocytochemical staining, which showed the reduction of neural progenitors in day 30 and an increase in blue cell number stained by Hoechst only.

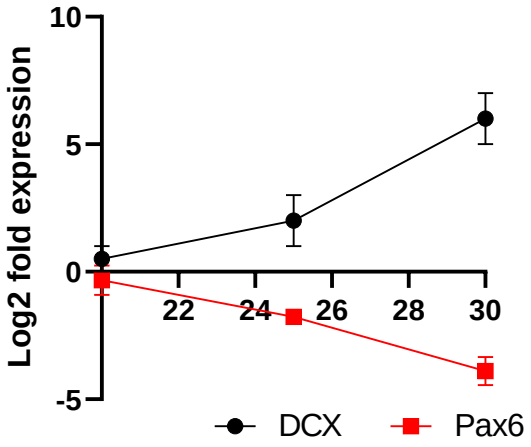

Figure 4.11. Log2 fold mRNA expression of post-mitotic marker *DCX* and NPC marker *PAX6* overtime.

PAX6 mRNA expression was significantly reduced in day 30 neurons compared to day 20, while *DCX* expression was increased (N= 9 controls; N=9 patients).

4.3.5. Cortical neurons are capable of forming functional synapses

Cortical neurons were subsequently stained for the presynaptic and postsynaptic markers Synaptophysin and PSD-95, respectively. In **Figure 4.12**, neurons were positive for both Synaptophysin and PSD-95 in Day 100 neurons. The percentage of cells positive for both markers was compared between Day 60 and Day 100. There was a significant increase in the number of cells positive for both synaptophysin and PSD95 at Day 100 compared to Day 60, indicating that the neurons were more capable of forming functional synapses overtime in culture. The percentage of Synaptophysin+ cells increased from 63% ± 3.2% to 89% ± 0.5% (**p=0.025), while the percentage of PSD95+ cells increased from 55% ± 1.7% to 83% ± 0.8% (***p<0.001) between day 60 and day 100 **(Figure 4.12)**. We then measured the expression of both markers on the RNA level and found there was no significant difference in Synaptophysin and PSD95 expression between patient and controls **(Figure 4.12)**.

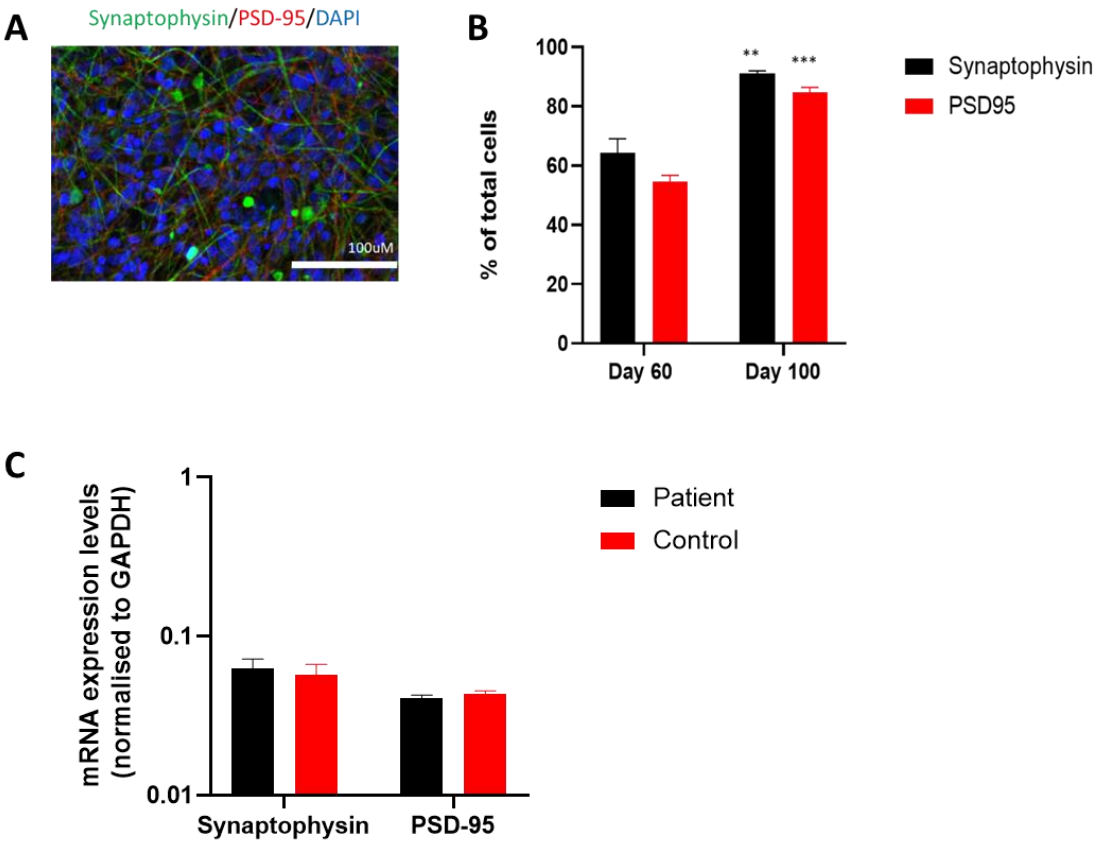

Figure 4.12. Immunocytochemistry and qPCR analysis of synaptic markers in Day 60 and Day 100 neurons.

(A) Day 100 neurons were positively stained for the synaptic markers synaptophysin and PSD-95. Representative image from EP2C001. **(B)** The markers were quantified using ImageJ. **(C)** RT-qPCR data from day 100 neurons showing relative mRNA expression levels of SYP gene coding for Synaptophysin and DLG4 coding for PSD-95. The mRNA expression levels were relative to the mRNA of the housekeeping gene *GAPDH*. Results are based on three biological and technical replicates. The data is presented as Mean ± SEM. Statistical significance (*p<0.05, **p<0.01, ***p<0.001) was evaluated using an unpaired parametric *t*-test.

4.3.6. Day 100 neurons are positive for cortical markers BRN2, SATB2, TBR1 and CTIP2

We next carried out immunocytochemistry with layer V cortical marker CTIP2, the layer VI cortical maker TBR1, and the layer II-IV marker SATB2 at Day 100 of the differentiated cultures to confirm the cortical identity of the neurons. As seen in **Figure 4.13**, approximately 56% ± 4.7% of neurons are positive for layer V marker CTIP2, 4.8% ± 1.6% are positive for layer II-IV marker SATB2, while approximately 10.1% ± 2.7% are positive for layer VI marker TBR1. We also found that some neurons were co-stained for TBR1 and SATB2 (1.9% ± 0.4%), which we were not expecting but has been reported before. We then measured the expression at the RNA level for the layer II/III markers of *POU3F2 (BRN2*) and *SATB2*, layer V *CTIP2* and layer VI *TBR1,* and found all genes were abundantly expressed, but there was no significant difference in the expression of all markers between patients and controls (**Figure 4.14**).

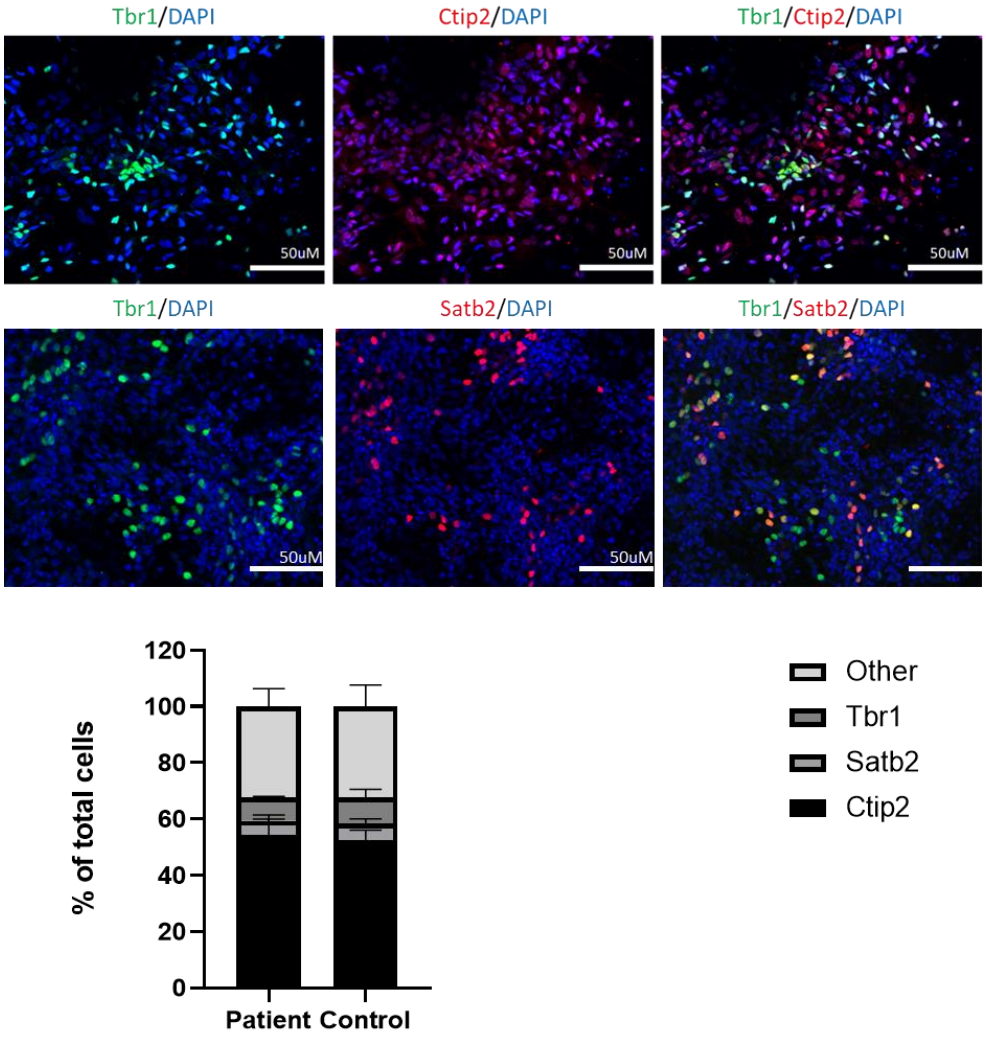

Figure 4.13. Immunocytochemistry and quantitative analysis of Layer II, V and VI cortical markers.

Day 100 neurons were positively stained for the cortical markers SATB2, CTIP2 and TBR1. The markers were quantified using ImageJ. Results are based on three biological and technical replicates. 3 lines for each mutation A265T, F261L and A294V and each sibling control were used. The data is presented as Mean ± SEM. Statistical significance (*p<0.05, **p<0.01, ***p<0.001) was evaluated using an unpaired parametric *t*-test. Total magnification of top panel is 20x. Representative images from F261L. Total magnification of bottom panel is 60x.

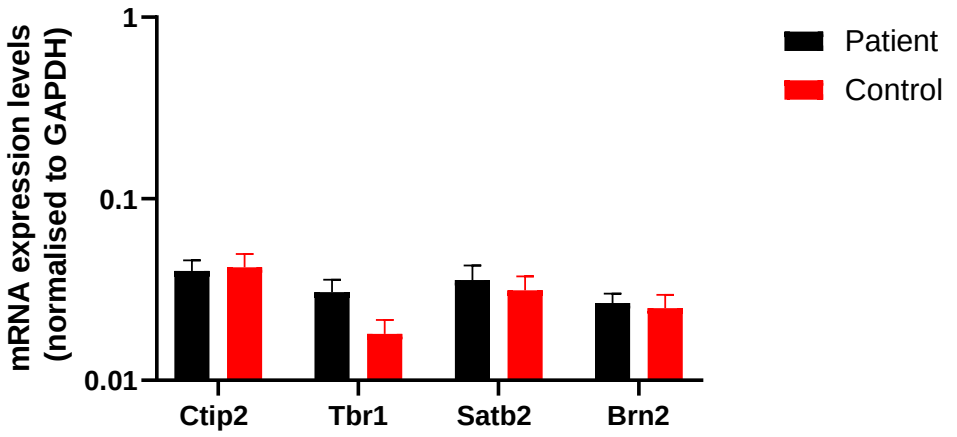

Figure 4.14. RT-qPCR Results indicate successful generation of cortical neurons.

Comparative analysis of expression levels of cortical layer V marker *CTIP2*, layer VI marker *TBR1*, layer II/II marker *SATB2* and *POU3F2 (BRN2)* in day 100 neurons using RT-qPCR. (Patient lines n=9, control lines n=9). Results are based on three technical replicates. The data is presented as Mean ± SEM.

4.3.7. Neurons are mainly glutamatergic with minimal GABAergic cells present at Day 100

Neurons were subsequently stained for the glutamatergic transporter VGLUT1 and the glutamatergic receptor GLUR1 at Day 100. Approximately 83% ± 3.2% of cells were positive for the glutamate receptor GLUR1 and approximately 87% ± 2.9% of cells were positive for the transporter VGLUT1 **(Figure 4.15)**, indicating the majority of cells were excitatory neurons. Additionally, we stained day 100 cultures for the GABAergic neuronal marker GAD67. Approximately 13% ± 3.4% of neurons were positive for GAD67 by immunocytochemistry **(Figure 4.15)**. For more precise quantification, RNA was extracted from cells at Day 100 and RT-qPCR was performed to quantify expression of glutamatergic and GABAergic neurons in our cultures. The RT-qPCR data confirmed that there were substantially higher level of *GLUR1* and *VGLUT1* mRNA expression than *GAD67*, however, there was no significant difference in the expression of each of these markers between patient and control neurons **(Figure 4.15)**, suggesting that epilepsy and control iPSCs are equally capable of differentiate into excitatory and inhibitory neurons.

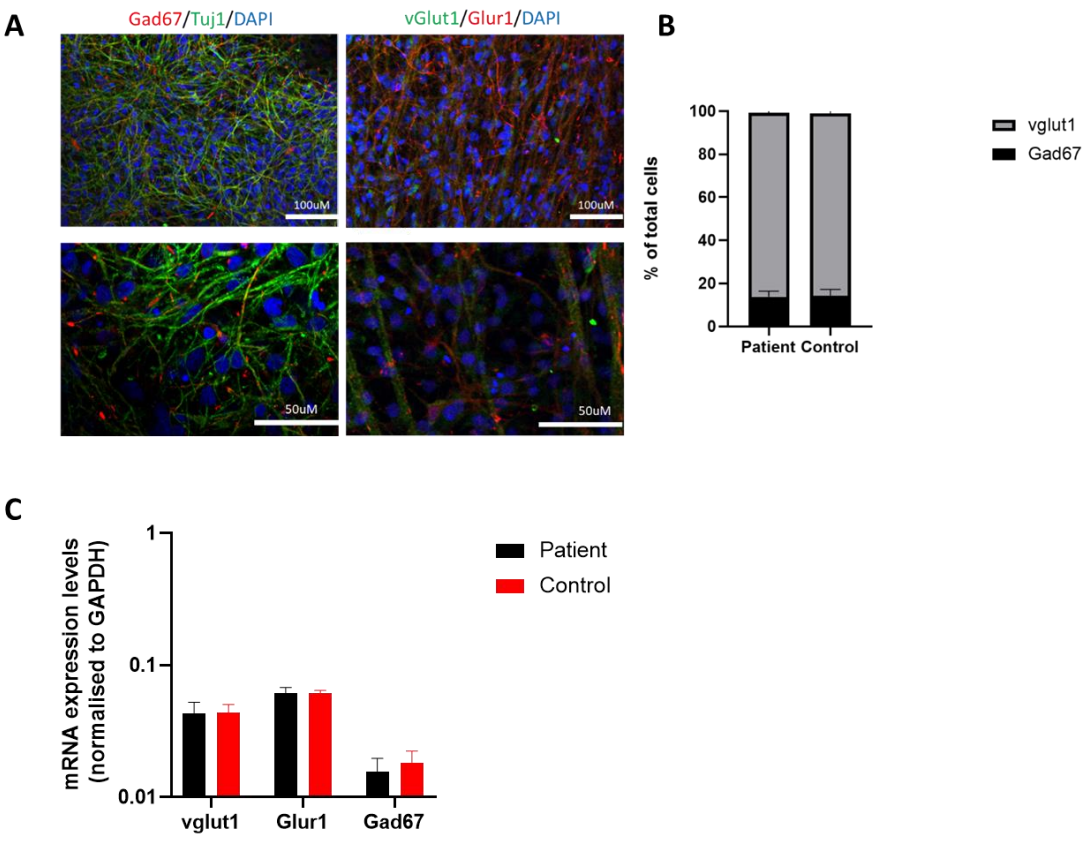

Figure 4.15. Immunocytochemistry and quantitative analysis confirm the presence of GABAergic and Glutamatergic markers in day 100 neurons.

(A) Day 100 neurons were positively stained for glutamatergic receptor and transporter, VGLUT1 and GLUR1 respectively. A small proportion of Gad67+ GABAergic neurons was also detected. Representative image from F261L. **(B)** The markers were quantified as percentage of total cells using ImageJ. **(C)** Relative mRNA expression levels of *VLGUT1, GLUR1* and *GAD67*. Results are based on three biological and technical replicates. 3 lines for each mutation A265T, F261L and A294V and each sibling control were used. The data were presented as Mean ± SEM. Statistical significance (*p<0.05, **p<0.01, ***p<0.001) was evaluated using an unpaired parametric *t*-test.

4.3.8 The presence of specific *KCNQ2*-DEE mutations (variants) are confirmed in patient neurons at Day 100 of the differentiation protocol

We then extracted DNA from the neurons at Day 100 to either (a) confirm the mutation is still present in the cells after the neuronal differentiation protocol or (b) confirm the absence of the mutation in the control cell lines. In **Figure 4.16**, the presence of each mutation was confirmed in their respective patient lines. In contrast to this, the absence of a mutation was also confirmed in the control cell lines.

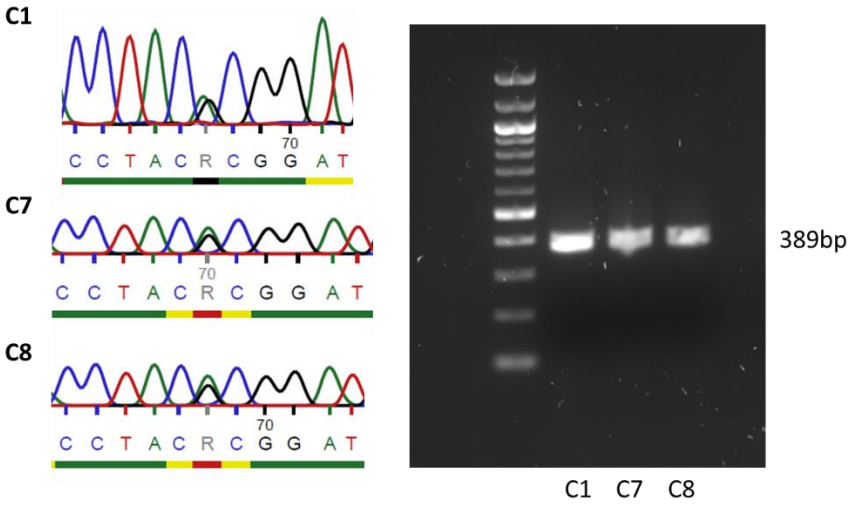

Figure 4.16. Sanger sequencing results confirm the presence of the mutation in differentiated neurons at Day 100.

Representative image of sequencing results confirming the variant (mutation A294V) is still present in patient-derived neurons (EP2004 C1, C7, C8) at day 100. DNA extracted from Day 100 neurons was sequenced using primers flanking the mutation site. A double peak can be seen annotated as 'R' at the point mutation site. The PCR product was also electrophoresed on an agarose gel to show the size of the PCR product.

4.3.9. *KCNQ2*-DEE neurons display an altered potassium and sodium channel gene expression at Day 100

To determine if there was any changes in the expression of other potassium channel genes in our *KCNQ2*-DEE neurons as a result of the mutation, we examined the expression of several key potassium genes by RT-qPCR. We found there was a significant upregulation of 7 other potassium genes in the *KCNQ2*-DEE neurons harbouring the mutation (A265T). The genes that were significantly upregulated were *KCNMA1* (*p= 0.032), *KCNMB1* (**p=0.008), *KCNA1* (***p<0.001), *KCNN1* (***p<0.001), *KCNN2* (***p<0.001), *KCNN3* (***p<0.001), and *KCNQ2* (**p=0.009) when compared to the sibling control lines **(Figure 4.17)**. In contrast to this, there was a significant downregulation of *KCNQ5* (*p=0.041) in the patient lines compared to the control lines. The upregulation of these genes in patient lines raises further questions as to the pathomechanisms of excitability and potential therapeutic targets.

As sodium channels also play an important role in action potentials, we also looked at any sodium channels that are closely related to *KCNQ2.* As shown in the string diagram **(Figure 4.18)**, *SCN1A*, *SCN2A* and *SCN8A* interact with *KCNQ2*. The relative expression of each of these genes is presented in **Figure 4.18**. There is a significant increase in all three sodium channels *SCN1A* (****P<0.0001), *SCN2A* (***P<0.001) and *SCN8A* (***P<0.001) in the *KCNQ2*-DEE neurons harbouring the mutation A294V, compared to controls.

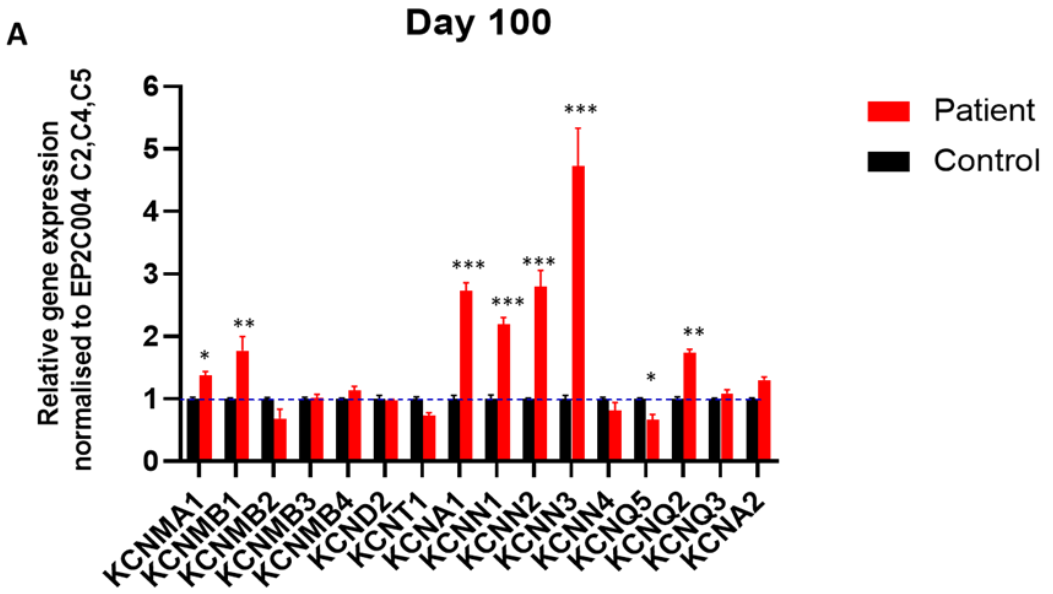

Figure 4.17. Expression of other potassium channels in *KCNQ2*-DEE neurons.

RT-qPCR results of the expression of other potassium channel genes in patient (A265T) and control neurons at day 100. GAPDH was used as the house-keeping gene. The fold change of gene expression in *KCNQ2*-DEE neurons was presented normalized to that of the healthy control neurons. The data are presented as mean ± SEM. Statistical significance (*p<0.05, **p<0.01, ***p<0.001) was evaluated using an unpaired parametric *t*-test.

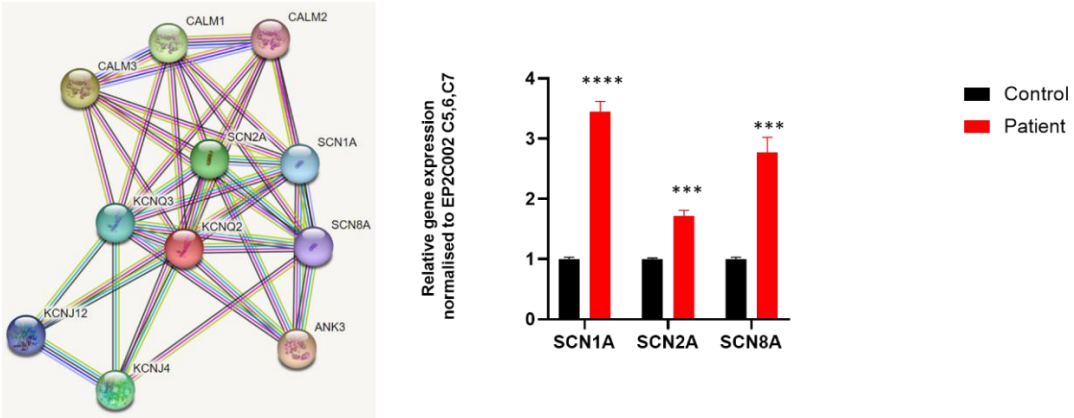

Figure 4.18. Expression of sodium channels *SCN1A, SCN2A* and *SCN8A in KCNQ2*-DEE neurons.

String analysis showing relationship between the sodium channels *SCN1A, SCN2A* and *SCN8A* with *KCNQ2.* RT-qPCR results showed the increased expression of the sodium channel genes *SCN1A, SCN2A*, and *SCN8A* in patient neurons (A294V) compared to controls at Day 100. GAPDH was used as the house-keeping gene. The fold change of gene expression in *KCNQ2*-DEE neurons was presented in relation to that of the healthy control neurons. The data are presented as Mean ± SEM. Statistical significance (*p<0.05, **p<0.01, ***p<0.001) was evaluated using an unpaired parametric *t*-test.

4.4 Discussion

The study of neurological diseases in humans has been revolutionised by the ability to generate neurons *in vitro* from renewable cell sources such as iPSCs. This can be achieved by utilising the factors and signalling pathways involved in foetal neural development in cell culture medium to differentiate PSCs into specific neuronal cell types. Early studies carried out in *Xenopus laevis* revealed that bone morphogenetic protein (BMP) inhibitors such as Noggin and Chordin have a crucial role in neural development in the embryo through the SMAD signalling pathway (Smith et al., 1992). Similarly, Noggin has also been shown to be highly expressed in adult mouse brain, acting as an important neural inducing factor (Valenzuela et al., 1995). Then, in 2008, Noggin was used to improve the efficiency of hESC differentiation into NPCs (Dottori et al., 2008). A small molecule, SB431542, which inhibits the transforming growth factor-beta (TGF-B) pathway, also leads to SMAD signalling inhibition (Patani et al., 2009). This small molecule was also shown to enhance differentiation of hESCs to a neural fate. Since then, these molecules have been used together extensively to successfully drive the generation of NPCs from hPSCs (Y. Shi, Kirwan, Smith, et al., 2012). Chambers et al. (2012), later discovered another BMP inhibitor, LDN193189, which can replace Noggin to promote neural induction through the ALK2, ALK3 and ALK6 receptors. In this study we have used the dual SMAD inhibition protocol with SB431542 and LDN193189 to generate cortical neurons from patient iPSCs harbouring a heterozygous *KCNQ2* mutation to investigate the disease phenotype.

Approximately 200 variants (mutations) in the *KCNQ2* gene have been reported to date (RIKEE DATABASE https://www.rikee.org/). Depending on the location of the mutation within the gene and the nature of the mutation itself, disease severity and phenotype can differ greatly. This is often due to the functional domain in which the mutation is present, i.e., the voltage-sensing domain which is crucial for voltage-dependent gating and expression of the Kv7.2 channels, or the pore-forming domain which controls K^+ permeability and selectivity. Mutations in these areas are predicted to cause a more severe phenotype due to the critical roles of these functional domains (Zhang et al., 2020).

In *KCNQ2*-related epilepsies, some studies suggest a genotype-phenotype correlation depending on the variant location in the Kv7.2 channel subunit. *KCNQ2* variants affecting Kv7.2 channels on the same residue have very rarely been reported to cause a different phenotype in patients (Laccetta et al., 2019). In this study, Patients EP2002 (c.783A>C, p.F261L) and EP2004 (c.793G>A, p.A265T) are located extracellularly, in the pore-forming

domain between S5 and S6. Patient EP2003 (c.638C>T, p.R213Q in S4) is located in the S4 voltage-sensing domain within the transmembrane region and patient EP2001 (c.881C>T, p. A294V) variant is located within the S6 transmembrane domain. Each of these locations are located in what have been termed 'mutational hotspots' and are predicted to cause a severe phenotype in patients and the *KCNQ2*-DEE clinical disorder. However, as these mutations sit within different locations of 2 functional domains, the precise pathomechanisms of each mutation may actually differ. Ultimately, the precise mechanisms of excitability in human neurons is unknown.

iPSCs underwent dual SMAD inhibition with SB431542 and LDN193189 to generate neural progenitor cells of cerebral cortical neurons after approximately 10 to 12 days depending on the cell line. During this time, the expression of the NPC marker *PAX6* was increased overtime, while the PSC marker *OCT4* was significantly decreased **(Figure 4.5)**. These results are indicative of a successful transformation of iPSCs to a neural progenitor cell fate (Zhang et al., 2010). In addition to this, cell morphology of iPSCs changed dramatically over the first 10 days, from the large, round nuclei of the iPSCs into elongated, columnar shaped nuclei of NPCs.

By day 8 of the neuronal differentiation protocol, the appearance of neural rosettes, a hallmark of NPC formation, could be seen forming **(Figure 4.4)**. As there are likely NSC, NPC and glial cells present in the cell culture at this time, we further characterised these cells at day 20 by immunocytochemistry. Cells were positively stained for the NSC/NPC markers PAX6, SOX2, NESTIN and FOXG1, the proliferation marker Ki67, and the glial cell marker S100B **(Figure 4.7)**. FOXG1 had the highest expression, being expressed in approximately 80% of cells, which is unsurprising as FOXG1 is also expressed in glial cells (Weise et al., 2018). Ki67 expression is indicative of dividing NPCs, which was expected to be highly expressed during this stage (Kee et al., 2002), however, the Ki67 protein expression is cell cycle-specific with the highest level in the M phase, and weaker signal in the other phase of cell cycle may be under-estimated by automated counting. Finally, we found approximately 40% of cells were positive for the glial cell marker S100B **(Figure 4.7)**. Glial cells are critical for NPC growth and maturation at this stage. We then quantified the expression of the same markers at the RNA level to confirm these findings **(Figure 4.8)**. This data revealed that there was no significant difference in gene expression of NPC markers between patient and control lines at day 20, suggesting that our *KCNQ2* mutations do not significantly affect the initiation of neural induction in these patients.

Between day 20 and day 30 of the neuronal differentiation protocol, cells began to change morphology and gene expression. Most markedly, we began to see a reduction in the expression of PAX6 in day 30 cells compared to day 20 **(Figure 4.11)**. Conversely, we observed an increase in the expression of DCX, a post-mitotic marker, and both suggest the birth of new neurons at this stage **(Figure 4.11)**. We then stained cells for the pan-neuronal marker *TUJ1* at day 30 and found that approximately 70% of cells were positive for *TUJ1* at this stage **(Figure 4.9)**. Most post-mitotic neurons in the cerebral cortex emerge from progenitor cells positive for $TUJ1^{+}$ cells, therefore, TUJ1 is a good pan-neuronal marker for neuronal development and maturation (Smith et al., 1998). Similarly, we stained neurons for the mature neuronal marker *MAP2* (microtubule associated protein) and found it was expressed in approximately 56% of cells **(Figure 4.9)**. *MAP2* is expressed shortly after the switch from neural precursor to neuron, making it a useful marker for neuronal maturation (Dehmelt et al., 2004). *MAP2* affects microtubule dynamics, neurite outgrowth and synaptogenesis (DeGiosio et al., 2022). The percentage of cells positive for *S100B* did not significantly change between day 20 and day 30, however, the positively stained cells appear to be dispersed more evenly between neurons at day 30 compared to day 20 **(Figure 4.9)**. Finally, we stained day 30 cells for NESTIN and Ki67 and both were significantly reduced. There was approximately an 18% reduction in NESTIN expressing cells and a 28% reduction in Ki67+ cells **(Figure 4.9)**. Together, these results indicate a reduction in the number of NPCs and proliferating cells, suggesting that at this stage, there is already a proportion of terminally differentiated neurons in the culture. We confirmed the expression of *TUJ1*, *MAP2* and *S100B* at the RNA level by RT-qPCR **(Figure 4.10)** and found there was no significant difference between patient and control lines. This is important to note, as alterations in the expression of *TUJ1* and *MAP2* can lead to developmental delay and Epilepsy.

In humans it takes approximately 100 days for cortical neurogenesis to be completed (Caviness et al., 1995). This timeframe has also been used to generate cortical neurons *in vitro* (Y. Shi, Kirwan, Smith, et al., 2012). In this study, we cultured neurons until day 100 and characterised the neurons at various time points. Between day 20 and day 100, neurons became larger, more dense and formed extensive connections with one another with some neurons forming clusters overtime **(Figure 4.6)**.

An important step in the formation of functional neuronal networks is the formation of synapses. Synapses are junctions designed for the fast transfer of electrical information unidirectionally from one neuron to another. At the presynaptic terminal, the neurotransmitter is released while the post-synaptic terminal senses neurotransmitters via

receptors (Südhof, 2018). We quantified the expression of the pre-synaptic marker synaptophysin and the post-synaptic marker PSD-95 at day 60 and day 100 of neuronal development. Neurons were stained with both markers at two timepoints and positive cells were calculated. We found there was a significant increase in both Syn1 and PSD-95 positive cells at day 100 compared to day 60 **(Figure 4.12)**. This suggests that neurons are still forming new synapses after 60 days in culture. We then measured the expression of both markers at the RNA level and found there was no significant difference between expression in patient and control neurons, suggesting that the *KCNQ2* variants (mutations) did not significantly affect synapse formation in our neuronal induction method **(Figure 4.12).**

During the establishment of the cerebral cortex, neurons are generated in successive waves to produce 6 layers of cells one on top of another, causing an inside-out patterning (Agirman et al., 2017). It has been shown that a *KCNQ2* variant caused hyperexcitability in pyramidal cells of cortical layers II, III and V of the motor cortex in a patient with Epileptic Encephalopathy (Niday et al., 2017). To verify that our neurons are of cortical origin, we measured the expression of cortical markers specific to different cortical layers. TBR1 was used to identify layer VI, CTIP2 for layer V, and BRN2 and SATB2 for layers II, III and IV. Immunocytochemistry staining revealed that in our neuronal culture we had neurons positive for TBR1, SATB2 and CTIP2. Over 50% of cells were positive for CTIP2, approximately 5% were positive for SATB2 and approximately 10% were positive for TBR1 **(Figure 4.13)**. Interestingly, we did find some cells that were positive for both TBR1 and SATB2. As SARB2 is widely expressed in layers II/III and IV/V, SATB2 positive neurons may have been derived from any of these cortical layers (Digilio et al., 2015). Double positive staining of neurons has been described previously. One study found that 7% of the rat neurons in their culture were positive for both CTIP2 and SATB2, markers which are known to suppress each other's expression (Arlotta et al., 2005). This concept has also been described *in vivo* in the human cortex (Nielsen et al., 2014). We then measured the expression of CTIP2, TBR1, SATB2 and BRN2 at the RNA level and found there was no significant difference between the expression levels of any of the markers in patient and control neurons **(Figure 4.14)**. Together, this data reveals the presence of both upper and lower layer excitatory cortical neurons in our neuronal culture at day 100.

Approximately 40% of neurons are glutamatergic, with the majority of these located in the frontal cortex (Gasiorowska et al., 2021). The most abundant neurotransmitter in the CNS, glutamate, has many important roles in brain function. Glutamate is involved in the formation of memories, learning and synaptic plasticity (Mayer et al., 1987). *GLUR1* is a post-

synaptic glutamate receptor that plays a direct role in excitatory synaptic transmission throughout the brain (Riedel, 2003). *vGLUT* is a glutamate transporter that is involved in controlling the amount of glutamate that is released into the synaptic cleft (Martineau et al., 2017). Glutamate plays an important role in epilepsy as it is involved in the initiation and spreading of seizure activity in the brain (Barker-Haliski et al., 2015). We found that over 80% of neurons were positive for *VGLUT*, while approximately 60% of neurons were positive for the receptor GLUR1 **(Figure 4.15)**.

GABAergic neurons are the inhibitory neurons of the brain, making up about 10-20% of all neurons. GABA is the main source of inhibition that counterbalances neuronal excitation in the brain (Caputi et al., 2013). Therefore, when generating an *in vitro* model of human epilepsy, the presence of GABAergic neurons is necessary for a physiologically relevant model. We stained the neurons for GAD67, a GABAergic marker involved in GABA synthesis, and found that approximately 13% of neurons were positive for the marker **(Figure 4.15).** We then measured the expression of *VGLUT1, GLUR1* and *GAD67* at the RNA level and found that there was no significant difference in the levels of each marker between patients and controls **(Figure 4.15)**. Many protocols exist for the generation of GABAergic neurons, which are then often co-cultured with glutamatergic neurons (S. Wang et al., 2023). This is an interesting method to model the disease which may be more physiologically relevant to directly control the percentage of GABAergic neurons. Although GABAergic neurons are well-known for their inhibitory effects, they have also been shown to play a role in seizure generation and maintenance (Magloire et al., 2019). This underscores their importance in the overall pathophysiology of epilepsy disorders and highlights their importance in disease modelling. Here, we present a network of mainly glutamatergic neurons with some cells positive for the GABAergic marker GAD67.

It is unknown whether the pathophysiology of *KCNQ2*-DEE is caused by an alteration in M current alone, or from maladaptive cellular re-organisation as a compensatory mechanism for *KCNQ2* channel dysfunction. One study looked at a specific *KCNQ2* mutation (R581Q) and found that the intrinsic action potential properties did not match up with a loss of M-current alone. Their data revealed that there was a gain of other voltage-gated potassium channels as a result of the mutation (Simkin et al., 2021). To analyse whether there was a similar dyshomeostatic effect in our neurons, we measured the expression of several other potassium channel genes that are involved in fast re-polarisation of action potentials and sodium channels that directly interact with *KCNQ2*. We found that a number of the potassium channel genes including *KCNMA1, KCNMB1, KCNA1, KCNN1, KCNN2, KCNN3*

KCNQ5 and *KCNQ2* were significantly upregulated in patients compared to controls **(Figure 4.17)**. *KCNMA1* and *KCNMB1* are BK channels, a type of Ca^{2+}-activated potassium channels, that have a large single channel conductance that enable a fast efflux of potassium ions, causing hyperpolarisation (Yang et al., 2015). *KCNN1, KCNN2* and *KCNN3* are SK channels. These are small conductance Ca^{2+}-activated potassium channels that mediate one part of the after-hyperpolarisation that occurs after an action potential (Faber et al., 2007). These genes have been previously implicated in epilepsy in both human and animal studies (Lerche et al., 2013). Our results suggest that either due to a loss of M-current, or simply the *KCNQ2* mutation, neurons undergo altered expression of ion channels to try control intrinsic excitability.

Similarly, we found that sodium channel genes *SCN1A, SCN2A* and *SCN8A* were all significantly upregulated in our patient neurons **(Figure 4.18)**. Sodium channels directly interact with *KCNQ2* and are all associated with epilepsy. *SCN1A* is one of the most common epilepsy-associated ion-channelopathies, and par excellence Dravet syndrome (or *SCN1A*-developmental and epileptic encephalopathy)(Ding et al., 2021). *SCN2A* and *SCN8A* are both associated with early onset (neonatal onset) developmental and epileptic encephalopathy (Zeng et al., 2022; Wagnon et al., 2015). Furthermore, sodium channels and potassium channels work together closely to regulate action potentials, especially with gain-of-function mutations, which resembles the timing of onset, interestingly, to *KCNQ2*-DEE, which is often in the neonatal period, whereas loss of function mutations of *SCN1A*, typically present later outside of this period. In addition, these results may also help explain why sodium channel blocker AEDs such as carbamazepine may help treat seizures in patients with *KCNQ2*-DEE as reported in the literature (Dilena et al., 2022).

In summary, we analysed the molecular basis of NPCs through to mature neurons over a 100 day dual SMAD inhibition protocol. We found that *KCNQ2* mutations had no significant effect on cell's ability to form NPCs, synapse formation, cortical cell identity, or the percentage of glutamatergic versus GABAergic neurons in our culture. However, when we looked at the expression of other potassium and sodium channels, we found that several genes were significantly upregulated in our patient neurons. These genes are all associated with epilepsies and DEE, it raises hypotheses surrounding the phenotypes associated with *KCNQ2*-DEE, which may not all be related to altered reduced M current conductance, or indeed may be related to altered expression patterns of other important potassium and sodium ion channel genes. We have successfully generated patient-specific 2D neuronal cell lines for further modelling of *KCNQ2*-DEE. A limitation of this model is that it relies almost exclusively

on excitatory neurons. The incorporation of well-defined inhibitory interneurons, and glia would be extremely beneficial as they are critical in the synchronisation of firing during epilepsy activity, as well as 3D modelling. Further phenotypic characterisation of the electrophysiological properties is also warranted to further model disease versus control neurons **(Chapter 5 and Chapter 6)**.

Chapter 5. Analysis of Functional Network Activities of *KCNQ2*-DEE iPSC-Derived Cortical Neurons by Multi-Electrode Array

5.1 Introduction

KCNQ2-DEE is characterised by the onset of severe intractable seizures often in the first few days of life. For many patients, these seizures are extremely drug-resistant, and a combinatorial drug approach is often needed to control seizures (Weckhuysen et al., 2013). A potassium channel opener drug called Retigabine was approved by the European Medicines Agency (EMA) and the Food and Drug Administarion (FDA) in 2011, which held great promise for epilepsy in general, with potential specificity in *KCNQ2*-related seizures, and in particular those with loss-of-function (LOF) mutaitons/variants **(Figure 5.1)** (Wickenden et al., 2000). However, this drug had several adverse effects such as dizziness, tinnitus, slurred speech, tremor, and skin discoloration (Porter et al., 2007). Additionally, this drug would likely not be useful for the more recently identified patients with a gain-of-function *KCNQ2* mutation/variant, where seizure exacerbation is plausibly the risk (Nissenkorn et al., 2021). Ultimately, retigabine may be considered as a type of precision therapy for patients with a loss of function mutation but is not an option for many patients, and clinical experience to date is still limited.

One of the major limitations in the development of improved therapies for monogenetic disorders such as *KCNQ2*, is the lack of appropriate human disease models. As discussed throughout this thesis, iPSC technology has now made it possible to create patient-specific neuronal models which can be used as a platform to both model the disease phenotype and perform drug screening. This facilitates a greater understanding of the disease phenotype which will help develop new therapies and also allows us to screen existing drugs. In this **Chapter**, I will give an overview of the evidence of altered electrophysiological properties of *KCNQ2*-DEE iPSC-derived cortical neurons with the pathogenic variants F261L, A65T, and A294V and discuss the known literature on the topic with a particular focus on the use of Multi-Electrode Array (MEA) technology.

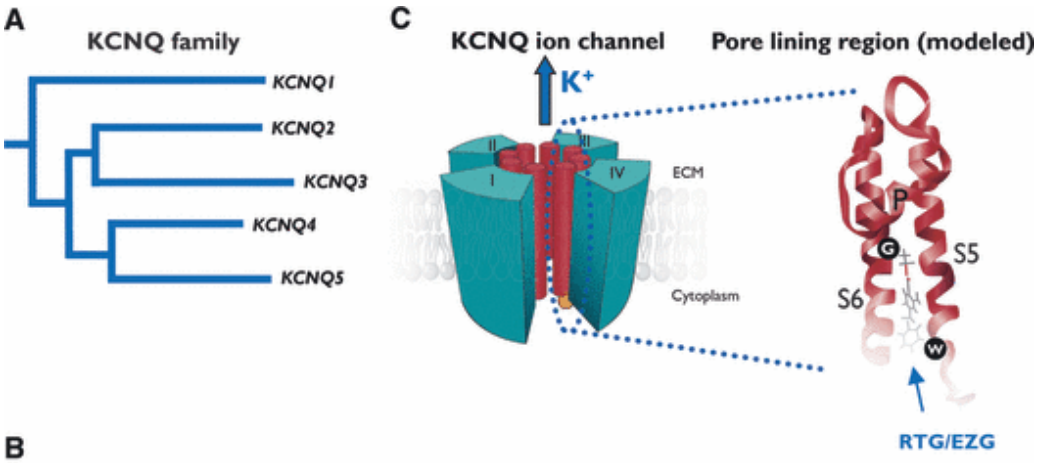

B

Assay	Effect	EC_{50} or IC_{50}
KCNQ2/3	Positive allosteric modulator	EC_{50} = 1.6 μM
KCNQ3/5	Positive allosteric modulator	EC_{50} = 1.4 μM
KCNQ2	Positive allosteric modulator	EC_{50} = 2.5 μM
KCNQ3	Positive allosteric modulator	EC_{50} = 0.6 μM
KCNQ4	Positive allosteric modulator	EC_{50} = 5.2 μM
KCNQ5	Positive allosteric modulator	EC_{50} = 6.4 μM
KCNQ1	Not a positive allosteric modulator Weak inhibitor	IC_{50} ~ 100 μM

Figure 5.1 Schematic illustration of the pharmacological potency and mechanism of action of Retigabine on KCNQ2/3 channels.

(A) The genes within the KCNQ potassium ion channel family. **(B)** The pharmacological potency of Retigabine (RTG) against all members of the KCNQ family. **(C)** Illustration of an assembled KCNQ2/3 channel, highlighting the binding site of Retigabine at the S5 and S6 region in the pore region (Gunthorpe et al., 2012). Abbreviations: RTG, retigabine; EZG (Ezogabine, alternative name for retigabine).

5.1.1. MEA-technology and iPSC-derived neurons

MEAs are a commonly used technique for recording the electrophysiological activities of neurons. MEAs consist of an array of planar or 3-Dimensional electrodes embedded in the base of a cell culture dish, that acts as an electrical interface which enables the detection of electrical activity by either spontaneous or evoked firing of neurons (Spira et al., 2013). MEAs can detect spikes and bursts which represent Action Potentials (APs) and multiple APs detected by patch clamping, respectively (Mendis et al., 2016).

MEA can record neuronal activity over long periods of time in a non-invasive manner making it extremely useful for functional characterisation, disease modelling and drug screening (Manz et al., 2021). However, it is important to note that MEA technology does have lower resolution than single-cell patch clamping as MEAs record the field potential electrical

activity from the extracellular space while single-cell patch clamping records the action potential electrical activity from an individual neuron (Jäckel et al., 2017). Therefore, for more precise information on neuronal response at the single-cell level, patch clamping is necessary.

5.1.2. MEA coating agents

One of the main considerations when performing MEA experiments is choosing an appropriate coating agent. Previous studies have reported that culturing neurons directly onto the MEA plates leads to cell clumping and poor cell attachment, which can affect the functional analysis of neurons (Charkhkar et al., 2012). Therefore, it's important that MEA plates are coated with an extracellular matrix (ECM) that will support cell attachment, proliferation, and connectivity *in vitro* (Barros et al., 2011). iPSC-derived neurons can continue to be cultured on Geltrex but only for short periods of time. It has shown to be an effective coating method until cells reach the neural progenitor stage, where they are then usually passaged to coating material more favourable for long term maturation of neurons (Schmidt et al., 2018). Additionally, Geltrex or Matrigel consist of undefined ECM components and growth factors, making it potentially xenogeneic (Hagbard et al., 2018). This has led to the use of chemically defined ECM molecules, whereby two substrates are usually combined, i.e. Poly-l-ornithine/Laminin (Liberio et al., 2014), Poly-l-ornithine/Fibronectin or Poly-d-lysine/Laminin (Liberio et al., 2014). These molecules support cell attachment however they are expensive to purchase and are prone to variability in quality between batches.

More recently, researchers have been using non-peptide polymer substrates as coating agents on MEA plates. These substrates are useful as they are resistant to enzymatic degradation (Fattahi et al., 2014). Examples of these polymers include polypropyleneimine, polyethyleneimine and polyelectrolyte multilayers (PEMs) which are often used alone or in combination with peptide-based coating agents such as Laminin (Yin et al., 2021). Combining peptide-based coating agents allows for a balance between resistance to protein degradation and biological compatibility with cells.

5.1.3. MEA literature and iPSC neuronal models of early onset developmental and epileptic encephalopathy (DEE)

As there has been limited functional characterisation carried out in iPSC-derived neurons in *KCNQ2* patients, I will also discuss studies involving other epilepsy-associated genes. There

is still little known about how the developmental expression of *KCNQ2* channels affect neuronal excitability. We don't understand how a change in M-current, either a gain or loss of current, alters the electrophysiological properties of neurons. In fact, it's not known whether the final pathophysiology mechanism of *KCNQ2* in neurons is caused by dysfunctional M current or from cellular re-organisation in an attempt to compensate for chronic *KCNQ2* channel dysfunction. To gain a better understanding of the electrophysiological properties of neurons with a *KCNQ2* mutation, Simkin and colleagues (Simkin et al., 2021) used MEA technology on iPSC-derived neurons with a *KCNQ2* variant (c.1742G>A, p.R581Q, in the C-terminal cytoplasmic tail). In electro-encephalograms (EEGs) of *KCNQ2* patients, an interictal burst-suppression pattern is often present early in the neonatal period (Weckhuysen et al., 2012). This involves large paroxysmal bursts of neuronal firing separated by periods of electrical silence. To determine whether they could recreate this phenotype *in vitro*, the researchers used MEA technology to study neuronal activity during neuronal development *in vitro* using human iPSCs. First, they assessed spontaneous neuronal activity over a 3-week period (days 15 to 31) of neuronal differentiation. They found that the distribution of spikes was significantly irregular compared to isogenic control neurons, indicated by an increased Interspike-Interval Coefficient of Variation (ISI CoV). Patient iPSC-derived neurons were susceptible to greater bursting, with significantly shorter intervals between spikes in bursts and significantly longer intervals between each burst. This phenotype is reminiscent of the interictal burst-suppression pattern seen in EEGs. When they examined the neuronal firing pattern over time, they found that patient neurons had more bursting electrodes which increased overtime as neurons matured in culture (Simkin et al., 2021). Simkin et al, 2021 then examined the effects of chronic M-current inhibition using XE-991 (1µM) on spontaneous neuronal firing in control neurons to compare with the electrophysiological properties of patient neurons. They found that chronic M current Inhibition led to significantly increased bursting activity and an irregular firing pattern seen in parameters such as the ISI CoV, number of bursts, number of spikes per burst, and burst frequency. Importantly, they found the effects of chronic M current inhibition to cause a more severe phenotype than the phenotype seen in patient neurons (Simkin et al., 2021). This is likely due to the patient having a less significant loss of *KCNQ2* channel function compared to a 100% loss of function by XE-991 treatment (Greene et al., 2017). Using MEA technology, these researchers successfully modelled the *KCNQ2* variant (R581Q) and revealed novel insight into the pathophysiology of the disease. Additionally, this model can also be used for subsequent drug-screening.

Another study looked at a mutation in the *KCNT1* gene, a sodium-activated potassium channel known to cause developmental and epileptic encephalopathy (*KCNT1*-DEE) as well as other epilepsy phenotypes such as autosomal dominant nocturnal epilepsy (Quraishi et al., 2019). To understand how these mutations contribute to hyperexcitability in neurons, they generated a hiPSC-derived neuronal line with a *KCNT1* (P924L, in the C-terminal cytoplasmic tail) mutation. They found that P924L expressing neurons had an increased mean firing rate, and burst frequency was more than doubled compared to the isogenic control. Interestingly, they found that burst intensity was increased for P924L-expressing neurons but burst durations were shorter. Finally, they assessed the synchrony index values and found they were significantly increased in P924L-expressing neurons compared to controls, suggesting firing patterns were irregular (Quraishi et al., 2019).

SCN2A is a sodium channel gene that closely interacts with *KCNQ2* and is one of the leading causes of DEE (Howell et al., 2015). *SCN2A* plays an important role in AP initiation and propagation during development (Rush et al., 2005). The L1342P mutation (in the Transmembrane S5), is a recurrent mutation that leads to DEE (Hackenberg et al., 2014), from which a reference hiPSC line was generated using CRISPR/CAS9 technology to analyse the electrophysiological properties of neurons *in vitro* (Que et al., 2021). L1342P iPSC derived neurons fired at a much higher level than control neurons during spontaneous neuronal network recordings on MEA. They also detected a significantly greater number of bursts in L1342P neurons compared to controls (Que et al., 2021). They then used this model to perform drug screening. They found that on MEA, 50µM of phenytoin could significantly reduce Mean Firing Rate (MFR) in L1342P neurons, while only 40µM of Phenytoin was required to significantly reduce MFR in controls, suggesting a gain of function (GOF) mutation. Similarly, a lower dose of phenytoin (30µM) could significantly reduce bursting in control neurons while 50uM of phenytoin was required in L1342P neurons (Que et al., 2021). This data suggests that neurons carrying the L1342P mutation have reduced sensitivity to phenytoin. This result could explain why patients carrying this mutation are largely resistant to this drug in the clinic. This data demonstrates the potential of MEA technology in disease modelling and drug screening.

5.1.4. Compound E use for neuronal maturation on MEA

A small molecule called Compound E has been shown to accelerate neuronal maturation *in vitro*. Compound E is a cell-permeable, selective inhibitor that blocks the gamma-secretase and cleavage of the notch intracellular domain. This molecule works by preventing the

generation of glia from the progenitor stage and accelerates neuralisation (Bianchi et al., 2018). This has been shown to generate post-mitotic neurons and substantially accelerate neuronal maturation in motor neurons (Chen et al., 2014). In this study, we incorporated Compound E (0.1μM) at day 20 for 6 days until day 26, as this was the peak of the progenitor stage, to analyse its effects on neuronal activity and maturation using MEA.

The aims of this **Chapter** are to 1) analyse the effect of Compound E on neuronal maturation and function. 2) perform extracellular electrophysiological recordings of iPSC-derived cortical neurons from 3 patients harbouring 3 different *KCNQ2* variants (p.A294V; p.F261L; p.A265T, respectively) on MEA plates to analyse neuronal excitability *in vitro*. We sought to compare the results to controls. To my knowledge these experiments have not been performed to date.

5.2. Materials and Methods

5.2.1 Preparation of MEA plate

5.2.1.1 Preparation of Poly-D-Lysine coating

Poly-D-Lysine (PDL) (Sigma, cat# P6407-5MG) was diluted in 5ml of DPBS to generate 1mg/ml stock solution. This was filtered with a 0.22µM sterile filter (Lennox, #A16534K) and aliquoted into 500µl stock vials. PDL was used at a working concentration of 10µg/ml by diluting a 500µl stock vial in 49.5ml DPBS for coating.

5.2.1.2 Preparation of Laminin

Laminin (Sigma, cat# L2020-1MG) was diluted in cold DPBS without calcium and magnesium (Thermo Fisher cat# 14190144) on ice and stored in 100µg/ml stock vials. Laminin was used at a working concentration of 10µg/ml by diluting 1ml stock vials in 9ml of DPBS.

5.2.1.3 Coating of MEA plate

MEA plates underwent a double coating treatment with PDL, and Laminin as described in **Chapter 4**. When coating the MEA plates, it was very important to only coat directly on top of the electrodes rather than the entire well to ensure cells attached to the electrodes. To do this, the wells were coated with an 8µl singular 'drop' of coating agents. Approximately 6-8ml of sterile water was added around the wells of the MEA plate to increase the humidity and prevent the coating agents from drying out during the incubation stages.

5.2.1.4 Seeding of cortical neuron progenitors onto MEA plate

Cortical neuron progenitor cells were seeded onto 48 well MEA plates at day 20 of the differentiation protocol as outlined in **Chapter 4**. Cells were seeded in triplicate at a density of 25 X 10^4, 50 X 10^4 and 75 X 10^4 in 8µl drops onto the centre of each well ensuring they covered the 16 electrodes. Different seeding densities were tested to determine the optimal density. The cells were allowed to attach to the coated plates for 1-2 hours at 37 °C and 5% CO2 before being topped up with 300µl of media. Y-27632 (Rock Inhibitor) was added into the medium for the first two days after replating to increase the survival of cells on the MEA plates. Cells underwent a half media change every other day. Cells were then allowed to differentiate into cortical neurons for 20 days before MEA recordings were started. The information on iPSC lines used for MEA recordings are outlined in **Table 5.1.**

Table 5.1. List of iPSC lines used for MEA analysis

Status	iPSC line	Gender	Age (years)	Mutation
N=3 *KCNQ2* mutations; N=9 iPSC lines	EP2004 C1	Female	7	c.793G>A(A265T)
	EP2004 C7	Female	7	c.793G>A(A265T)
	EP2004 C8	Female	7	c.793G>A(A265T)
	EP2002 C1	Female	4	c.783A>C (F261L)
	EP2002 C2	Female	4	c.783A>C (F261L)
	EP2002 C3	Female	4	c.783A>C (F261L)
	EP2001 C4	Male	5	c.881C>T(A294V)
	EP2001 C5	Male	5	c.881C>T (A294V)
	EP2001 C8	Male	5	c.881C>T (A294V)
N= 3 healthy donors; N= 9 iPSC lines	EP2C004 C2	Female	12	N/A
	EP2C004 C4	Female	12	N/A
	EP2C004 C5	Female	12	N/A
	EP2C002 C5	Male	4	N/A
	EP2C002 C6	Male	4	N/A
	EP2C002 C7	Male	4	N/A
	EP2C001 C1	Male	15	N/A
	EP2C001 C2	Male	15	N/A
	EP2C001 C4	Male	15	N/A

5.2.2 MEA data recording

MEA recordings were taken every other day for a 3-week period from day 40 to day 61, before changing the media of the cells. The 48 well MEA plate was loaded into the MAESTRO MEA recording amplifier (Axiom Biosystems). The temperature was maintained at 37°C by switching on the heater option. Signals were sampled at 12.5 kHz, digitised, and analysed using Axion Integrated Studio Navigator (AxIS) 2.5.2 with a 300 Hz high pass and a 5 kHz low pass filter. An adaptive spike detection threshold is set at 6 times the standard deviation for each electrode with 1s binning according to the settings from the published paper (**Figure 5.1**) (Simkin et al., 2021). Raw data (.raw), filtered data(.raw) and spike data (.spk) were saved for analysis.

5.2.3 MEA data analysis using the Neural Metric Tool and Axion Metric Plotting Tool

The exported spike files (.spk) were batch-processed using the Neural Metric Tool (Axion Biosystems). The settings used in the software are presented in **Figure 5.2**. Briefly, the Active Electrode Criteria was defined as a minimum of 5 spikes/min. The Single Electrode Burst detector was set to detect the Inter-Spike Interval (ISI) threshold with a minimum of 5 spikes in a maximum of 100 ms ISI. The Network Burst detector was set to a minimum of 50 spikes with a maximum of 100 ms of ISI and a minimum of 35% of active electrodes involved in

bursting. To analyse the spontaneous activity of the cells, the first 300s (5min) of MEA recording was used. All the processed data were exported as a comma format (.csv file). For group comparison (i.e., time-course, control-patient pair, or treatment), the .csv file was uploaded to the Axion Metric Plotting Tool. The summarised .csv file with parameters was exported for statistical analysis using Graph Pad.

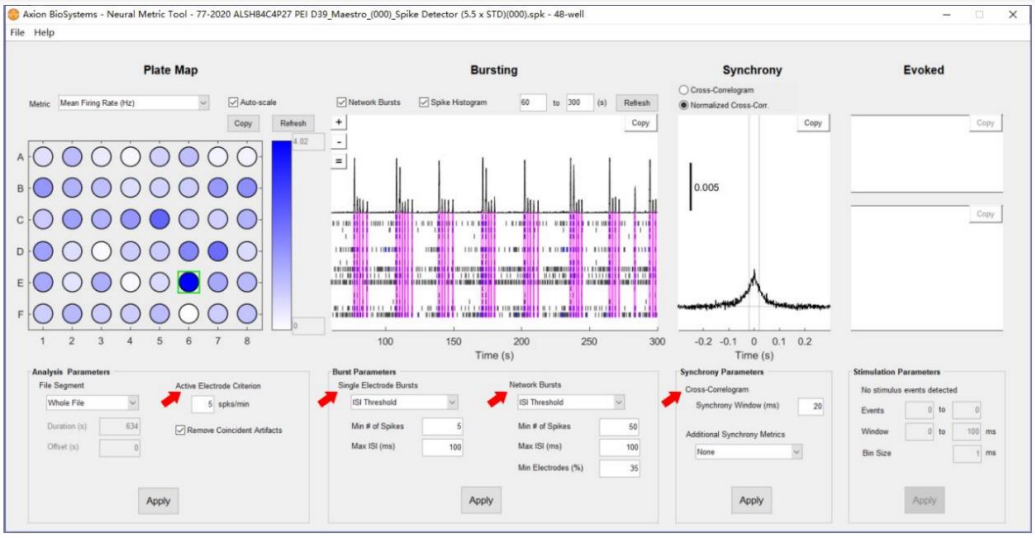

Figure 5.2. Settings used in Neural metric tool for analysis.

Red arrows indicate the parameters chosen for analysis.

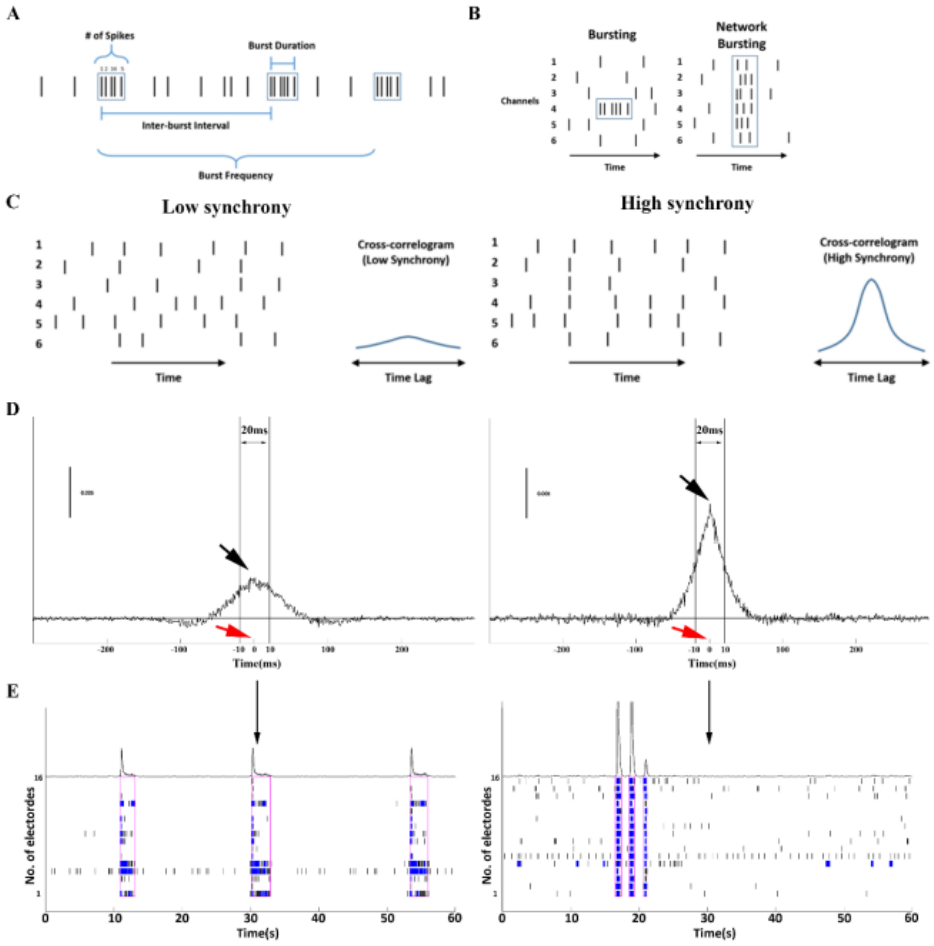

Figure 5.3 Metrics diagram showing types of neuronal activity detected on MEA.

(A) Each black line represents an AP, or "spike" detected by recording electrodes in a single or cluster form (blue boxes). A cluster or group of spikes on a single electrode is called a burst. The period between two single spikes is known as the Inter-Spike-Interval (ISI). In our parameters, If ≥ 5 spikes are detected from a single electrode in 100 ms ISI, the cluster of spikes is considered a burst. **(B)** A network burst is a coordinated cluster of spikes across multiple electrodes (there are 16 electrodes in each well of a 48-well MEA plate) (blue box in the right panel). If >35% of electrodes in a well detect ≥ 50 spikes in 100ms ISI, the coordinated cluster of spikes is considered a network burst. **(C)** Schematic diagram showing low (left) and high (right) synchrony. Synchrony indicates the level of coordinated or simultaneous spiking between electrodes which is quantified using a cross-correlogram between spiking on pairs of electrodes and then pooling across all pairwise combinations in a well (Halliday et al., 2006). The cross correlogram assesses the probability of a spike occurring on electrode A at times relative to a spike on electrode B. This probability is summed across all spikes in electrode B to produce the cross-correlogram. For example, if both electrodes always fire together, the cross-correlogram would have a sharp peak at time 0. **(D)** The Neural Metric Tool computes synchrony by first finding the cross-correlation. Phase lags of zero (x-axis on correlogram, red arrow) indicate synchronous spiking between electrodes. When more electrodes have a similar phase relationship, the probability (y-axis height on the correlogram, black arrow) of that phase-lag (zero for synchrony) increases. The normalized cross-correlation normalizes the cross-correlation to remove the autocorrelation - each electrode's cross-correlation with itself. Tall, sharp cross-correlograms indicate high synchrony (right panel). Short, wide cross-correlograms indicate low synchrony (left panel). **(E)** Raster plot showing low (left) and high (right) neuronal network activities. Data were presented from one patient iPSC-derived cortical neurons.

Table 5.2. Definition of parameters used in this study

Metric	Definition
Mean Firing Rate (Hz)	The total number of spikes divided by the duration of the analysis.
Number of Active Electrodes	The number of electrodes with activity greater than the minimum threshold of 5 spikes/min.
Weighted Mean Firing Rate (Hz)	The total number of spikes in only the active electrodes divided by the duration of the analysis.
Burst Frequency (Hz)	A single electrode burst is described as a train of spikes (> 5 spikes) detected by a single electrode in a defined timeframe (100ms). Burst frequency is total electrode bursts divided by the duration of the analysis.
Network Burst Frequency (Hz)	Network bursts are described as almost perfectly synchronous spikes across electrodes in a well in a defined timeframe (100ms). Total number of network bursts divided by the duration of the analysis equals Network Burst Frequency.
Synchrony index	Area under the well-wide pooled inter-electrode cross-correlation normalized to the autocorrelations is used to present the synchrony. This is normalised between 0 and 1, when fully synchronous firing equals to 1 and fully asynchronous neurons equal to 0.
Network Burst Percentage (%)	The number of spikes in network bursts divided by the total number of spikes, multiplied by 100. This indicates the proportion of neurons involved in the neuronal network communication and transmission.
Network Burst Duration	The length of time in seconds between the first spike and the last spike in a network burst. A longer burst duration is associated with greater excitation and less inhibition.
Number of Spikes per Network Burst	The average number of spikes in a network burst indicates the number of spikes involved in neuronal network activities.
Inter-Spike Interval Coefficient of Variation in Network burst (Network ISI CoV)	Average across network bursts of the ISI CoV (standard deviation/mean of the inter-spike interval) within network bursts. The CoV in combination reflects the distribution of spikes in Network bursts. Small values close to 0 indicate regular firing while larger values close to or >1 indicate irregular firing.

5.2.4. Cleaning and Sterilisation of MEA plates

MEA plates can be sterilised for re-use according to manufacturer's instructions. Briefly, MEA plates were rinsed 3 times with DPBS without calcium and magnesium to remove any cellular debris from the plates. Then, 0.5% trypsin was added to each well and incubated at 37℃ for 30 min to ensure all cells were detached from the plates. Plates were rinsed 3 more times with sterile deionised water to remove any debris or trace proteins that remained. The MEA plates were examined closely under the microscope to ensure all wells were clear of any cellular debris. An additional trypsination step may be added here if any cells are remaining.

Once the plates were clear, the entire plate was filled with 70% ethanol and left for 10 min in the biological safety cabinet to sterilise the plates. The plates were then rinsed once with 90% ethanol, followed by 3 washes with deionised water. To ensure all water was removed from the plates, they were shaken upside down and left open in the biological safety cabinet with the UV on. Once plates were completely dry, they could then be coated in the appropriate coating agent.

5.2.5. Acute drug treatment

MEA recordings were used to record the electrophysiological properties of neurons both spontaneously and after the addition of specific acute drugs with compounds that target either ion channels or neurotransmitter receptors based on published literature (Simkin et al., 2021). The different compounds used are listed in **Table 5.3.** Each compound was dissolved in either water or DMSO, according to manufacturer's instructions, to generate stock concentrations of approximately 1000 times greater than the working concentration. All drugs were stored at -80℃. On the day of drug treatment, the stock concentration of the drugs was freshly diluted with Neural Maturation Medium into a 10-fold working concentration, and 1/10 volume of drug-containing medium, i.e., 33.3µl, was added into each 48-well that contained 300 µl of culture medium.

The timeline for the drug administration is shown below in **Fig 5.4.** First the spontaneous activity of the cells was recorded for 300s, then one of the drugs was added within the 60s, and then the plate was recorded for another 300s. The 60s interval was considered drug administration time. If two doses of a specific drug were being tested, the lower dose would be tested as described above and then the second higher dose would be added at a second 60s interval and recorded for an additional 300s.

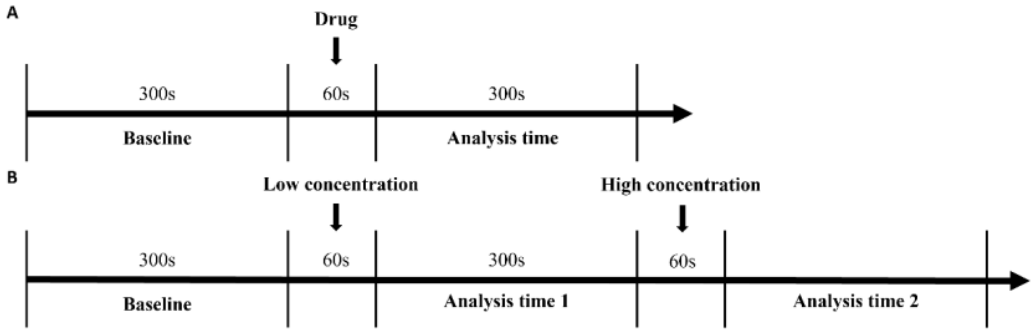

Figure 5.4. Timeline for acute drug administration.

The MEA plate was continuously recorded, with the first 300s recording used as a Baseline. **(A)** A drug was added within the 60s, and the plate was recorded for an additional 300s after adding the drug, which was analysed for drug effect in comparison to baseline. **(B)** If the drug was tested in two concentrations, the low dose was added and recorded first, following the higher dose to determine any dose-dependent effect.

5.2.6. Chronic drug treatment

For chronic drug treatment, the drug was added to the medium at a lower dose as outlined in **Table 5.3.** with every media change and spontaneous MEA recordings were performed every other day.

Table 5.3. List of drugs used for MEA recordings

Drug	Dose 1 (low dose)	Dose 2 (high dose)	Days of administration	Mechanism of action
TTX (Tetrodotoxin)	2.5nM	25nM	45, 55, 65	Na^+ channel blocker
CNQX (cyanquixaline)	5µM	50µM	45, 55, 65	AMPA/kainite receptor antagonist
Glutamate	10µM	100µM	45, 55, 65	Excitatory neurotransmitter
Paxilline	20µM	N/A	50	BK channel blocker
Apamin	500nM	N/A	50	SK channel blocker
XE991	20µM	N/A	45, 55, 65	Blocker of Kv7.2 and Kv7.3
XE991 (chronic treatment)	1µM	N/A	Every other day from Day 30 to Day 60.	Blocker of Kv7.2 and Kv7.3
Carbamazepine	100µM	N/A	50	Na+ Channel blocker

Retigabine	10µM	N/A	50	Kv7.2 and Kv7.3 channel opener

5.2.7 Statistical analysis

Statistical analyses were performed using GraphPad Prism version 9.3.1. Two-tailed either paired or unpaired t-test with multiple-comparison correction or ANOVA was used as indicated. P values are presented as follows: *=p <0.05, **=p<0.01, ***=p<0.001, ****=p<0.0001.

5.3 Results

5.3.1 MEA plate preparation and plating of cortical neurons

The day before the cortical neurons were plated, MEA plates were coated with PDL (10 µg/ml) and Laminin (10 µg/ml) and incubated overnight. The neurons were then passaged by scraping the cells from the surface of the plate to keep the cells in small pieces. The cells were seeded onto the MEA plates at a density of 25 $x10^3$ cells per well of a 48 well plate. Once the cells had attached, 300µl of media was added to each well after 2 hours and images of the cells were taken after 24 hours **(Figure 5.5)**.

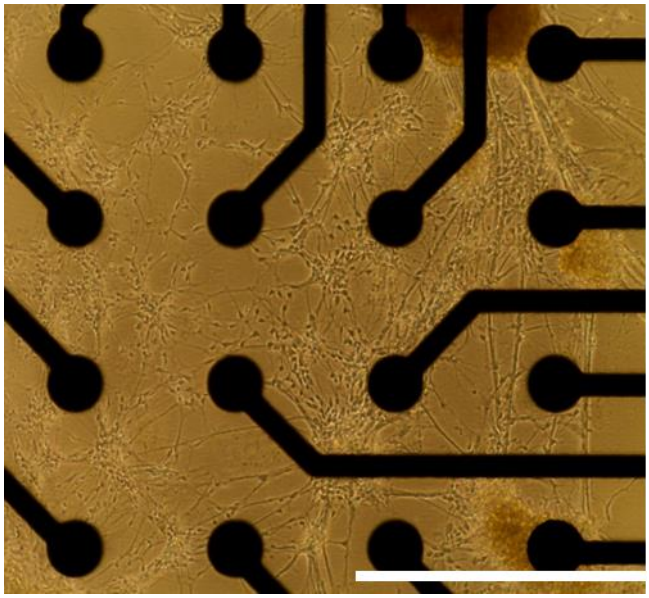

Figure 5.5: Representative image of cortical neurons seeded onto MEA plate after 24 hours.

25 x 10^5 cortical neurons were seeded onto PDL and Laminin coated MEA plates. Scale bar is 100µM.

5.3.2 Compound E increases weighted mean firing rate in cortical neurons

To analyse to impact of Compound E on neuronal maturation and function, we measured several different parameters on MEA in neurons cultured in standard neuronal maintenance medium and neurons cultured in neuronal maintenance medium supplemented with compound E (0.1µM). Compound E was added to the medium every other day for 6 days (Day 20 to 26). MEA recordings were performed from day 40 to day 61. We found that there was no significant difference between the number of active electrodes in both control and patient lines (A265T) between groups. The number of active electrodes increased overtime for each group **(Figure 5.6)**. However, there is an increased weighted mean firing rate (wMFR) in both patient and control neurons cultured in Compound E supplemented medium.

This difference is greater in patient-derived (*KCNQ2*-DEE) lines and increases overtime in culture **(Figure 5.6)**. At day 50, wMFR was significantly higher in the patient line cultured with Compound E than without (*p=0.033, 2.24 Hz ± 0.11 Hz compared to 2.08 Hz ± 0.10 Hz). This difference in wMFR increased overtime. At day 60, wMFR in the patient line + E was 4.62 Hz ± 0.29 Hz compared to patient line alone at 3.14 Hz ± 0.48 Hz. (**p=0.008). Compound E also caused a significant increase in wMFR in control neurons, but only at day 60 (*p=0.042, 1.44 Hz ± 0.03 Hz compared to 1.12 Hz ± 0.08 Hz).

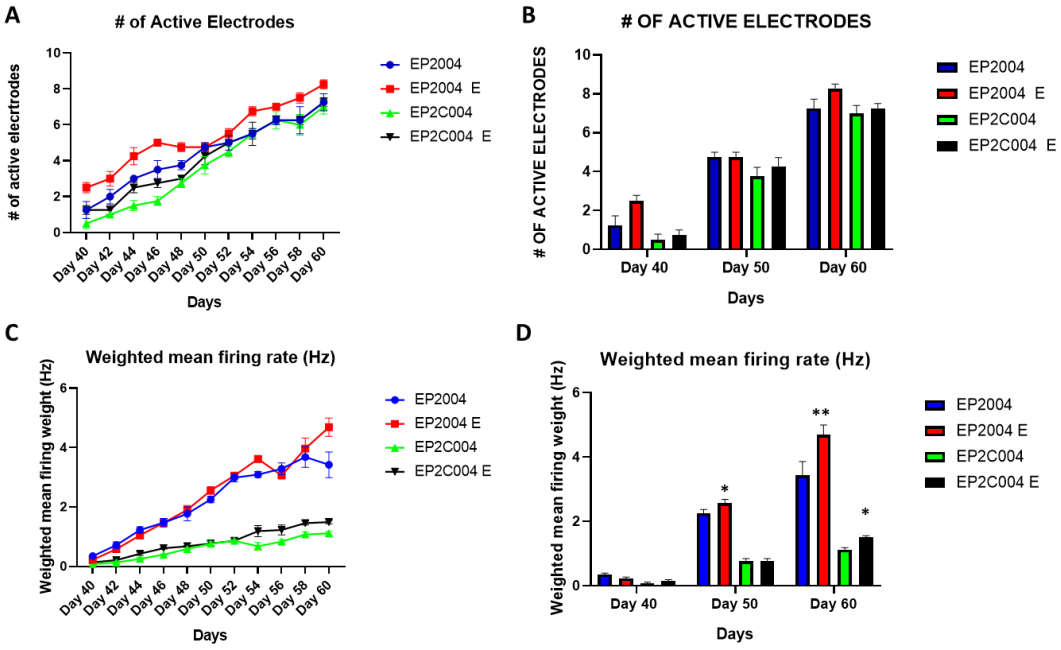

Figure 5.6. Compound E significantly increases the weighted mean firing rate of patient and control neurons.

(A) The number of active electrodes (with 5 spikes/min) during longitudinal recording showing the functional maturity of cortical neurons between the groups. **(B)** Statistical analysis of number of active electrodes between neurons grown with or without compound E (annotated E in the diagram) in 3 lines of EP2004 (A265T) and EP2C004 (n= 6 for each condition). **(C)** The weighted mean firing rate of neurons during longitudinal recording showing a significantly higher MFR (mean firing rate) in neurons cultured with compound E. **(D)** Statistical analysis of wMFR between groups in 3 lines of EP2004 and EP2C004 (n= 6 for each condition). Statistical significance (*p<0.05, **p<0.01, ***p<0.001) was evaluated using an unpaired parametric *t*-test.

5.3.3 Compound E significantly increases the number of bursts seen in *KCNQ2*-DEE neurons

Next, we wanted to analyse whether compound E could affect the bursting firing patterns of neurons. To do this, we measured the number of bursts and number of spikes per burst in each group. As seen in **Figure 5.7**, medium + E causes a significant increase in the number of

bursts seen in patient neurons and this difference increases overtime. On day 50, patient neurons (A265T) cultured in medium + E fired 83 ± 4 bursts compared to 47 ± 4 bursts in normal medium (**p= 0.007). At day 60, patient neurons cultured in medium + E fired 171 ± 5 bursts compared to 88 ± 6 bursts in normal medium (***p<0.001). In contrast to this, there is no significant difference in the number of bursts seen in control neurons with or without the addition of Compound E. Similarly, there is an increased number of spikes/burst in patient neurons cultured in media supplemented with Compound E. This difference can be seen from as early as the first day of recording on MEA (*p= 0.031, 6.5 ± 0.7 compared to 4 ± 0.5). However, no significant difference is seen again until the last timepoint at day 60 (*p=0.012, 15.5 ± 0.7 compared to 13.5 ± 0.5). Again, there is no difference in the number of spikes per burst seen in control neurons **(Figure 5.7).**

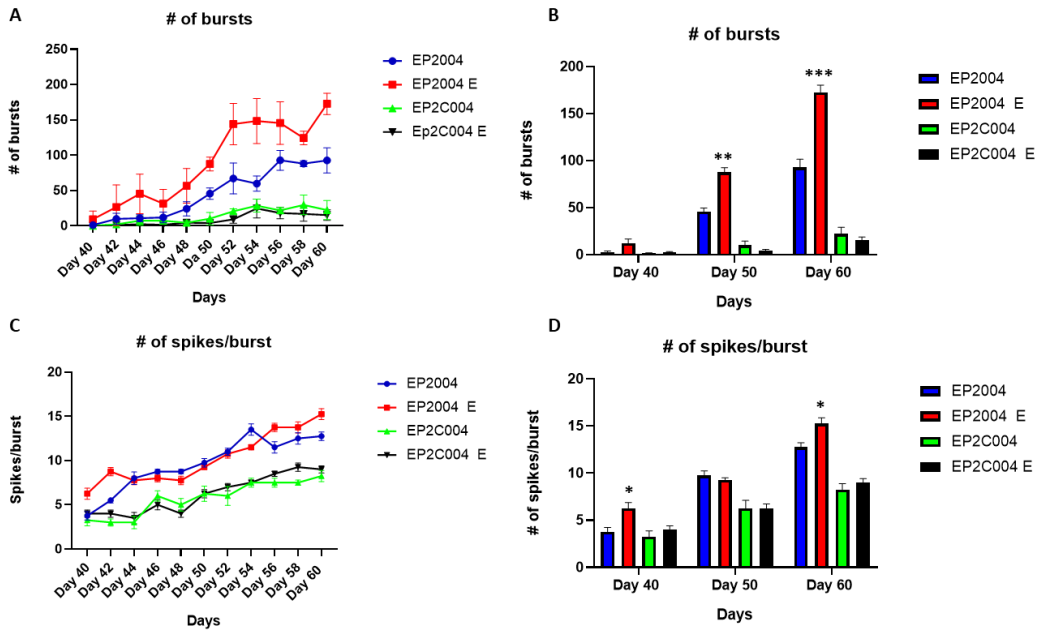

Figure 5.7. Compound E significantly increases the number of bursts in patient neurons.

(A) The number of bursts recorded during a longitudinal recording between the groups comparing the effect of compound E on bursting behaviour. **(B)** Statistical analysis of the number of bursts between groups overtime. **(C)** The number of spikes per burst recorded during a longitudinal recording between the groups. **(D)** Statistical analysis of the number of spikes per burst between groups in 3 lines of EP2004 (A265T) and EP2C004 (N= 6 replicates per group). Statistical significance (*p<0.05, **p<0.01, ***p<0.001) was evaluated using an unpaired parametric *t*-test.

5.3.4 Compound E has no effect on burst frequency or ISI CoV in neurons

Finally, we looked at whether Compound E affected the Burst frequency and ISI CoV of neurons overtime in culture. We found that there was no significant difference between ISI CoV or Burst frequency in neurons grown in media supplemented with Compound E in either

patient or control lines **(Figure 5.8)**. There was a slight trend showing an increase in both burst frequency and ISI CoV due to the addition of compound E in patient lines (Burst Frequency at day 60 p=0.067, 0.043 Hz ± 0.005 Hz compared to 0.038 Hz ± 0.004 Hz)(ISI CoV at day 60 p= 0.084, 3.5 ± 0.3 compared to 3.3 ± 0.2), However, this was not significant **(Figure 5.8)**.

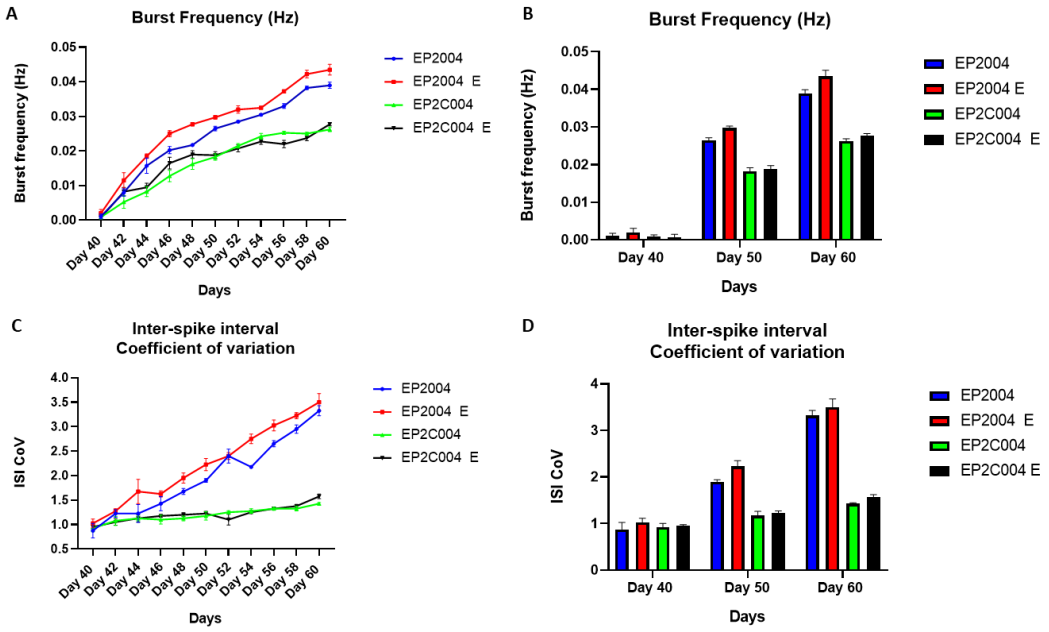

Figure 5.8. Compound E has no significant effect on burst frequency or Inter-spike interval coefficient of variation.

(A) The burst frequency with no significant difference between neurons grown with or without compound E. **(B)** Statistical analysis of burst frequency in neurons between groups in 3 lines from both EP2004 (A265T) and EP2C004 (n=6 replicates per group). **(C)** The ISI CoV of neurons showing no difference between groups. **(D)** Statistical analysis of the ISI CoV between groups in 3 lines from both EP2004 (A265T) and EP2C004 (n=6 replicates per group). Statistical significance (*p<0.05, **p<0.01, ***p<0.001) was evaluated using an unpaired parametric *t*-test.

5.3.5 Spontaneous firing activities are driven by voltage-gated Na^+ channels

During an action potential (AP), the neuron becomes depolarised when Na^+ enters the cell. This process is initiated when glutamate binds to voltage-gated Na^+ channels. Tetrodotoxin (TTX) is a Na^+ channel blocker which blocks this event from occurring in neurons (Narahashi, 2008). Therefore, to confirm that the signals detected in our culture are Na^+ channel mediated APs, we treated our neurons with two different doses of TTX (2.5nM, 25nM) at Day 50. The drug was administered according to the timeline in **Figure 5.4**. Briefly, the baseline was recorded for 300s, then the low dose of 2.5nM was added and recorded for 300s, then

the high dose of 25nM was added and recorded for 300s. We analysed the data using weighted mean firing (wMFR) rate to remove data from any inactive electrodes (less than 5 spikes per min).

We found that there was a significant difference between patient and control lines at baseline. Patient lines had a significantly greater wMFR at baseline compared to control lines (***p<0.001, 3.8 Hz ± 0.4 Hz compared to 1.4 ± 0.3 Hz) **(Figure 5.9)**. The addition of the low dose (2.5nM) of TTX significantly reduced the wMFR in both patient (***p<0.001, 3.8 Hz ± 0.4 Hz to 0.2 Hz ± 0.01 Hz) and control lines (****p<0.001, 1.4 Hz ± 0.3 Hz to 0.2 Hz ± 0.005 Hz) **(Figure 5.9)**. Following the second dose of TTX (25nM), firing was almost entirely eliminated (raw voltage traces showed almost no neuronal spiking). These results suggest that the firing signal detected on MEA are caused by voltage-gated Na^+ channels, as almost the entirety of the signal was diminished by treatment with Na^+ channel blocker TTX.

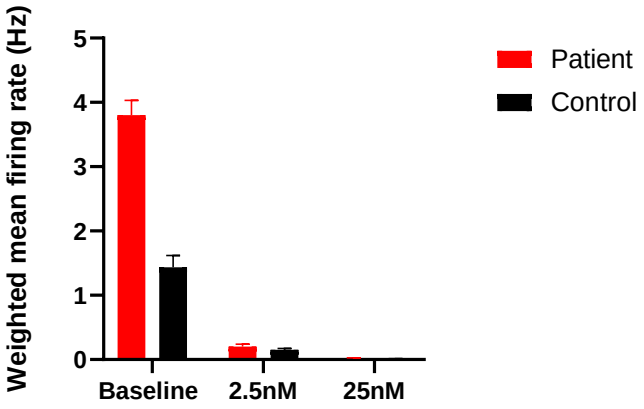

Figure 5.9. Spike activities detected by MEA are voltage-gated Na+ channel-mediated APs.

Baseline recordings were recorded at Day 50 for 300s before two concentrations of TTX were added to determine the dose-dependent response in 3 lines from each patient (F261L, A265T, A294V) and 3 lines from each control. Drugs were administered according to the timeline in **Figure 5.4**. wMFR was significantly reduced at the low dose and completely blocked at the higher dose in both the patient and control group. The total number of used wells was n= 27 from 9 control lines and n=27 from 9 patient lines. Statistical significance (*p<0.05, **p<0.01, ***p<0.001) was evaluated using an unpaired parametric *t*-test.

5.3.6. Formation of functionally matured synapses is confirmed by the response to AMPA antagonist CNQX

Glutamate is the most abundant excitatory neurotransmitter in the CNS which acts via different types of glutamate receptors including AMPA, NMDA and kainate receptors. CNQX is an AMPA antagonist that blocks glutamate, indirectly isolating GABA receptor-mediated

spontaneous inhibitory post-synaptic currents (Brickley et al., 2001). To assess the contribution of AMPA receptors to neurotransmission, we treated iPSC-derived neurons with AMPA antagonist CNQX at day 60. We tested two escalating doses (5μM, 50μM) to monitor if there was a dose-dependent response **(Figure 5.10)**. We found that for patient and control lines, CNQX treatment resulted in a dose-dependent blocking. We measured the wMFR at baseline and found that wMFR was significantly higher in patients (3.6 Hz ±0.3 Hz) compared to controls (1.4 Hz ± 0.05 Hz)(***p<0.001). After the low dose of 5μM, CNQX resulted in a significant reduction in wMFR in both patient (1.9 Hz ± 0.3 Hz) and controls (0.9 Hz ± 0.15 Hz)(***p<0.001). After the high dose of 50μM, CNQX treatment resulted in a further reduction of wMFR in both patient (0.43 Hz ± 0.07 Hz) and controls (0.22 Hz ± 0.03 Hz) (****p<0.0001) **(Figure 5.10)**. This data indicates that a substantial proportion of our excitatory neurons are AMPA- mediated. However, as CNQX did not cause a complete blocking of wMFR, there are likely NMDA and kainate-mediated receptors as well as inhibitory neurons present in our cultures.

We then looked at the effect of the addition of the excitatory neurotransmitter glutamate, on neurons. Extracellular glucose is known to increase spontaneous activity of neurons *in vivo* by binding to glutamate receptors (Sun et al., 2001) and has since been shown in *in vitro* studies using MEA (Demchenko et al., 2022). To analyse the effect of glutamate treatment on our cortical neurons, we used two escalating doses (10μM, 100μM) **(Figure 5.10)**. We found that for both patient and controls, glutamate caused a dose-dependent increase in wMFR. After the low dose of 10μM, wMFR significantly increased in patients (4.8 Hz ± 0.3 Hz) compared to baseline (3.7 Hz ± 0.4 Hz)(**p= 0.006). There was no significant difference in wMFR in controls in response to low dose (10μM). At the higher dose of 100μM, wMFR was increased even further in patients (6.6 Hz ± 0.6 Hz)(***p<0.001) and controls (4.5 Hz ± 0.3 Hz)(***p<0.001)**(Figure 5.10)**.

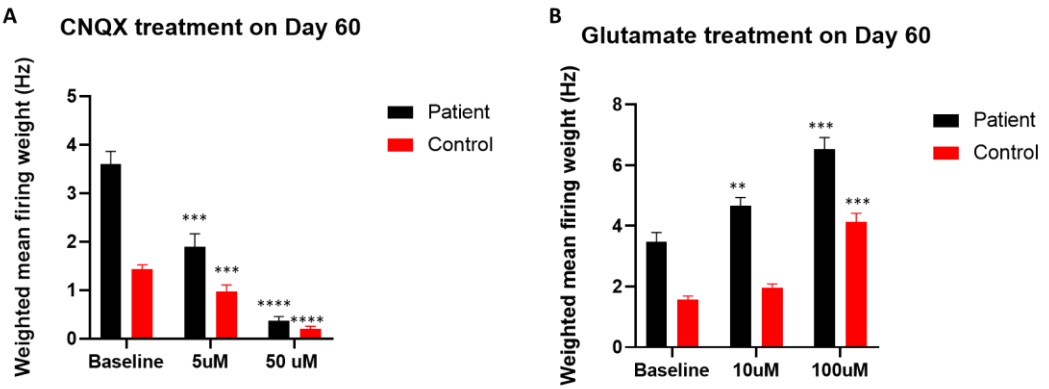

Figure 5.10 AMPA mediated functional synapses were confirmed using antagonists CNQX and glutamate.

(A) The effect of CNQX showed a concentration-dependent blocking (n=27 from 9 control lines and 9 patient lines. (3 lines from each of the pathogenic variants F261F, A65T and A294V). **(B)** The effect of glutamate showed a concentration-dependent increase in neuronal excitability (n=27 from 9 control lines and 9 patient lines). Statistical significance (*p<0.05, **p<0.01, ***p<0.001, ****p<0.0001) was evaluated using an unpaired parametric *t*-test.

5.3.7 *KCNQ2*-DEE neurons exhibit increased spontaneous bursting

One of the main hallmarks of *KCNQ2*-DEE is hyperexcitability in the form of a phasic burst-suppression firing pattern; this is a hallmark severely abnormal pattern on the early neonatal EEG waveforms. The exact mechanism by which the expression of *KCNQ2* (Kv7.2) channels during development affects neuronal excitability is not clear. To determine the effect of the *KCNQ2* mutations in this study on neuronal excitability, we measured neuronal activity on MEA recordings over a 3-week period from Day 40 to Day 61. As each mutation is different, the results will be presented separately for each of the 3 mutations (F261L, A265T, A294V) as phenotypes between patients may differ.

First, we recorded the number of active electrodes over a 3-week period and found there was no significant difference between the number of active electrodes in patient and control cell lines **(Figure 5.11)**. We measured the wMFR of neurons overtime and the mean firing rate in both patient and control neurons increased overtime, and there was a significantly higher wMFR in patient neurons compared to controls. In EP2004 (A265T), wMFR was significantly increased in each line compared to controls at Day 50 (C1= 2.5 Hz ± 0.2 Hz ****p<0.0001, C7= 2.1 Hz ± 0.3 Hz ***p<0.001, C8= 2.4 Hz ± 0.2 Hz ***p<0.001 compared to 0.8 Hz ± 0.2 Hz for controls) **(Figure 5.11)**. By day 60, wMFR increased for both patient and control lines and patient lines (C1= 4.1 Hz ± 0.3 Hz ***p<0.001, C7= 3.4 Hz ± 0.6 Hz ***p<0.001, C8= 4.3 Hz ± 0.5 Hz ***p<0.001 had a significantly higher wMFR than control lines (1.7 Hz ± 0.1 Hz)**(Figure 5.11).** These data reveal that *KCNQ2* (A265T) neurons have a significantly higher wMFR than control neurons and that all neurons' wMFR increases overtime in culture. Similar results were obtained from MEA recordings of EP2001 (A294V) and EP2002 (F261F) which are presented in the supplementary information **(Figure S5.1)**.

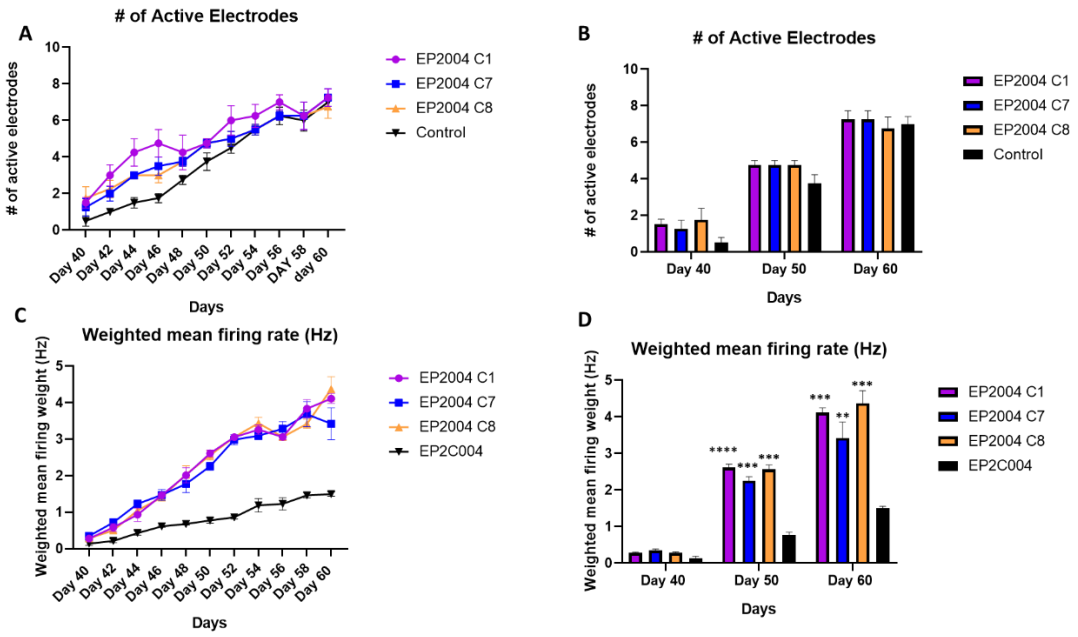

Figure 5.11 *KCNQ2*-DEE neurons show an increased spontaneous firing rate.

(A) Longitudinal recording of the number of active electrodes in *KCNQ2*-DEE neurons and patient neurons. **(B)** Statistical analysis comparing the number of active electrodes between groups. **(C)** Longitudinal recording of the weighted mean firing rate in *KCNQ2*-DEE neurons and controls. **(D)** Statistical analysis comparing the weighted mean firing rate between groups. Three lines from both EP2004 (A265T) and EP2C004 (N= 3 replicates per group) were used. Statistical significance (*p<0.05, **p<0.01, ***p<0.001, ****p<0.0001) was evaluated using an unpaired parametric *t*-test.

As *KCNQ2*-DEE patients often present with a burst-suppression firing pattern on EEG, we hypothesised that *KCNQ2*-DEE neurons would be more likely to fire in bursts than control neurons. To determine this, we measured the number of bursts and number of spikes per burst for patient and control lines. We found that patient neurons (**Day 50**: C1= 62 ± 5 **p=0.006, C7= 49 ± 4 **p=0.009, C8= 88 ± 6 ****p<0.0001)(**Day 60**: C1= 122 ± 11 ****p<0.0001, C7= 98 ± 8 ***p<0.001, C8= 143 ± 6 ***p<0.001) had (i) a significantly higher number of bursts than control neurons at day 50 (14 ± 4) and day 60 (26 ± 7). Interestingly, this difference increased overtime in culture as neurons matured **(Figure 5.12)**. At Day 40 during the first recording period, there was no significant difference between the number of bursts in two groups. Similarly, we found (ii) the number of spikes per burst was also significantly increased in patient neurons (**Day 50**: C1= 10.5 ± 0.5 **p=0.006, C7= 9.5 ± 0.6**p=0.009, C8= 9 ± 0.3 ****p<0.0001)(**Day 60**: C1= 14 ± 1.2 ****p<0.0001, C7= 13 ± 0.2 ***p<0.001, C8= 15 ± 0.4 ***p<0.001) compared to controls at **Day 50 (**6.5 ± 1.0) and **Day 60 (**8.4 ± 0.9) **(Figure 5.12)**. Similar results were obtained from MEA recordings of EP2001

(A294V) and EP2002 (F261L) which are presented in the supplementary information **(Figure S5.2)**.

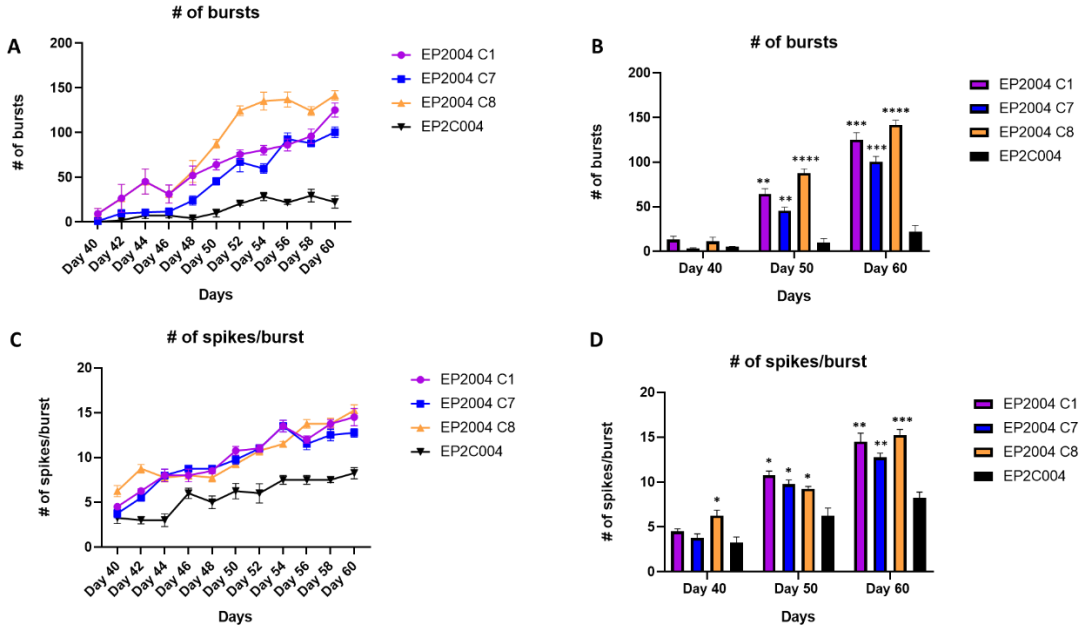

Figure 5.12 *KCNQ2*-DEE neurons have an increased number of bursts and number of spikes per burst.

(A) Longitudinal recording of the number of bursts in *KCNQ2*-DEE neurons and patient neurons. **(B)** Statistical analysis comparing the number of bursts between groups. **(C)** Longitudinal recording of the number of spikes per burst in *KCNQ2*-DEE neurons and controls. **(D)** Statistical analysis comparing the number of spikes per burst between groups. Three lines from both EP2004 (A265T) and EP2C004 (N= 3 replicates per group). Statistical significance (*p<0.05, **p<0.01, ***p<0.001, ****p<0.0001) was evaluated using an unpaired parametric *t*-test.

We next found that there was (iii) an increased frequency of bursts in patient lines (**Day 50**: C1= 0.027 ± 0.001 **p=0.005, C7= 0.027 ± 0.002 **p=0.005, C8= 0.030 ± 0.001 ***p<0.001)(**Day 60**: C1= 0.041 ± 0.001 ****p<0.0001, C7= 0.039 ± 0.002 ***p<0.001, C8= 0.043 ± 0.005 ***p<0.001) compared to control lines (**Day 50**: 0.019 ± 0.003)(**Day 60**: 0.028 ± 0.002) at day 50 and day 60. For both patients and controls, burst frequency increased overtime in culture **(Figure 5.13)**.

The variation in the ISI is described by using the co-efficient of variation which is the standard deviation of the ISI divided by the mean of the ISI. Lower values close to zero represent regular firing while larger values greater than 1, indicate irregular firing. We measured the ISI CoV for patient and control neurons overtime and found that (iv) patient neurons lines (**Day 50**: C1= 1.95 ± 0.01 **p=0.006, C7= 1.91 ± 0.02 **p=0.005, C8= 2.16 ± 0.03 **p=0.003)(**Day 60**: C1= 3.72 ± 0.1 ****p<0.0001, C7= 3.56 ± 0.3 ***p<0.001, C8= 3.68 ± 0.4

***p<0.001) had a significantly higher CoV than control neurons (**Day 50**: 1.21 ± 0.3)(**Day 60**: 1.47 ± 0.1). This increase in ISI CoV seen in patient neurons became more pronounced overtime and values reached as high as 3.7, suggesting that firing pattern in patient neurons was extremely irregular. Similar results were obtained from MEA recordings of EP2001 (A294V) and EP2002 (F261L) which are presented in the supplementary information **(Figure S5.3)**.

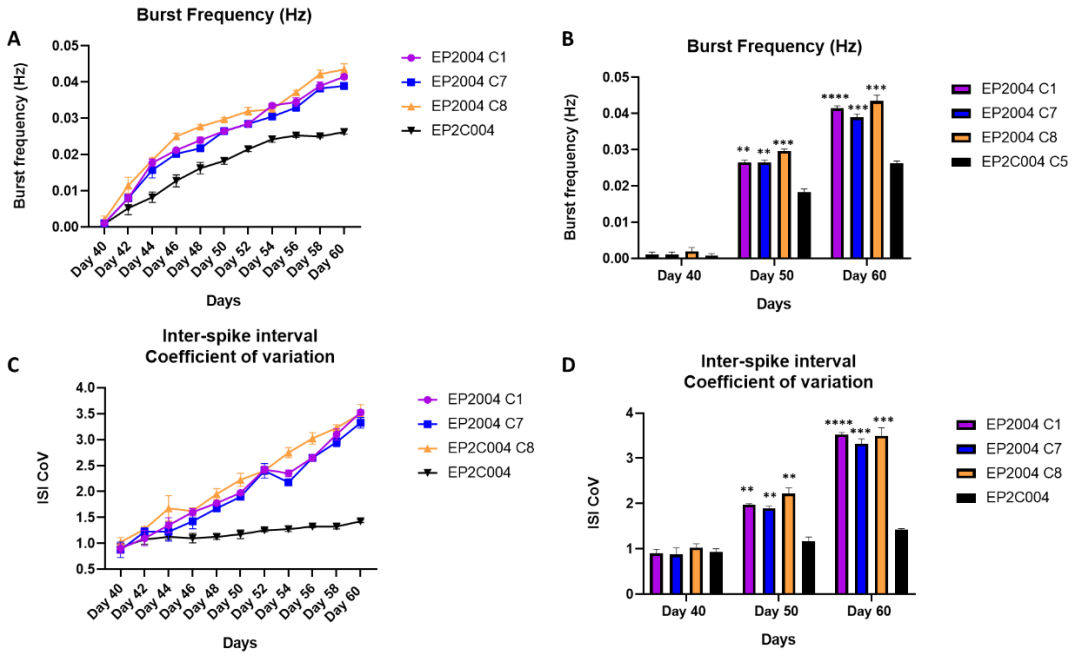

Figure 5.13. *KCNQ2*-DEE neurons have an irregular firing pattern and burst frequency.

(A) Longitudinal recording of the burst frequency in *KCNQ2*-DEE neurons and control neurons. **(B)** Statistical analysis comparing the burst frequency between groups. **(C)** Longitudinal recording of the number of the inter-spike interval Coefficient of variation (ISI CoV) in *KCNQ2*-DEE neurons and controls. **(D)** Statistical analysis comparing the ISI CoV between groups. Three lines from both EP2004 (A265T) and EP2C004 (N= 3 replicates per group) were analysed. Statistical significance (*p<0.05, **p<0.01, ***p<0.001, ****p<0.0001) was evaluated using an unpaired parametric *t*-test.

5.3.8. Chronic M current inhibition in control neurons mimics the phenotype seen in *KCNQ2*-DEE neurons

We already know that *KCNQ2*-encoded Kv7.2 and *KCNQ3*-encoded Kv7.3 channels control the M current, and the mutations in this study all result in a loss of M current. Therefore, we chronically treated control neurons with a low dose of XE-991 (a Kv7.2 and Kv7.3 channel blocker) to determine if the phenotype was comparable with patient neurons (A265T). We treated control neurons (EP2C004) with a low dose of 1µM XE-991 every other day from day 30 to day 60, with recordings starting at day 40. First, we measured the number of spikes per

burst and found that XE-991 treated controls (**Day 50**: 12 ± 0.6 *p=0.045, **Day 60**: 16 ± 0.5 *p=0.033) had a significantly increased number of spikes per burst compared to patient neurons (**Day 50**: 10 ± 0.5, **Day 60**: 13.5 ± 0.7) **(Figure 5.14).** Next, we compared the number of bursts and found that XE-991 treated controls (**Day 50**: 82 ± 7, **Day 60**: 172 ± 4 *p= 0.026) had a significantly greater number of bursts than patient neurons (**Day 50**: 94 ± 3, **Day 60**: 147 ± 5) as neurons matured overtime in culture. There was no significant difference in the number of bursts at the earlier timepoints **(Figure 5.14)**. Finally, we measured the ISI CoV and found that XE-991 treated controls (**Day 50**: 2.9 ±0.21 **p=0.0068, **Day 60**: 3.9 ±0.14 *p=0.036) had a significantly higher ISI CoV than patient neurons (**Day 50**: 2.05 ±0.01, **Day 60**: 3.3 ± 0.3)**(Figure 5.14)**. These results indicate that the effect of XE-991 treatment on controls neurons was more dramatic than the irregular bursting phenotype of patient neurons (A265T), most likely due to the less severe loss of M current function associated with the mutation compared to the loss of function with XE-991 treatment in controls.

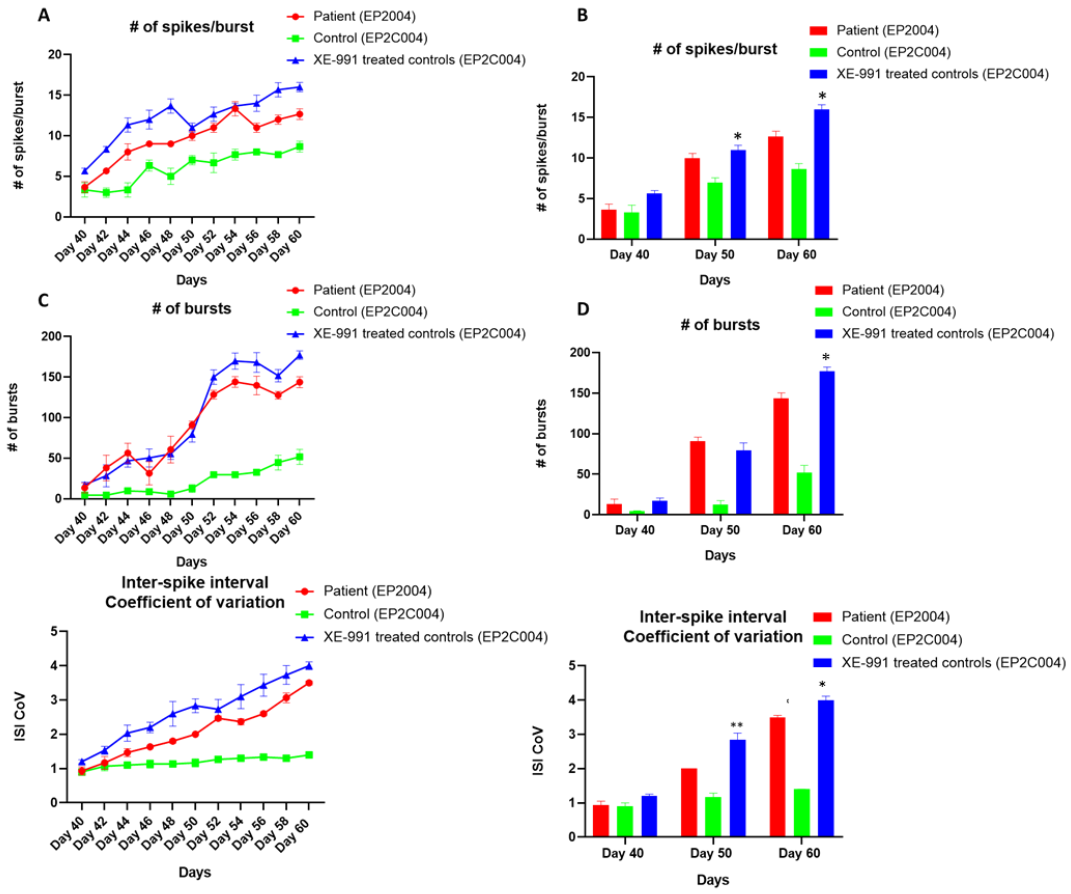

Figure 5.14 Chronic M current inhibition in control neurons phenocopies *KCNQ2*-DEE neurons.

(A) Longitudinal recording of the number of spikes per bursts in *KCNQ2*-DEE neurons, control neurons and XE-991 treated controls. **(B)** Statistical analysis comparing the number of spikes per bursts between groups. **(C)** Longitudinal recording of the number of bursts in *KCNQ2*-DEE neurons, control

neurons and XE-991 treated controls. **(D)** Statistical analysis comparing the number of bursts between groups. **(E)** Longitudinal recording of the number of the inter-spike interval Coefficient of variation (ISI CoV) in *KCNQ2*-DEE neurons, controls and XE-991 treated controls **(F)** Statistical analysis comparing the ISI CoV between groups. Three lines from both EP2004 (A265T) and EP2C004 (N= 3 replicates per group) were analysed. Statistical significance (*p<0.05, **p<0.01, ***p<0.001, ****p<0.0001) was evaluated using an unpaired parametric *t*-test.

5.3.9 SK and BK channel antagonists reduce irregular firing pattern in *KCNQ2*-DEE neurons

Due to the upregulation of BK channels (*KCNMA1, KCNMB1*) and SK channels (*KCNN1, KCNN2, KCNN3*) in our *KCNQ2*-DEE neurons **(Figure 4.16)**, we applied the SK channel antagonist apamin (500nM) and the BK channel antagonist paxilline (20μM) to patient (EP2004 A265T) and control (EP2C004) neurons during spontaneous MEA recording on day 50. Since there was most significant upregulation in SK channels, we treated cells with an SK channel antagonist alone and then a combinatorial treatment of an SK channel and BK channel antagonist. We found that treatment with apamin and paxilline combined was the most successful at significantly reducing the ISI CoV, number of bursts and number of spikes per burst in patient neurons **(Figure 5.15)**. We found that treatment did not significantly affect control neurons **(Figure S5.3)**. First, we measured the ISI CoV at baseline (2.36 ±0.14) and again after treatment with apamin and paxilline. We found that both apamin alone (1.48 ± 0.11, **p=0.0078) and a combinatorial treatment of apamin and paxilline (1.29 ± 0.10, **p= 0.0059) resulted in a significantly lower ISI CoV in patient neurons **(Figure 5.15)**. Next, we measured the burst frequency and found that apamin (0.019 ± 0.002, **P= 0.0091) and apamin + paxilline (0.017 ± 0.0005, **P= 0.0083) treatment significantly reduced burst frequency in patient neurons compared to baseline recording (0.028 ± 0.001). Again, we found that treatment with these SK and BK antagonists had no significant effect on control neurons **(Figure S5.3)**. Finally, we measured the number of spikes per burst and found that apamin alone (7.8 ± 1.7 compared to 8.5 ± 1.9 baseline, p= 0.065) had no significant effect on the number of spikes per burst in patient neurons. However, the combination of apamin and paxilline resulted in a significant reduction in the number of spikes per burst (6.6 ± 1.6 compared to 8.5 ± 1.9 baseline, *p= 0.044)**(Figure 5.15).** Together, this data suggests that inhibition of SK and BK channels in *KCNQ2*-DEE (C.881C>T) neurons reduces bursting and irregular firing patterns.

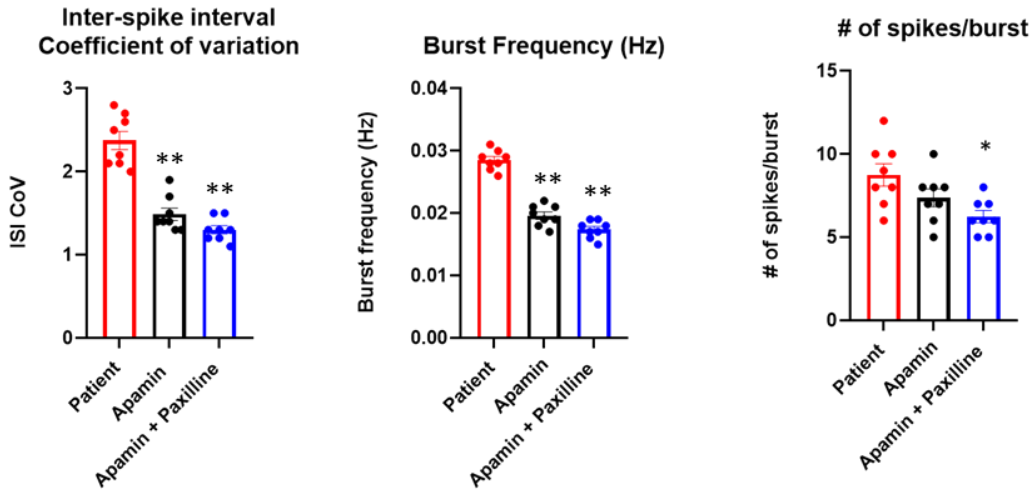

Figure 5.15. SK and BK channel antagonists reduce irregular firing pattern in *KCNQ2*-DEE neurons.

KCNQ2-DEE (A265T) neurons were treated with SK channel blocker Apamin (500nM) alone, and SK and BK channel blocker Paxilline (20µM) combined. Combinatorial treatment of apamin and paxilline significantly decreased the ISI CoV, Burst Frequency, and number of spikes per burst in *KCNQ2*-DEE neurons. Three lines from EP2002 (N= 4 replicates per line) were analysed. Statistical significance (*p<0.05, **p<0.01, ***p<0.001, ****p<0.0001) was evaluated using an unpaired parametric *t*-test.

5.3.10 Carbamazepine treatment significantly reduces bursting and irregular firing patterns in *KCNQ2*-DEE neurons

Due to the upregulation of the sodium channel genes *SCN1A, SCN2A* and *SCN8A* we detected in *KCNQ2*-DEE neurons (A294V)**(Figure 4.17)**, we treated patient neurons with the sodium channel blocker carbamazepine. Carbamazepine is a commonly used anti-seizure medication in clinical practice (Marson et al., 2002) and in a small percentage of young infants treated, associated with seizure reduction. We found that treatment with carbamazepine resulted in significantly reduced number of bursts, number of spikes per burst and ISI CoV, nearly to the level of controls. Carbamazepine treatment caused a significant reduction in the number of bursts in patients from (61 ± 6) to (42 ± 5)**(Figure 5.16)**. Similarly, we also saw a reduction in the number of spikes per burst in patients from 9.8 ± 0.7 to 7.7 ± 0.3 **(Figure 5.16).** Finally, we detected a significant reduction in the ISI CoV in patient neurons after treatment with carbamazepine from (2.08 ± 0.4) to (1.55 ± 0.2)**(Figure 5.16)**. Together, these results show that carbamazepine treatment reduces the increased bursting and irregular firing seen in *KCNQ2*-DEE neurons.

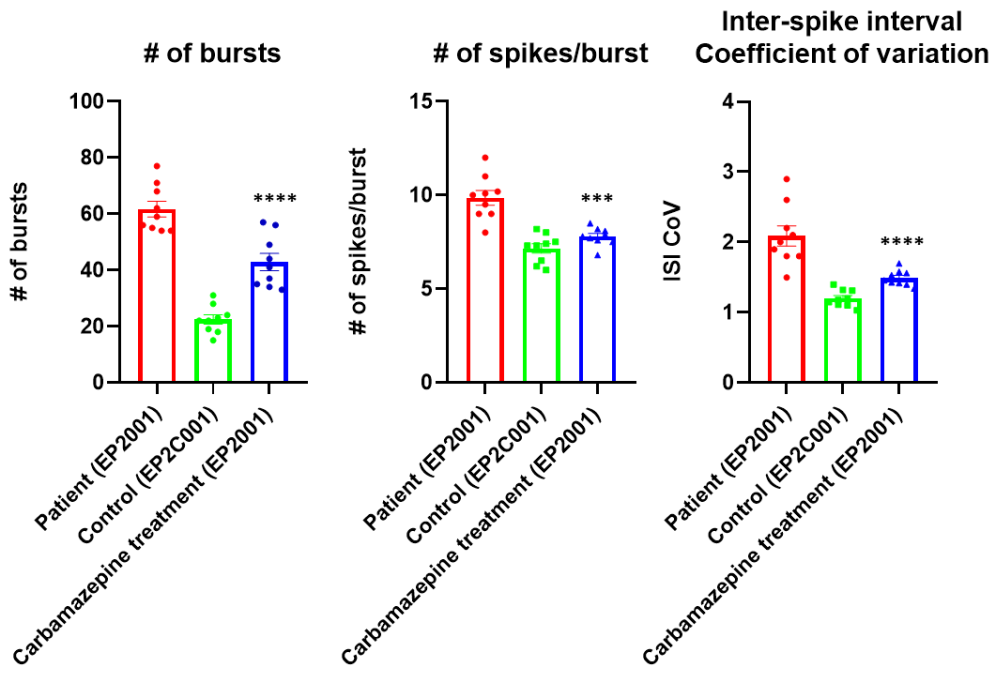

Figure 5.16: Anti-seizure drug carbamazepine significantly reduces the number of bursts and the ISI CoV in *KCNQ2*-DEE neurons.

KCNQ2-DEE neurons (A294V) were treated with the sodium channel blocker carbamazepine (100μM) at Day 50 on MEA. Carbamazepine treatment significantly reduced the number of bursts, number of spikes per burst and the ISI CoV in patient neurons. Three lines from EP2001 (A294V) and three lines from EP2C001 (N= 3 replicates per line) were analysed. Statistical significance (*p<0.05, **p<0.01, ***p<0.001, ****p<0.0001) was evaluated using a One-way ANOVA and Tukey's multiple comparison test.

5.3.11 Retigabine treatment significantly reduces bursting and irregular firing patterns in *KCNQ2*-DEE neurons

Retigabine is a Kv7.2 and Kv7.3 specific potassium channel opener that promotes the activation of KCNQ2/KCNQ3 (Kv7.2/7.3) potassium channels. To analyse the effect of this drug on our model, we treated *KCNQ2*-DEE neurons (A294V) with retigabine (10μM) at day 50. We found that treatment with retigabine resulted in significantly reduced number of bursts, number of spikes per burst and ISI CoV. Retigabine treatment caused a significant reduction in the number of bursts in patients from (62 ± 7) to (38 ± 6)**(Figure 5.17)**. Similarly, we also observed a reduction in the number of spikes per burst in patients from (10.1 ± 0.8) to (7.7 ± 0.5)**(Figure 5.17).** Finally, we detected a significant reduction in the ISI CoV in patient neurons after treatment with retigabine from (2.35 ± 0.5) to (1.26 ± 0.3)**(Figure 5.17)**.

Together, these results show that retigabine treatment reduces the increased bursting and irregular firing seen in *KCNQ2*-DEE neurons.

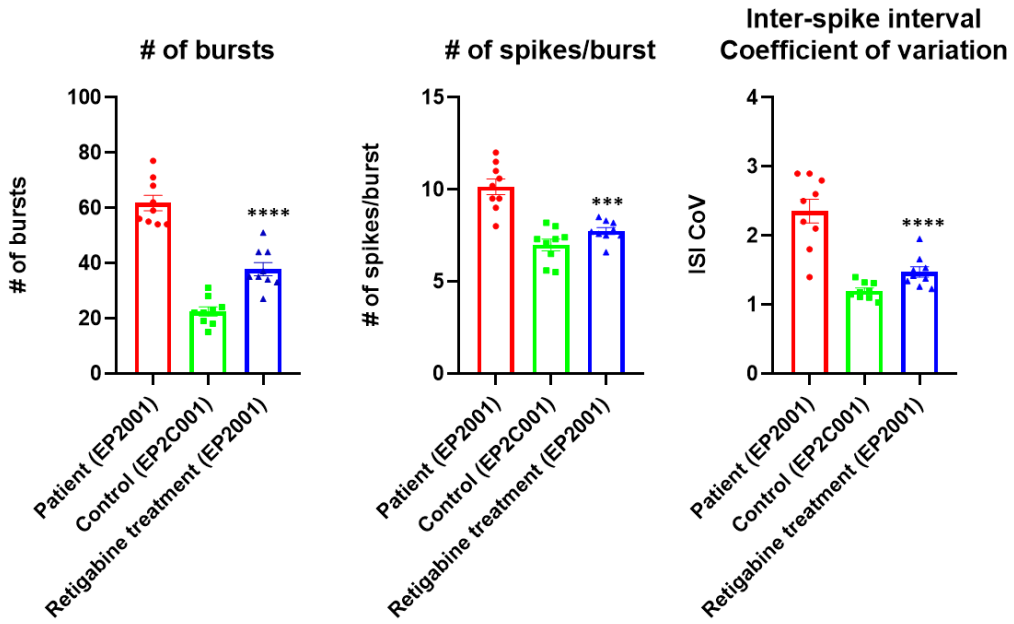

Figure 5.17 Treatment with Retigabine significantly reduces the number of bursts and ISI CoV in *KCNQ2*-DEE neurons.

KCNQ2-DEE neurons (A294V) were treated with the potassium channel opener retigabine (10µM) at day 50 on MEA. Retigabine treatment significantly reduced the number of bursts and the ISI CoV in patient neurons. Three lines from EP2001 (A294V) and three lines from EP2C001 (N= 3 replicates per line) were analysed. Statistical significance (*p<0.05, **p<0.01, ***p<0.001, ****p<0.0001) was evaluated using a One-way ANOVA and Tukey's multiple comparison test.

5.4 Discussion

Over the past decade, MEAs have been increasingly used for functional phenotyping, especially in iPSC disease modelling studies. MEAs enable a greater understanding of changes in network dynamics in disease models by simultaneously recording electrical activity in a culture which records population-wide electrical activity. This technology is particularly useful for studying neurodevelopmental disorders, which alter inherent excitability properties, such as *KCNQ2*-DEE, and track over time as the technology is non-destructive to cells which enables the same neurons to be monitored over multiple weeks as the neurons mature *in vitro*. Here, I will discuss the results we obtained from this study, draw comparisons to other studies and discuss the opportunities and limitations of applying MEA technology to iPSC disease modelling studies.

Choosing an appropriate seeding density and coating agent(s) is essential for optimal cell attachment, proliferation, and survival (Ferguson et al., 2019). We trialled three different seeding densities of 25,000, 50,000 and 75,000 cells per well in a 48-well plate and found that 25,000 cells resulted in the most uniform distribution of cell attachment. Cells were not too crowded and didn't form too many clumps **(Figure 5.5)**. Based on previous protocols used in our laboratory by other researchers, we chose to coat the MEA plates with PDL (10ug/ml) and Laminin (10 µg/ml). We found that this coating technique enabled the long-term culture of neurons without any noticeable cell detachment over the course of the recording period. However, we did find that overtime neurons were prone to form clumps in some of the wells. However, when we performed MEA analysis, the cell clumps did not prevent sufficient electrical activity from being recorded. They were still able to meet the criteria for an active electrode (The number of electrodes with activity greater than the minimum threshold of 5 spikes/min) in sufficient numbers for all cell lines. Studies have shown that alternative coating agents such as PEI can reduce the level of clumping seen in 2D neuronal studies (Overland et al., n.d.). Similarly, co-culturing with astrocytes has also been shown to reduce neuronal clumping (Buttermore, 2022). This is particularly useful for neurons generated using transcription factors such as NGN2, as this results in an almost pure population of neurons. Our dual SMAD inhibition protocol resulted in approximately 40% of glial cells, which may have played a role in preventing substantial neuronal clumping.

To determine whether the addition of the Notch signalling Inhibitor Compound E, could promote neuronal maturation, we added Compound E (0.1µM) to patient (EP2004, A265T) and control (EP2C004) neurons and analysed the neurons using MEA. We found that addition

of Compound E could effectively promote the maturation of neurons, evidenced by increased wMFR and bursting. We found that there was no significant difference between the number of active electrodes in patients and controls with or without Compound E **(Figure 5.6)**. However, from day 50, there was a significant increase in wMFR in patient neurons with Compound E compared to patient neurons without Compound E. This difference increases over time and becomes significant in control neurons with Compound E at day 60 **(Figure 5.6)**. We also found there was a significant increase in the number of bursts in patient neurons with Compound E, compared to patient neurons without Compound E. Interestingly, this was not seen in control neurons, where Compound E had no significant effect on the number of bursts **(Figure 5.7)**. Finally, we showed that Compound E had no effect on bursting frequency of ISI CoV in patient or control lines **(Figure 5.8)**. Together, these results indicate that Compound E may accelerate neuronal maturation, as evidenced here by increased wMFR and an increased number of bursts. Interestingly, these effects are amplified in patient neurons, where wMFR and bursting is much greater than control neurons at these stages of development **(Figure 5.11, Figure 5.12)**. As there has been no published studies using Compound E in cortical neuron differentiation coupled with the varying effects of Compound E between patient and control lines, we chose to perform all further analysis without addition of Compound E to align with previous studies.

Tetrodotoxin (TTX) is a voltage-gated Na^+ channel blocker that prevents the passage of sodium into neurons, resulting in the inhibition of AP firing. Here, we tested whether our iPSC-derived neurons could respond to TTX treatment. We found that the lower dose (2.5nM) almost completely abolished electrical activity, as wMFR was reduced to almost 0 Hz, while the higher dose completely abolished all electrical activity **(Figure 5.9)**. These results suggest that the firing signal detected on MEA in our experiments are caused by voltage gated Na^+ channels. To further characterise the cells, we treated the neurons with the AMPA antagonist CNQX, and found that the wMFR was significantly reduced after treatment, suggesting that a large proportion of the excitatory neurons are AMPA-mediated **(Figure 5.10)**. The remainder of the firing is likely originating from synaptic transmission mediated via other glutamatergic receptors (Miyazaki et al., 2021). AMPA-mediated excitatory neurons make up the majority of mature fast excitatory neurons (Puglia et al., 2009). However, the use of antagonists towards other glutamate receptor subtypes such as NMDA receptors and Kainite receptors, would provide further information for characterising excitatory neurons.

The iPSC-derived *KCNQ2*-DEE neuronal phenotype that we observe in this study presents the opportunity to examine the functional effects of three different *KCNQ2* mutations (F261L, A265T, A294V) *in vitro* during neuronal development for the first time. Based on studies of epilepsy in both experimental models and human models, we know that repetitive burst firing of APs is associated with chronic epilepsy (Gast et al., 2016). Our findings reveal that for each *KCNQ2* mutation, neurons had significantly higher wMFR, a greater number of bursts and burst frequency and had a higher ISI CoV. Patient neurons preferred to fire in bursts compared to single tonic spikes seen in control neurons **(Figure S5.1, S5.5 - S5.7)**. This increased firing and bursting phenotype became more pronounced as neurons matured overtime. The Inter Spike Interval (ISI) reveals how regular or irregular neuronal firing patterns are in the culture. Lower values close to zero indicate regular firing while higher vales greater than one indicate irregular firing (Taube, 2010). In our data, patient neurons have a significantly higher ISI CoV, which increases as neurons mature. This data suggests that during development, the *KCNQ2*-DEE neuronal aberrant firing pattern becomes more irregular as neurodevelopment progresses, perhaps suggesting that immediate treatments will be required for *KCNQ2*-DEE disease modification, and further experimentation in the future for example with pharmacological manipulation in iPSC models may help elucidate further this hypothesis.

The phenotype seen in our neurons was not surprising as it is reminiscent of the interictal burst suppression pattern seen on *KCNQ2* patient EEGs. Additionally, a recent study using iPSC derived *KCNQ2* neurons harbouring the mutation (R581Q), recorded spontaneous electrical activity during neural development (Simkin et al., 2021). Their results revealed that their patient excitatory cortical neurons were prone to firing in bursts, evidenced by an increased number of bursts, number of spikes per burst and the percentage of spikes that occur within bursts (Simkin et al., 2021). One difference we saw from this study was that we found no difference in the number of active electrodes between patients and controls. In their study, they found there was a significant increase in the number of active electrodes in patient neurons throughout the entirety of the recording period. Another study using mice, also analysed the phenotype of GABAergic interneurons that had a selective deletion of the M current channels Kv7.2 and Kv7.3. They found that the deletion of these channels on interneurons also led to hyperexcitability (Soh et al., 2018). This reveals a limitation of our study that it is primarily composed of excitatory glutamatergic neurons, but nevertheless shows in human iPSC-derived neuronal models of disease and healthy an important role in excitatory neurons. GABAergic neurons are known to play a crucial role in synchronising

firing in epilepsy, thus their presence in *in vitro* epilepsy models will provide a more physiologically relevant disease model in the future.

It remains unclear whether the phenotype seen in *KCNQ2*-DEE patients is caused as a direct result of reduced M current or if it's caused by maladaptive cellular re-organisation and gene expression during neurodevelopment as a result of particular mutations, and there are many different mutations, different effects, or mechanisms may be occurring in different patients. Importantly, many patients with a *KCNQ2* mutation have a less severe phenotype known as Benign Familial Neonatal Seizures (BFNS), where seizures usually go away and development is normal (Singh, 2003). Therefore, it's possible that maladaptive cellular re-organisation or gene expression possibly as a result of severely reduced M current or frequent seizure activity leads to the more severe *KCNQ2*-DEE phenotype. It is likely that there is mutation-specific phenotypes also. In a recently conducted study, 60% of mothers of patients with *KCNQ2*-related epilepsy believed that the child experienced seizures in the utero (Weckhuysen et al., 2022). It is likely that iPSC-derived neurons may recapitulate early neuronal development. We chronically treated control neurons with a low dose of XE-991 (Kv7.2 and Kv7.3 channel blocker) to supress M current from day 30 to day 60. Using MEA, we then compared the phenotype between patients and M current-supressed controls. We found that XE-991 treated control neurons fired more bursts, and the firing pattern was more irregular, as determined by the ISI CoV **(Figure 5.14)**. These results suggest that the more severe phenotype seen in XE-991 treated controls is due to a complete or greater loss of M current in wild type than the mutation. However, the level of M current reduction caused by the pharmacological treatment with XE-991 was not determined here. In the study by Simkin (Simkin et al., 2021), they used patch clamping to show that chronic XE-991 (1µM) treatment resulted in significantly reduced AP half-width and fAHP, confirming a reduction in M current compared to the wild type mutation (Simkin et al., 2021). Another limitation of our study is that we did not compare our findings with those of the milder "Benign Familial Neonatal Seizures (BFNS)" mutation which may shed further light on the developmental effects of the more severe mutations in comparison, on burst-firing patterns for example.

One of the main advantages of the MEA platform is the ability to easily perform drug screening, which also offers the opportunity to examine a neuronal phenotype. We previously showed that our patient neurons (EP2004; A265T) had an upregulation of several BK and SK channels **(Chapter 4)**. To determine if BK and SK channel antagonists could ameliorate the phenotype in patient neurons, we treated neurons with paxilline and apamin. We found that a combinatorial treatment resulted in the most significant reduction in the ISI

CoV, burst frequency and number of spikes per burst **(Figure 5.15)**. Similarly, we detected an upregulation of the Na^+ channels *SCN1A, SCN2A* and *SCN8A* in patient neurons (EP2001; A294V). Therefore, we treated neurons with the commonly prescribed Na^+ channel blocker carbamazepine (100µM) and found that treatment significantly reduced the irregular, bursting phenotype in patients **(Figure 5.16)**. This was consistent with clinical data of this drug which has been shown to effectively treat seizures in patients in the clinic (Dilena et al., 2022). Finally, we treated neurons with retigabine (10µM), a specific Kv7.2 and Kv7.3 potassium channel opener, and found that again, treatment significantly improved the phenotype in patient neurons (EP2001; A294V) **(Figure 5.17)**. While each of the drugs we tested improved the phenotype on MEA, none were successful in restoring the phenotype to the level of control neurons. These results suggest that higher doses may be required, for complete early seizure abolition, but it is also likely that neurons may have undergone complex altered plasticity in response to the mutation, as well as other dyshomeostatic mechanisms, and fits with the notion which could help explain why *KCNQ2*-mutations of this type lead to an underlying brain developmental disorder, above and beyond the seizures themselves. It would be interesting to examine other mechanisms, in addition to excitability mechanisms, the structure and morphology of neuronal development, omics differences and actual sub-cellular locations of Kv7.2 channels in disease and control neurons.

5.5: Supplementary Information

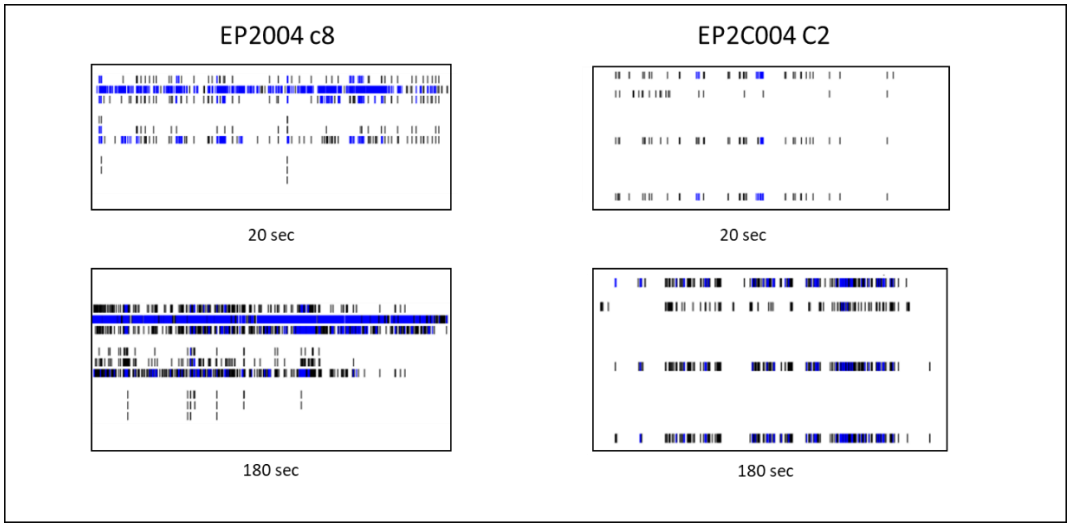

Figure S5.1 Representative images of Raster plots taken from spontaneous recordings of *KCNQ2*-DEE patient (EP2004, A265T neurons (left) and control (EP2C004) neurons (right) at day 60.

Each black line represents a single spike while blue lines indicate bursts or a train of spikes. EP2004 (A265T) neurons have significantly more spikes and bursts than EP2C004 neurons. Similarly, the firing pattern in EP2004 C8 neurons is much more irregular than the firing pattern in EP2C004 C2 neurons.

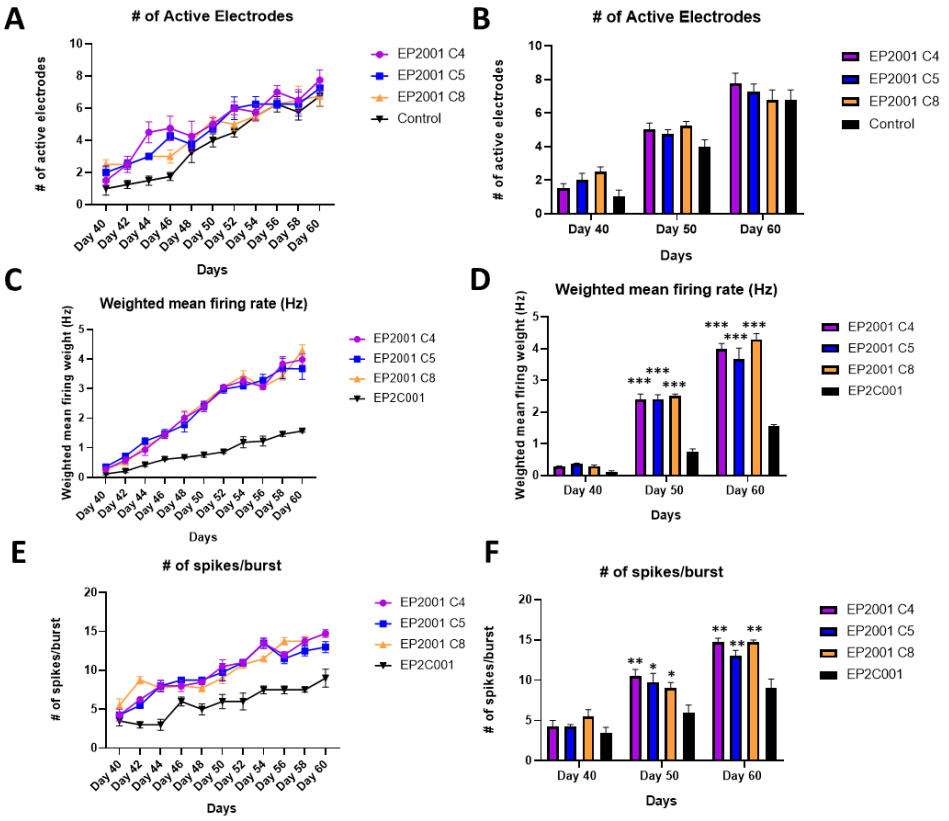

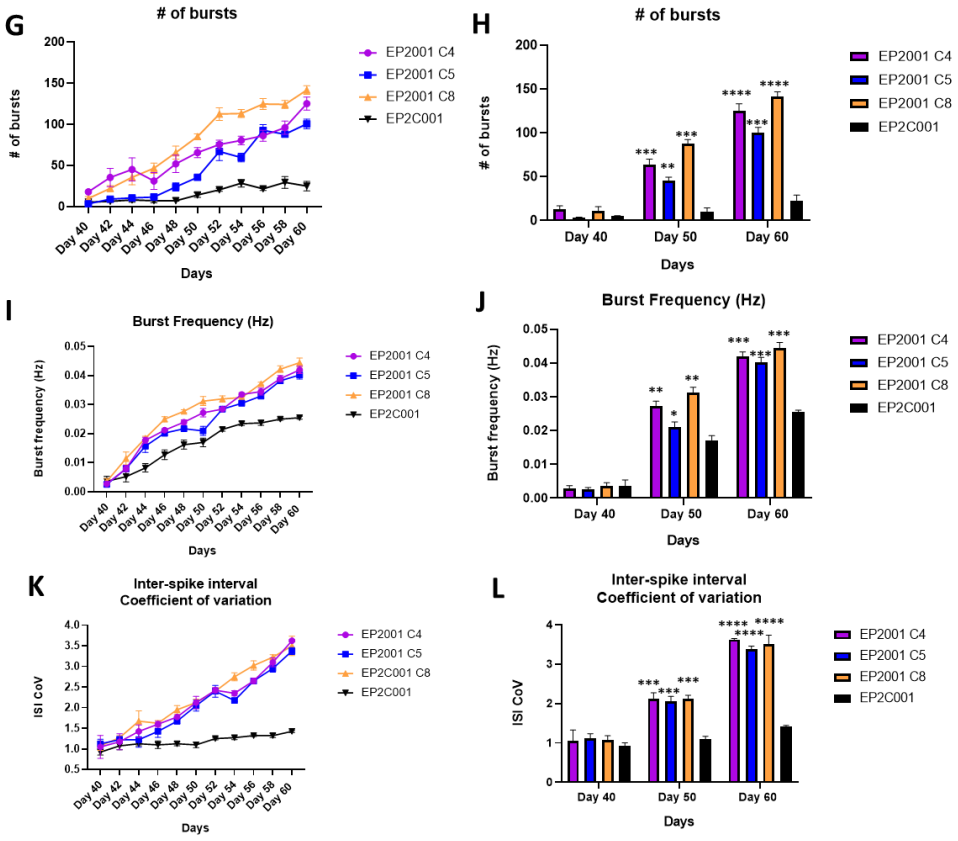

Figure S5.2 MEA data from EP2001 (A294V) and EP2C001 illustrating number of active electrodes, weighted Mean Firing Rate, number of spikes per burst, number of bursts, burst frequency and ISI CoV.

(A) Longitudinal recording of the number of active electrodes in *KCNQ2*-DEE neurons and patient neurons. **(B)** Statistical analysis comparing the number of active electrodes between groups. **(C)** Longitudinal recording of the weighted mean firing rate in *KCNQ2*-DEE neurons and controls. **(D)** Statistical analysis comparing the weighted mean firing rate between groups **(E)** Longitudinal recording of the number of bursts in *KCNQ2*-DEE neurons and patient neurons. **(F)** Statistical analysis comparing the number of bursts between groups. **(G)** Longitudinal recording of the number of spikes per burst in *KCNQ2*-DEE neurons and controls. **(H)** Statistical analysis comparing the number of spikes per burst between groups. **(I)** Longitudinal recording of the burst frequency in KCNQ2-DEE neurons and patient neurons. **(J)** Statistical analysis comparing the burst frequency between groups. **(K)** Longitudinal recording of the number of the inter-spike interval Coefficient of variation (ISI CoV) in *KCNQ2*-DEE neurons and controls. **(L)** Statistical analysis comparing the ISI CoV between groups. Three lines from both EP2001 (A294V) and EP2C001 (N= 3 replicates per group) were used. Statistical significance (*p<0.05, **p<0.01, ***p<0.001, ****p<0.0001) was evaluated using an unpaired parametric *t*-test.

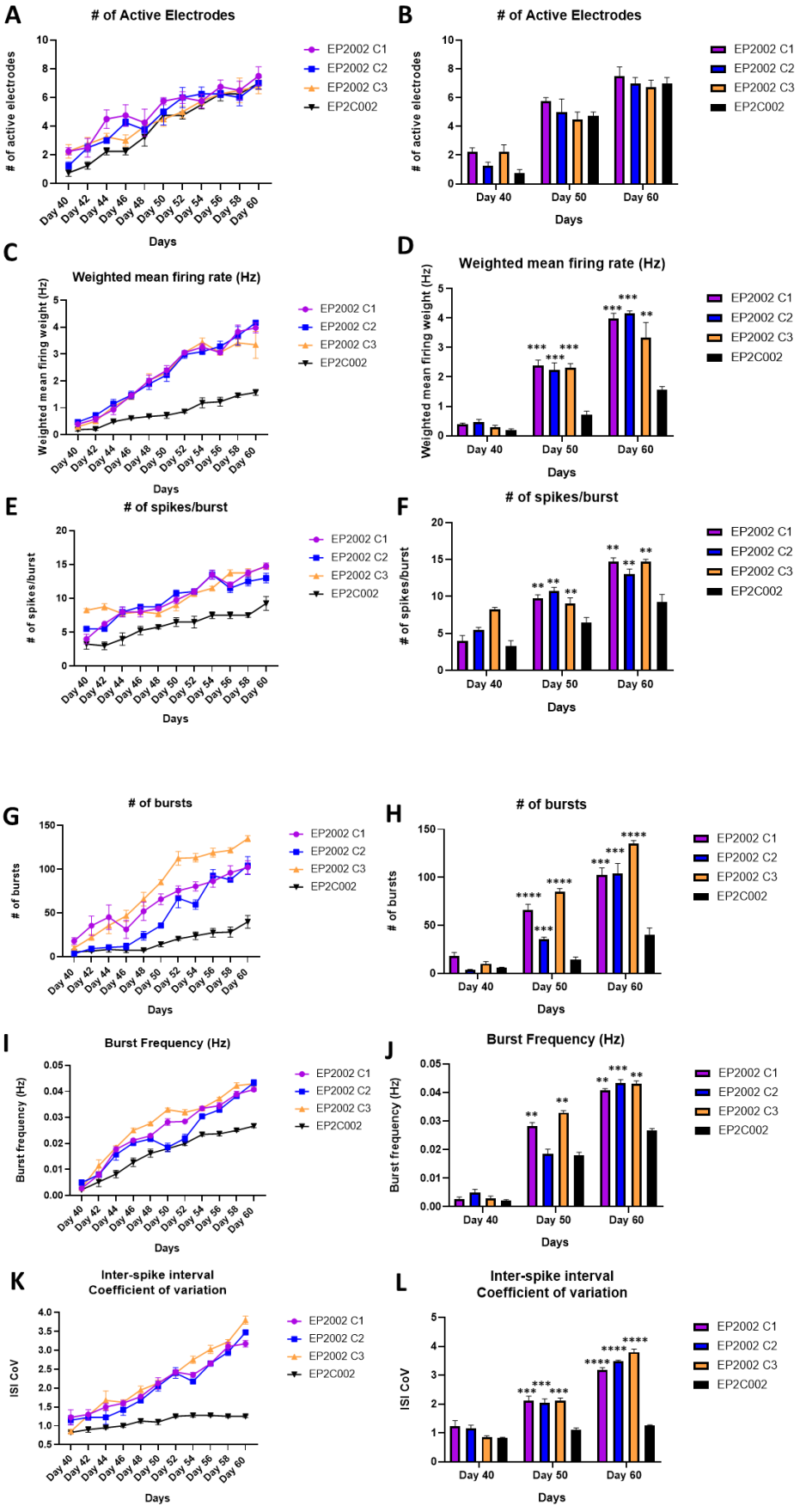
A
# of Active Electrodes
# of active electrodes
Days
EP2002 C1
EP2002 C2
EP2002 C3
EP2C002
B
# of Active Electrodes
# of active electrodes
Day 40
Day 50
Day 60
Days
C
Weighted mean firing rate (Hz)
Weighted mean firing weight (Hz)
D
E
# of spikes/burst
# of spikes/burst
F
G
# of bursts
# of bursts
H
I
Burst Frequency (Hz)
Burst frequency (Hz)
J
K
Inter-spike interval
Coefficient of variation
ISI CoV
L

Figure S5.3 MEA data from EP2002 (F261L) and EP2C002 illustrating number of active electrodes, weighted Mean Firing Rate, number of spikes per burst, number of bursts, burst frequency and ISI CoV.

(A) Longitudinal recording of the number of active electrodes in *KCNQ2*-DEE neurons and patient neurons. **(B)** Statistical analysis comparing the number of active electrodes between groups. **(C)** Longitudinal recording of the weighted mean firing rate in *KCNQ2*-DEE neurons and controls. **(D)** Statistical analysis comparing the weighted mean firing rate between groups. **(E)** Longitudinal recording of the number of bursts in *KCNQ2*-DEE neurons and patient neurons. **(F)** Statistical analysis comparing the number of bursts between groups. **(G)** Longitudinal recording of the number of spikes per burst in *KCNQ2*-DEE neurons and controls. **(H)** Statistical analysis comparing the number of spikes per burst between groups. **(I)** Longitudinal recording of the burst frequency in *KCNQ2*-DEE neurons and patient neurons. **(J)** Statistical analysis comparing the burst frequency between groups. **(K)** Longitudinal recording of the number of the inter-spike interval Coefficient of variation (ISI CoV) in *KCNQ2*-DEE neurons and controls. **(L)** Statistical analysis comparing the ISI CoV between groups. Three lines from both EP2002 and EP2C002 (N= 3 replicates per group) were used. Statistical significance (*p<0.05, **p<0.01, ***p<0.001, ****p<0.0001) was evaluated using an unpaired parametric *t*-test.

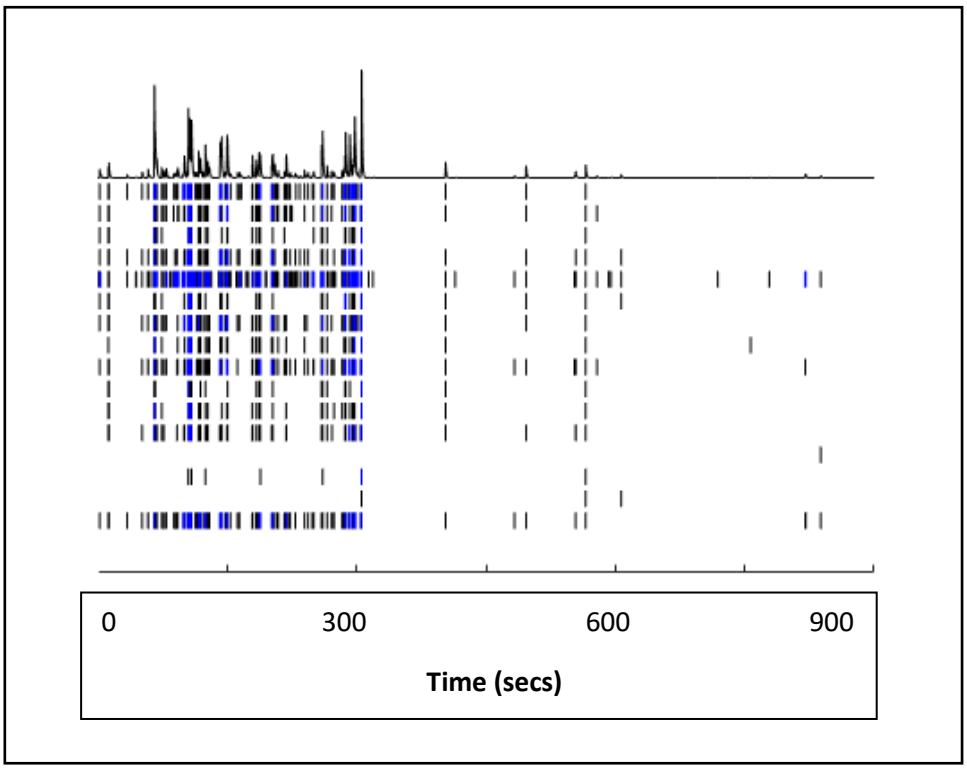

Figure S5.4: Representative image of Raster plots taken from *KCNQ2*-DEE patient EP2004 C1 (A265T) after TTX treatment. Spontaneous recordings of A265T were taken for 300s. Low dose TTX (2.5nM) administration was given at 300s, followed by high dose TTX (25nM) at 600s. TTX treatment blocks almost all firing in A265T neurons.

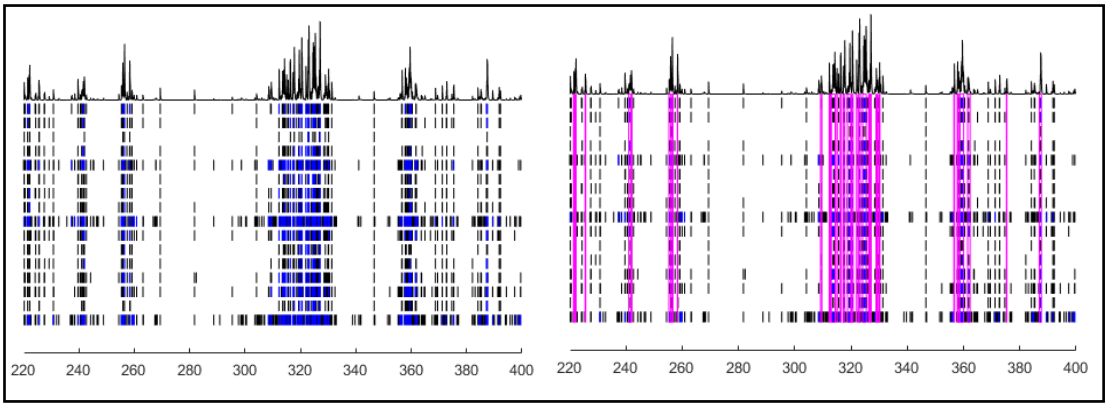

Figure S5.5 Representative raster plot image of spontaneous firing pattern in EP2004 C1 (A265T) neurons illustrating the burst suppression pattern seen in patient neurons.

(Left) Raster plot without bursts highlighted. (Right) Purple boxes indicate areas of bursting, determined by the software. The spikes at the top represent areas of bursting. Periods of electrical silence are seen between areas of bursts.

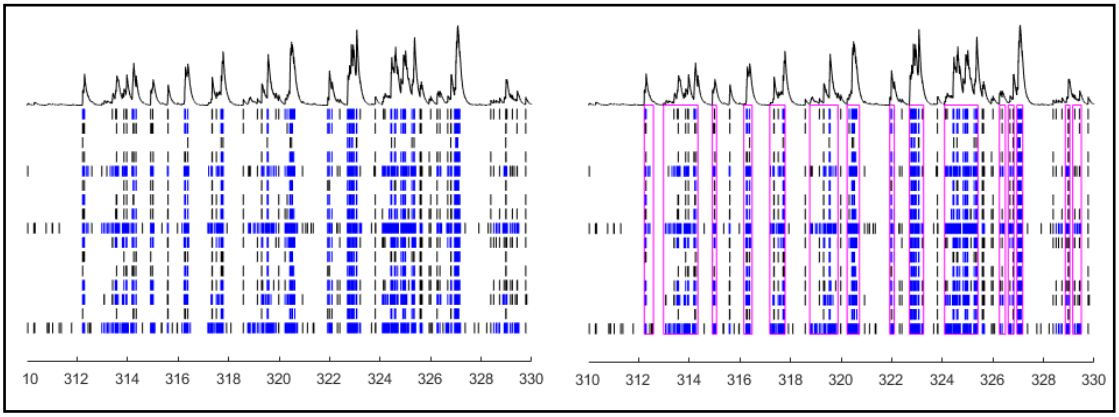

Figure S5.6 Representative raster plot image of spontaneous firing pattern in EP2002 C2 (F261L) neurons illustrating the burst suppression pattern seen in patient neurons.

(Left) Raster plot without bursts highlighted. (Right) Purple boxes indicate areas of bursting, determined by the software. The spikes at the top represent areas of bursting. Periods of electrical silence are seen between areas of bursts.

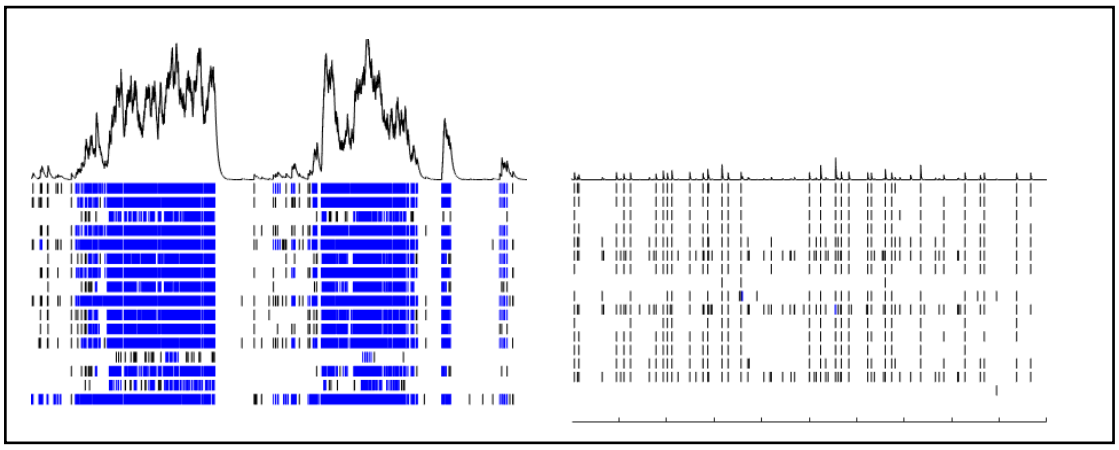

Figure S5.7 Representative raster plot image of spontaneous firing pattern in EP2001 C4 (A294V) and EP2C001 neurons illustrating the burst suppression pattern seen in patient neurons.

(Left) Blue lines indicate bursts, and the spikes represent the intensity of the burst. Periods of electrical silence are seen after bursting in *KCNQ2*-DEE (A294V) neurons. (Right) spontaneous firing pattern in a sibling control line (EP2C001 C2) is more uniform with less bursts.

Chapter 6: Functional Characterisation of iPSC-Derived Cortical Neurons by Calcium Imaging

6.1 Introduction

Ca^{2+} ions are known to assist in depolarisation, synaptic transmission, plasticity, regulate neuronal gene expression, and many other neuronal processes involved in learning and memory (Michaelsen et al., 2010; Gleichmann et al., 2011). As a result, neurons have developed extensive Ca^{2+} signalling pathways (Kawamoto et al., 2012). Due to the critical role Ca^{2+}plays in neuronal plasticity, it's no surprise that any changes in Ca^{2+} homeostasis can lead to functional (and structural) alterations in neurons, as commonly seen in neurological disorders (Rajakulendran et al., 2016). In this **Chapter**, I will first discuss the main roles of Ca^{2+} in neuronal physiology, diseased neurons, and genetic alterations in Ca^{2+} channel genes associated with epilepsy. To test if iPSC-derived neuronal networks with a *KCNQ2* pathogenic variant (p.A265T) have altered Ca^{2+} dynamics in our system, we preloaded the cells with the calcium indicator Fluo-4AM and recorded spontaneous calcium transients. Finally, I will discuss our results drawing comparisons to other studies.

6.1.1 Role of Ca^{2+} in neuronal physiology

Ca^{2+} homeostasis is achieved by the tight regulation of Ca^{2+} influx from and efflux to the extracellular space, achieved by specific Ca^{2+} channels (Gleichmann et al., 2011). Typically, the extracellular free Ca^{2+} concentration is approximately 1.2mM compared to the much lower resting cytosolic free Ca^{2+} concentration of 100nM. This 10,000-fold concentration gradient causes a huge increase in intracellular Ca^{2+} after a neuron becomes depolarised. This is unique to Ca^{2+} ions, as Na^{2+} and K^{+} ions mainly affect the membrane potential and have minimal effect on cytosolic levels of Ca^{2+} ions (Benarroch, 2010). There are two main types of calcium channels located in the plasma membrane which regulate the entry of Ca^{2+} into the cell: voltage-gated calcium channels (VGCCs) and ionotropic glutamate receptors (iGluRs) (Tsien et al., 1988).

6.1.2 Voltage Gated Calcium Channels

VGCCs control Ca^{2+} influx in response to depolarisation and result in many important functions in the nervous system as well as the cardiac and endocrine systems (Catterall, 2011). VGCCs can be divided into three main families and 10 individual isoforms as outlined in **Table 6.1**. N- and P/Q- types of VGCCs are located on the presynaptic membrane where

they play an important role in neurotransmitter release (Nimmrich et al., 2012)**(See Figure 6.1)**. Upon opening of these channels, Ca^{2+} enters the cell rapidly, causing the release of neurotransmitters into the synaptic cleft. This neurotransmitter release activates other Ca^{2+} receptors like iGluRs, located in the post-synaptic membrane, resulting in the generation of Ca^{2+} signals which triggers an array of cellular responses specific to the neurotransmitter that was released (Reiner et al., 2018). In contrast, L- or R- types of VGCCs are located on the post-synaptic membrane and play a role in Ca^{2+}-dependent gene activation and neuronal plasticity (Moyer et al., 1994). The fundamental importance of calcium channels is underscored by the very many neurological disorders, including developmental and epileptic encephalopathies that may also occur, when pathogenic mutations arise, however it is beyond the scope of this thesis to discuss further.

Table 6.1 List of Calcium Channel subunits

Gene	Protein	Current type	Location	Role
CACNA1A	Cav2.1	P/Q	Pre-synaptic	Forms conducting pore
CACNA1B	Cav2.2	N	Pre-synaptic	Forms conducting pore
CACNA1C	Cav1.2	L	Synapses and dendrites	Forms conducting pore
CACNA1D	Cav1.3	L	Post-synaptic	Mediates entry of Ca^{2+} into excitable cells
CACNA1E	Cav2.3	R	Pre & Post-synaptic	Mediates entry of Ca^{2+} into excitable cells
CACNA1F	Cav1.4	L	Pre-synaptic	Mediates entry of Ca^{2+} into excitable cells
CACNA1G	Cav3.1	T	Post-synaptic	Mediates entry of Ca^{2+} into excitable cells
CACNA1H	Cav3.2	T	Plasma Membrane	Forms conducting pore
CACNA1I	Cav3.3	T	Plasma Membrane	Forms conducting pore
CACNA1S	Cav1.1	L	Plasma Membrane	Forms conducting pore

6.1.3 Ionotropic Glutamate Receptors

In the synaptic cleft, glutamate release will activate ionotropic glutamate receptors NMDA, AMPA and kainite receptors (KARS), allowing the rapid influx of ions into the post-synaptic terminal (Kawamoto et al., 2012). NMDA (N-Methyl-D-Aspartate) receptors play a crucial role in the CNS as they control post-synaptic Ca^{2+} influx which is known to regulate CREB-dependent (C-AMP Response Element-Binding Protein) gene transcription required for long term synaptic plasticity memory and learning (Hollmann et al., 1994). Evidence also suggests that normal NMDA receptor activation promotes the survival of numerous neuronal cell types while chronic activation of NMDA receptors, such as after seizure activity, can cause neuronal cell death (Hardingham et al., 2010). AMPA receptors are different type of iGluRs.

These receptors form heterotetrameric structures of subunits encoded by the genes Glur1, Glur2, Glur3 and Glur4 (Kawamoto et al., 2012). The Glur2 subunit is responsible for permeability to Ca^{2+} ions i.e., only the AMPA receptors that lack Glur2 have Ca^{2+} permeability, however with a lower affinity when compared with NMDA receptors (Dingledine et al., 1999). These Glur2 lacking AMPA receptors are located throughout the CNS, playing an important role in synaptic transmission. Finally, KARs (Kainate Receptors), can respond to kainate, glutamate and to a lesser extent and AMPA (Hollmann et al., 1994). Their precise role is poorly understood, but it is believed they act as modulators of excitatory and inhibitory synaptic transmission (Contractor et al., 2011). As these three types of receptors all play an important role in controlling neuronal excitability, they are critical targets when investigating the electrophysiological properties of neurons.

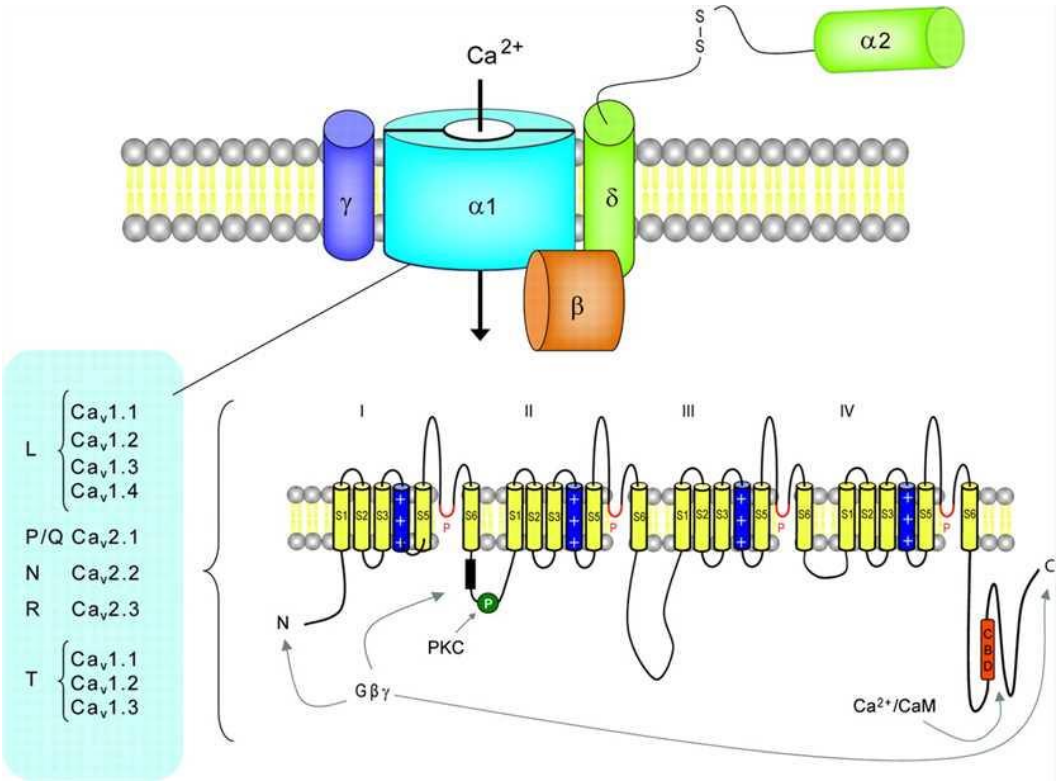

Figure 6.1. General Structure of Voltage Gated Calcium Channels.

Schematic illustration of the structure of VGCCs, the different calcium channel genes and their subtypes (Benarroch, 2010).

6.1.4 Ca^{2+} homeostasis and the endoplasmic reticulum

Another mechanism of Ca^{2+} release is through the endoplasmic reticulum (ER). This is mainly controlled by the two channels, IP_3Rs (inositol-1,4,5-triphosphate receptors) and RyRs

(Ryanodine receptors), however some Ca^{2+} also exits the ER through the leak channel (Tu et al., 2006). RyRs are located in both muscle cells and neurons and are triggered by increased intracellular Ca^{2+} known as Ca^{2+}-induced Ca^{2+}-release (CICR). Conversely, IP_3Rs are expressed in many cell types and are regulated by a wide array of factors (Prole et al., 2019). There are very elaborate and complex regulatory mechanisms involved in ER-related Ca^{2+} homeostasis which will not be discussed here.

6.1.5 Dyshomeostasis of Ca^{2+} in epilepsy models

A large number of genetic mutations have been identified in genes encoding almost all of the CaV channels, such as *CACNA1C* (CaV1.2), *CACNA1D* (CaV1.3), *CACNA1A* (CaV2.1), *CACNA1B* (CaV2.2), *CACNA1E* (CaV2.3) and *CACNA1H* (CaV3.2), and consequently a variety of seizure related neurological disorders (Bozarth et al., 2018). Disease phenotype and severity differs between CaV genes, some of which are associated with developmental and epileptic encephalopathy (DEE) (Jouvenceau et al., 2001). Like that seen in *KCNQ2*-related disorders, both gain-of-function or loss-of-function CaV gene mutations have been reported. Mutations that cause a reduced expression of P/Q- type calcium channels have been shown to increase the T-type calcium current in thalamic neurons, which is believed to play a role in some genetic forms of absence epilepsy (Zhang et al., 2002). In one study, two commonly used SOCE (store operated calcium entry) inhibitors were shown to successfully reduce the calcium concentration in neurons along with reduced firing and increased synchrony in primary neuronal cultures (Gruszczynska-Biegala et al., 2011).

IP_3R and RYR-mediated CICR plays important roles in maintaining calcium homeostasis in epilepsy models (Chong et al., 2018). Furthermore, its believed that constant changes in cytosolic calcium after periods of epileptogenesis may cause plasticity changes (Pal et al., 2001). In some rare situations, *RYR2* mutations can cause neurological disorders with epilepsy (Ma et al., 2021). Finally, NCXs are a group of channels that remove calcium from cells by coupling with sodium influx (Bode et al., 2018). In models of kainate-induced epilepsy, NCXs (sodium-calcium exchanger are expressed in the hippocampus and the amygdala during epileptogenesis. Inhibition of these NCXs with pentylenetetrazol (PTZ) successfully controlled the tonic-flexion convulsions, suggesting that NCXs may play an inhibitory role in PTZ-induced convulsions (Saito et al., 2009).

6.1.6 Role of calcium binding proteins in epilepsy

Cytosolic Ca^{2+} overload may result in Ca^{2+} dyshomeostasis. During this process, a group of proteins known as calcium-binding proteins (CaBPs), act as Ca^{2+} reservoirs in an attempt to control increased cytosolic Ca^{2+} levels and increase the neuronal tolerance to excitotoxicity (Nejatbakhsh et al., 2011). CaBPs also regulate other ion channels and can act as Ca^{2+} sensors, suggesting a possible role of CaBPs in epilepsy. Examples of these CaBPs include calmodulin, calbindin, calretinin, and parvalbumin (Xu et al., 2018). *KCNQ2* encodes Kv7.2 channels which must associate with calmodulin to function properly, hence the calmodulin-binding region of the Kv7.2 channel is a known mutational hotspot in *KCNQ2*-DEE (Zhou et al., 2022). One study showed that a mutation R353G, found in the calmodulin binding functional domain of Kv7.2, inhibited calmodulin binding which resulted in the retention of KCNQ2 within the ER, reducing the number of Kv7.2 channels capable of reaching the plasma membrane (Etxeberria et al., 2008). Overexpression of calmodulin has been shown to partially restore the lost outward K^+ current, reduced neuronal hyperexcitability (Ambrosino et al., 2015).

In this **Chapter**, we recorded (i) spontaneous and (ii) evoked calcium transients in iPSC-derived cortical neurons harbouring the *KCNQ2*-DEE pathogenic variant (A265T) using Fluo-4-AM dye, firstly as a parameter for functionally matured neurons and secondly to examine any alterations in Ca^{2+} transients between *KCNQ2* pathogenic variants and sibling controls.

6.2. Materials and Methods

6.2.1 Cell culture

iPSC-derived cortical neurons were seeded onto 15mm round coverslips (VWR, #MENZCB00150RAC20) in 12-well plates on Day 20 of the cortical neuronal differentiation protocol as outlined in **Chapter 4**. Coverslips underwent a double coating step with PDL, and laminin as previously described. Media was changed every other day until the day of analysis. A summary of the cell lines, the sample size and the drugs used are presented in **Table 6.2.**

Table 6.2. List of iPSC lines and experimental set up for Calcium Imaging experiments

Status	Cell line	Number of coverslips		Cell number		Treatment
		D60	D100	D60	D100	D100
Healthy controls (N = 1 donors; 3 iPSC lines)	EP2C004 C2	n=3	n=3	3,285	3,655	1* TTX 1,211 1*Glu 499 1*CNQX 1,425
	EP2C004 C4	n=3	n=3	4,167	4,481	1* TTX 1,457 1*Glu 752 1*CNQX 1,510
	EP2C004 C5	n=3	n=3	2,971	3,727	1* TTX 1,084 1*Glu 707 1*CNQX 1,444
KCNQ2 mutations (N = 1 donors; 3 iPSC lines)	EP2004 (A265T) C1	n=3	n=3	4,159	4,429	1* TTX 1,289 1*Glu 676 1*CNQX 1,684
	EP2004 (A265T) C7	n=3	n=3	3,268	3,576	1* TTX 1,364 1*Glu 814 .1*CNQX 1,595
	EP2004 (A265T) C8	n=3	n=3	5,438	5,206	1* TTX 1,560 1*Glu 696 1*CNQX 1,372
Abbreviations: TTX: tetrodotoxin, Glu: glutamate, CNQX: cyanquixaline						

6.2.2 Calcium imaging and data acquisition

Cells were labelled with a Fluo-4 AM dye to visualise Ca^{2+} transients. Briefly, 50µg of Fluo-4 AM (Thermo Fisher Scientific, F14201, MW. 1096.95) was dissolved in 50µl of DMSO to generate a 1mM stock solution which was protected from light. The Fluo-4 AM stock solution was diluted (500X) in culture media to make a working solution of 2µM. The artificial cerebrospinal fluid (ACSF) solution consisted of 140mM NaCl (Sigma Aldrich, 71387), 5 mM KCl (Sigma-Aldrich, P9333), 2mM $CaCl_2$ (Sigma-Aldrich, C5670), 2mM $MgCl_2$ (Sigma-Aldrich,

M8266), 10mM HEPES potassium salt (Sigma- Aldrich, H0527) and 10mM Glucose (Sigma Aldrich, 1083469029). The pH of the solution was adjusted to 7.4 using the pH meter.

Firstly, the cell culture media was removed from the wells and the cells were washed twice with ACSF solution. The media containing 2µM Fluo-4 AM dye was then added to the cells and incubated for 30 min at 37℃. The excess dye was then removed, and the cells were washed 2X with ACSF again. Fresh media was then added to the cells and incubated for 20 min at 37℃. The coverslip was then carefully removed using a tweezers and placed on the imaging chamber under a Zeiss Axiovert 200 microscope. 300µl of ACSF solution was added to the imaging chamber to prevent the coverslip from drying out. Images were taken under 10X magnification at room temperature using an Ocular Image Acquisition software with an interval of 1s for 120s to 600s and stored as uncompressed image sequences for analyses.

6.2.3 Drugs used in calcium imaging experiments

Drug testing (pharmacological manipulation of the model) workflow is outlined below in **Figure 6.2** (drugs listed in **Table 6.3**)**.** Briefly, coverslips were prepared as described above, and spontaneous calcium transients were recorded for the first 120s. Then the drug being tested was added directly to the ACSF solution covering the cells and the drug effect was recorded for a subsequent 300s.

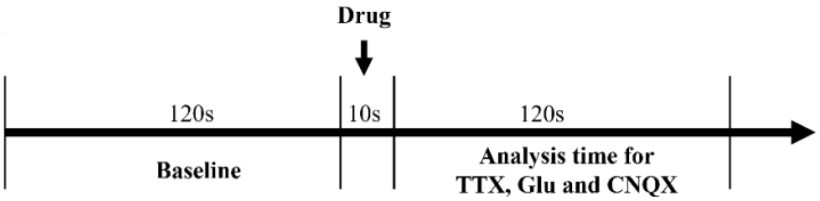

Figure 6.2. Outline of drug administration timeline.

Spontaneous calcium activity was measured for 120s which was considered as baseline. The drug was then directly added to the ACSF surrounding the neurons. The following 120s recording was considered as drug effect.

Table 6.3. List of drugs used in Calcium experiments

Name	Concentration	Manufacturer	Cat #	Function
TTX	1uM	Alomone labs	T-550	Na^+ channel blocker
CNQX	50uM	Alomone labs	C-140	Block AMPA/ kainate glutamate receptors
Glutamate	100uM	Sigma Aldrich	G8415	Activate neurons

6.2.4 Processing of calcium data using FluoroSNNAP

To analyse the calcium imaging data, a software called FluoroSNNAP (Fluorescence Single Neuron and Network Analysis Package) was used. FluoroSNNAP is a package in MATLAB (Mathworks, Inc.), which is used for the visualisation of calcium signalling in individual neurons or networks to study different patterns of activity overtime. In this project, we chose to analyse fluorescent variations over time in each individual neuron, defined as region of interest (ROI). There are 5 main steps involved in FluoroSNNAP's analysis; (1) Time-lapse analysis of neurons in a specified time window, (2) Identification of neuronal cell bodies (ROI) using Batch segmentation, (3) Pre-processing of automated segmentation to remove areas with cell aggregates using Segmentation GUI (Graphical User Interface). (4) Computation of time-varying fluorescence variations of each ROI. (5) Exportation and analysis of delta F/F0 trace of single cells to determine their calcium transient kinetics. These steps are outlined in more detail in **Figure 6.3**.

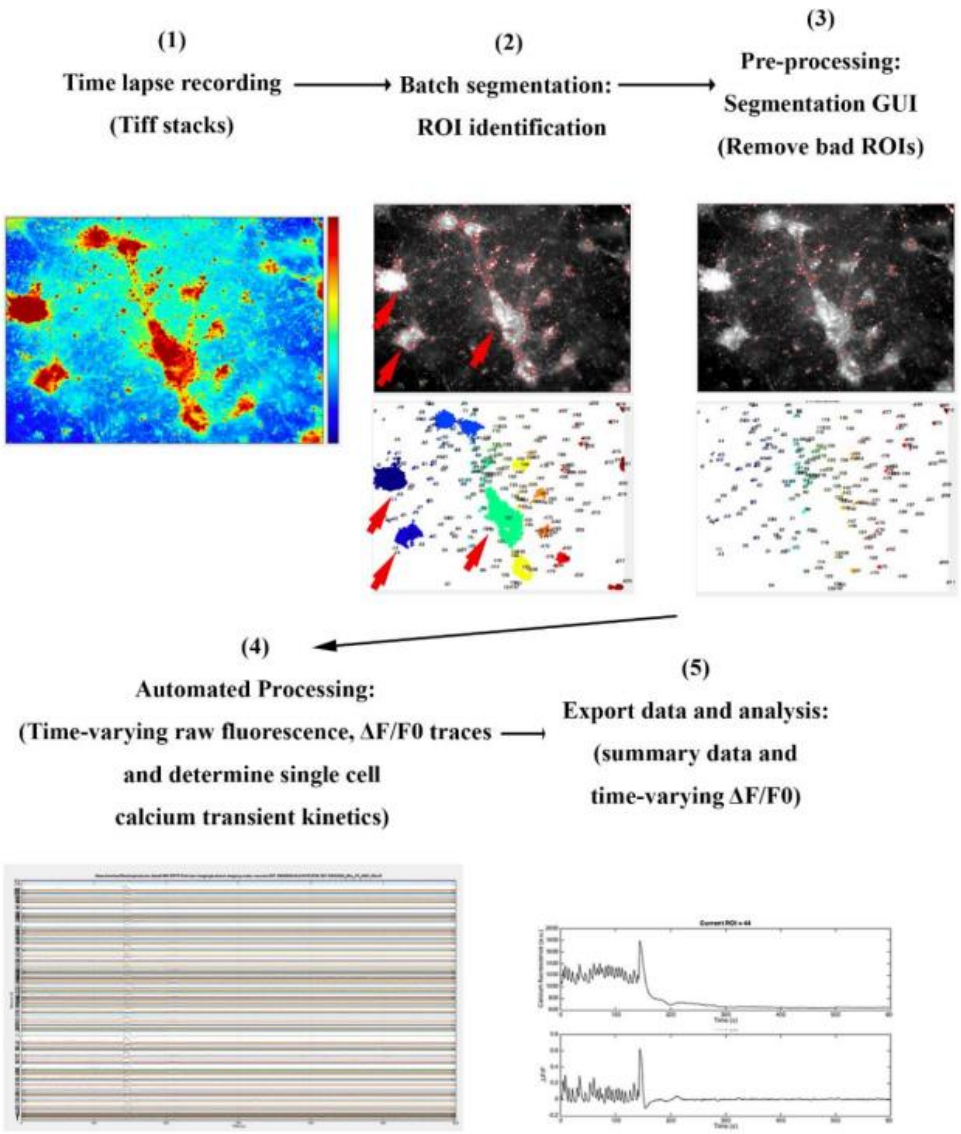

Figure 6.3. FluoroSNNAP workflow for the analysis of time-lapse recording of calcium imaging.

(1) Live calcium imaging was performed by acquiring stacks of images for 120-600 seconds. (2) cell bodies were identified as the Region of Interests (ROI). (3) areas with cell aggregates were removed (red arrowed) before calcium imaging analysis. (4) the time-varying fluorescence trace (ΔF/F0) were used to define ROI. (5) data of each ROI were exported for analyses of the calcium dynamics in each single cells. (Image taken from FluoroSNNAP manual).

Steps 1-3: Timelapse recordings and segmentation of ROI's

Firstly, a time-lapse recording was taken using the computer. Next, the ROI was identified using an algorithm within the FluoroSNNAP software. It identifies sources of fluorescence with variations over time, based on the principle that mature neurons have active calcium influx. Known as the active contour method, the software selects ROI's that automatically

delineate neurons from the background. However, iPSC-derived cortical neurons may form large aggregates over long periods of culture time, compromising the fluorescence variations of single cells. Therefore, these false and large areas of "ROIs" of cell aggregates were manually deleted using the Segmentation GUI tool prior to data analyses.

Step 4: Identification of ROI's and computation of time course fluorescence variations

Once the ROIs have been identified, the next step is to trace the single neuron fluorescence variations. The software computes fluorescence-versus-time trace for each ROI (=cell). The mean of the lower 50% fluorescence value in the first 10 seconds (excluding transient peak) was averaged as the baseline F0 for each ROI, which is automatically summarized by the FluoroSNNAP software. F is the raw fluorescence value of a given time point. ΔF was calculated by subtracting each raw fluorescence value with F0 (ΔF=F-F0). ΔF/F0 was defined as the amplitude of calcium transient.

Step 5: Determination of single cell calcium transient kinetics.

Two files were exported for data analysis on FluoroSNNAP: delta F/F0 and the automatically saved summary data. To identify the onset of calcium transients, we applied a threshold of 0.05 for ΔF/F0 amplitudes, and the ΔF/F0 $\leq$5% change in fluorescence intensity was regarded as noise or background. Only the cells with an amplitude ΔF/F0 of more than 0.05 in the duration of analysis was defined as an active cell and referred to as spontaneous calcium transient (Fig 6.2)

6.2.5 Definitions used for the properties of calcium transients

1. Number of active cells %: If an ROI has a value of ΔF/F0 ≥0.05 in the analysis, it is defined as an active cell. The number of active cells % is calculated by dividing the total number of active ROIs by the total number of segmented ROIs **(Fig 6.4)**.

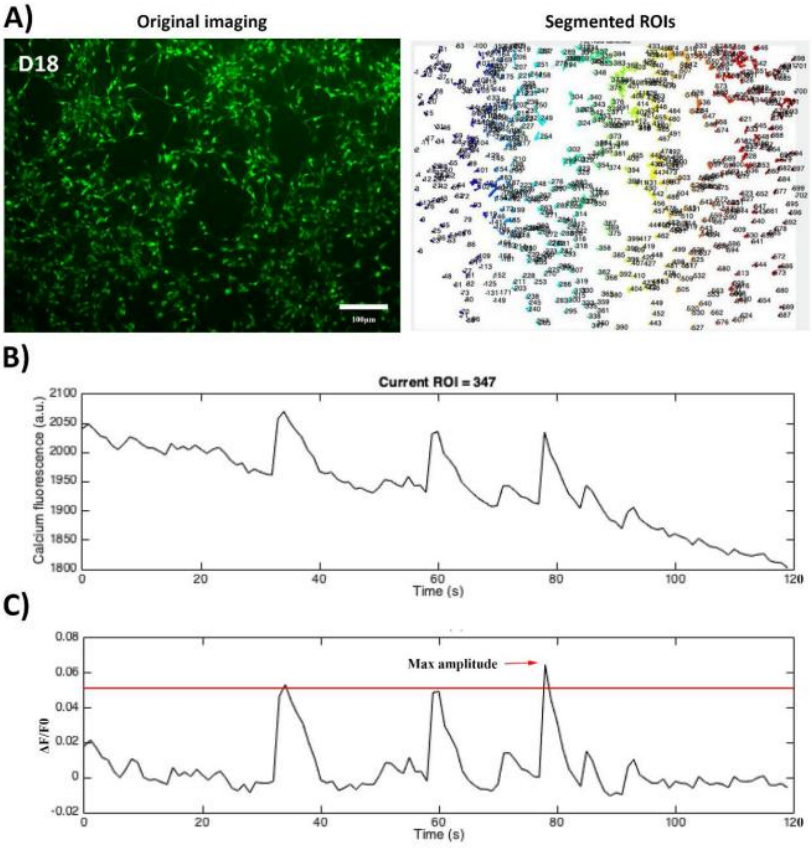

Figure 6.4. Detection of fluorescence in a single cell.

(**A**) Image of cells with fluorescent Ca^{2+} dye and segmentation of ROIs by software revealing individual cells. (**B**) Individual ROI shows Ca^{2+} fluorescence for an individual cell. (**C**) Frequency of Ca^{2+} transients overtime showing max amplitude.

2. Frequency of calcium transients: The frequency of calcium transients is calculated by dividing the number of the calcium transients with a ΔF/F0 value ≥0.05 by the duration of the analysis.

3. The maximal amplitude of calcium transients: The maximal amplitude is calculated by calculating the mean of the Max Intensity of all active ROIs (the highest peak) in the duration of the analysis. The amplitude was defined as the maximum change in fluorescence over the baseline following the onset of a calcium transient.

4. Intracellular Ca^{2+} concentrations [Ca^{2+}]i: The baseline calcium fluorescence (F0) is used to indicate the [Ca2+]i. The F0 of each ROI was quantified by averaging parts of the fluorescence trace at 2s before the onset and 10s after all calcium transients, which is automatically summarized by the FluroSNNAP software.

6.2.6 Statistical analysis

Statistical analyses were performed using GraphPad Prism version 9.3.1. Statistical analyses were performed using paired or unpaired non-parametric t-test with a level of significance set at *p<0.5, **p<0.01, ***p<0.001. All data are presented as mean ± SEM.

6.3 Results

6.3.1 Spontaneous calcium activity is increased in cortical neurons overtime

Action potentials and calcium transients are necessary for the normal functioning of the CNS. The different characteristics of calcium transients play an important role in neurotransmitter release and signalling transmission in both immature and mature neurons. In this study, we firstly investigated calcium transients in iPSC-derived cortical neurons in a control (EP2C004) at an early time point (Day 60) and at a later time point (Day 100) of differentiation **(Figure 6.5).**

Spontaneous calcium transients were recorded for 120s to compare the calcium kinetics overtime in culture as neurons matured. We found that there was a significantly greater percentage of spontaneously active cells at day 100 (32% ± 2.7%) compared to day 60 (19% ± 3.4%; p<0.001)**(Figure 6.5 C)**. Similarly, the frequency (D60= 0.08 ± .02 Hz, D100= 0.15 ± .04 Hz; p<0.001) and the amplitude (D60 ΔF/F0 = .09 ± .04 Hz, D100 ΔF/F0 = .14 ± .06 Hz; p=.0082) were significantly increased at day 100 compared to day 60 **(Figure 6.5 D and E)**. Furthermore, there was also a significant increase in relative fluorescence intensity of baseline (F0) in cells at day 100 (1324 ± 92%) compared to day 60 (782 ± 62%, p<0.0001) **(Figure 6.5 F).** These results indicate a higher concentration of intracellular Ca^{2+} in cells at day 100.

Next, we performed the same analysis in patient-derived cells to determine whether the *KCNQ2* mutation altered the Ca^{2+} dynamics during neuronal maturation. We found that patient neurons (A265T) displayed a similar pattern to control neurons over the culture time, with the percentage of spontaneously active cells (D60 = 22 ± 1.8%, D100 = 37 ± 2.1%; p=<0.001) , the frequency (D60 = 0.09 ± .009 Hz, D100 = 0.195 ± .018 Hz; p=<0.0001), the amplitude (D60 ΔF/F0 = 0.105 ± .015 Hz, D100 ΔF/F0 = .152 ± .017 Hz; p=<0.001) and the relative florescence intensity (D60 = 862 ± 78%, D100 = 1579 ± 84%; p= <0.0001), all of which were increased from day 60 to day 100, indicating the mutation was not impeding neuronal maturation **(Figure 6.6)**.

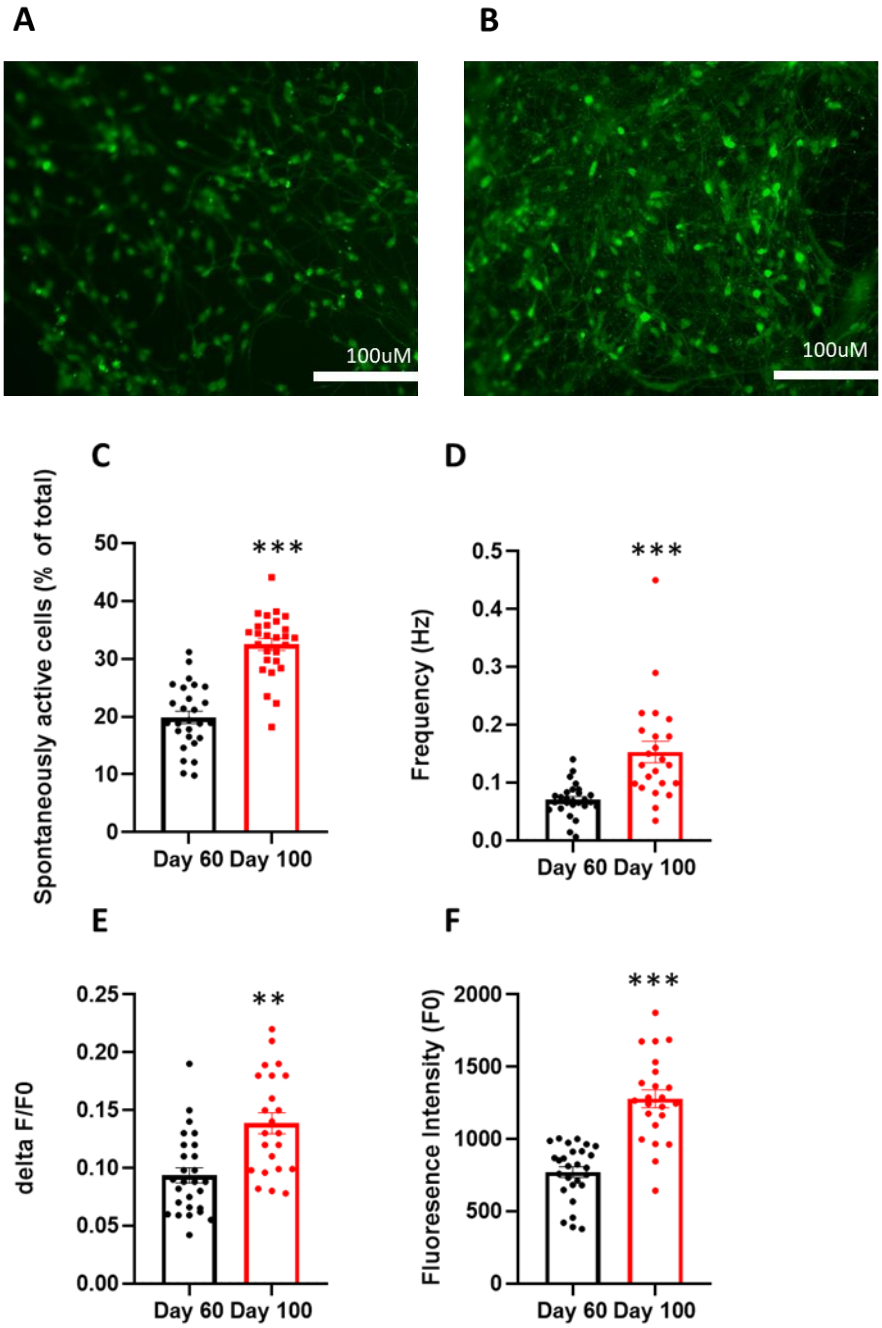

Figure 6.5: Spontaneous Ca^{2+} transient properties were increased in <u>control</u> iPSC-derived neurons overtime in culture between day 60 and day 100.

(A) Representative image of cells from day 60 in control cell line EP2C004 C2. **(B)** Representative image of cells from day 100 in control cell line EP2C004 C2. **(C)** The percentage of spontaneously active cells in control neurons at day 60 and 100. **(D)** The frequency, **(E)** Amplitude and **(F)** Fluorescence intensity of Ca^{2+} transients at day 60 and day 100 (For each timepoint n = 27). The data was analysed from 3 different areas per coverslip, 3 coverslips per cell line, 3 lines per donor). The total number of cells examined at day 60 = 10,423 and at day 100 = 11,863. The data are presented as Mean ± SEM. Statistical significance (*p<0.05, **p<0.01, ***p<0.001) was evaluated using an unpaired parametric *t*-test.

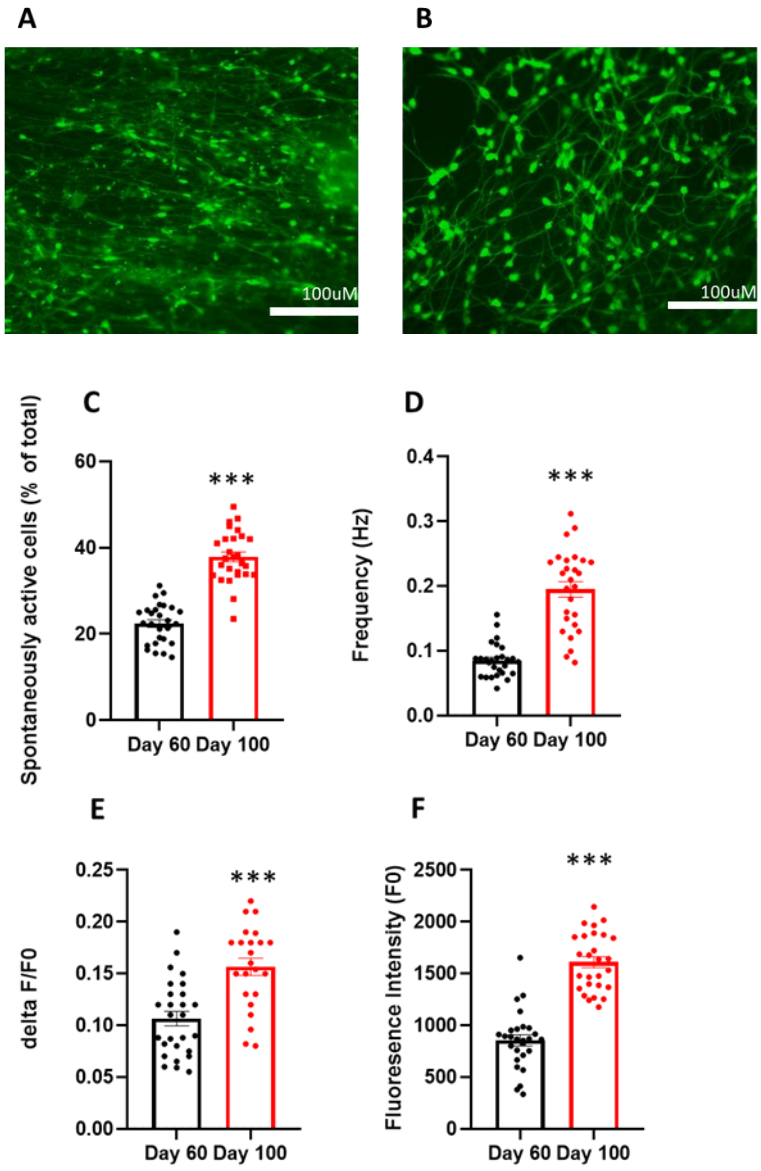

Figure 6.6: Spontaneous Ca^{2+} transient properties were increased in patient (A265T) iPSC-derived neurons overtime in culture between day 60 and day 100.

(A) Representative image of cells from day 60 in the patient cell line EP2004 C8 (A65T). **(B)** Representative image of cells from day 100 in patient cell line EP2004 C8. **(C)** The percentage of spontaneously active cells in control neurons at day 60 and 100. **(D)** The frequency, **(E)** Amplitude and **(F)** Fluorescence intensity of Ca^{2+} transients at day 60 and day 100 (For each timepoint n = 27). The data was analysed from 3 different areas per coverslip, 3 coverslips per cell line, 3 lines per donor). The total number of cells examined at day 60 = 12,865 and at day 100 = 13,211. The data are presented as Mean ± SEM. Statistical significance (*p<0.05, **p<0.01, ***p<0.001) was evaluated using an unpaired parametric *t*-test.

6.3.2 Spontaneous calcium transients were largely driven by voltage-gated Na^+ channels through action potential propagation

An AP is initiated by rising intracellular Na^+ concentration through voltage-gated Na^+ channels which causes an influx of Ca^{2+}. Tetrodotoxin (TTX) is a widely used voltage-gated Na+ channel blocker that inhibits the initiation of an AP. To investigate whether these spontaneous calcium transients were associated with membrane depolarizations, we applied 1µM of TTX to the iPSC-derived cortical neurons at day 100 **(Figure 6.7)**. We found that 1µM TTX abolished 83.7 ± 4.8% of calcium transients of active cells in patient cells and 83.2% ± 5.3% in control cells on day 100 **(Figure 6.7 C)**. Additionally, we also observed a reduction in the frequency of the remaining active cells in patients (53.8 ± 4.1%) and controls (49.1 ± 7.2%)**(Figure 6.7 D)**. However, there was no significant difference in the effect of TTX on patient and control lines. These results indicate that the spontaneous calcium transients in our cortical neurons were largely controlled by voltage-gated Na^+ channels through Action Potentials.

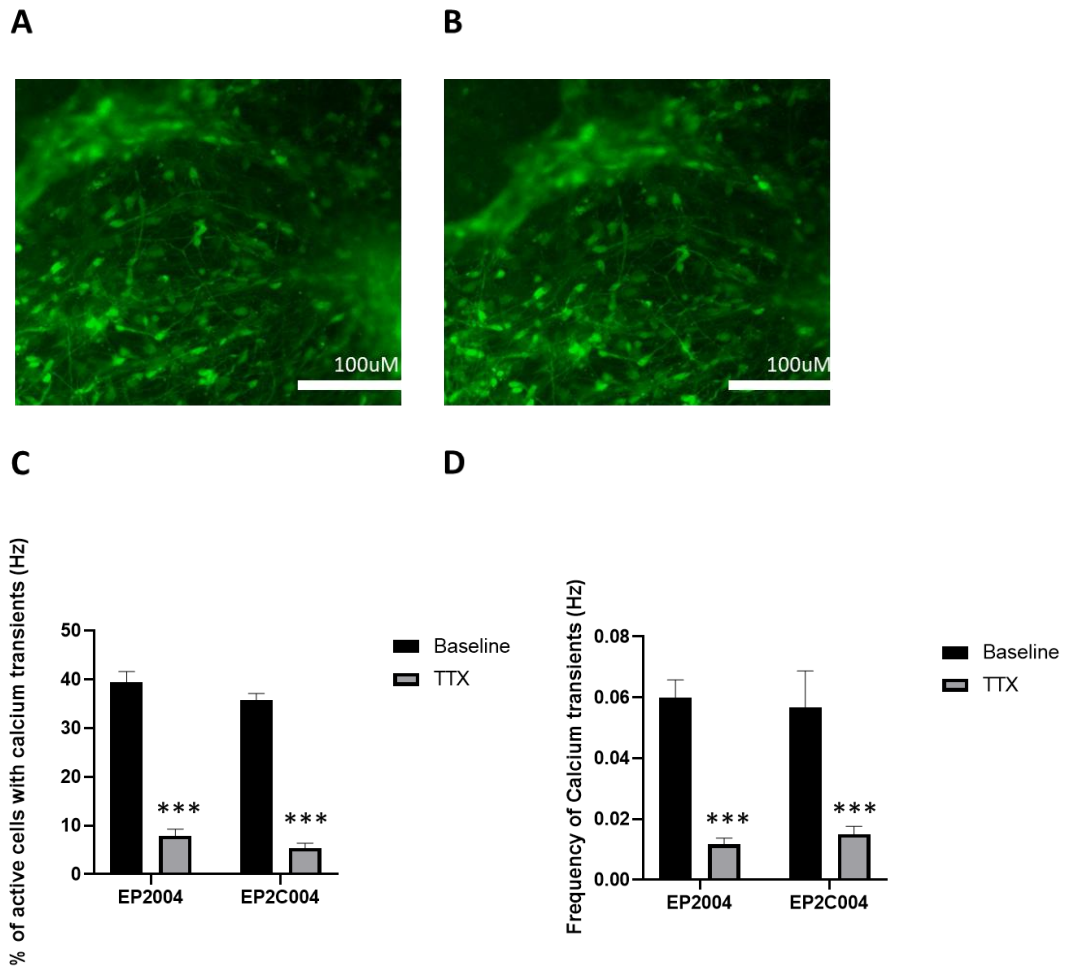

Figure 6.7: Spontaneous Ca^{2+} transients were largely driven by Na^{+} channels though action potential propagation.

(A) Representative image of cells from EP2004 C7 (A265T) at day 100 before TTX addition. **(B)** Representative image of cells from EP2004 C7 (A65T) at day 100 after 1µM TTX addition. **(C)** Reduction of the % of active cells in EP2004 (A265T) and EP2C004 at day 100 showed a successful blocking effect of Na^{+} channel blocker TTX (n= 9, 3 coverslips, 3 lines). **(D)** Reduction % of the frequency of calcium transients in EP2004 (A265T) and EP2C004 cells at day 100 in the remaining active cells showed a time-dependent manner (n= 3/9). The total number of cells analysed was EP2004 = 4,213, EP2C004 = 3,752. The data are presented as Mean ± SEM. Statistical significance (*p<0.05, **p<0.01, ***p<0.001) was evaluated using an unpaired parametric *t*-test.

6.3.3 iPSC-derived cortical neurons respond positively to glutamate addition

As cortical neurons are excitatory neurons, we investigated whether our iPSC-derived cortical neurons are responsive to the excitatory neurotransmitter glutamate (Glu) **(Figure 6.8)**. Glu treatment was shown to increase the percentage of active cells with calcium transients in patient cells from 39.2 % ± 2.2% to 87.1% ± 7.1%($p \leq 0.0001$) and in control cells from 36.7% ± 3.5% to 83.4 % ±7.3% ($p \leq 0.0001$) at day 100 **(Figure 6.8 C)**. The frequency of

calcium transients were also increased in patient cells (0.05 ± .04 Hz to 0.19 ± .03 Hz; p=<0.0001) and control cells (.09 ± .005 Hz to .16 ± .015 Hz; p=<0.0001)**(Figure 6.8 D)**. These results show that the majority of our iPSC-derived cortical neurons were excitatory neurons possessing functional glutamate receptors.

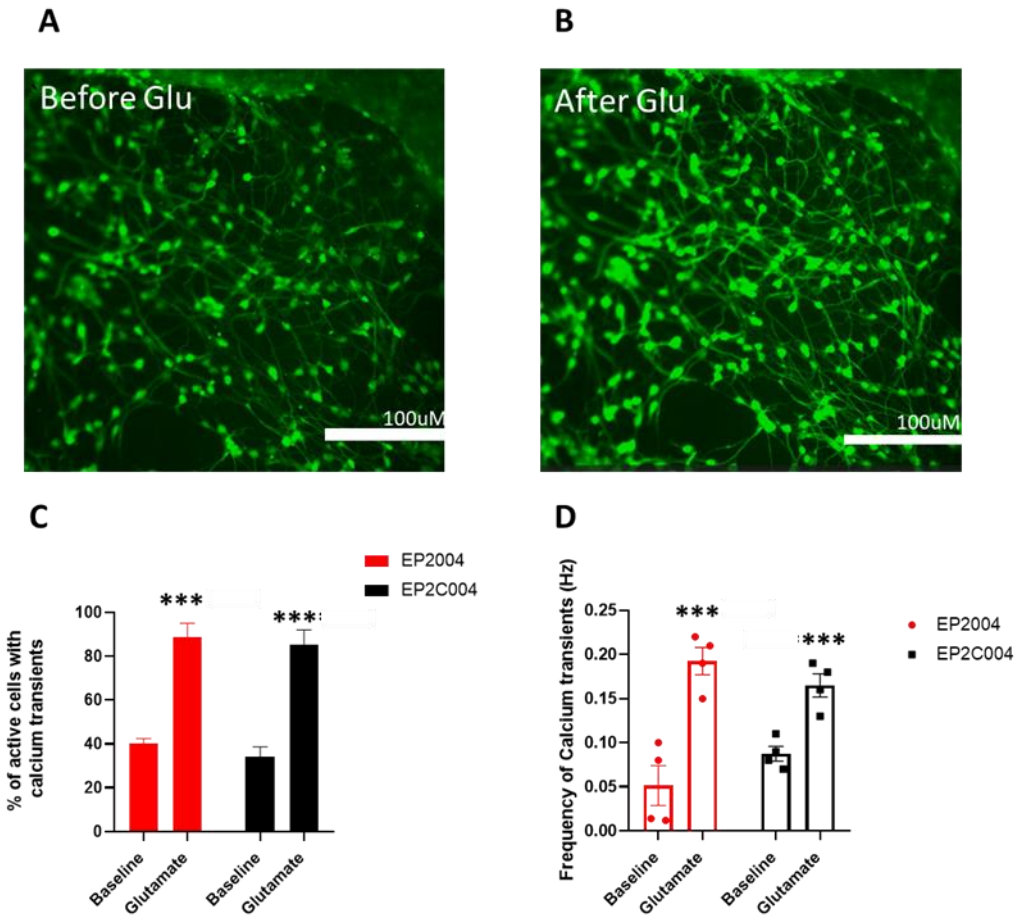

Figure 6.8. iPSC-derived cortical neurons displayed a positive response to glutamate treatment.

(A) Representative image of cells from EP2004 C1 (A265T) at day 100 before Glutamate addition. **(B)** Representative image of cells from EP2004 C1 at day 100 after Glutamate addition. **(C)** An increase in the % of active cells with calcium transients showed a positive response to Glutamate addition **(D)** Increased % of the frequency of calcium transients in EP2004 (A265T) and EP2C004 cells at day 100 showed a positive response to Glutamate addition (n= 4). The total number of cells used was EP2004 = 2,186, EP2C004 = 1,958. The data are presented as Mean ± SEM. Statistical significance (*p<0.05, **p<0.01, ***p<0.001) was evaluated using an unpaired parametric *t*-test.

6.3.4 iPSC-derived cortical neurons displayed an inhibitory response to treatment with CNQX

CNQX is a commonly used AMPA glutamate receptor antagonist. To further verify the functionality of iPSC-derived cortical neurons, we applied CNQX (50µM) to our cortical neurons at day 100 **(Figure 6.9)**. We demonstrated that CNQX successfully blocked 81.1 ± 2.9% of calcium transients in patient cells (A265T) and 71.4% ± 2.3% in control cells **(Figure 6.9 C)**. This was accompanied with a decreased frequency of calcium transients in the remaining active cells in patient cells from 0.112 ± .036Hz to 0.037 ± .013Hz (p=<0.001) and in control cells from 0.083 ± .024Hz to 0.042 ± .014Hz (p=<0.001)**(Figure 6.9 D)**. These data suggest that the calcium transients in the iPSC-derived cortical neurons were largely driven by AMPA-mediated glutamatergic synaptic transmission. However, since we did not observe a blocking effect as dramatic as with TTX treatment, it is likely that there are other forms of synaptic transmission in our cells such as via other glutamatergic receptors such as NMDA.

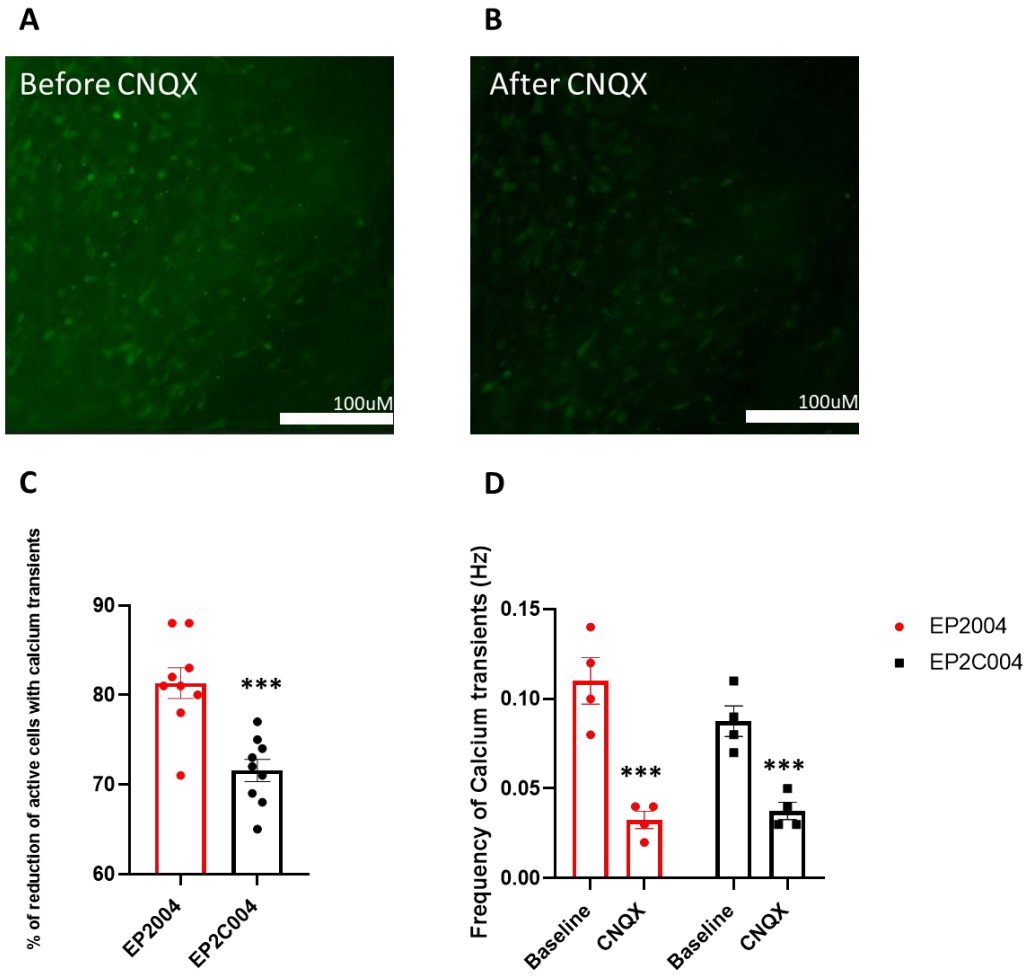

Figure 6.9. iPSC- derived cortical neurons are glutamatergic with a negative response to CNQX treatment.

(A) Representative image of cells from EP2004 C8 (A265T) at day 100 before CNQX addition. **(B)** Representative image of cells from EP2004 C8 (A265T) at day 100 after CNQX addition. **(C)** Reduction of the % of active cells in EP2004 (A265T) and EP2C004 at day 100 showed a successful blocking effect of CNQX. (n= 9, 3 coverslips, 3 lines). **(D)** Frequency of calcium transients showed a reduction due to CNQX treatment (n= 4/9). The total number of cells analysed was EP2004 = 4,651, EP2C004 = 4,379. The data are presented as Mean ± SEM. Statistical significance (*p<0.05, **p<0.01, ***p<0.001) was evaluated using an unpaired parametric *t*-test.

6.3.5 Calcium dynamics are altered in *KCNQ2*-neurons at day 100

As disrupted Ca^{2+} homeostasis is a hypothesis of epilepsy pathogenesis, we compared the properties of spontaneous calcium transients in *KCNQ2*-neurons and control neurons. As iPSC-derived cortical neurons showed higher maturity at day 100 and were responsive to glutamate and CNQX treatments, we analysed spontaneous calcium transients at this timepoint between patient and control groups. The characteristics of spontaneous calcium transients were evaluated in 3 *KCNQ2*-DEE mutated lines (A265T) and 3 healthy sibling control lines. We found there was a significantly greater percentage of spontaneously active cells in patient lines (42.1% ± 1.2%) compared to controls (36.6% ± 1.5%; p=0.006)**(Figure 6.10 A)**. Similarly, there was a significant increase in the frequency (Control: 0.185 ±.018 Hz, Patient: 0.202 ± .019 Hz; p= 0.024) and amplitude (Control: 0.108 ± .013 Hz, Patient: .149 ± .034 Hz; p= 0.007) in patient lines compared to controls **(Figure 6.10 B and C)**. In addition, the relative fluorescence intensity to baseline was significantly higher in patient lines (1763 ± 74%) compared to controls (1579 ±84%; p=0.008)**(Figure 6.10 D).** These data demonstrate that spontaneous calcium transients are altered in patient neurons compared to their sibling controls.

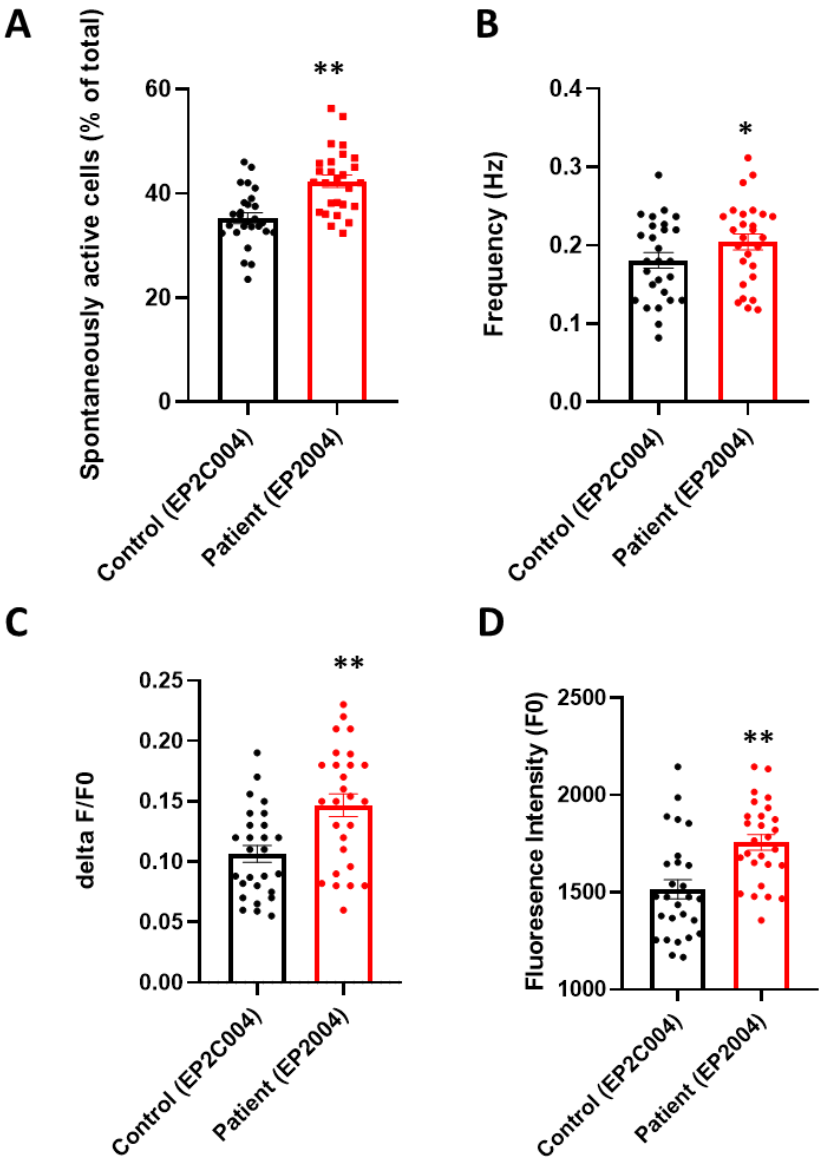

Figure 6.10*: KCNQ2*- iPSC derived cortical neurons display altered calcium dynamics at day 100.

(A) The percentage of spontaneously active cells in control neurons EP2C004 and patient neurons EP2004 (A265T) at day 100. **(B)** The frequency, **(C)** Amplitude and **(D)** Fluorescence intensity of Ca^{2+} transients at day 100 in patient and control neurons (for each donor n = 27). The data was analysed from 3 different areas per coverslip, 3 coverslips per cell line, 3 lines per donor). The total number of cells examined at day 100 is EP2004 = 11,215 and EP2C004 = 10,838. The data are presented as Mean ± SEM. Statistical significance (*p<0.05, **p<0.01, ***p<0.001) was evaluated using an unpaired parametric *t*-test.

6.4 Discussion

In our *KCNQ2*-DEE (A265T) model, we showed that calcium dynamics were altered in *KCNQ2*-DEE (A265T) neurons compared to sibling controls. Calcium dynamics including spontaneously active cells, amplitude, frequency, and fluorescence intensity were significantly increased in *KCNQ2* mutant neurons, reflective of the hyperexcitable phenotype we witnessed using MEA technology.

Intracellular Ca^{2+} concentration in neurons is critical for triggering and propagating seizure activity (Steinlein, 2014). As discussed, calcium binding proteins help regulate Ca^{2+} concentration in the cytosol and act as both Ca^{2+} transporters and sensors (Xu et al., 2018). As such, Ca^{2+} binding proteins play a role in the pathogenesis of epilepsy. In *KCNQ2*, the Ca^{2+} binding protein Calmodulin is of particular importance as this protein is necessary for the activation of the *KCNQ2* channel, Kv7.2 (Wen et al., 2002). The overexpression of calmodulin has been shown to increase K^+ current release by Kv7.2 channels, causing a reduction in neuronal activity. Conversely, knockdown of Calmodulin causes a reduction in Kv7.2 current, resulting in increased neuronal activity (Zhou et al., 2016). The calmodulin-binding helix B and helix B-C linker have been categorised as mutational hotspots in *KCNQ2*-DEE (Zhang et al., 2020). Numerous studies have shown that mutations that are located with these Calmodulin-binding regions of the C-terminus decrease or prevent the interaction between calmodulin and the Kv7.2 channel. This decreased interaction prevents Kv7.2 channel expression at the plasma membrane by interrupting with trafficking of the channel (Zhou et al., 2016). Another study showed that a *KCNQ2* mutation R581Q, located in the coiled-coil domain of the C-helix, resulted in the functional enhancement of Ca^{2+} activated K^+ channels likely due to increased cytosolic Ca^{2+} concentrations (Simkin et al., 2021). What is poorly understood is how Ca^{2+} dynamics are altered in *KCNQ2* neurons where the mutation is not located within the calmodulin binding domain. To my knowledge, there has been no studies which examine the calcium dynamics of neurons with a *KCNQ2* mutation within the pore-forming region. In this study, we discovered that Ca^{2+} dynamics were significantly altered in the *KCNQ2* mutation A265T (c.793G>A), located within the pore of the Kv7.2 channel.

First, we compared the spontaneous Ca^{2+} transients in control neurons at two timepoints: day 60 and day 100, and found that at day 100, neurons had a greater percentage of active cells, a higher frequency and amplitude of calcium transients and a significantly increased relative fluorescence of baseline compared to day 60 neurons **(Figure 6.5)**. These results suggest a higher level of calcium signalling at day 100, indicative of higher neuronal

maturation, as calcium transients reflect electrical events. A study showed that Ca^{2+} transients had a higher frequency and amplitude in post-migratory neurons compared to migratory neurons, suggesting that increased spontaneous calcium transients contribute to terminating migration in excitatory cortical neurons during development (Bando et al., 2016). Together with our data, this suggests that our neurons have undergone further neuronal maturation between day 60 and day 100. Next, we analysed the spontaneous Ca^{2+} transients in *KCNQ2* (A265T) neurons at the same timepoints. We found that patient neurons displayed a similar pattern of increased calcium activity overtime **(Figure 6.6)**. These results suggest that the A265T mutation was not impeding the development of new Ca^{2+} connections during maturation between day 60 and day 100, though we also sought to explore differences calcium dynamics between control and *KCNQ2*-DEE neurons (discussed below).

To further validate our excitatory cortical neurons, we applied glutamate to the cells at day 100 and recorded spontaneous calcium transients. Glutamate addition significantly increased the percentage of active cells as well as the frequency of calcium transients **(Figure 6.8)**. Additionally, we showed an 80% reduction in active cells in patient cells and a 70% reduction in control cells when treated with the AMPA-antagonist CNQX **(Figure 6.9)**. Taken together, these results show that our cell population are largely glutamatergic and that glutamatergic synaptic activity drives calcium transients in culture. We have no data here on other glutamatergic receptors such as NMDA, which has been previously recorded to be necessary for synaptic function (Evans et al., 2012). As CNQX treatment did not result in a complete ablation of Ca^{2+} transients in our cultures, it is reasonable to assume that Ca^{2+} mediated synaptic transmission is also partially mediated by other glutamatergic receptors including NMDA receptors.

While Ca^{2+} imaging is a useful tool for analysing neuronal properties and maturation, we were also interested is understanding whether *KCNQ2*-disease cortical neurons displayed altered Ca^{2+} dynamics when compared to controls. As shown in **Chapter 5**, *KCNQ2*-DEE (A265T) cortical neurons exhibited an increased firing and bursting phenotype on MEA plates **(Chapter 5)**. Therefore, we hypothesised that Ca^{2+} dynamics would also be altered as Ca^{2+} transients are initiated by action potentials (APs). On day 100, we analysed a total of 11,215 patient cells and 10,838 control cells and recorded the spontaneous Ca^{2+} transients for 120s. We found that *KCNQ2*-DEE (A265T) neurons had increased excitability, evidenced by a higher percentage of active cells and a higher frequency compared to control cells **(Figure 6.10)**. Additionally, *KCNQ2*-DEE (A265T) neurons had a significantly higher amplitude and

fluorescence intensity **(Figure 6.10)**. These results together convincingly demonstrated iPSC-derived cortical neurons recapitulate a hyperexcitability phenotype.

Altered Ca^{2+} dynamics, either decreased or increased, have previously been reported in iPSC-derived neuronal epilepsy models. In a study by Marchetto et al., they generated an iPSC-derived neuronal model of Rett syndrome from patients with different mutations in the MeCP2 gene. To analyse whether their Rett-iPSCs-derived neuronal networks had altered Ca^{2+} dynamics, they preloaded the cells with the calcium indicator fluo-4AM. They recorded the spontaneous Ca^{2+} transients in neurons and found that the frequency of calcium transients in patient neurons was abnormally decreased when compared to controls, suggesting a deficiency in the neuronal network connectivity and activity dynamics. These altered Ca^{2+} dynamics are consistent with their other electrophysiological findings which showed that patients neurons had decreased frequency of spontaneous postsynaptic currents using whole cell patch clamping and reduced glutamatergic synapse number (Marchetto et al., 2010). In a hyperexcitable iPSC-derived neuronal model of bipolar disorder consisting of hippocampal dentate gyrus (DG) granule cell-like neurons, the authors examined whether the enhanced excitability of single neurons could also generate neural network hyperactivity by analysing spontaneous Ca^{2+} transients using the calcium indicator, Fluo-4AM. They found that patient neurons showed a significantly higher frequency of Ca^{2+} events, reflective of the hyperexcitability seen in their patch-clamping experiments (Mertens et al., 2015). These studies, as well as our study reveal that Ca^{2+} transients can be used as an indicator of excitability in neurons in combination with electrophysiological approaches such as MEA and whole-cell patch clamping.

One study which looked at a mouse model of epilepsy using adult born granule cells found that intracellular calcium was elevated in the disease models. To determine the source of this elevated intracellular Ca^{2+}, they treated neurons with TTX and found no difference in the spontaneous calcium transients amplitude or frequency. They then treated the neurons with the GABA inhibitor bicuculline (20µM) and found a significant reduction in spontaneous Ca^{2+} transient frequency (Lybrand et al., 2021). In our study, we found that TTX resulted in an 80% reduction of active cells with calcium transients, suggesting a large component of the calcium transients are driven by voltage-gated Na^{+} channels during an AP. However, of the remaining active cells the frequency of calcium transients was reduced by approximately 50%. An interesting follow up experiment would be to treat neurons with a GABA inhibitor such as bicuculline to determine whether the frequency of the remaining active cells could be further reduced. I hypothesise that GABAergic neurons may be responsible for some of the increased

Ca^{2+} activity seen in *KCNQ2* cells compared to controls as we know GABAergic neurons play an important role in genetic epilepsies. For example, there is impaired GABA synthesis in human pyridoxine deficiency, a disorder characterized by the onset of seizures in infancy (Treiman, 2001). A greater reduction in Ca^{2+} transient frequency in patient cells after bicuculline treatment compared to controls, could reveal a potential involvement of these GABAergic neurons in the disease phenotype. Although we showed in **Chapter 4** that our neurons are positive for GABAergic markers, a distinct co-culture of glutamatergic and GABAergic neurons in known proportions would be more advantageous.

Astrocytes play an important role in Ca^{2+} signalling and epilepsy-related disorders. We know that astrocytes interact closely with neurons by supporting them metabolically and also crucial for maintaining homeostasis by controlling the levels of extracellular glutamate and potassium levels (Danbolt et al., 2016). Astrocytes are also believed to be involved in brain signalling (Lundgaard et al., 2015). Ca^{2+} signals within astrocytes control the release of gliotransmitters such as Glutamate, which interacts directly with neurons (Perea et al., 2014). Astrocyte-neuron interactions which involve Ca^{2+} signalling are associated with ictogenesis, or the initiation of seizure activity (Patel et al., 2019). One study showed that by eliciting Ca^{2+} signals in astrocytes, by applying ATP and mGlur5 agonists, slow inward Ca^{2+} currents were triggered in neighbouring neurons, which were not affected by the treatment of the Na^{+} channel antagonist TTX (Fellin et al., 2004). Furthermore, another study showed that during experimental seizure induction, Ca^{2+} mediated glutamate release by astrocytes also resulted in slow inward Ca^{2+} currents in neighbouring neurons (Tian et al., 2005). These studies reveal the close relationship between astrocytes and neurons in seizure generation. An interesting follow on experiment could be to analyse *KCNQ2* astrocytes using Ca^{2+} imaging and compare their Ca^{2+} dynamics with control astrocytes, as we showed earlier in **Chapter 4**, that glial cells including astrocytes make up approximately 40% of our culture.

In summary, we performed functional analysis of iPSC-derived cortical neurons from a *KCNQ2* pathogenic variant (p.A265T; c.793G>A), via calcium imaging of day 60 and day 100 of cortical differentiation. We found that calcium dynamics were altered in *KCNQ2* neurons compared to sibling controls. Calcium dynamics including spontaneously active cells, amplitude, frequency, and fluorescence intensity were significantly increased in *KCNQ2* mutant neurons, reflective of the hyperexcitable phenotype we witnessed using MEA technology. We hypothesise that this increase in Ca^{2+} transients is likely due to increased action potential firing in both glutamatergic and GABAergic neurons. Additional experiments, as discussed above, would facilitate further understanding of the mechanisms.

7.1 Discussion

7.1.1. Summary

The primary aim of this PhD work was to generate iPSC lines from 3 children affected by *KCNQ2*-developmental and epileptic encephalopathy (*KCNQ2*-DEE), and healthy controls, and secondly, to develop a 2D-cortical neuronal model. Ultimately, we generated and analysed patient-derived iPSC-based models of 3 specific pathogenic heterozygous mutations (variants) in *KCNQ2* (F261L, A265T, A294V) for the first time, providing novel insights into the phenotype of *KCNQ2*-DEE. We then chose to focus on one mutation, A265T, for further calcium imaging and gene expression analysis. The results of the neuronal models for these loss-of-function (LOF) mutations reveal that excitatory, cortical neurons, display progressive escalation of burst firing and altered calcium dynamics as they matured over time in culture. Furthermore, patient neurons (A265T) exhibited an altered expression of other key K^+ and Na^+ channels associated with epilepsy. Our findings suggest that in our *KCNQ2*-DEE LOF neuronal models, neurons are hyperexcitable, display irregular firing patterns and have altered gene expression of critical epilepsy (brain developmental potassium ion channel)-related genes.

The experimental design of this project focused on 6 key pipelines (involving a diverse range of laboratory techniques) described across various Chapters in this thesis as follows: In **Chapter 2**, we derived patient-specific and sibling control iPSCs from dermal fibroblasts creating a bank of 24 iPSC lines. In **Chapter 3**, we performed gene editing using CRISPR/CAS9 technology and used miRNA approaches to control gene expression of upregulated genes in patient (A265T) lines. In **Chapter 4**, we differentiated iPSCs into excitatory, cortical neurons using the dual-SMAD inhibition protocol. In **Chapter 5**, we performed electrophysiological characterisation of iPSC-derived neurons using MEA recordings and finally in **Chapter 6**, we performed Ca^{2+} imaging and Ca^{2+} profile analyses.

7.1.2. Skin fibroblasts versus other iPSC sources

The discovery of iPSCs was a huge breakthrough development in the field of biomedical science. As iPSCs overcome the ethical and immunogenic challenges associated with hESCs, iPSCs have become a popular cell choice for disease modelling, stem cell therapy and personalised medicine (Liu et al., 2017). A wide range of iPSC sources exist. In theory, almost any mature cell type in the human body can be reprogrammed into iPSCs but the most

frequently used sources include dermal fibroblasts, umbilical cord blood cells, bone marrow cells, peripheral blood cells, keratinocytes, and more recently, cells in urine (Liu et al., 2020). In this study, as outlined in **Chapter 2,** we chose to derive iPSCs from dermal fibroblasts, taken from a skin biopsy due to the combined experience in our lab. Dermal fibroblasts have been the gold standard choice for reprogramming and there are bodies of research highlighting the reliability and reproducibility of dermal fibroblasts as a cell source for generating iPSCs (Plath et al., 2011). In more recent years, urine has been used a cell source for generating iPSCs and has many advantages as the process is easy, relatively costless to obtain, repeatable, and non-invasive (Huang et al., 2020). These advantages coupled with their ability for successful downstream generation of nerve cells, makes urine a particularly suitable cell choice for young children with neurological disorders such as those in our study (Kim et al., 2016). In the future, I would like to use urine as a cell source for generating iPSCs to eliminate any discomfort for patients and remove the requirement for a trained professional to obtain the starting material as is the case for dermal fibroblasts.

In this study, we chose to use a non-integrating Sendai Virus (SeV) due to its highly effective, non-integrating nature, to deliver the transcription factors *OCT4*, *SOX2*, *C-MYC*, and *KLF4* to the cells. Using this method, we had a 100% success rate in generating 24 iPSC lines from 8 donors. We found no difference in the ability between patient and control lines to differentiate into the 3 germ layers or any variances in the expression of the pluripotency markers, suggesting the *KCNQ2*-DEE variants had no visible effects on early neurogenesis. In 2007, Yamanaka and colleagues discovered that only the four [(*OCT4*, *SOX2*, *KLF4*, and *C-MYC* (abbreviated as OSKM)] of the twenty-four previously used pluripotency transcription factors are necessary to reprogram human fibroblasts into an embryonic stem cell-like state, creating iPSCs (Takahashi et al., 2007). It has been shown that *OCT4* is the most critical PSC reprogramming factor, while *KLF4* and *C-MYC* can be replaced by *NANOG* and *LIN28* (Shi et al., 2010). Shortly after the discovery of Yamanaka's OSKM factors, Yu and colleagues described a modified four-factor induction protocol using *OCT4*, *SOX2*, *NANOG*, and *LIN28*, which exhibit reprogramming with an efficiency similar to that obtained with the Yamanaka factors (Yu et al., 2007). When choosing an iPSC reprogramming method, it is important to reduce introducing any possible risk while also maintaining pluripotency and the ability to direct specific cell fate development of the desired lineage. In initial reprogramming studies, viral vectors such as retroviruses and lentiviruses, were used for the delivery of reprogramming factors (Shao et al., 2010). Unfortunately, the possibility of viral integration of transcription factor genes may cause genomic alterations, including oncogenic changes

in *Klf4* and *c-Myc*, which hinders the translation of these protocols to clinical application (Maherali et al., 2008). This is an important consideration for using iPSCs in cellular therapy, however delivery of iPSC-derived neuronal cells/tissues to human patients was not the aim of this study, which set out to determine an in vitro experimental neuronal model.

7.1.3. iPSC-derived experimental models of neurological disease

Given that many monogenic diseases such as *KCNQ2*-DEE affect specific cell types with great penetrance, disease-relevant phenotypes will be most predictable from iPSCs carrying the same genetic constellation (Xu et al., 2013). For this reason, many disease models for genetic disorders are utilising patient-derived iPSCs to examine phenotypes and pathophysiology that may occur because of the mutation (Brooks et al., 2022). They may also therefore provide models, to correct the phenotype with various experimental and therapeutic approaches. Ebert *et al*, published the first study of a neurological disease illustrating that human iPSCs could be used to model a monogenic disorder in a patient with SMA, due to a mutation in the survival motor neuron (*SMN1*) gene (Ebert et al., 2009). This study revealed that motor neurons derived from SMA iPSCs were selectively reduced in quantity and size compared to controls. In epilepsy models, the Na^+ channel, Nav1.1 has been extensively studied in the human iPSC models. Using epilepsy patient iPSCs-derived inhibitory neurons, it has been revealed that neurons carrying a LOF *SCN1A* mutation (S1328P) had a reduced Na^+ current amplitude (Sun et al., 2016). Meanwhile, *SCN1A* (c.4261G>T/c.3576_3580del TCAAA) mutated neurons displayed decreased Na^+ current density (Kim et al., 2018). To date, there has been very few studies using patient-derived iPSCs to model *KCNQ2*-DEE disorders. The most significant study was published recently by Simkin et al, who derived iPSCs from a patient harbouring a *KCNQ2*-DEE variant R581Q, who showed that the disease-causing mutation caused a dyshomeostatic modulation of other Ca^{2+} activated K^+ channels, findings that would not have been revealed using other models (Simkin et al., 2021).

CRISPR/Cas9-based gene therapy holds great promise in both correcting monogenic diseases to generate isogenic control lines and introduce a mutation to generate isogenic mutant lines (Tărlungeanu et al., 2018). In this study, as outlined in **Chapter 3** we utilised CRSIPR/CAS9 technology to try to create both isogenic mutant and control lines, to generate a model that would enable us to attribute any discovered phenotypic differences to the genetic variant. Both attempts at either (a) correcting the mutation in the patient cell line or (b) introducing the mutation in the control cell line, were unsuccessful. As previously discussed, this was likely due to problems during delivery of the RNP complex to the cells via electroporation.

Incorporation of a fluorescent label during reprogramming may be a useful indicator to include in future experiments for immediate confirmation that RNP components were successfully delivered to the cells. Due to time constraints, we were not in a position to repeat these experiments once we realised that we may have experienced a delivery issue. It is suggested when developing neuronal phenotypes for specific mutations, that isogenic mutant lines are also included for power analysis, and therefore this is a limitation of regarding any phenotype seen in our patient lines to the pathogenic variant (Simkin et al., 2022). As we have already designed the guide RNAs and templates required for both mutation-induction and mutation-correction, we would plan to re-do these experiments using a different electroporation system in the future. Nevertheless, as the same experiments were applied to three different mutations in 9 iPSC neuronal cell lines, as compared to controls, with similar striking results, the findings corroborate previous hypothesis for the only other published study (and a single mutation) to date for *KCNQ2*-DEE (Simkin et al., 2021), as discussed in **Chapters 5 and 6** and in the following text.

7.1.4. iPSC derived cortical neuronal models and *KCNQ2*

As Kv7.2 channels are highly expressed in the human cortex, we chose to generate patient iPSC-derived cortical neurons (Zhu et al., 2022). Various protocols now exist for the derivation of human cerebral neural stem cells (NSCs) and functional neurons from iPSCs which has greatly facilitated functional studies of cortex development, cortical disease modelling and potential drug discovery (Alsanie et al., 2020). Some earlier protocols lacked the ability to generate secondary progenitor cells, creating a population of mainly early born deep cortical neurons (Eiraku et al., 2008). We chose to use a modified version of the protocol published by Y. Shi, Kirwan, & Livesey, 2012, as this protocol generates both primary neuroepithelial cells and secondary cortical stem/progenitor cells. In our protocol, we utilised the dual SMAD inhibition pathway using the two small molecules, SB-431542 and LDN-193189, to direct differentiation toward the anterior neuroectodermal lineage (Chambers et al., 2009). Using this approach, the efficiency of cortical neural induction from iPSCs was very high in all nine cell lines generated **(Figure 4.7, Chapter 4)**. We found that deep layer, early born projection neurons were the most abundant in our cell population by immunocytochemistry **(Figure 4.13, Chapter 4)**. This could be explained by the fact that these neurons are produced first whereas the later-born, layer 2 neurons are produced as late as day 90 of differentiation (Y. Shi, Kirwan, Smith, et al., 2012). In the original paper, they reported approximately equal numbers of deep- and upper-layer neurons in their cultures. We hypothesise that a potential

reason for a reduced number of upper layer neurons in our culture may be a consequence of their late production. If repeating such experiments again, I would measure the quantity of upper layer neurons as late as day 120 to analyse this further. Furthermore, the method of iPSC maintenance may affect the delay in the presence of these upper layer neurons, as other media such as mTESR has been shown to prime for neuronal differentiation. Another possible explanation could be poor staining using the marker for *SATB2*, because when we measured relative mRNA expression levels, the number of deep layer neurons (*CTIP2*) and upper layer neurons *(SATB2)* appeared more equal, which could also be due to transcripts being present before the protein is produced **(Figure 4.14, Chapter 4)**.

The ability to generate disease-relevant cell types will contribute to the elucidation of the mechanisms of cell type–specific disease onset, in addition to the validation of potential drugs and therapies in the appropriate target cell types (Y. Shi, Kirwan, & Livesey, 2012). Choosing the correct cell-type(s) to model the disease of interest is critical. Kv7.2 channels are expressed in excitatory neurons, inhibitory neurons, and astrocytes (Dirkx et al., 2020). One limitation, therefore, was that our protocol did not incorporate the use of inhibitory neurons or glial cells in a controlled manner. As the NPCs generated in our protocol do produce glial cells, we found that ~40% of cells in our culture were glial cells by S100 staining **(Figure 4.9)**. However, these cell types were never characterised further. Similarly, we saw that a small percentage of cells (<20%) were positive for the inhibitory neuronal marker, Gad67, suggesting a small number of inhibitory neurons may have been present **(Figure 4.15)**. A previous (non-iPSC derived) study showed that Kv7.2/Kv7.3 channels in inhibitory neurons likely play a fundamental role in normal neurophysiology, demonstrating that a selective deletion of these channels in parvalbumin GABAergic interneurons leads to hyperexcitability and enhanced excitatory transmission in pyramidal neurons (Soh et al., 2018). As GABA has previously been shown to exert excitatory effects in early developing neurons, this enhanced excitation may have been due to excitatory GABA (Cherubini et al., 1991). This data suggests that using a protocol with defined quantities of both excitatory and inhibitory neurons may generate a model that more accurately recapitulates what is happening in the human brain or at least a slightly more complex neuronal network. In another study on bulk RNA extracted from isolated cell types from both fetal and adult human cortex, a high expression of *KCNQ2* was found in fetal astrocytes or astrocyte precursor cells (Zhang et al., 2016). Conversely, on the UCSC cell browser, there was no clear evidence of expression of *KCNQ2* in astrocytes, suggesting expression in astrocytes is restricted to the early neurodevelopmental period (Ambrosino et al., 2015). To date, there is

no evidence to suggest that Kv7.2 channels have a functional role in astrocytes, but it could be interesting to study this further as astrocytes interact closely with neurons in a number of ways. Aside from their expression of Kv7.2 channels, astrocytes also promote functional maturation of neurons, which is extremely useful as iPSC-derived neurons often have reduced maturity (Shan et al., 2021).

Despite the major discoveries that have been made using 2D cellular models including the findings we report here, 2D models do not usually provide the complex organization that mimics complicated biological processes such as embryonic development, cellular networking, and disease development (Dang et al., 2016). Furthermore, the diversity of iPSC-derived neurons and glial precursors are sometimes too immature to provide the metabolic and neuronal activity that is observed in the mature neurons (for example adult brain) (Liu et al., 2018). Lastly, the genomic and epigenomic signatures are more vulnerable to alterations in 2D cellular systems overtime (Bose et al., 2021). These limitations have led to an increased interest in the development of 3D organoids that more accurately recapitulate the human organs. Human iPSC-derived 3D brain organoids can differentiate into multi-lineages and self-organize to create heterogeneous cell populations with tissue-like architecture (Lee et al., 2017). The 3D environment within brain organoids favours the differentiation of specific cell types that reflects the early stages of neuronal maturation in the human CNS.

Various protocols have been designed to generate neural and cerebral 3D organoids from differentiating iPSCs (Völkner et al., 2016; Lancaster et al., 2013). iPSCs can be differentiated into cerebral organoids containing NSCs, astrocytes, neurons, and synaptic structures in approx. 1–2 months and can be maintained for up to 1 year. These protocols have since been improved by applying advanced technologies (Kelava et al., 2016). For example, one of the most significant advancements was the development and characterization of vascularized organoids that prevented necrosis (Mansour et al., 2018; Monzel et al., 2017; Zhao et al., 2021). Recently, organ-on-a-chip technology, which can model various organs including the brain on a microfluidic chip is capable of controlling the microenvironment and perfusion of oxygen and nutrients (Zhang et al., 2017). Due to time constraints and lack of appropriate equipment required for the generation of these organoids, and the number of *KCNQ2*-patients and controls we set out to recruit, we chose to focus on iPSC generation of cell lines, to initially explore some neuronal preliminary phenotyping using a 2D model protocol that had been used successfully in our lab in the past.

7.1.5. iPSC-patient derived neuronal *KCNQ2*-phenotype and pharmacologic manipulation

Epilepsy is a chronic condition associated with unprovoked, recurrent seizures with specific irregular EEG patterns (Shneker et al., 2003). In both animal and human models of epilepsy, repeated bursts of AP firing is common (Karoly et al., 2017). One of the main clinical characteristics of *KCNQ2*-DEE on EEG recordings is an interictal burst-suppression pattern (i.e., bursts of firing activity interspersed with periods of electrical silence). Simkin et al. (Simkin et al., 2021) revealed that the firing patterns of the *KCNQ2*-DEE (R581Q) patient neurons were drastically irregular compared to isogenic control neurons. This irregular firing pattern was associated with a greater tendency for neurons to fire in bursts, with short intervals between spikes in bursts and longer intervals or periods of silence between bursts, reflective of patients EEG recordings (Simkin et al., 2021). Here, we showed for the first time that the *KCNQ2*-DEE pathogenic variants F261L, A265T and A294V all displayed an irregular bursting phenotype and were hyperexcitable in cortical neurons derived from patient-iPSCs compared to sibling controls using MEA technology. This hyperexcitability became more pronounced and bursting became more irregular overtime. This disease model resembles the neonatal seizure activity makes an ideal platform for drug testing and discovery using the MEA platform. To further analyse the phenotype of patient neurons, we performed Ca^{2+} imaging experiments only in the A265T model due to time constraints and discovered that Ca^{2+} dynamics were significantly altered. Patient neurons had a higher percentage of active cells and a higher frequency compared to control cells **(Figure 6.10)**. Additionally, *KCNQ2* neurons (A265T) had a significantly higher amplitude and fluorescence intensity **(Figure 6.10)**. These results together demonstrated iPSC-derived cortical neurons recapitulated a severe hyperexcitability phenotype, as seen in *KCNQ2* patients.

Each of the mutations included in this study were LOF mutations, as previously reported usually in non-neuronal heterologous expression systems, such as two-microelectrode voltage-clamping in Xenopus Oocytes or patch-clamping in CHO or HEK cells studies (Yang et al., 2023; Lee et al., 2020). While I did perform some whole cell patch clamping in a small number of patient neurons, due to time constraints, we could not obtain statistically relevant numbers (data not shown) and therefore I did not directly determine (as not the primary focus) the level of M current loss. Here, we treated control neurons with the M current blocker XE-991 and found that XE-991 treated neurons fired even more bursts, and the firing pattern was more irregular, than patient neurons, suggesting that the more severe phenotype seen in XE-991 treated controls is due to a complete or greater loss of M current

in WT than the mutation. In a recent study, Yang et al. (Yang et al., 2023), studied five *KCNQ2*-DEE pathogenic variants including one of the same variants as in our study, A265T. They showed that this mutation caused the most minimal reduction in M current (36%) compared to the other 4 mutations. This may explain why we saw a much higher number of bursts and burst frequency in XE-991 treated controls than in our pathogenic variants **(Figure 5.14)**.

Retigabine, a K_V7 channel opener, has shown to be an effective anticonvulsant for several *KCNQ2*-DEE patients with LOF mutations (Stas et al., 2016). Here, we showed that retigabine treatment (10μM) of A294V patient neurons significantly reduced the number of bursts and irregular firing pattern **(Figure 5.17)**. Importantly, retigabine was unable to reduce the phenotype to the level of the sibling control suggesting that diseased neurons may have undergone maladaptive cellular reorganisation or differential gene expression as a result of the mutation which is contributing to the disease phenotype. In the future, the use of an isogenic control line in these experiments would be very interesting. Furthermore, I would have liked to treat the other two lines (A265T) and (F261L) with retigabine to determine if the drug efficiency is impacted by the location of the mutation. Moreover, it would be interesting to monitor the effect of the drug overtime to check if long term disease phenotype can be altered via MEA experiments. To my knowledge, this is the first time retigabine has been experimented in human iPSC-derived neurons harbouring a *KCNQ2*-DEE pathogenic variant.

Here, we report that in cortical neurons harbouring the A265T pathogenic variant (other variants not examined with this approach due to time constraints), there is a significant upregulation of various other Ca^{2+} activated potassium channels **(Figure 4.17)** and Na^+ channels **(Figure 4.18)**. Similar findings were previously published by Simkin et al. for the *KCNQ2*-DEE R581Q pathogenic variant, where they found upregulation of several other key potassium channel genes (Simkin et al., 2021). The majority of upregulated potassium channels were BK and SK channels, so we treated neurons with the SK and BK channel antagonists Apamin and Paxilline, respectively to analyse the effect of these drugs on the disease phenotype. We showed that a combinatorial treatment of these drugs was the most effective in reducing the hyperexcitable, irregular bursting seen in patient neurons, however it was unable to reduce levels to that of controls **(Figure 5.15)**. Similarly, we detected a significant upregulation of the Na^+ channels *SCN1A, SCN2A* and *SCN8A* in patient (A265T) neurons. Therefore, we treated neurons with the commonly prescribed Na^+ channel blocker carbamazepine (100μM) and found that treatment significantly reduced the irregular, bursting phenotype in patients **(Figure 5.16)**. This is consistent with clinical data of

carbamazepine which has been shown to effectively treat seizures in patients in the clinic (Dilena et al., 2022) These results may suggest that the dysregulation of other genes may contribute to the phenotype associated with this pathogenic variant. Therefore, targeting altered ion currents could potentially offer an alternative therapeutic strategy for *KCNQ2*-DEE seizures. However, the phenotype was normalised, and the over-time and overall effects of KCNQ2-mutations in brain development were not examined in this thesis. The iPSC-based platform we have developed here, nevertheless may be valuable to identify potential therapeutic screening for antiseizure medications in cortical excitatory neurons, and further uncover mechanisms of *KCNQ2*-DEE.

miRNAs are endogenous non-coding RNAs that play a role in post-transcriptional regulation and gene expression in eukaryotes (Wang et al., 2021). miRNA acts by inhibiting mRNA expression by identifying a complementary ribonucleotide sequence in the 3'-untranslated region (UTR) of the target messenger RNA (mRNA) (Bartel, 2004). miRNAs are an endogenous class of small non-coding RNA that hold great therapeutic promise for a number of reasons. Firstly, Individual miRNAs target many genes making them 'meta-controllers' capable of targeting more than one pathway (Friedman et al., 2009). Secondly, many functions under miRNA control are central to epileptogenesis, such as neuronal death, gliosis, inflammation, and neuronal microstructure (Henshall, 2013). This enables miRNAs to interrupt pathogenic pathways not previously possible and to potentially control protein levels in epilepsy. In this study we showed that the miRNA miR34-a, was capable of downregulating the expression of two potassium channel genes *KCNN2* and *KCNN3*, upregulated in our patient model **(Figure 3.11)**. The target scan database revealed that miR-34a with both of these channels and also our mutant gene, *KCNQ2*. However, we saw no significant change in *KCNQ2* expression in our patient lines, though important for hypothesis testing, a subject for further investigation. In a pilocarpine-induced epileptic mouse model, miR-137 overexpression was induced by an intrahippocampal injection of a specific agomir. Treatment with miR-137 increased the latency period of spontaneously recurring seizures and reduced the severity of epilepsy (Wang et al., 2016). Further research in miRNAs involved in epilepsy pathogenesis, may enable miRNA-targeted intervention to treat epilepsy.

7.2 Conclusion

In summary, the focus of this study was to generate *KCNQ2*-iPSC lines and begin to examine neuronal models of this untreatable profound neurodevelopmental and severe epilepsy-related potassium ion channelopathy. In this thesis we generated 24 iPSC lines from 4

pathogenic variants of *KCNQ2*-DEE and 4 sibling controls. We then generated 18 cortical neuronal lines (9 patient, 9 control) from these human iPSCs to generate an apparently effective patient-specific *in vitro* disease model. Using electrophysiological approaches, we showed that *KCNQ2*-DEE neurons are hyperexcitable and display an irregular, bursting phenotype compared to controls. Moreover, we showed that Ca^{2+} dynamics are dysregulated with higher amplitude, activity, and frequency, in patient neurons, reminiscent of a hyperexcitable phenotype. Furthermore, *KCNQ2*-DEE neurons exhibit an altered expression of several other potassium and sodium channels which could be partially controlled by treatment with appropriate ASMs. Finally, we showed that miR-34a could regulate gene expression of *KCNN2* and *KCNN3* in our disease model.

7.3 Future directions

In our study we have not included the use of isogenic cell lines due to technical difficulties and time-constraints encountered. We have used age-matched sibling controls which offer an ideal control aside from isogenic lines. In the future, it would be favourable to generate isogenic lines (ideally a control and a mutant) and to include these lines in future phenotypic experiments. For future generation of a neuronal model, we would aim to use a protocol that is less time consuming than 100 days and that incorporates controlled amounts of excitatory neurons, inhibitory neurons, and astrocytes. A future direction for this work would be to include recapitulate more closely the in vivo network architecture, generating 3D cortical organoids using our patient-derived iPSCs to model the phenotype in a model that contains excitatory neurons, inhibitory neurons, and astrocytes. This would encompass electrophysiological and other -omics approaches, over time, and network phenotypes, given the role of *KCNQ2* in brain development not just seizures. For further characterisation of the electrophysiological properties of single neurons, it would be useful to also perform whole cell patch clamping to compare potassium conductance in patient and control neurons. Finally, in the future we would like to investigate additional therapeutic approaches. Further miRNA studies analysing different miRNAs and different genes could reveal new therapeutic targets, including anti-sense oligonucleotides. Targeted patient-specific designed siRNAs could be used to target the mutant allele only in these heterozygous mutations.

8. Bibliography

Abidi, A., Devaux, J. J., Molinari, F., Alcaraz, G., Michon, F.-X., Sutera-Sardo, J., Becq, H., Lacoste, C., Altuzarra, C., Afenjar, A., Mignot, C., Doummar, D., Isidor, B., Guyen, S. N., Colin, E., De La Vaissière, S., Haye, D., Trauffler, A., Badens, C., … Anikstejn, L. (2015). A recurrent KCNQ2 pore mutation causing early onset epileptic encephalopathy has a moderate effect on M current but alters subcellular localization of Kv7 channels. *Neurobiology of Disease*, *80*, 80–92. https://doi.org/10.1016/j.nbd.2015.04.017

Agirman, G., Broix, L., & Nguyen, L. (2017). Cerebral cortex development: an outside-in perspective. *FEBS Letters*, *591*(24), 3978–3992. https://doi.org/10.1002/1873-3468.12924

Allen, N. M., Weckhuysen, S., Gorman, K., King, M. D., & Lerche, H. (2020). Genetic potassium channel-associated epilepsies: Clinical review of the Kv family. *European Journal of Paediatric Neurology*, *24*, 105–116. https://doi.org/10.1016/j.ejpn.2019.12.002

Almannai, M., Al Mahmoud, R. A., Mekki, M., & El-Hattab, A. W. (2021). Metabolic Seizures. *Frontiers in Neurology*, *12*. https://doi.org/10.3389/fneur.2021.640371

Alsanie, W. F., Bahri, O. A., Habeeballah, H. H., Alhomrani, M., Almehmadi, M. M., Alsharif, K., Felemban, E. M., Althobaiti, Y. S., Almalki, A. H., Alsaab, H. O., Gaber, A., Hassan, M. M., Hardy, A. M. G., & Alhadidi, Q. (2020). Generating homogenous cortical preplate and deep-layer neurons using a combination of 2D and 3D differentiation cultures. *Scientific Reports*, *10*(1), 6272. https://doi.org/10.1038/s41598-020-62925-9

Ambrosino, P., Alaimo, A., Bartollino, S., Manocchio, L., De Maria, M., Mosca, I., Gomis-Perez, C., Alberdi, A., Scambia, G., Lesca, G., Villarroel, A., Taglialatela, M., & Soldovieri, M. V. (2015a). Epilepsy-causing mutations in Kv7.2 C-terminus affect binding and functional modulation by calmodulin. *Biochimica et Biophysica Acta (BBA) - Molecular Basis of Disease*, *1852*(9), 1856–1866. https://doi.org/10.1016/j.bbadis.2015.06.012

Angel, M. J., & Young, G. B. (2011). Metabolic Encephalopathies. *Neurologic Clinics*, *29*(4), 837–882. https://doi.org/10.1016/j.ncl.2011.08.002

Arbini, A., Gilmore, J., King, M. D., Gorman, K. M., Krawczyk, J., McInerney, V., O'Brien, T., Shen, S., & Allen, N. M. (2020). Generation of three induced pluripotent stem cell (iPSC) lines from a patient with developmental epileptic encephalopathy due to the pathogenic KCNA2 variant c.869T>G; p.Leu290Arg (NUIGi052-A, NUIGi052-B, NUIGi052-C). *Stem Cell Research*, *46*. https://doi.org/10.1016/j.scr.2020.101853

Arlotta, P., Molyneaux, B. J., Chen, J., Inoue, J., Kominami, R., & Macklis, J. D. (2005). Neuronal Subtype-Specific Genes that Control Corticospinal Motor Neuron Development In Vivo. *Neuron*, *45*(2), 207–221. https://doi.org/10.1016/j.neuron.2004.12.036

Avazzadeh, A. (2018a). *Title Stem cell modelling for the role of NRXN1 deletion in Autism Spectrum Disorder*. http://hdl.handle.net/10379/14898

Balaram, P., Hackett, & Kaas, J. (2011). VGLUT1 mRNA and protein expression in the visual system of prosimian galagos (Otolemur garnetti). *Eye and Brain*, 81. https://doi.org/10.2147/EB.S23007

Balestrini, S., Arzimanoglou, A., Blümcke, I., Scheffer, I. E., Wiebe, S., Zelano, J., & Walker, M. C. (2021). The aetiologies of epilepsy. *Epileptic Disorders*, *23*(1), 1–16. https://doi.org/10.1684/epd.2021.1255

Bandaranayake, A. D., & Almo, S. C. (2014). Recent advances in mammalian protein production. *FEBS Letters*, *588*(2), 253–260. https://doi.org/10.1016/j.febslet.2013.11.035

Bando, Y., Irie, K., Shimomura, T., Umeshima, H., Kushida, Y., Kengaku, M., Fujiyoshi, Y., Hirano, T., & Tagawa, Y. (2016). Control of Spontaneous Ca $^{2+}$ Transients Is Critical for Neuronal Maturation in the Developing Neocortex. *Cerebral Cortex*, *26*(1), 106–117. https://doi.org/10.1093/cercor/bhu180

Barker-Haliski, M., & White, H. S. (2015). Glutamatergic Mechanisms Associated with Seizures and Epilepsy. *Cold Spring Harbor Perspectives in Medicine*, *5*(8), a022863. https://doi.org/10.1101/cshperspect.a022863

Barros, C. S., Franco, S. J., & Muller, U. (2011). Extracellular Matrix: Functions in the Nervous System. *Cold Spring Harbor Perspectives in Biology*, *3*(1), a005108–a005108. https://doi.org/10.1101/cshperspect.a005108

Bartel, D. P. (2004). MicroRNAs. *Cell*, *116*(2), 281–297. https://doi.org/10.1016/S0092-8674(04)00045-5

Bartolini, E. (2021). Inherited Developmental and Epileptic Encephalopathies. *Neurology International*, *13*(4), 555–568. https://doi.org/10.3390/neurolint13040055

Batista Napotnik, T., Polajžer, T., & Miklavčič, D. (2021). Cell death due to electroporation – A review. *Bioelectrochemistry*, *141*, 107871. https://doi.org/10.1016/j.bioelechem.2021.107871

Battefeld, A., Tran, B. T., Gavrilis, J., Cooper, E. C., & Kole, M. H. P. (2014). Heteromeric K $_{v}$ 7.2/7.3 Channels Differentially Regulate Action Potential Initiation and Conduction in Neocortical Myelinated Axons. *The Journal of Neuroscience*, *34*(10), 3719–3732. https://doi.org/10.1523/JNEUROSCI.4206-13.2014

Beekhuis-Hoekstra, S. D., Watanabe, K., Werme, J., de Leeuw, C. A., Paliukhovich, I., Li, K. W., Koopmans, F., Smit, A. B., Posthuma, D., & Heine, V. M. (2021). Systematic assessment of variability in the proteome of iPSC derivatives. *Stem Cell Research*, *56*. https://doi.org/10.1016/j.scr.2021.102512

Beghi, E. (2020). The Epidemiology of Epilepsy. *Neuroepidemiology*, *54*(2), 185–191. https://doi.org/10.1159/000503831

Benarroch, E. E. (2010). Neuronal voltage-gated calcium channels: Brief overview of their function and clinical implications in neurology. *Neurology*, *74*(16), 1310–1315. https://doi.org/10.1212/WNL.0b013e3181da364b

Berg, A. T., Berkovic, S. F., Brodie, M. J., Buchhalter, J., Cross, J. H., van Emde Boas, W., Engel, J., French, J., Glauser, T. A., Mathern, G. W., Moshé, S. L., Nordli, D., Plouin, P., & Scheffer, I. E. (2010). Revised terminology and concepts for organization of seizures and epilepsies: Report of the ILAE Commission on Classification and Terminology, 2005-2009. *Epilepsia*, *51*(4), 676–685. https://doi.org/10.1111/j.1528-1167.2010.02522.x

Bhutani, K., Nazor, K. L., Williams, R., Tran, H., Dai, H., Dzakula, Z., Cho, E. H., Pang, A. W. C., Rao, M., Cao, H., Schork, N. J., & Loring, J. F. (2016). Whole-genome mutational burden analysis of three pluripotency induction methods. *Nature Communications*, *7*. https://doi.org/10.1038/ncomms10536

Bianchi, F., Malboubi, M., Li, Y., George, J. H., Jerusalem, A., Szele, F., Thompson, M. S., & Ye, H. (2018). Rapid and efficient differentiation of functional motor neurons from human iPSC for neural injury modelling. *Stem Cell Research*, *32*, 126–134. https://doi.org/10.1016/j.scr.2018.09.006

Birey, F., Andersen, J., Makinson, C. D., Islam, S., Wei, W., Huber, N., Fan, H. C., Metzler, K. R. C., Panagiotakos, G., Thom, N., O'Rourke, N. A., Steinmetz, L. M., Bernstein, J. A., Hallmayer, J., Huguenard, J. R., & Paşca, S. P. (2017). Assembly of functionally integrated human forebrain spheroids. *Nature*, *545*(7652), 54–59. https://doi.org/10.1038/nature22330

Blumcke, I., Spreafico, R., Haaker, G., Coras, R., Kobow, K., Bien, C. G., Pfäfflin, M., Elger, C., Widman, G., Schramm, J., Becker, A., Braun, K. P., Leijten, F., Baayen, J. C., Aronica, E., Chassoux, F., Hamer, H., Stefan, H., Rössler, K., … Avanzini, G. (2017). Histopathological Findings in Brain Tissue Obtained during Epilepsy Surgery. *New England Journal of Medicine*, *377*(17), 1648–1656. https://doi.org/10.1056/NEJMoa1703784

Bock, C., Surur, A. S., Beirow, K., Kindermann, M. K., Schulig, L., Bodtke, A., Bednarski, P. J., & Link, A. (2019). Sulfide Analogues of Flupirtine and Retigabine with Nanomolar K_V 7.2/K_V 7.3 Channel Opening Activity. *ChemMedChem*, *14*(9), 952–964. https://doi.org/10.1002/cmdc.201900112

Bode, K., & O'Halloran, D. M. (2018). NCX-DB: a unified resource for integrative analysis of the sodium calcium exchanger super-family. *BMC Neuroscience*, *19*(1), 19. https://doi.org/10.1186/s12868-018-0423-2

Bose, R., Banerjee, S., & Dunbar, G. L. (2021). Modeling Neurological Disorders in 3D Organoids Using Human-Derived Pluripotent Stem Cells. *Frontiers in Cell and Developmental Biology*, *9*. https://doi.org/10.3389/fcell.2021.640212

Bozarth, X., Dines, J. N., Cong, Q., Mirzaa, G. M., Foss, K., Lawrence Merritt, J., Thies, J., Mefford, H. C., & Novotny, E. (2018). Expanding clinical phenotype in *CACNA1C* related disorders: From neonatal onset severe epileptic encephalopathy to late-onset epilepsy. *American Journal of Medical Genetics Part A*, *176*(12), 2733–2739. https://doi.org/10.1002/ajmg.a.40657

Brickley, S. G., Farrant, M., Swanson, G. T., & Cull-Candy, S. G. (2001). CNQX increases GABA-mediated synaptic transmission in the cerebellum by an AMPA/kainate receptor-independent mechanism. *Neuropharmacology*, *41*(6), 730–736. https://doi.org/10.1016/S0028-3908(01)00135-6

Brookhouser, N., Raman, S., Potts, C., & Brafman, David. (2017). May I Cut in? Gene Editing Approaches in Human Induced Pluripotent Stem Cells. *Cells*, *6*(1), 5. https://doi.org/10.3390/cells6010005

Brooks, I. R., Garrone, C. M., Kerins, C., Kiar, C. S., Syntaka, S., Xu, J. Z., Spagnoli, F. M., & Watt, F. M. (2022). Functional genomics and the future of iPSCs in disease modeling. *Stem Cell Reports*, *17*(5), 1033–1047. https://doi.org/10.1016/j.stemcr.2022.03.019

Broughton, J. P., Lovci, M. T., Huang, J. L., Yeo, G. W., & Pasquinelli, A. E. (2016). Pairing beyond the Seed Supports MicroRNA Targeting Specificity. *Molecular Cell*, *64*(2), 320–333. https://doi.org/10.1016/j.molcel.2016.09.004

BRUNKLAUS, A., DORRIS, L., ELLIS, R., REAVEY, E., LEE, E., FORBES, G., APPLETON, R., CROSS, J. H., FERRIE, C., HUGHES, I., JOLLANDS, A., KING, M. D., LIVINGSTON, J., LYNCH, B., PHILIP, S., SCHEFFER, I. E., WILLIAMS, R., & ZUBERI, S. M. (2013). The clinical utility of an *SCN1A* genetic diagnosis in infantile-onset epilepsy. *Developmental Medicine & Child Neurology*, *55*(2), 154–161. https://doi.org/10.1111/dmcn.12030

Buttermore, E. D. (2022). Phenotypic assay development with iPSC-derived neurons: technical considerations from plating to analysis. In *Phenotyping of Human iPSC-derived Neurons: Patient-Driven Research* (pp. 25–43). Elsevier. https://doi.org/10.1016/B978-0-12-822277-5.00015-8

Bystron, I., Blakemore, C., & Rakic, P. (2008). Development of the human cerebral cortex: Boulder Committee revisited. *Nature Reviews Neuroscience*, *9*(2), 110–122. https://doi.org/10.1038/nrn2252

Cadwell, C. R., Bhaduri, A., Mostajo-Radji, M. A., Keefe, M. G., & Nowakowski, T. J. (2019). Development and Arealization of the Cerebral Cortex. *Neuron*, *103*(6), 980–1004. https://doi.org/10.1016/j.neuron.2019.07.009

Caputi, A., Melzer, S., Michael, M., & Monyer, H. (2013). The long and short of GABAergic neurons. *Current Opinion in Neurobiology*, *23*(2), 179–186. https://doi.org/10.1016/j.conb.2013.01.021

Catterall, W. A. (2011). Voltage-Gated Calcium Channels. *Cold Spring Harbor Perspectives in Biology*, *3*(8), a003947–a003947. https://doi.org/10.1101/cshperspect.a003947

Cavaretta, J. P., Sherer, K. R., Lee, K. Y., Kim, E. H., Issema, R. S., & Chung, H. J. (2014). Polarized Axonal Surface Expression of Neuronal KCNQ Potassium Channels Is Regulated by Calmodulin Interaction with KCNQ2 Subunit. *PLoS ONE*, *9*(7), e103655. https://doi.org/10.1371/journal.pone.0103655

Caviness, V. S., Takahashi, T., & Nowakowski, R. S. (1995). Numbers, time and neocortical neuronogenesis: a general developmental and evolutionary model. *Trends in Neurosciences*, *18*(9), 379–383. https://doi.org/10.1016/0166-2236(95)93933-O

Centeno, E. G. Z., Cimarosti, H., & Bithell, A. (2018a). 2D versus 3D human induced pluripotent stem cell-derived cultures for neurodegenerative disease modelling. *Molecular Neurodegeneration*, *13*(1), 27. https://doi.org/10.1186/s13024-018-0258-4

Chambers, S. M., Fasano, C. A., Papapetrou, E. P., Tomishima, M., Sadelain, M., & Studer, L. (2009a). Highly efficient neural conversion of human ES and iPS cells by dual inhibition

of SMAD signaling. *Nature Biotechnology*, *27*(3), 275–280. https://doi.org/10.1038/nbt.1529

Chambers, S. M., Qi, Y., Mica, Y., Lee, G., Zhang, X.-J., Niu, L., Bilsland, J., Cao, L., Stevens, E., Whiting, P., Shi, S.-H., & Studer, L. (2012). Combined small-molecule inhibition accelerates developmental timing and converts human pluripotent stem cells into nociceptors. *Nature Biotechnology*, *30*(7), 715–720. https://doi.org/10.1038/nbt.2249

Chan, E. M., Ratanasirintrawoot, S., Park, I. H., Manos, P. D., Loh, Y. H., Huo, H., Miller, J. D., Hartung, O., Rho, J., Ince, T. A., Daley, G. Q., & Schlaeger, T. M. (2009). Live cell imaging distinguishes bona fide human iPS cells from partially reprogrammed cells. *Nature Biotechnology*, *27*(11), 1033–1037. https://doi.org/10.1038/nbt.1580

Chang, R. S., Leung, C. Y. W., Ho, C. C. A., & Yung, A. (2017). Classifications of seizures and epilepsies, where are we? – A brief historical review and update. *Journal of the Formosan Medical Association*, *116*(10), 736–741. https://doi.org/10.1016/j.jfma.2017.06.001

Charkhkar, H., Knaack, G. L., Gnade, B. E., Keefer, E. W., & Pancrazio, J. J. (2012). Development and demonstration of a disposable low-cost microelectrode array for cultured neuronal network recording. *Sensors and Actuators B: Chemical*, *161*(1), 655–660. https://doi.org/10.1016/j.snb.2011.10.086

Chatterjee, N., & Walker, G. C. (2017). Mechanisms of DNA damage, repair, and mutagenesis. *Environmental and Molecular Mutagenesis*, *58*(5), 235–263. https://doi.org/10.1002/em.22087

Chen, H., Qian, K., Du, Z., Cao, J., Petersen, A., Liu, H., Blackbourn, L. W., Huang, C.-L., Errigo, A., Yin, Y., Lu, J., Ayala, M., & Zhang, S.-C. (2014). Modeling ALS with iPSCs Reveals that Mutant SOD1 Misregulates Neurofilament Balance in Motor Neurons. *Cell Stem Cell*, *14*(6), 796–809. https://doi.org/10.1016/j.stem.2014.02.004

Cherubini, E., Gaiarsa, J. L., & Ben-Ari, Y. (1991). GABA: an excitatory transmitter in early postnatal life. *Trends in Neurosciences*, *14*(12), 515–519. https://doi.org/10.1016/0166-2236(91)90003-D

Child, N. D., & Benarroch, E. E. (2014). Differential distribution of voltage-gated ion channels in cortical neurons: Implications for epilepsy. *Neurology*, *82*(11), 989–999. https://doi.org/10.1212/WNL.0000000000000228

Chong, P. N., Sangu, M., Huat, T. J., Reza, F., Begum, T., Mohamed Yusoff, A. A., Jaafar, H., & Abdullah, J. M. (2018). Trkb-IP3 Pathway Mediating Neuroprotection in Rat Hippocampal Neuronal Cell Culture Following Induction of Kainic Acid. *Malaysian Journal of Medical Sciences*, *25*(6), 28–45. https://doi.org/10.21315/mjms2018.25.6.4

Chuang, K., Fields, M. A., & Del Priore, L. V. (2017). Potential of Gene Editing and Induced Pluripotent Stem Cells (iPSCs) in Treatment of Retinal Diseases. *The Yale Journal of Biology and Medicine*, *90*(4), 635–642.

Chun, Y. S., Byun, K., & Lee, B. (2011). Induced pluripotent stem cells and personalized medicine: current progress and future perspectives. *Anatomy & Cell Biology*, *44*(4), 245. https://doi.org/10.5115/acb.2011.44.4.245

Contractor, A., Mulle, C., & Swanson, G. T. (2011). Kainate receptors coming of age: milestones of two decades of research. *Trends in Neurosciences*, *34*(3), 154–163. https://doi.org/10.1016/j.tins.2010.12.002

Cooper, E. C., Aldape, K. D., Abosch, A., Barbaro, N. M., Berger, M. S., Peacock, W. S., Jan, Y. N., & Jan, L. Y. (2000). Colocalization and coassembly of two human brain M-type potassium channel subunits that are mutated in epilepsy. *Proceedings of the National Academy of Sciences*, *97*(9), 4914–4919. https://doi.org/10.1073/pnas.090092797

Coppola, A., Cellini, E., Stamberger, H., Saarentaus, E., Cetica, V., Lal, D., Djémié, T., Bartnik-Glaska, M., Ceulemans, B., Helen Cross, J., Deconinck, T., Masi, S. De, Dorn, T., Guerrini, R., Hoffman-Zacharska, D., Kooy, F., Lagae, L., Lench, N., Lemke, J. R., … Zuffardi, O. (2019). Diagnostic implications of genetic copy number variation in epilepsy plus. *Epilepsia*, *60*(4), 689–706. https://doi.org/10.1111/epi.14683

Costamagna, G., Andreoli, L., Corti, S., & Faravelli, I. (2019). iPSCs-based neural 3D systems: A multidimensional approach for disease modeling and drug discovery. *Cells*, *8*(11). https://doi.org/10.3390/cells8111438

Danbolt, N. C., Furness, D. N., & Zhou, Y. (2016). Neuronal vs glial glutamate uptake: Resolving the conundrum. *Neurochemistry International*, *98*, 29–45. https://doi.org/10.1016/j.neuint.2016.05.009

Dang, J., Tiwari, S. K., Lichinchi, G., Qin, Y., Patil, V. S., Eroshkin, A. M., & Rana, T. M. (2016). Zika Virus Depletes Neural Progenitors in Human Cerebral Organoids through Activation of the Innate Immune Receptor TLR3. *Cell Stem Cell*, *19*(2), 258–265. https://doi.org/10.1016/j.stem.2016.04.014

D'Antonio, M., Woodruff, G., Nathanson, J. L., D'Antonio-Chronowska, A., Arias, A., Matsui, H., Williams, R., Herrera, C., Reyna, S. M., Yeo, G. W., Goldstein, L. S. B., Panopoulos, A. D., & Frazer, K. A. (2017). High-Throughput and Cost-Effective Characterization of Induced Pluripotent Stem Cells. *Stem Cell Reports*, *8*(4), 1101–1111. https://doi.org/10.1016/j.stemcr.2017.03.011

De Masi, C., Spitalieri, P., Murdocca, M., Novelli, G., & Sangiuolo, F. (2020a). Application of CRISPR/Cas9 to human-induced pluripotent stem cells: from gene editing to drug discovery. *Human Genomics*, *14*(1), 25. https://doi.org/10.1186/s40246-020-00276-2

De Sousa, P. A., Steeg, R., Wachter, E., Bruce, K., King, J., Hoeve, M., Khadun, S., McConnachie, G., Holder, J., Kurtz, A., Seltmann, S., Dewender, J., Reimann, S., Stacey, G., O'Shea, O., Chapman, C., Healy, L., Zimmermann, H., Bolton, B., … Allsopp, T. E. (2017). Rapid establishment of the European Bank for induced Pluripotent Stem Cells (EBiSC) - the Hot Start experience. *Stem Cell Research*, *20*, 105–114. https://doi.org/10.1016/j.scr.2017.03.002

DeGiosio, R. A., Grubisha, M. J., MacDonald, M. L., McKinney, B. C., Camacho, C. J., & Sweet, R. A. (2022). More than a marker: potential pathogenic functions of MAP2. *Frontiers in Molecular Neuroscience*, *15*. https://doi.org/10.3389/fnmol.2022.974890

Dehmelt, L., & Halpain, S. (2004). The MAP2/Tau family of microtubule-associated proteins. *Genome Biology*, *6*(1), 204. https://doi.org/10.1186/gb-2004-6-1-204

Demchenko, I., Tassone, V. K., Kennedy, S. H., Dunlop, K., & Bhat, V. (2022). Intrinsic Connectivity Networks of Glutamate-Mediated Antidepressant Response: A Neuroimaging Review. *Frontiers in Psychiatry*, *13*. https://doi.org/10.3389/fpsyt.2022.864902

Digilio, L., Yap, C. C., & Winckler, B. (2015). Ctip2-, Satb2-, Prox1-, and GAD65-Expressing Neurons in Rat Cultures: Preponderance of Single- and Double-Positive Cells, and Cell Type-Specific Expression of Neuron-Specific Gene Family Members, Nsg-1 (NEEP21) and Nsg-2 (P19). *PLOS ONE*, *10*(10), e0140010. https://doi.org/10.1371/journal.pone.0140010

Dilena, R., Mauri, E., Di Fonzo, A., Bana, C., Ajmone, P. F., Rigamonti, C., Catenio, T., Gangi, S., Striano, P., & Fumagalli, M. (2022a). Case Report: Effect of Targeted Therapy With Carbamazepine in KCNQ2 Neonatal Epilepsy. *Frontiers in Neurology*, *13*, 942582. https://doi.org/10.3389/fneur.2022.942582

Ding, J., Li, X., Tian, H., Wang, L., Guo, B., Wang, Y., Li, W., Wang, F., & Sun, T. (2021). SCN1A Mutation—Beyond Dravet Syndrome: A Systematic Review and Narrative Synthesis. *Frontiers in Neurology*, *12*. https://doi.org/10.3389/fneur.2021.743726

Dingledine, R., Borges, K., Bowie, D., & Traynelis, S. F. (1999). The glutamate receptor ion channels. *Pharmacological Reviews*, *51*(1), 7–61.

Dirkx, N., Miceli, F., Taglialatela, M., & Weckhuysen, S. (2020a). The Role of Kv7.2 in Neurodevelopment: Insights and Gaps in Our Understanding. *Frontiers in Physiology*, *11*. https://doi.org/10.3389/fphys.2020.570588

Dottori, M., & Pera, M. F. (2008). *Neural Differentiation of Human Embryonic Stem Cells* (pp. 19–30). https://doi.org/10.1007/978-1-59745-133-8_3

Doudna, J. A. (2020). The promise and challenge of therapeutic genome editing. *Nature*, *578*(7794), 229–236. https://doi.org/10.1038/s41586-020-1978-5

Duchaine, T. F., & Fabian, M. R. (2019). Mechanistic Insights into MicroRNA-Mediated Gene Silencing. *Cold Spring Harbor Perspectives in Biology*, *11*(3), a032771. https://doi.org/10.1101/cshperspect.a032771

Dunn, P., Albury, C. L., Maksemous, N., Benton, M. C., Sutherland, H. G., Smith, R. A., Haupt, L. M., & Griffiths, L. R. (2018). Next Generation Sequencing Methods for Diagnosis of Epilepsy Syndromes. *Frontiers in Genetics*, *9*. https://doi.org/10.3389/fgene.2018.00020

Ebert, A. D., Yu, J., Rose, F. F., Mattis, V. B., Lorson, C. L., Thomson, J. A., & Svendsen, C. N. (2009). Induced pluripotent stem cells from a spinal muscular atrophy patient. *Nature*, *457*(7227), 277–280. https://doi.org/10.1038/nature07677

Eggenschwiler, R., Loya, K., Wu, G., Sharma, A. D., Sgodda, M., Zychlinski, D., Herr, C., Steinemann, D., Teckman, J., Bals, R., Ott, M., Schambach, A., Schöler, H. R., & Cantz, T. (2013). Sustained Knockdown of a Disease-Causing Gene in Patient-Specific Induced Pluripotent Stem Cells Using Lentiviral Vector-Based Gene Therapy. *Stem Cells Translational Medicine*, *2*(9), 641–654. https://doi.org/10.5966/sctm.2013-0017

Eiraku, M., Watanabe, K., Matsuo-Takasaki, M., Kawada, M., Yonemura, S., Matsumura, M., Wataya, T., Nishiyama, A., Muguruma, K., & Sasai, Y. (2008). Self-Organized Formation of Polarized Cortical Tissues from ESCs and Its Active Manipulation by Extrinsic Signals. *Cell Stem Cell*, *3*(5), 519–532. https://doi.org/10.1016/j.stem.2008.09.002

Etxeberria, A., Aivar, P., Rodriguez-Alfaro, J. A., Alaimo, A., Villace, P., Gomez-Posada, J. C., Areso, P., & Villarroel, A. (2008). Calmodulin regulates the trafficking of KCNQ2 potassium channels. *The FASEB Journal*, *22*(4), 1135–1143. https://doi.org/10.1096/fj.07-9712com

Evans, R. C., Morera-Herreras, T., Cui, Y., Du, K., Sheehan, T., Kotaleski, J. H., Venance, L., & Blackwell, K. T. (2012). The Effects of NMDA Subunit Composition on Calcium Influx and Spike Timing-Dependent Plasticity in Striatal Medium Spiny Neurons. *PLoS Computational Biology*, *8*(4), e1002493. https://doi.org/10.1371/journal.pcbi.1002493

Faber, E. L., & Sah, P. (2007). FUNCTIONS OF SK CHANNELS IN CENTRAL NEURONS. *Clinical and Experimental Pharmacology and Physiology*, *34*(10), 1077–1083. https://doi.org/10.1111/j.1440-1681.2007.04725.x

Falco-Walter, J. J., Scheffer, I. E., & Fisher, R. S. (2018). The new definition and classification of seizures and epilepsy. *Epilepsy Research*, *139*, 73–79. https://doi.org/10.1016/j.eplepsyres.2017.11.015

Fattahi, P., Yang, G., Kim, G., & Abidian, M. R. (2014). A Review of Organic and Inorganic Biomaterials for Neural Interfaces. *Advanced Materials*, *26*(12), 1846–1885. https://doi.org/10.1002/adma.201304496

Fellin, T., Pascual, O., Gobbo, S., Pozzan, T., Haydon, P. G., & Carmignoto, G. (2004). Neuronal Synchrony Mediated by Astrocytic Glutamate through Activation of Extrasynaptic NMDA Receptors. *Neuron*, *43*(5), 729–743. https://doi.org/10.1016/j.neuron.2004.08.011

Ferguson, M., Sharma, D., Ross, D., & Zhao, F. (2019). A Critical Review of Microelectrode Arrays and Strategies for Improving Neural Interfaces. *Advanced Healthcare Materials*, *8*(19), 1900558. https://doi.org/10.1002/adhm.201900558

Fernandopulle, M. S., Prestil, R., Grunseich, C., Wang, C., Gan, L., & Ward, M. E. (2018). Transcription Factor-Mediated Differentiation of Human iPSCs into Neurons. *Current Protocols in Cell Biology*, *79*(1), e51. https://doi.org/10.1002/cpcb.51

Fiest, K. M., Sauro, K. M., Wiebe, S., Patten, S. B., Kwon, C.-S., Dykeman, J., Pringsheim, T., Lorenzetti, D. L., & Jetté, N. (2017). Prevalence and incidence of epilepsy. *Neurology*, *88*(3), 296–303. https://doi.org/10.1212/WNL.0000000000003509

Fisher, R. S., Acevedo, C., Arzimanoglou, A., Bogacz, A., Cross, J. H., Elger, C. E., Engel, J., Forsgren, L., French, J. A., Glynn, M., Hesdorffer, D. C., Lee, B. I., Mathern, G. W., Moshé, S. L., Perucca, E., Scheffer, I. E., Tomson, T., Watanabe, M., & Wiebe, S. (2014). ILAE Official Report: A practical clinical definition of epilepsy. *Epilepsia*, *55*(4), 475–482. https://doi.org/10.1111/epi.12550

Fitsiori, A., Hiremath, S., Boto, J., Garibotto, V., & Vargas, M. (2019). Morphological and Advanced Imaging of Epilepsy: Beyond the Basics. *Children*, *6*(3), 43. https://doi.org/10.3390/children6030043

Freeman, M. R. (2006). Sculpting the nervous system: glial control of neuronal development. *Current Opinion in Neurobiology*, *16*(1), 119–125. https://doi.org/10.1016/j.conb.2005.12.004

Frew, J. W., Hawkes, J. E., Sullivan-Whalen, M., Gilleaudeau, P., & Krueger, J. G. (2019). Inter-rater reliability of phenotypes and exploratory genotype–phenotype analysis in inherited hidradenitis suppurativa. *British Journal of Dermatology*, *181*(3), 566–571. https://doi.org/10.1111/bjd.17695

Friedman, R. C., Farh, K. K.-H., Burge, C. B., & Bartel, D. P. (2009). Most mammalian mRNAs are conserved targets of microRNAs. *Genome Research*, *19*(1), 92–105. https://doi.org/10.1101/gr.082701.108

Fusaki, N., Ban, H., Nishiyama, A., Saeki, K., & Hasegawa, M. (2009a). Efficient induction of transgene-free human pluripotent stem cells using a vector based on Sendai virus, an RNA virus that does not integrate into the host genome. *Proceedings of the Japan Academy Series B: Physical and Biological Sciences*, *85*(8), 348–362. https://doi.org/10.2183/pjab.85.348

Gardella, E., Marini, C., Trivisano, M., Fitzgerald, M. P., Alber, M., Howell, K. B., Darra, F., Siliquini, S., Bölsterli, B. K., Masnada, S., Pichiecchio, A., Johannesen, K. M., Jepsen, B., Fontana, E., Anibaldi, G., Russo, S., Cogliati, F., Montomoli, M., Specchio, N., … Møller, R. S. (2018). The phenotype of *SCN8A* developmental and epileptic encephalopathy. *Neurology*, *91*(12), e1112–e1124. https://doi.org/10.1212/WNL.0000000000006199

Gasiorowska, A., Wydrych, M., Drapich, P., Zadrozny, M., Steczkowska, M., Niewiadomski, W., & Niewiadomska, G. (2021). The Biology and Pathobiology of Glutamatergic, Cholinergic, and Dopaminergic Signaling in the Aging Brain. *Frontiers in Aging Neuroscience*, *13*. https://doi.org/10.3389/fnagi.2021.654931

Gasiunas, G., Barrangou, R., Horvath, P., & Siksnys, V. (2012). Cas9–crRNA ribonucleoprotein complex mediates specific DNA cleavage for adaptive immunity in bacteria. *Proceedings of the National Academy of Sciences*, *109*(39). https://doi.org/10.1073/pnas.1208507109

Gast, H., Niediek, J., Schindler, K., Boström, J., Coenen, V. A., Beck, H., Elger, C. E., & Mormann, F. (2016). Burst firing of single neurons in the human medial temporal lobe changes before epileptic seizures. *Clinical Neurophysiology*, *127*(10), 3329–3334. https://doi.org/10.1016/j.clinph.2016.08.010

Geis, C., Planagumà, J., Carreño, M., Graus, F., & Dalmau, J. (2019). Autoimmune seizures and epilepsy. *Journal of Clinical Investigation*, *129*(3), 926–940. https://doi.org/10.1172/JCI125178

Gelman, D. M., & Marín, O. (2010). Generation of interneuron diversity in the mouse cerebral cortex. *European Journal of Neuroscience*, *31*(12), 2136–2141. https://doi.org/10.1111/j.1460-9568.2010.07267.x

Gibson, S. B., Downie, J. M., Tsetsou, S., Feusier, J. E., Figueroa, K. P., Bromberg, M. B., Jorde, L. B., & Pulst, S. M. (2017). The evolving genetic risk for sporadic ALS. *Neurology*, *89*(3), 226–233. https://doi.org/10.1212/WNL.0000000000004109

Gleichmann, M., & Mattson, M. P. (2011). Neuronal Calcium Homeostasis and Dysregulation. *Antioxidants & Redox Signaling*, *14*(7), 1261–1273. https://doi.org/10.1089/ars.2010.3386

Gómez-Herreros, F. (2019). DNA Double Strand Breaks and Chromosomal Translocations Induced by DNA Topoisomerase II. *Frontiers in Molecular Biosciences*, *6*. https://doi.org/10.3389/fmolb.2019.00141

Goto, A., Ishii, A., Shibata, M., Ihara, Y., Cooper, E. C., & Hirose, S. (2019). Characteristics of *<scp>KCNQ</scp> 2* variants causing either benign neonatal epilepsy or developmental and epileptic encephalopathy. *Epilepsia*, *60*(9), 1870–1880. https://doi.org/10.1111/epi.16314

Granata, T., Cross, H., Theodore, W., & Avanzini, G. (2011). Immune-mediated epilepsies. *Epilepsia*, *52*, 5–11. https://doi.org/10.1111/j.1528-1167.2011.03029.x

Gras, D., Roze, E., Caillet, S., Méneret, A., Doummar, D., Billette de Villemeur, T., Vidailhet, M., & Mochel, F. (2014). GLUT1 deficiency syndrome: An update. *Revue Neurologique*, *170*(2), 91–99. https://doi.org/10.1016/j.neurol.2013.09.005

Greene, D. L., Kang, S., & Hoshi, N. (2017). XE991 and Linopirdine Are State-Dependent Inhibitors for Kv7/KCNQ Channels that Favor Activated Single Subunits. *Journal of Pharmacology and Experimental Therapeutics*, *362*(1), 177–185. https://doi.org/10.1124/jpet.117.241679

Gruszczynska-Biegala, J., Pomorski, P., Wisniewska, M. B., & Kuznicki, J. (2011). Differential Roles for STIM1 and STIM2 in Store-Operated Calcium Entry in Rat Neurons. *PLoS ONE*, *6*(4), e19285. https://doi.org/10.1371/journal.pone.0019285

Guerrini, R., & Dobyns, W. B. (2014). Malformations of cortical development: clinical features and genetic causes. *The Lancet Neurology*, *13*(7), 710–726. https://doi.org/10.1016/S1474-4422(14)70040-7

Gunthorpe, M. J., Large, C. H., & Sankar, R. (2012). The mechanism of action of retigabine (ezogabine), a first-in-class K+ channel opener for the treatment of epilepsy. *Epilepsia*, *53*(3), 412–424. https://doi.org/10.1111/j.1528-1167.2011.03365.x

Guo, N. N., Liu, L. P., Zheng, Y. W., & Li, Y. M. (2020). Inducing human induced pluripotent stem cell differentiation through embryoid bodies: A practical and stable approach. In *World Journal of Stem Cells* (Vol. 12, Issue 1, pp. 25–34). Baishideng Publishing Group Co. https://doi.org/10.4252/wjsc.v12.i1.25

GURDON, J. B. (1962). The developmental capacity of nuclei taken from intestinal epithelium cells of feeding tadpoles. *Journal of Embryology and Experimental Morphology*, *10*, 622–640.

Ha, M., & Kim, V. N. (2014). Regulation of microRNA biogenesis. *Nature Reviews Molecular Cell Biology*, *15*(8), 509–524. https://doi.org/10.1038/nrm3838

Hackenberg, A., Baumer, A., Sticht, H., Schmitt, B., Kroell-Seger, J., Wille, D., Joset, P., Papuc, S., Rauch, A., & Plecko, B. (2014). Infantile Epileptic Encephalopathy, Transient Choreoathetotic Movements, and Hypersomnia due to a De Novo Missense Mutation

in the SCN2A Gene. *Neuropediatrics*, *45*(04), 261–264. https://doi.org/10.1055/s-0034-1372302

Hadjantonakis, A. K. (2014). From pluripotency to differentiation: Laying foundations for the body pattern in the mouse embryo. In *Philosophical Transactions of the Royal Society B: Biological Sciences* (Vol. 369, Issue 1657). Royal Society of London. https://doi.org/10.1098/rstb.2013.0535

Hagbard, L., Cameron, K., August, P., Penton, C., Parmar, M., Hay, D. C., & Kallur, T. (2018). Developing defined substrates for stem cell culture and differentiation. *Philosophical Transactions of the Royal Society B: Biological Sciences*, *373*(1750), 20170230. https://doi.org/10.1098/rstb.2017.0230

Halliday, D. M., Rosenberg, J. R., Breeze, P., & Conway, B. A. (2006). Neural spike train synchronization indices: Definitions, interpretations, and applications. *IEEE Transactions on Biomedical Engineering*, *53*(6), 1056–1066. https://doi.org/10.1109/TBME.2006.873392

Hamdan, F. F., Myers, C. T., Cossette, P., Lemay, P., Spiegelman, D., Laporte, A. D., Nassif, C., Diallo, O., Monlong, J., Cadieux-Dion, M., Dobrzeniecka, S., Meloche, C., Retterer, K., Cho, M. T., Rosenfeld, J. A., Bi, W., Massicotte, C., Miguet, M., Brunga, L., … Michaud, J. L. (2017). High Rate of Recurrent De Novo Mutations in Developmental and Epileptic Encephalopathies. *American Journal of Human Genetics*, *101*(5), 664–685. https://doi.org/10.1016/j.ajhg.2017.09.008

Han, J. W., & Yoon, Y. S. (2011). Induced pluripotent stem cells: Emerging techniques for nuclear reprogramming. In *Antioxidants and Redox Signaling* (Vol. 15, Issue 7, pp. 1799–1820). https://doi.org/10.1089/ars.2010.3814

Hardingham, G. E., & Bading, H. (2010). Synaptic versus extrasynaptic NMDA receptor signalling: implications for neurodegenerative disorders. *Nature Reviews Neuroscience*, *11*(10), 682–696. https://doi.org/10.1038/nrn2911

Henshall, D. C. (2013). MicroRNAs in the pathophysiology and treatment of status epilepticus. *Frontiers in Molecular Neuroscience*, *6*. https://doi.org/10.3389/fnmol.2013.00037

Hmeljak, J., & Justice, M. J. (2019). From gene to treatment: supporting rare disease translational research through model systems. *Disease Models & Mechanisms*, *12*(2). https://doi.org/10.1242/dmm.039271

Ho, S.-M., Hartley, B. J., TCW, J., Beaumont, M., Stafford, K., Slesinger, P. A., & Brennand, K. J. (2016). Rapid Ngn2-induction of excitatory neurons from hiPSC-derived neural progenitor cells. *Methods*, *101*, 113–124. https://doi.org/10.1016/j.ymeth.2015.11.019

Hollmann, M., & Heinemann, S. (1994). Cloned Glutamate Receptors. *Annual Review of Neuroscience*, *17*(1), 31–108. https://doi.org/10.1146/annurev.ne.17.030194.000335

Howell, K. B., McMahon, J. M., Carvill, G. L., Tambunan, D., Mackay, M. T., Rodriguez-Casero, V., Webster, R., Clark, D., Freeman, J. L., Calvert, S., Olson, H. E., Mandelstam, S., Poduri, A., Mefford, H. C., Harvey, A. S., & Scheffer, I. E. (2015). *SCN2A*

encephalopathy. *Neurology*, *85*(11), 958–966. https://doi.org/10.1212/WNL.0000000000001926

Hu, Y., Shan, Y., Du, Q., Ding, Y., Shen, C., Wang, S., Ding, M., & Xu, Y. (2021). Gender and Socioeconomic Disparities in Global Burden of Epilepsy: An Analysis of Time Trends From 1990 to 2017. *Frontiers in Neurology*, *12*. https://doi.org/10.3389/fneur.2021.643450

Huang, P., Li, Y., Nasser, M. I., Guo, H., Huang, H., Zhao, M., & Zhu, P. (2020). Urine-Derived Induced Pluripotent Stem Cells in Cardiovascular Disease. *Cardiology Research and Practice*, *2020*, 1–8. https://doi.org/10.1155/2020/3563519

Huff, J. S., & Murr, N. (2023). *Seizure*.

Hulme, A. J., McArthur, J. R., Maksour, S., Miellet, S., Ooi, L., Adams, D. J., Finol-Urdaneta, R. K., & Dottori, M. (2020). Molecular and Functional Characterization of Neurogenin-2 Induced Human Sensory Neurons. *Frontiers in Cellular Neuroscience*, *14*. https://doi.org/10.3389/fncel.2020.600895

Humphries, E. S. A., & Dart, C. (2015). Neuronal and Cardiovascular Potassium Channels as Therapeutic Drug Targets: Promise and Pitfalls. *SLAS Discovery*, *20*(9), 1055–1073. https://doi.org/10.1177/1087057115601677

Husari, K. S., & Dubey, D. (2019). Autoimmune Epilepsy. *Neurotherapeutics*, *16*(3), 685–702. https://doi.org/10.1007/s13311-019-00750-3

Hussein, S. M., Batada, N. N., Vuoristo, S., Ching, R. W., Autio, R., Narvä, E., Ng, S., Sourour, M., Hämälä, R., Olsson, C., Lundin, K., Mikkola, M., Trokovic, R., Peitz, M., Brüstle, O., Bazett-Jones, D. P., Alitalo, K., Lahesmaa, R., Nagy, A., & Otonkoski, T. (2011). Copy number variation and selection during reprogramming to pluripotency. *Nature*, *471*(7336), 58–62. https://doi.org/10.1038/nature09871

Jäckel, D., Bakkum, D. J., Russell, T. L., Müller, J., Radivojevic, M., Frey, U., Franke, F., & Hierlemann, A. (2017). Combination of High-density Microelectrode Array and Patch Clamp Recordings to Enable Studies of Multisynaptic Integration. *Scientific Reports*, *7*(1). https://doi.org/10.1038/s41598-017-00981-4

Jafari, N., Kim, H., Park, R., Li, L., Jang, M., Morris, A. J., Park, J., & Huang, C. (2017). CRISPR-Cas9 Mediated NOX4 Knockout Inhibits Cell Proliferation and Invasion in HeLa Cells. *PLOS ONE*, *12*(1), e0170327. https://doi.org/10.1371/journal.pone.0170327

Jang, Y., Kim, D. W., Yang, K. I., Byun, J.-I., Seo, J.-G., No, Y. J., Kang, K. W., Kim, D., Kim, K. T., Cho, Y. W., & Lee, S.-T. (2020). Clinical Approach to Autoimmune Epilepsy. *Journal of Clinical Neurology*, *16*(4), 519. https://doi.org/10.3988/jcn.2020.16.4.519

Jauhari, A., Singh, T., Singh, P., Parmar, D., & Yadav, S. (2018). Regulation of miR-34 Family in Neuronal Development. *Molecular Neurobiology*, *55*(2), 936–945. https://doi.org/10.1007/s12035-016-0359-4

Javaid, M. S., Tan, T., Dvir, N., Anderson, A., J. O'Brien, T., Kwan, P., & Antonic-Baker, A. (2022). Human In Vitro Models of Epilepsy Using Embryonic and Induced Pluripotent Stem Cells. *Cells*, *11*(24), 3957. https://doi.org/10.3390/cells11243957

Jiang, P., Rushing, S. N., Kong, C., Fu, J., Lieu, D. K.-T., Chan, C. W., Deng, W., & Li, R. A. (2010). Electrophysiological properties of human induced pluripotent stem cells. *American Journal of Physiology-Cell Physiology*, *298*(3), C486–C495. https://doi.org/10.1152/ajpcell.00251.2009

Jinek, M., Chylinski, K., Fonfara, I., Hauer, M., Doudna, J. A., & Charpentier, E. (2012). A Programmable Dual-RNA–Guided DNA Endonuclease in Adaptive Bacterial Immunity. *Science*, *337*(6096), 816–821. https://doi.org/10.1126/science.1225829

Jouvenceau, A., Eunson, L. H., Spauschus, A., Ramesh, V., Zuberi, S. M., Kullmann, D. M., & Hanna, M. G. (2001). Human epilepsy associated with dysfunction of the brain P/Q-type calcium channel. *The Lancet*, *358*(9284), 801–807. https://doi.org/10.1016/S0140-6736(01)05971-2

Karoly, P. J., Nurse, E. S., Freestone, D. R., Ung, H., Cook, M. J., & Boston, R. (2017). Bursts of seizures in long-term recordings of human focal epilepsy. *Epilepsia*, *58*(3), 363–372. https://doi.org/10.1111/epi.13636

Katyayan, A., & Diaz-Medina, G. (2021). Epilepsy. *Neurologic Clinics*, *39*(3), 779–795. https://doi.org/10.1016/j.ncl.2021.04.002

Kawamoto, E. M., Vivar, C., & Camandola, S. (2012). Physiology and Pathology of Calcium Signaling in the Brain. *Frontiers in Pharmacology*, *3*. https://doi.org/10.3389/fphar.2012.00061

Kee, N., Sivalingam, S., Boonstra, R., & Wojtowicz, J. M. (2002). The utility of Ki-67 and BrdU as proliferative markers of adult neurogenesis. *Journal of Neuroscience Methods*, *115*(1), 97–105. https://doi.org/10.1016/S0165-0270(02)00007-9

Kelava, I., & Lancaster, M. A. (2016). Dishing out mini-brains: Current progress and future prospects in brain organoid research. *Developmental Biology*, *420*(2), 199–209. https://doi.org/10.1016/j.ydbio.2016.06.037

Khamdiyeva, O., Tileules, Z., Baratzhanova, G., Perfilyeva, A., & Djansugurova, L. (2021). The study of sodium and potassium channel gene single-nucleotide variation significance in non-mechanical forms of epilepsy. *Egyptian Journal of Medical Human Genetics*, *22*(1). https://doi.org/10.1186/s43042-020-00123-y

Kim, D. M., & Nimigean, C. M. (2016). Voltage-Gated Potassium Channels: A Structural Examination of Selectivity and Gating. *Cold Spring Harbor Perspectives in Biology*, *8*(5), a029231. https://doi.org/10.1101/cshperspect.a029231

Kim, E. Y., Page, P., Dellefave-Castillo, L. M., McNally, E. M., & Wyatt, E. J. (2016). Direct reprogramming of urine-derived cells with inducible MyoD for modeling human muscle disease. *Skeletal Muscle*, *6*(1), 32. https://doi.org/10.1186/s13395-016-0103-9

Kim, H. W., Quan, Z., Kim, Y.-B., Cheong, E., Kim, H. D., Cho, M., Jang, J., Yoo, Y. R., Lee, J. S., Kim, J. H., Kim, Y. I., Kim, D.-S., & Kang, H.-C. (2018a). Differential effects on sodium current impairments by distinct SCN1A mutations in GABAergic neurons derived from Dravet syndrome patients. *Brain and Development*, *40*(4), 287–298. https://doi.org/10.1016/j.braindev.2017.12.002

Kim, K., Doi, A., Wen, B., Ng, K., Zhao, R., Cahan, P., Kim, J., Aryee, M. J., Ji, H., Ehrlich, L. I. R., Yabuuchi, A., Takeuchi, A., Cunniff, K. C., Hongguang, H., McKinney-Freeman, S., Naveiras, O., Yoon, T. J., Irizarry, R. A., Jung, N., … Daley, G. Q. (2010). Epigenetic memory in induced pluripotent stem cells. *Nature*, *467*(7313), 285–290. https://doi.org/10.1038/nature09342

Kim, Y., Rim, Y. A., Yi, H., Park, N., Park, S. H., & Ju, J. H. (2016). The Generation of Human Induced Pluripotent Stem Cells from Blood Cells: An Efficient Protocol Using Serial Plating of Reprogrammed Cells by Centrifugation. *Stem Cells International*, *2016*. https://doi.org/10.1155/2016/1329459

Klyachko, V. A., & Stevens, C. F. (2003). Connectivity optimization and the positioning of cortical areas. *Proceedings of the National Academy of Sciences*, *100*(13), 7937–7941. https://doi.org/10.1073/pnas.0932745100

Knott, G. J., & Doudna, J. A. (2018). CRISPR-Cas guides the future of genetic engineering. *Science*, *361*(6405), 866–869. https://doi.org/10.1126/science.aat5011

Krey, J. F., Paşca, S. P., Shcheglovitov, A., Yazawa, M., Schwemberger, R., Rasmusson, R., & Dolmetsch, R. E. (2013). Timothy syndrome is associated with activity-dependent dendritic retraction in rodent and human neurons. *Nature Neuroscience*, *16*(2), 201–209. https://doi.org/10.1038/nn.3307

Kriegstein, A. R. (2005). Constructing Circuits: Neurogenesis and Migration in the Developing Neocortex. *Epilepsia*, *46*(s7), 15–21. https://doi.org/10.1111/j.1528-1167.2005.00304.x

Kudva, Y. C., Ohmine, S., Greder, L. V., Dutton, J. R., Armstrong, A., De Lamo, J. G., Khan, Y. K., Thatava, T., Hasegawa, M., Fusaki, N., Slack, J. M. W., & Ikeda, Y. (2012). Transgene-Free Disease-Specific Induced Pluripotent Stem Cells from Patients with Type 1 and Type 2 Diabetes. *Stem Cells Translational Medicine*, *1*(6), 451–461. https://doi.org/10.5966/sctm.2011-0044

Kuersten, M., Tacke, M., Gerstl, L., Hoelz, H., Stülpnagel, C. v., & Borggraefe, I. (2020). Antiepileptic therapy approaches in KCNQ2 related epilepsy: A systematic review. *European Journal of Medical Genetics*, *63*(1), 103628. https://doi.org/10.1016/j.ejmg.2019.02.001

Kyttälä, A., Moraghebi, R., Valensisi, C., Kettunen, J., Andrus, C., Pasumarthy, K. K., Nakanishi, M., Nishimura, K., Ohtaka, M., Weltner, J., Van Handel, B., Parkkonen, O., Sinisalo, J., Jalanko, A., Hawkins, R. D., Woods, N. B., Otonkoski, T., & Trokovic, R. (2016). Genetic Variability Overrides the Impact of Parental Cell Type and Determines iPSC Differentiation Potential. *Stem Cell Reports*, *6*(2), 200–212. https://doi.org/10.1016/j.stemcr.2015.12.009

Laccetta, G., Fiori, S., Giampietri, M., Ferrari, A., Cetica, V., Bernardini, M., Chesi, F., Mazzotti, S., Parrini, E., Ciantelli, M., Guzzetta, A., & Ghirri, P. (2019). A de novo KCNQ2 Gene Mutation Associated With Non-familial Early Onset Seizures: Case Report and Revision of Literature Data. *Frontiers in Pediatrics*, *7*. https://doi.org/10.3389/fped.2019.00348

Laddach, A., Ng, J. C. F., & Fraternali, F. (2021). Pathogenic missense protein variants affect different functional pathways and proteomic features than healthy population variants. *PLOS Biology*, *19*(4), e3001207. https://doi.org/10.1371/journal.pbio.3001207

Lancaster, M. A., & Knoblich, J. A. (2014). Generation of cerebral organoids from human pluripotent stem cells. *Nature Protocols*, *9*(10), 2329–2340. https://doi.org/10.1038/nprot.2014.158

Lancaster, M. A., Renner, M., Martin, C.-A., Wenzel, D., Bicknell, L. S., Hurles, M. E., Homfray, T., Penninger, J. M., Jackson, A. P., & Knoblich, J. A. (2013a). Cerebral organoids model human brain development and microcephaly. *Nature*, *501*(7467), 373–379. https://doi.org/10.1038/nature12517

Lee, C.-T., Bendriem, R. M., Wu, W. W., & Shen, R.-F. (2017). 3D brain Organoids derived from pluripotent stem cells: promising experimental models for brain development and neurodegenerative disorders. *Journal of Biomedical Science*, *24*(1), 59. https://doi.org/10.1186/s12929-017-0362-8

Lee, I.-C., Yang, J.-J., Liou, Y.-M., & Wong, S.-H. (2022). KCNQ2 Selectivity Filter Mutations Cause Kv7.2 M-Current Dysfunction and Configuration Changes Manifesting as Epileptic Encephalopathies and Autistic Spectrum Disorders. *Cells*, *11*(5), 894. https://doi.org/10.3390/cells11050894

Lee, I.-C., Yang, J.-J., Wong, S.-H., Liou, Y.-M., & Li, S.-Y. (2020). Heteromeric Kv7.2 current changes caused by loss-of-function of KCNQ2 mutations are correlated with long-term neurodevelopmental outcomes. *Scientific Reports*, *10*(1), 13375. https://doi.org/10.1038/s41598-020-70212-w

Lee, J. Y. (2019). Normal and Disordered Formation of the Cerebral Cortex : Normal Embryology, Related Molecules, Types of Migration, Migration Disorders. *Journal of Korean Neurosurgical Society*, *62*(3), 265–271. https://doi.org/10.3340/jkns.2019.0098

Lemke, G. (2001). Glial Control of Neuronal Development. *Annual Review of Neuroscience*, *24*(1), 87–105. https://doi.org/10.1146/annurev.neuro.24.1.87

Lerche, H., Shah, M., Beck, H., Noebels, J., Johnston, D., & Vincent, A. (2013). Ion channels in genetic and acquired forms of epilepsy. *The Journal of Physiology*, *591*(4), 753–764. https://doi.org/10.1113/jphysiol.2012.240606

Li, X.-J., & Zhang, S.-C. (n.d.). In Vitro Differentiation of Neural Precursors From Human Embryonic Stem Cells. In *Human Embryonic Stem Cell Protocols* (pp. 168–178). Humana Press. https://doi.org/10.1385/1-59745-046-4:168

Li, X.-L., Li, G.-H., Fu, J., Fu, Y.-W., Zhang, L., Chen, W., Arakaki, C., Zhang, J.-P., Wen, W., Zhao, M., Chen, W. V, Botimer, G. D., Baylink, D., Aranda, L., Choi, H., Bechar, R., Talbot, P., Sun, C.-K., Cheng, T., & Zhang, X.-B. (2018). Highly efficient genome editing via CRISPR–Cas9 in human pluripotent stem cells is achieved by transient BCL-XL overexpression. *Nucleic Acids Research*, *46*(19), 10195–10215. https://doi.org/10.1093/nar/gky804

Liberio, M. S., Sadowski, M. C., Soekmadji, C., Davis, R. A., & Nelson, C. C. (2014). Differential Effects of Tissue Culture Coating Substrates on Prostate Cancer Cell

Adherence, Morphology and Behavior. *PLoS ONE*, *9*(11), e112122. https://doi.org/10.1371/journal.pone.0112122

Liu, C., Oikonomopoulos, A., Sayed, N., & Wu, J. C. (2018). Modeling human diseases with induced pluripotent stem cells: from 2D to 3D and beyond. *Development*, *145*(5). https://doi.org/10.1242/dev.156166

Liu, G., David, B. T., Trawczynski, M., & Fessler, R. G. (2020). Advances in Pluripotent Stem Cells: History, Mechanisms, Technologies, and Applications. *Stem Cell Reviews and Reports*, *16*(1), 3–32. https://doi.org/10.1007/s12015-019-09935-x

Liu, J.-J., Orlova, N., Oakes, B. L., Ma, E., Spinner, H. B., Baney, K. L. M., Chuck, J., Tan, D., Knott, G. J., Harrington, L. B., Al-Shayeb, B., Wagner, A., Brötzmann, J., Staahl, B. T., Taylor, K. L., Desmarais, J., Nogales, E., & Doudna, J. A. (2019). CasX enzymes comprise a distinct family of RNA-guided genome editors. *Nature*, *566*(7743), 218–223. https://doi.org/10.1038/s41586-019-0908-x

Liu, M.-L., Zang, T., Zou, Y., Chang, J. C., Gibson, J. R., Huber, K. M., & Zhang, C.-L. (2013). Small molecules enable neurogenin 2 to efficiently convert human fibroblasts into cholinergic neurons. *Nature Communications*, *4*(1), 2183. https://doi.org/10.1038/ncomms3183

Liu, X., Li, F., Stubblefield, E. A., Blanchard, B., Richards, T. L., Larson, G. A., He, Y., Huang, Q., Tan, A.-C., Zhang, D., Benke, T. A., Sladek, J. R., Zahniser, N. R., & Li, C.-Y. (2012). Direct reprogramming of human fibroblasts into dopaminergic neuron-like cells. *Cell Research*, *22*(2), 321–332. https://doi.org/10.1038/cr.2011.181

Liu, X., Li, W., Fu, X., & Xu, Y. (2017). The Immunogenicity and Immune Tolerance of Pluripotent Stem Cell Derivatives. *Frontiers in Immunology*, *8*. https://doi.org/10.3389/fimmu.2017.00645

Liu, Y., Lopez-Santiago, L. F., Yuan, Y., Jones, J. M., Zhang, H., O'Malley, H. A., Patino, G. A., O'Brien, J. E., Rusconi, R., Gupta, A., Thompson, R. C., Natowicz, M. R., Meisler, M. H., Isom, L. L., & Parent, J. M. (2013). Dravet syndrome patient-derived neurons suggest a novel epilepsy mechanism. *Annals of Neurology*, *74*(1), 128–139. https://doi.org/10.1002/ana.23897

Löscher, W. (2011). Critical review of current animal models of seizures and epilepsy used in the discovery and development of new antiepileptic drugs. *Seizure*, *20*(5), 359–368. https://doi.org/10.1016/j.seizure.2011.01.003

Lundgaard, I., Li, B., Xie, L., Kang, H., Sanggaard, S., Haswell, J. D. R., Sun, W., Goldman, S., Blekot, S., Nielsen, M., Takano, T., Deane, R., & Nedergaard, M. (2015). Direct neuronal glucose uptake heralds activity-dependent increases in cerebral metabolism. *Nature Communications*, *6*(1), 6807. https://doi.org/10.1038/ncomms7807

Lybrand, Z. R., Goswami, S., Zhu, J., Jarzabek, V., Merlock, N., Aktar, M., Smith, C., Zhang, L., Varma, P., Cho, K.-O., Ge, S., & Hsieh, J. (2021). A critical period of neuronal activity results in aberrant neurogenesis rewiring hippocampal circuitry in a mouse model of epilepsy. *Nature Communications*, *12*(1), 1423. https://doi.org/10.1038/s41467-021-21649-8

Ma, M.-G., Liu, X.-R., Wu, Y., Wang, J., Li, B.-M., Shi, Y.-W., Su, T., Li, B., Liu, D.-T., Yi, Y.-H., & Liao, W.-P. (2021). RYR2 Mutations Are Associated With Benign Epilepsy of Childhood With Centrotemporal Spikes With or Without Arrhythmia. *Frontiers in Neuroscience*, *15*. https://doi.org/10.3389/fnins.2021.629610

Ma, Q., Kintner, C., & Anderson, D. J. (1996). Identification of neurogenin, a Vertebrate Neuronal Determination Gene. *Cell*, *87*(1), 43–52. https://doi.org/10.1016/S0092-8674(00)81321-5

MacArthur, C. C., Fontes, A., Ravinder, N., Kuninger, D., Kaur, J., Bailey, M., Taliana, A., Vemuri, M. C., & Lieu, P. T. (2012). Generation of human-induced pluripotent stem cells by a nonintegrating RNA Sendai virus vector in feeder-free or xeno-free conditions. *Stem Cells International*. https://doi.org/10.1155/2012/564612

Maetzel, D., Sarkar, S., Wang, H., Abi-Mosleh, L., Xu, P., Cheng, A. W., Gao, Q., Mitalipova, M., & Jaenisch, R. (2014). Genetic and chemical correction of cholesterol accumulation and impaired autophagy in hepatic and neural cells derived from niemann-pick type C patient-specific iPS cells. *Stem Cell Reports*, *2*(6), 866–880. https://doi.org/10.1016/j.stemcr.2014.03.014

Magloire, V., Mercier, M. S., Kullmann, D. M., & Pavlov, I. (2019). GABAergic Interneurons in Seizures: Investigating Causality With Optogenetics. *The Neuroscientist*, *25*(4), 344–358. https://doi.org/10.1177/1073858418805002

Maherali, N., & Hochedlinger, K. (2008). Guidelines and Techniques for the Generation of Induced Pluripotent Stem Cells. *Cell Stem Cell*, *3*(6), 595–605. https://doi.org/10.1016/j.stem.2008.11.008

Málaga, I., Sánchez-Carpintero, R., Roldán, S., Ramos-Lizana, J., & García-Peñas, J. J. (2019). New anti-epileptic drugs in paediatrics. *Anales de Pediatría (English Edition)*, *91*(6), 415.e1-415.e10. https://doi.org/10.1016/j.anpede.2019.09.005

Malerba, F., Alberini, G., Balagura, G., Marchese, F., Amadori, E., Riva, A., Vari, M. S., Gennaro, E., Madia, F., Salpietro, V., Angriman, M., Giordano, L., Accorsi, P., Trivisano, M., Specchio, N., Russo, A., Gobbi, G., Raviglione, F., Pisano, T., … Striano, P. (2020). Genotype-phenotype correlations in patients with de novo *KCNQ2* pathogenic variants. *Neurology Genetics*, *6*(6), e528. https://doi.org/10.1212/NXG.0000000000000528

Mansour, A. A., Gonçalves, J. T., Bloyd, C. W., Li, H., Fernandes, S., Quang, D., Johnston, S., Parylak, S. L., Jin, X., & Gage, F. H. (2018). An in vivo model of functional and vascularized human brain organoids. *Nature Biotechnology*, *36*(5), 432–441. https://doi.org/10.1038/nbt.4127

Manz, K. M., Siemann, J. K., McMahon, D. G., & Grueter, B. A. (2021). Patch-clamp and multi-electrode array electrophysiological analysis in acute mouse brain slices. *STAR Protocols*, *2*(2), 100442. https://doi.org/10.1016/j.xpro.2021.100442

Manzini, S., Viiri, L. E., Marttila, S., & Aalto-Setälä, K. (2015). A Comparative View on Easy to Deploy non-Integrating Methods for Patient-Specific iPSC Production. *Stem Cell Reviews and Reports*, *11*(6), 900–908. https://doi.org/10.1007/s12015-015-9619-3

Marchetto, M. C. N., Carromeu, C., Acab, A., Yu, D., Yeo, G. W., Mu, Y., Chen, G., Gage, F. H., & Muotri, A. R. (2010). A Model for Neural Development and Treatment of Rett Syndrome Using Human Induced Pluripotent Stem Cells. *Cell*, *143*(4), 527–539. https://doi.org/10.1016/j.cell.2010.10.016

Mariani, J., Simonini, M. V., Palejev, D., Tomasini, L., Coppola, G., Szekely, A. M., Horvath, T. L., & Vaccarino, F. M. (2012). Modeling human cortical development in vitro using induced pluripotent stem cells. *Proceedings of the National Academy of Sciences*, *109*(31), 12770–12775. https://doi.org/10.1073/pnas.1202944109

Marson, A. G., Williamson, P. R., Clough, H., Hutton, J. L., Chadwick, D. W., & On Behalf Of The Epilepsy Monothera. (2002). Carbamazepine versus Valproate Monotherapy for Epilepsy: A Meta-analysis. *Epilepsia*, *43*(5), 505–513. https://doi.org/10.1046/j.1528-1157.2002.20801.x

Martineau, M., Guzman, R. E., Fahlke, C., & Klingauf, J. (2017). VGLUT1 functions as a glutamate/proton exchanger with chloride channel activity in hippocampal glutamatergic synapses. *Nature Communications*, *8*(1). https://doi.org/10.1038/s41467-017-02367-6

Martire, M., Castaldo, P., D'Amico, M., Preziosi, P., Annunziato, L., & Taglialatela, M. (2004). M Channels Containing KCNQ2 Subunits Modulate Norepinephrine, Aspartate, and GABA Release from Hippocampal Nerve Terminals. *The Journal of Neuroscience*, *24*(3), 592–597. https://doi.org/10.1523/JNEUROSCI.3143-03.2004

Mattick, J. (2010). Video Q&A: Non-coding RNAs and eukaryotic evolution - a personal view. *BMC Biology*, *8*(1), 67. https://doi.org/10.1186/1741-7007-8-67

Mayer, M. L., & Westbrook, G. L. (1987). The physiology of excitatory amino acids in the vertebrate central nervous system. *Progress in Neurobiology*, *28*(3), 197–276. https://doi.org/10.1016/0301-0082(87)90011-6

McGinn, R. J., Von Stein, E. L., Summers Stromberg, J. E., & Li, Y. (2022). *Precision medicine in epilepsy* (pp. 147–188). https://doi.org/10.1016/bs.pmbts.2022.04.001

Mehravar, M., Shirazi, A., Mehrazar, M. M., & Nazari, M. (2019). In Vitro Pre-validation of Gene Editing by CRISPR/Cas9 Ribonucleoprotein. *Avicenna Journal of Medical Biotechnology*, *11*(3), 259–263.

Mendis, G. D. C., Morrisroe, E., Petrou, S., & Halgamuge, S. K. (2016). Use of adaptive network burst detection methods for multielectrode array data and the generation of artificial spike patterns for method evaluation. *Journal of Neural Engineering*, *13*(2), 026009. https://doi.org/10.1088/1741-2560/13/2/026009

Mertens, J., Wang, Q.-W., Kim, Y., Yu, D. X., Pham, S., Yang, B., Zheng, Y., Diffenderfer, K. E., Zhang, J., Soltani, S., Eames, T., Schafer, S. T., Boyer, L., Marchetto, M. C., Nurnberger, J. I., Calabrese, J. R., Oedegaard, K. J., McCarthy, M. J., Zandi, P. P., … Yao, J. (2015). Differential responses to lithium in hyperexcitable neurons from patients with bipolar disorder. *Nature*, *527*(7576), 95–99. https://doi.org/10.1038/nature15526

Miceli, F., Millevert, C., Soldovieri, M. V., Mosca, I., Ambrosino, P., Carotenuto, L., Schrader, D., Lee, H. K., Riviello, J., Hong, W., Risen, S., Emrick, L., Amin, H., Ville, D., Edery, P., de Bellescize, J., Michaud, V., Van-Gils, J., Goizet, C., … Weckhuysen, S. (2022). KCNQ2

R144 variants cause neurodevelopmental disability with language impairment and autistic features without neonatal seizures through a gain-of-function mechanism. *EBioMedicine*, *81*, 104130. https://doi.org/10.1016/j.ebiom.2022.104130

Miceli, F., Soldovieri, M. V., Weckhuysen, S., Cooper, E., & Taglialatela, M. (1993). *KCNQ2-Related Disorders*.

Michaelsen, K., & Lohmann, C. (2010). Calcium dynamics at developing synapses: mechanisms and functions. *European Journal of Neuroscience*, *32*(2), 218–223. https://doi.org/10.1111/j.1460-9568.2010.07341.x

Milh, M., Roubertoux, P., Biba, N., Chavany, J., Spiga Ghata, A., Fulachier, C., Collins, S. C., Wagner, C., Roux, J., Yalcin, B., Félix, M., Molinari, F., Lenck-Santini, P., & Villard, L. (2020). A knock-in mouse model for *KCNQ2* -related epileptic encephalopathy displays spontaneous generalized seizures and cognitive impairment. *Epilepsia*, *61*(5), 868–878. https://doi.org/10.1111/epi.16494

Millichap, J. J., Miceli, F., De Maria, M., Keator, C., Joshi, N., Tran, B., Soldovieri, M. V., Ambrosino, P., Shashi, V., Mikati, M. A., Cooper, E. C., & Taglialatela, M. (2017). Infantile spasms and encephalopathy without preceding neonatal seizures caused by *KCNQ2* R198Q, a gain-of-function variant. *Epilepsia*, *58*(1), e10–e15. https://doi.org/10.1111/epi.13601

Millichap, J. J., Park, K. L., Tsuchida, T., Ben-Zeev, B., Carmant, L., Flamini, R., Joshi, N., Levisohn, P. M., Marsh, E., Nangia, S., Narayanan, V., Ortiz-Gonzalez, X. R., Patterson, M. C., Pearl, P. L., Porter, B., Ramsey, K., McGinnis, E. L., Taglialatela, M., Tracy, M., … Cooper, E. C. (2016a). *KCNQ2* encephalopathy. *Neurology Genetics*, *2*(5), e96. https://doi.org/10.1212/NXG.0000000000000096

Mirjalili, A., Parmoor, E., Moradi Bidhendi, S., & Sarkari, B. (2005). Microbial contamination of cell cultures: A 2 years study. *Biologicals*, *33*(2), 81–85. https://doi.org/10.1016/j.biologicals.2005.01.004

Miyazaki, T., Morimoto-Tomita, M., Berthoux, C., Konno, K., Noam, Y., Yamasaki, T., Verhage, M., Castillo, P. E., Watanabe, M., & Tomita, S. (2021). Excitatory and inhibitory receptors utilize distinct post- and trans-synaptic mechanisms in vivo. *ELife*, *10*. https://doi.org/10.7554/eLife.59613

Modarai, S. R., Man, D., Bialk, P., Rivera-Torres, N., Bloh, K., & Kmiec, E. B. (2018). Efficient Delivery and Nuclear Uptake Is Not Sufficient to Detect Gene Editing in CD34+ Cells Directed by a Ribonucleoprotein Complex. *Molecular Therapy - Nucleic Acids*, *11*, 116–129. https://doi.org/10.1016/j.omtn.2018.01.013

Monzon, F. A., Hagenkord, J. M., Lyons-Weiler, M. A., Balani, J. P., Parwani, A. V., Sciulli, C. M., Li, J., Chandran, U. R., Bastacky, S. I., & Dhir, R. (2008). Whole genome SNP arrays as a potential diagnostic tool for the detection of characteristic chromosomal aberrations in renal epithelial tumors. *Modern Pathology*, *21*(5), 599–608. https://doi.org/10.1038/modpathol.2008.20

Morris, G. (2021). Limitations of animal epilepsy research models: Can epileptic human tissue provide translational benefit? *ALTEX*. https://doi.org/10.14573/altex.2007082

Moshé, S. L., Perucca, E., Ryvlin, P., & Tomson, T. (2015). Epilepsy: new advances. *The Lancet*, *385*(9971), 884–898. https://doi.org/10.1016/S0140-6736(14)60456-6

Moyer, J. R., & Disterhoft, J. F. (1994). Nimodipine decreases calcium action potentials in rabbit hippocampal CA1 neurons in an age-dependent and concentration-dependent manner. *Hippocampus*, *4*(1), 11–17. https://doi.org/10.1002/hipo.450040104

Mullen, S. A., Berkovic, S. F., Lowenstein, D. H., Kato, M., Cross, H., Satishchandra, P., De Jonghe, P., Goldman, A., Petrou, S., Tan, N. C. K., Helbig, I., Mefford, H. C., & Jiang, Y. (2018). Genetic generalized epilepsies. *Epilepsia*, *59*(6), 1148–1153. https://doi.org/10.1111/epi.14042

Muratore, C. R., Srikanth, P., Callahan, D. G., & Young-Pearse, T. L. (2014). Comparison and Optimization of hiPSC Forebrain Cortical Differentiation Protocols. *PLoS ONE*, *9*(8), e105807. https://doi.org/10.1371/journal.pone.0105807

Nadarajah, B., & Parnavelas, J. G. (2002). Modes of neuronal migration in the developing cerebral cortex. *Nature Reviews Neuroscience*, *3*(6), 423–432. https://doi.org/10.1038/nrn845

Nägler, K., Mauch, D. H., & Pfrieger, F. W. (2001). Glia-derived signals induce synapse formation in neurones of the rat central nervous system. *The Journal of Physiology*, *533*(3), 665–679. https://doi.org/10.1111/j.1469-7793.2001.00665.x

Nagoshi, N., Tsuji, O., Nakamura, M., & Okano, H. (2019). Cell therapy for spinal cord injury using induced pluripotent stem cells. *Regenerative Therapy*, *11*, 75–80. https://doi.org/10.1016/j.reth.2019.05.006

Nappi, M., Barrese, V., Carotenuto, L., Lesca, G., Labalme, A., Ville, D., Smol, T., Rama, M., Dieux-Coeslier, A., Rivier-Ringenbach, C., Soldovieri, M. V., Ambrosino, P., Mosca, I., Pusch, M., Miceli, F., & Taglialatela, M. (2022). Gain of function due to increased opening probability by two *KCNQ5* pore variants causing developmental and epileptic encephalopathy. *Proceedings of the National Academy of Sciences*, *119*(15). https://doi.org/10.1073/pnas.2116887119

Nappi, P., Miceli, F., Soldovieri, M. V., Ambrosino, P., Barrese, V., & Taglialatela, M. (2020). Epileptic channelopathies caused by neuronal Kv7 (KCNQ) channel dysfunction. *Pflügers Archiv - European Journal of Physiology*, *472*(7), 881–898. https://doi.org/10.1007/s00424-020-02404-2

NARAHASHI, T. (2008). Tetrodotoxin -A brief history-. *Proceedings of the Japan Academy, Series B*, *84*(5), 147–154. https://doi.org/10.2183/pjab.84.147

Navarro, P., Festuccia, N., Colby, D., Gagliardi, A., Mullin, N. P., Zhang, W., Karwacki-Neisius, V., Osorno, R., Kelly, D., Robertson, M., & Chambers, I. (2012). OCT4/SOX2-independent Nanog autorepression modulates heterogeneous Nanog gene expression in mouse ES cells. *EMBO Journal*, *31*(24), 4547–4562. https://doi.org/10.1038/emboj.2012.321

Nejatbakhsh, N., & Feng, Z. (2011). Calcium binding protein-mediated regulation of voltage-gated calcium channels linked to human diseases. *Acta Pharmacologica Sinica*, *32*(6), 741–748. https://doi.org/10.1038/aps.2011.64

Nelakanti, R. V., Kooreman, N. G., & Wu, J. C. (2015). Teratoma formation: A tool for monitoring pluripotency in stem cell research. *Current Protocols in Stem Cell Biology*, *2015*, 4a.8.1-4a.8.17. https://doi.org/10.1002/9780470151808.sc04a08s32

Ngugi, A. K., Bottomley, C., Kleinschmidt, I., Wagner, R. G., Kakooza-Mwesige, A., Ae-Ngibise, K., Owusu-Agyei, S., Masanja, H., Kamuyu, G., Odhiambo, R., Chengo, E., Sander, J. W., & Newton, C. R. (2013). Prevalence of active convulsive epilepsy in sub-Saharan Africa and associated risk factors: cross-sectional and case-control studies. *The Lancet Neurology*, *12*(3), 253–263. https://doi.org/10.1016/S1474-4422(13)70003-6

Niday, Z., Hawkins, V. E., Soh, H., Mulkey, D. K., & Tzingounis, A. V. (2017). Epilepsy-Associated KCNQ2 Channels Regulate Multiple Intrinsic Properties of Layer 2/3 Pyramidal Neurons. *The Journal of Neuroscience*, *37*(3), 576–586. https://doi.org/10.1523/JNEUROSCI.1425-16.2016

Nielsen, J. V., Thomassen, M., Møllgård, K., Noraberg, J., & Jensen, N. A. (2014). Zbtb20 Defines a Hippocampal Neuronal Identity Through Direct Repression of Genes That Control Projection Neuron Development in the Isocortex. *Cerebral Cortex*, *24*(5), 1216–1229. https://doi.org/10.1093/cercor/bhs400

Nimmrich, V., & Gross, G. (2012). P/Q-type calcium channel modulators. *British Journal of Pharmacology*, *167*(4), 741–759. https://doi.org/10.1111/j.1476-5381.2012.02069.x

Nishihara, K., Shiga, T., Nakamura, E., Akiyama, T., Sasaki, T., Suzuki, S., Ko, M. S. H., Tada, N., Okano, H., & Akamatsu, W. (2019). Induced Pluripotent Stem Cells Reprogrammed with Three Inhibitors Show Accelerated Differentiation Potentials with High Levels of 2-Cell Stage Marker Expression. *Stem Cell Reports*, *12*(2), 305–318. https://doi.org/10.1016/j.stemcr.2018.12.018

Nissenkorn, A., Kornilov, P., Peretz, A., Blumkin, L., Heimer, G., Ben-Zeev, B., & Attali, B. (2021). Personalized treatment with retigabine for pharmacoresistant epilepsy arising from a pathogenic variant in the KCNQ2 selectivity filter. *Epileptic Disorders*, *23*(5), 695–705. https://doi.org/10.1684/epd.2021.1315

Noh, W., Pak, S., Choi, G., Yang, S., & Yang, S. (2019). Transient Potassium Channels: Therapeutic Targets for Brain Disorders. *Frontiers in Cellular Neuroscience*, *13*. https://doi.org/10.3389/fncel.2019.00265

Olarerin-George, A. O., & Hogenesch, J. B. (2015). Assessing the prevalence of mycoplasma contamination in cell culture via a survey of NCBI's RNA-seq Archive. *Nucleic Acids Research*, *43*(5), 2535–2542. https://doi.org/10.1093/nar/gkv136

Olson, H. E., Kelly, M., LaCoursiere, C. M., Pinsky, R., Tambunan, D., Shain, C., Ramgopal, S., Takeoka, M., Libenson, M. H., Julich, K., Loddenkemper, T., Marsh, E. D., Segal, D., Koh, S., Salman, M. S., Paciorkowski, A. R., Yang, E., Bergin, A. M., Sheidley, B. R., & Poduri, A. (2017). Genetics and genotype-phenotype correlations in early onset epileptic encephalopathy with burst suppression. *Annals of Neurology*, *81*(3), 419–429. https://doi.org/10.1002/ana.24883

O'Shea, O., Steeg, R., Chapman, C., Mackintosh, P., & Stacey, G. N. (2020). Development and implementation of large-scale quality control for the European bank for induced

Pluripotent Stem Cells. *Stem Cell Research*, *45*. https://doi.org/10.1016/j.scr.2020.101773

Overland, A. C., Rauch, J. N., Oupicka, L., Rock, D. M., & Appledorn, D. M. (n.d.). *APPLICATION NOTE IncuCyte ® Live-Cell Analysis System Quantitative live-cell analysis for optimization of culture conditions and evaluation of cell health in human induced pluripotent stem cell-derived neurons*.

Oyrer, J., Maljevic, S., Scheffer, I. E., Berkovic, S. F., Petrou, S., & Reid, C. A. (2018a). Ion Channels in Genetic Epilepsy: From Genes and Mechanisms to Disease-Targeted Therapies. *Pharmacological Reviews*, *70*(1), 142–173. https://doi.org/10.1124/pr.117.014456

Pal, S., Sun, D., Limbrick, D., Rafiq, A., & DeLorenzo, R. J. (2001). Epileptogenesis induces long-term alterations in intracellular calcium release and sequestration mechanisms in the hippocampal neuronal culture model of epilepsy. *Cell Calcium*, *30*(4), 285–296. https://doi.org/10.1054/ceca.2001.0236

Park, I. H., Zhao, R., West, J. A., Yabuuchi, A., Huo, H., Ince, T. A., Lerou, P. H., Lensch, M. W., & Daley, G. Q. (2008). Reprogramming of human somatic cells to pluripotency with defined factors. *Nature*, *451*(7175), 141–146. https://doi.org/10.1038/nature06534

Paszkiel, S. (2020). *Data Acquisition Methods for Human Brain Activity* (pp. 3–9). https://doi.org/10.1007/978-3-030-30581-9_2

Patani, R., Compston, A., Puddifoot, C. A., Wyllie, D. J. A., Hardingham, G. E., Allen, N. D., & Chandran, S. (2009). Activin/Nodal Inhibition Alone Accelerates Highly Efficient Neural Conversion from Human Embryonic Stem Cells and Imposes a Caudal Positional Identity. *PLoS ONE*, *4*(10), e7327. https://doi.org/10.1371/journal.pone.0007327

Patel, D. C., Tewari, B. P., Chaunsali, L., & Sontheimer, H. (2019). Neuron–glia interactions in the pathophysiology of epilepsy. *Nature Reviews Neuroscience*, *20*(5), 282–297. https://doi.org/10.1038/s41583-019-0126-4

Perea, G., Sur, M., & Araque, A. (2014). Neuron-glia networks: integral gear of brain function. *Frontiers in Cellular Neuroscience*, *8*. https://doi.org/10.3389/fncel.2014.00378

Pérez-Palma, E., May, P., Iqbal, S., Niestroj, L.-M., Du, J., Heyne, H. O., Castrillon, J. A., O'Donnell-Luria, A., Nürnberg, P., Palotie, A., Daly, M., & Lal, D. (2020). Identification of pathogenic variant enriched regions across genes and gene families. *Genome Research*, *30*(1), 62–71. https://doi.org/10.1101/gr.252601.119

Peterson, S. E., & Loring, J. F. (2014). Genomic instability in pluripotent stem cells: Implications for clinical applications. In *Journal of Biological Chemistry* (Vol. 289, Issue 8, pp. 4578–4584). American Society for Biochemistry and Molecular Biology Inc. https://doi.org/10.1074/jbc.R113.516419

Piao, Y., Hung, S. S.-C., Lim, S. Y., Wong, R. C.-B., & Ko, M. S. H. (2014). Efficient Generation of Integration-Free Human Induced Pluripotent Stem Cells From Keratinocytes by Simple Transfection of Episomal Vectors. *Stem Cells Translational Medicine*, *3*(7), 787–791. https://doi.org/10.5966/sctm.2013-0036

Plath, K., & Lowry, W. E. (2011). Progress in understanding reprogramming to the induced pluripotent state. *Nature Reviews Genetics*, *12*(4), 253–265. https://doi.org/10.1038/nrg2955

Pontious, A., Kowalczyk, T., Englund, C., & Hevner, R. F. (2008). Role of Intermediate Progenitor Cells in Cerebral Cortex Development. *Developmental Neuroscience*, *30*(1–3), 24–32. https://doi.org/10.1159/000109848

Porter, R. J., Partiot, A., Sachdeo, R., Nohria, V., & Alves, W. M. (2007). Randomized, multicenter, dose-ranging trial of retigabine for partial-onset seizures. *Neurology*, *68*(15), 1197–1204. https://doi.org/10.1212/01.wnl.0000259034.45049.00

Poryo, M., Clasen, O., Oehl-Jaschkowitz, B., Christmann, A., Gortner, L., & Meyer, S. (2017). Dravet syndrome: a new causative SCN1A mutation? *Clinical Case Reports*, *5*(5), 613–615. https://doi.org/10.1002/ccr3.787

Prole, D. L., & Taylor, C. W. (2019). Structure and Function of IP_3 Receptors. *Cold Spring Harbor Perspectives in Biology*, *11*(4), a035063. https://doi.org/10.1101/cshperspect.a035063

Puglia, M. P., & Valenzuela, C. F. (2009). AMPAR-mediated synaptic transmission in the CA1 hippocampal region of neonatal rats: unexpected resistance to repeated ethanol exposure. *Alcohol*, *43*(8), 619–625. https://doi.org/10.1016/j.alcohol.2009.10.004

Qasim, W., Zhan, H., Samarasinghe, S., Adams, S., Amrolia, P., Stafford, S., Butler, K., Rivat, C., Wright, G., Somana, K., Ghorashian, S., Pinner, D., Ahsan, G., Gilmour, K., Lucchini, G., Inglott, S., Mifsud, W., Chiesa, R., Peggs, K. S., … Veys, P. (2017). Molecular remission of infant B-ALL after infusion of universal TALEN gene-edited CAR T cells. *Science Translational Medicine*, *9*(374). https://doi.org/10.1126/scitranslmed.aaj2013

Qi, L. S., Larson, M. H., Gilbert, L. A., Doudna, J. A., Weissman, J. S., Arkin, A. P., & Lim, W. A. (2013). Repurposing CRISPR as an RNA-Guided Platform for Sequence-Specific Control of Gene Expression. *Cell*, *152*(5), 1173–1183. https://doi.org/10.1016/j.cell.2013.02.022

Qian, X., Nguyen, H. N., Song, M. M., Hadiono, C., Ogden, S. C., Hammack, C., Yao, B., Hamersky, G. R., Jacob, F., Zhong, C., Yoon, K., Jeang, W., Lin, L., Li, Y., Thakor, J., Berg, D. A., Zhang, C., Kang, E., Chickering, M., … Ming, G. (2016). Brain-Region-Specific Organoids Using Mini-bioreactors for Modeling ZIKV Exposure. *Cell*, *165*(5), 1238–1254. https://doi.org/10.1016/j.cell.2016.04.032

Que, Z., Olivero-Acosta, M. I., Zhang, J., Eaton, M., Tukker, A. M., Chen, X., Wu, J., Xie, J., Xiao, T., Wettschurack, K., Yunis, L., Shafer, J. M., Schaber, J. A., Rochet, J.-C., Bowman, A. B., Yuan, C., Huang, Z., Hu, C.-D., Trader, D. J., … Yang, Y. (2021). Hyperexcitability and Pharmacological Responsiveness of Cortical Neurons Derived from Human iPSCs Carrying Epilepsy-Associated Sodium Channel Nav1.2-L1342P Genetic Variant. *The Journal of Neuroscience*, *41*(49), 10194–10208. https://doi.org/10.1523/JNEUROSCI.0564-21.2021

Quraishi, I. H., Stern, S., Mangan, K. P., Zhang, Y., Ali, S. R., Mercier, M. R., Marchetto, M. C., McLachlan, M. J., Jones, E. M., Gage, F. H., & Kaczmarek, L. K. (2019). An Epilepsy-Associated KCNT1 Mutation Enhances Excitability of Human iPSC-Derived Neurons by

Increasing Slack K_{Na} Currents. *The Journal of Neuroscience*, *39*(37), 7438–7449. https://doi.org/10.1523/JNEUROSCI.1628-18.2019

Raab, S., Klingenstein, M., Liebau, S., & Linta, L. (2014a). A Comparative View on Human Somatic Cell Sources for iPSC Generation. *Stem Cells International*, *2014*, 1–12. https://doi.org/10.1155/2014/768391

Rahimpour, A., Ahani, R., Najaei, A., Adeli, A., Barkhordari, F., & Mahboudi, F. (2016). Development of Genetically Modified Chinese Hamster Ovary Host Cells for the Enhancement of Recombinant Tissue Plasminogen Activator Expression. *The Malaysian Journal of Medical Sciences : MJMS*, *23*(2), 6–13.

RAHMAN, S., FOOTITT, E. J., VARADKAR, S., & CLAYTON, P. T. (2013). Inborn errors of metabolism causing epilepsy. *Developmental Medicine & Child Neurology*, *55*(1), 23–36. https://doi.org/10.1111/j.1469-8749.2012.04406.x

Rajakulendran, S., & Hanna, M. G. (2016). The Role of Calcium Channels in Epilepsy. *Cold Spring Harbor Perspectives in Medicine*, *6*(1), a022723. https://doi.org/10.1101/cshperspect.a022723

Ranjan, R., Logette, E., Marani, M., Herzog, M., Tâche, V., Scantamburlo, E., Buchillier, V., & Markram, H. (2019). A Kinetic Map of the Homomeric Voltage-Gated Potassium Channel (Kv) Family. *Frontiers in Cellular Neuroscience*, *13*. https://doi.org/10.3389/fncel.2019.00358

Raybaud, C., & Widjaja, E. (2011). Development and Dysgenesis of the Cerebral Cortex: Malformations of Cortical Development. *Neuroimaging Clinics of North America*, *21*(3), 483–543. https://doi.org/10.1016/j.nic.2011.05.014

Re, S., Dogan, A. A., Ben-Shachar, D., Berger, G., Werling, A. M., Walitza, S., & Grünblatt, E. (2018). Improved generation of induced pluripotent stem cells from hair derived keratinocytes – A tool to study neurodevelopmental disorders as ADHD. *Frontiers in Cellular Neuroscience*, *12*. https://doi.org/10.3389/fncel.2018.00321

Reiner, A., & Levitz, J. (2018). Glutamatergic Signaling in the Central Nervous System: Ionotropic and Metabotropic Receptors in Concert. *Neuron*, *98*(6), 1080–1098. https://doi.org/10.1016/j.neuron.2018.05.018

Remy, S., Chenouard, V., Tesson, L., Usal, C., Ménoret, S., Brusselle, L., Heslan, J.-M., Nguyen, T. H., Bellien, J., Merot, J., De Cian, A., Giovannangeli, C., Concordet, J.-P., & Anegon, I. (2017). Generation of gene-edited rats by delivery of CRISPR/Cas9 protein and donor DNA into intact zygotes using electroporation. *Scientific Reports*, *7*(1), 16554. https://doi.org/10.1038/s41598-017-16328-y

Richards, S., Aziz, N., Bale, S., Bick, D., Das, S., Gastier-Foster, J., Grody, W. W., Hegde, M., Lyon, E., Spector, E., Voelkerding, K., & Rehm, H. L. (2015). Standards and guidelines for the interpretation of sequence variants: a joint consensus recommendation of the American College of Medical Genetics and Genomics and the Association for Molecular Pathology. *Genetics in Medicine*, *17*(5), 405–424. https://doi.org/10.1038/gim.2015.30

Riedel, G. (2003). Glutamate receptor function in learning and memory. *Behavioural Brain Research*, *140*(1–2), 1–47. https://doi.org/10.1016/S0166-4328(02)00272-3

Rippon, H. J., & Bishop, A. E. (2004). Embryonic stem cells. *Cell Proliferation*, *37*(1), 23–34. https://doi.org/10.1111/j.1365-2184.2004.00298.x

Rodda, D. J., Chew, J. L., Lim, L. H., Loh, Y. H., Wang, B., Ng, H. H., & Robson, P. (2005). Transcriptional regulation of Nanog by OCT4 and SOX2. *Journal of Biological Chemistry*, *280*(26), 24731–24737. https://doi.org/10.1074/jbc.M502573200

Roden, D. M., Wilke, R. A., Kroemer, H. K., & Stein, C. M. (2011). Pharmacogenomics. *Circulation*, *123*(15), 1661–1670. https://doi.org/10.1161/CIRCULATIONAHA.109.914820

Rundfeldt, C., & Netzer, R. (2000). The novel anticonvulsant retigabine activates M-currents in Chinese hamster ovary-cells tranfected with human KCNQ2/3 subunits. *Neuroscience Letters*, *282*(1–2), 73–76. https://doi.org/10.1016/S0304-3940(00)00866-1

Rush, A. M., Dib-Hajj, S. D., & Waxman, S. G. (2005). Electrophysiological properties of two axonal sodium channels, $Na_v1.2$ and $Na_v1.6$, expressed in mouse spinal sensory neurones. *The Journal of Physiology*, *564*(3), 803–815. https://doi.org/10.1113/jphysiol.2005.083089

Safiulina, V. F., Zacchi, P., Taglialatela, M., Yaari, Y., & Cherubini, E. (2008). Low expression of Kv7/M channels facilitates intrinsic and network bursting in the developing rat hippocampus. *The Journal of Physiology*, *586*(22), 5437–5453. https://doi.org/10.1113/jphysiol.2008.156257

Saito, R., Kaneko, E., Tanaka, Y., Honda, K., Matsuda, T., Baba, A., Komuro, I., Kita, S., Iwamoto, T., & Takano, Y. (2009). Involvement of Na+/Ca2+ Exchanger in Pentylenetetrazol-Induced Convulsion by Use of Na+/Ca2+ Exchanger Knockout Mice. *Biological and Pharmaceutical Bulletin*, *32*(11), 1928–1930. https://doi.org/10.1248/bpb.32.1928

Sakaguchi, H., Kadoshima, T., Soen, M., Narii, N., Ishida, Y., Ohgushi, M., Takahashi, J., Eiraku, M., & Sasai, Y. (2015). Generation of functional hippocampal neurons from self-organizing human embryonic stem cell-derived dorsomedial telencephalic tissue. *Nature Communications*, *6*(1), 8896. https://doi.org/10.1038/ncomms9896

Sansom, M. S. P., Shrivastava, I. H., Bright, J. N., Tate, J., Capener, C. E., & Biggin, P. C. (2002). Potassium channels: structures, models, simulations. *Biochimica et Biophysica Acta (BBA) - Biomembranes*, *1565*(2), 294–307. https://doi.org/10.1016/S0005-2736(02)00576-X

Sato, M., Inohaya, A., Yasuda, E., Mogami, H., Chigusa, Y., Kawasaki, K., Kawamura, Y., Ueda, Y., Takai, H., Mandai, M., & Kondoh, E. (2021). Three-dimensional human placenta-like bud synthesized from induced pluripotent stem cells. *Scientific Reports*, *11*(1), 14167. https://doi.org/10.1038/s41598-021-93766-9

Scheffer, I. E., Berkovic, S., Capovilla, G., Connolly, M. B., French, J., Guilhoto, L., Hirsch, E., Jain, S., Mathern, G. W., Moshé, S. L., Nordli, D. R., Perucca, E., Tomson, T., Wiebe, S., Zhang, Y., & Zuberi, S. M. (2017). <scp>ILAE</scp> classification of the epilepsies: Position paper of the <scp>ILAE</scp> Commission for Classification and Terminology. *Epilepsia*, *58*(4), 512–521. https://doi.org/10.1111/epi.13709

Scheffer, I. E., & Liao, J. (2020a). Deciphering the concepts behind “Epileptic encephalopathy” and “Developmental and epileptic encephalopathy.” *European Journal of Paediatric Neurology*, *24*, 11–14. https://doi.org/10.1016/j.ejpn.2019.12.023

Scheiner, Z. S., Talib, S., & Feigal, E. G. (2014). The Potential for Immunogenicity of Autologous Induced Pluripotent Stem Cell-derived Therapies. *Journal of Biological Chemistry*, *289*(8), 4571–4577. https://doi.org/10.1074/jbc.R113.509588

Schmidt, S., Lilienkampf, A., & Bradley, M. (2018). New substrates for stem cell control. *Philosophical Transactions of the Royal Society B: Biological Sciences*, *373*(1750), 20170223. https://doi.org/10.1098/rstb.2017.0223

Schubert-Bast, S., & Strzelczyk, A. (2021). Review of the treatment options for epilepsy in tuberous sclerosis complex: towards precision medicine. *Therapeutic Advances in Neurological Disorders*, *14*, 175628642110311. https://doi.org/10.1177/17562864211031100

Shan, L., Zhang, T., Fan, K., Cai, W., & Liu, H. (2021). Astrocyte-Neuron Signaling in Synaptogenesis. *Frontiers in Cell and Developmental Biology*, *9*. https://doi.org/10.3389/fcell.2021.680301

Shao, L., & Wu, W.-S. (2010). Gene-delivery systems for iPS cell generation. *Expert Opinion on Biological Therapy*, *10*(2), 231–242. https://doi.org/10.1517/14712590903455989

Shellhaas, R. A., Wusthoff, C. J., Tsuchida, T. N., Glass, H. C., Chu, C. J., Massey, S. L., Soul, J. S., Wiwattanadittakun, N., Abend, N. S., & Cilio, M. R. (2017). Profile of neonatal epilepsies. *Neurology*, *89*(9), 893–899. https://doi.org/10.1212/WNL.0000000000004284

Shi, G., & Jin, Y. (2010). Role of Oct4 in maintaining and regaining stem cell pluripotency. *Stem Cell Research & Therapy*, *1*(5), 39. https://doi.org/10.1186/scrt39

Shi, Y., Kirwan, P., Smith, J., Robinson, H. P. C., & Livesey, F. J. (2012). Human cerebral cortex development from pluripotent stem cells to functional excitatory synapses. *Nature Neuroscience*, *15*(3), 477–486. https://doi.org/10.1038/nn.3041

Shneker, B. F., & Fountain, N. B. (2003). Epilepsy. *Disease-a-Month*, *49*(7), 426–478. https://doi.org/10.1016/S0011-5029(03)00065-8

Simkin, D., Ambrosi, C., Marshall, K. A., Williams, L. A., Eisenberg, J., Gharib, M., Dempsey, G. T., George, A. L., McManus, O. B., & Kiskinis, E. (2022a). ‘Channeling’ therapeutic discovery for epileptic encephalopathy through iPSC technologies. *Trends in Pharmacological Sciences*, *43*(5), 392–405. https://doi.org/10.1016/j.tips.2022.03.001

Simkin, D., & Kiskinis, E. (2018a). Modeling Pediatric Epilepsy through iPSC-Based Technologies. *Epilepsy Currents*, *18*(4), 240–245. https://doi.org/10.5698/1535-7597.18.4.240

Simkin, D., Marshall, K. A., Vanoye, C. G., Desai, R. R., Bustos, B. I., Piyevsky, B. N., Ortega, J. A., Forrest, M., Robertson, G. L., Penzes, P., Laux, L. C., Lubbe, S. J., Millichap, J. J., George, A. L., & Kiskinis, E. (2021). Dyshomeostatic modulation of Ca2+-activated K+

channels in a human neuronal model of KCNQ2 encephalopathy. *ELife*, *10*. https://doi.org/10.7554/eLife.64434

Singh, N. A. (2003). KCNQ2 and KCNQ3 potassium channel genes in benign familial neonatal convulsions: expansion of the functional and mutation spectrum. *Brain*, *126*(12), 2726–2737. https://doi.org/10.1093/brain/awg286

Singh, N. A., Charlier, C., Stauffer, D., DuPont, B. R., Leach, R. J., Melis, R., Ronen, G. M., Bjerre, I., Quattlebaum, T., Murphy, J. V., McHarg, M. L., Gagnon, D., Rosales, T. O., Peiffer, A., Anderson, V. E., & Leppert, M. (1998). A novel potassium channel gene, KCNQ2, is mutated in an inherited epilepsy of newborns. *Nature Genetics*, *18*(1), 25–29. https://doi.org/10.1038/ng0198-25

Sledzinski, P., Dabrowska, M., Nowaczyk, M., & Olejniczak, M. (2021). Paving the way towards precise and safe CRISPR genome editing. *Biotechnology Advances*, *49*, 107737. https://doi.org/10.1016/j.biotechadv.2021.107737

Smith, C. M., & Luskin, M. B. (1998). Cell cycle length of olfactory bulb neuronal progenitors in the rostral migratory stream. *Developmental Dynamics*, *213*(2), 220–227. https://doi.org/10.1002/(SICI)1097-0177(199810)213:2<220::AID-AJA7>3.0.CO;2-I

Smith, J. S., Iannotti, C. A., Dargis, P., Christian, E. P., & Aiyar, J. (2001). Differential Expression of KCNQ2 Splice Variants: Implications to M Current Function during Neuronal Development. *The Journal of Neuroscience*, *21*(4), 1096–1103. https://doi.org/10.1523/JNEUROSCI.21-04-01096.2001

Smith, W. C., & Harland, R. M. (1992). Expression cloning of noggin, a new dorsalizing factor localized to the Spemann organizer in Xenopus embryos. *Cell*, *70*(5), 829–840. https://doi.org/10.1016/0092-8674(92)90316-5

Soh, H., Park, S., Ryan, K., Springer, K., Maheshwari, A., & Tzingounis, A. V. (2018a). Deletion of KCNQ2/3 potassium channels from PV+ interneurons leads to homeostatic potentiation of excitatory transmission. *ELife*, *7*. https://doi.org/10.7554/eLife.38617

Soldovieri, M. V., Freri, E., Ambrosino, P., Rivolta, I., Mosca, I., Binda, A., Murano, C., Ragona, F., Canafoglia, L., Vannicola, C., Solazzi, R., Granata, T., Castellotti, B., Messina, G., Gellera, C., Labalme, A., Lesca, G., DiFrancesco, J. C., & Taglialatela, M. (2020). Gabapentin treatment in a patient with KCNQ2 developmental epileptic encephalopathy. *Pharmacological Research*, *160*, 105200. https://doi.org/10.1016/j.phrs.2020.105200

Specchio, N., & Curatolo, P. (2021). Developmental and epileptic encephalopathies: what we do and do not know. *Brain*, *144*(1), 32–43. https://doi.org/10.1093/brain/awaa371

Spira, M. E., & Hai, A. (2013). Multi-electrode array technologies for neuroscience and cardiology. In *Nature Nanotechnology* (Vol. 8, Issue 2, pp. 83–94). Nature Publishing Group. https://doi.org/10.1038/nnano.2012.265

Squier, W., & Jansen, A. (2010). Abnormal development of the human cerebral cortex. *Journal of Anatomy*, *217*(4), 312–323. https://doi.org/10.1111/j.1469-7580.2010.01288.x

Stacey, G. N., Crook, J. M., Hei, D., & Ludwig, T. (2013). Banking human induced pluripotent stem cells: Lessons learned from embryonic stem cells? In *Cell Stem Cell* (Vol. 13, Issue 4, pp. 385–388). Cell Press. https://doi.org/10.1016/j.stem.2013.09.007

Stadtfeld, M., & Hochedlinger, K. (2010). Induced pluripotency: history, mechanisms, and applications. *Genes & Development*, *24*(20), 2239–2263. https://doi.org/10.1101/gad.1963910

Stadtfeld, M., Nagaya, M., Utikal, J., Weir, G., & Hochedlinger, K. (2008). Induced pluripotent stem cells generated without viral integration. *Science*, *322*(5903), 945–949. https://doi.org/10.1126/science.1162494

Stanurova, J., Neureiter, A., Hiber, M., de Oliveira Kessler, H., Stolp, K., Goetzke, R., Klein, D., Bankfalvi, A., Klump, H., & Steenpass, L. (2016). Angelman syndrome-derived neurons display late onset of paternal UBE3A silencing. *Scientific Reports*, *6*(1), 30792. https://doi.org/10.1038/srep30792

Stark, J. M., Pierce, A. J., Oh, J., Pastink, A., & Jasin, M. (2004). Genetic Steps of Mammalian Homologous Repair with Distinct Mutagenic Consequences. *Molecular and Cellular Biology*, *24*(21), 9305–9316. https://doi.org/10.1128/MCB.24.21.9305-9316.2004

Stas, J. I., Bocksteins, E., Jensen, C. S., Schmitt, N., & Snyders, D. J. (2016). The anticonvulsant retigabine suppresses neuronal KV2-mediated currents. *Scientific Reports*, *6*(1), 35080. https://doi.org/10.1038/srep35080

Štefková, K., Procházková, J., & Pacherník, J. (2015). Alkaline phosphatase in stem cells. In *Stem Cells International* (Vol. 2015). Hindawi Publishing Corporation. https://doi.org/10.1155/2015/628368

Steinhäuser, C., Grunnet, M., & Carmignoto, G. (2016). Crucial role of astrocytes in temporal lobe epilepsy. *Neuroscience*, *323*, 157–169. https://doi.org/10.1016/j.neuroscience.2014.12.047

Steinlein, O. K. (2008). Genetics and epilepsy. *Dialogues in Clinical Neuroscience*, *10*(1), 29–38. https://doi.org/10.31887/DCNS.2008.10.1/oksteinlein

Steinlein, O. K. (2014). Calcium signaling and epilepsy. *Cell and Tissue Research*, *357*(2), 385–393. https://doi.org/10.1007/s00441-014-1849-1

Stenshorne, I., Syvertsen, M., Ramm-Pettersen, A., Henning, S., Weatherup, E., Bjørnstad, A., Brüggemann, N., Spetalen, T., Selmer, K. K., & Koht, J. (2022). Monogenic developmental and epileptic encephalopathies of infancy and childhood, a population cohort from Norway. *Frontiers in Pediatrics*, *10*. https://doi.org/10.3389/fped.2022.965282

Stewart, R., Gadoud, C., Krawczyk, J., McInerney, V., O'Brien, T., Shen, S., & Allen, N. M. (2023). Generation of three induced pluripotent stem cell lines from a patient with KCNQ2 developmental and epileptic encephalopathy as a result of the pathogenic variant c.638C > T; p.Arg213Gln (NUIGi063-A, NUIGi063-B, NUIGi063-C) and 3 healthy controls (NUIGi064-A, NUIGi064-B, NUIGi064-C). *Stem Cell Research*, *69*, 103093. https://doi.org/10.1016/j.scr.2023.103093

Stockler, S., Plecko, B., Gospe, S. M., Coulter-Mackie, M., Connolly, M., van Karnebeek, C., Mercimek-Mahmutoglu, S., Hartmann, H., Scharer, G., Struijs, E., Tein, I., Jakobs, C., Clayton, P., & Van Hove, J. L. K. (2011). Pyridoxine dependent epilepsy and antiquitin deficiency. *Molecular Genetics and Metabolism*, *104*(1–2), 48–60. https://doi.org/10.1016/j.ymgme.2011.05.014

Streckfuss-Bömeke, K., Wolf, F., Azizian, A., Stauske, M., Tiburcy, M., Wagner, S., Hübscher, D., Dressel, R., Chen, S., Jende, J., Wulf, G., Lorenz, V., Schön, M. P., Maier, L. S., Zimmermann, W. H., Hasenfuss, G., & Guan, K. (2013). Comparative study of human-induced pluripotent stem cells derived from bone marrow cells, hair keratinocytes, and skin fibroblasts. *European Heart Journal*, *34*(33), 2618–2629. https://doi.org/10.1093/eurheartj/ehs203

Südhof, T. C. (2018). Towards an Understanding of Synapse Formation. *Neuron*, *100*(2), 276–293. https://doi.org/10.1016/j.neuron.2018.09.040

Sugita, S., Hono, A., Fujino, S., Futatsugi, Y., Yunomae, Y., Shimizu, N., & Takahashi, M. (2021). Detection of mycoplasma contamination in transplanted retinal cells by rapid and sensitive polymerase chain reaction test. *International Journal of Molecular Sciences*, *22*(22). https://doi.org/10.3390/ijms222212555

Sun, D. A., Sombati, S., & DeLorenzo, R. J. (2001). Glutamate Injury–Induced Epileptogenesis in Hippocampal Neurons. *Stroke*, *32*(10), 2344–2350. https://doi.org/10.1161/hs1001.097242

Sun, D., Gao, W., Hu, H., & Zhou, S. (2022). Why 90% of clinical drug development fails and how to improve it? *Acta Pharmaceutica Sinica B*, *12*(7), 3049–3062. https://doi.org/10.1016/j.apsb.2022.02.002

Sun, H., & Yu, G. (2019). New insights into the pathogenicity of non-synonymous variants through multi-level analysis. *Scientific Reports*, *9*(1), 1667. https://doi.org/10.1038/s41598-018-38189-9

Sun, Y., Paşca, S. P., Portmann, T., Goold, C., Worringer, K. A., Guan, W., Chan, K. C., Gai, H., Vogt, D., Chen, Y.-J. J., Mao, R., Chan, K., Rubenstein, J. L., Madison, D. V, Hallmayer, J., Froehlich-Santino, W. M., Bernstein, J. A., & Dolmetsch, R. E. (2016a). A deleterious Nav1.1 mutation selectively impairs telencephalic inhibitory neurons derived from Dravet Syndrome patients. *ELife*, *5*. https://doi.org/10.7554/eLife.13073

Sun, Y., Paşca, S. P., Portmann, T., Goold, C., Worringer, K. A., Guan, W., Chan, K. C., Gai, H., Vogt, D., Chen, Y.-J. J., Mao, R., Chan, K., Rubenstein, J. L., Madison, D. V, Hallmayer, J., Froehlich-Santino, W. M., Bernstein, J. A., & Dolmetsch, R. E. (2016b). A deleterious Nav1.1 mutation selectively impairs telencephalic inhibitory neurons derived from Dravet Syndrome patients. *ELife*, *5*. https://doi.org/10.7554/eLife.13073

Supèr, H., Soriano, E., & Uylings, H. B. M. (1998). The functions of the preplate in development and evolution of the neocortex and hippocampus. *Brain Research Reviews*, *27*(1), 40–64. https://doi.org/10.1016/S0165-0173(98)00005-8

Swijnenburg, R.-J., Schrepfer, S., Govaert, J. A., Cao, F., Ransohoff, K., Sheikh, A. Y., Haddad, M., Connolly, A. J., Davis, M. M., Robbins, R. C., & Wu, J. C. (2008). Immunosuppressive therapy mitigates immunological rejection of human embryonic stem cell xenografts.

Proceedings of the National Academy of Sciences, *105*(35), 12991–12996. https://doi.org/10.1073/pnas.0805802105

Syvertsen, M., Nakken, K. O., Edland, A., Hansen, G., Hellum, M. K., & Koht, J. (2015). Prevalence and etiology of epilepsy in a Norwegian county-A population based study. *Epilepsia*, *56*(5), 699–706. https://doi.org/10.1111/epi.12972

Szostak, J. W., Orr-Weaver, T. L., Rothstein, R. J., & Stahl, F. W. (1983). The double-strand-break repair model for recombination. *Cell*, *33*(1), 25–35. https://doi.org/10.1016/0092-8674(83)90331-8

Takahashi, K., Tanabe, K., Ohnuki, M., Narita, M., Ichisaka, T., Tomoda, K., & Yamanaka, S. (2007a). Induction of Pluripotent Stem Cells from Adult Human Fibroblasts by Defined Factors. *Cell*, *131*(5), 861–872. https://doi.org/10.1016/j.cell.2007.11.019

Takahashi, K., & Yamanaka, S. (2006a). Induction of Pluripotent Stem Cells from Mouse Embryonic and Adult Fibroblast Cultures by Defined Factors. *Cell*, *126*(4), 663–676. https://doi.org/10.1016/j.cell.2006.07.024

Tan, K. N., McDonald, T. S., & Borges, K. (2015). Metabolic Dysfunctions in Epilepsy and Novel Metabolic Treatment Approaches. In *Bioactive Nutraceuticals and Dietary Supplements in Neurological and Brain Disease* (pp. 461–473). Elsevier. https://doi.org/10.1016/B978-0-12-411462-3.00048-5

Tărlungeanu, D. C., & Novarino, G. (2018). Genomics in neurodevelopmental disorders: an avenue to personalized medicine. *Experimental & Molecular Medicine*, *50*(8), 1–7. https://doi.org/10.1038/s12276-018-0129-7

Taube, J. S. (2010). Interspike Interval Analyses Reveal Irregular Firing Patterns at Short, But Not Long, Intervals in Rat Head Direction Cells. *Journal of Neurophysiology*, *104*(3), 1635–1648. https://doi.org/10.1152/jn.00649.2009

Tavakoli, K., Pour-Aboughadareh, A., Kianersi, F., Poczai, P., Etminan, A., & Shooshtari, L. (2021). Applications of CRISPR-Cas9 as an Advanced Genome Editing System in Life Sciences. *BioTech*, *10*(3), 14. https://doi.org/10.3390/biotech10030014

Telezhkin, V., Straccia, M., Yarova, P., Pardo, M., Yung, S., Vinh, N.-N., Hancock, J. M., Barriga, G. G.-D., Brown, D. A., Rosser, A. E., Brown, J. T., Canals, J. M., Randall, A. D., Allen, N. D., & Kemp, P. J. (2018). Kv7 channels are upregulated during striatal neuron development and promote maturation of human iPSC-derived neurons. *Pflügers Archiv - European Journal of Physiology*, *470*(9), 1359–1376. https://doi.org/10.1007/s00424-018-2155-7

Thanaskody, K., Jusop, A. S., Tye, G. J., Wan Kamarul Zaman, W. S., Dass, S. A., & Nordin, F. (2022). MSCs vs. iPSCs: Potential in therapeutic applications. *Frontiers in Cell and Developmental Biology*, *10*. https://doi.org/10.3389/fcell.2022.1005926

Thijs, R. D., Surges, R., O'Brien, T. J., & Sander, J. W. (2019). Epilepsy in adults. *The Lancet*, *393*(10172), 689–701. https://doi.org/10.1016/S0140-6736(18)32596-0

Thoma, E. C., Wischmeyer, E., Offen, N., Maurus, K., Sirén, A.-L., Schartl, M., & Wagner, T. U. (2012). Ectopic Expression of Neurogenin 2 Alone is Sufficient to Induce Differentiation

of Embryonic Stem Cells into Mature Neurons. *PLoS ONE*, *7*(6), e38651. https://doi.org/10.1371/journal.pone.0038651

Tian, G.-F., Azmi, H., Takano, T., Xu, Q., Peng, W., Lin, J., Oberheim, N., Lou, N., Wang, X., Zielke, H. R., Kang, J., & Nedergaard, M. (2005). An astrocytic basis of epilepsy. *Nature Medicine*, *11*(9), 973–981. https://doi.org/10.1038/nm1277

Torres-Ruiz, R., & Rodriguez-Perales, S. (2017). CRISPR-Cas9 technology: applications and human disease modelling. *Briefings in Functional Genomics*, *16*(1), 4–12. https://doi.org/10.1093/bfgp/elw025

Treiman, D. M. (2001). GABAergic Mechanisms in Epilepsy. *Epilepsia*, *42*, 8–12. https://doi.org/10.1046/j.1528-1157.2001.042suppl.3008.x

Trimmer, J. S. (2015). Subcellular Localization of K+ Channels in Mammalian Brain Neurons: Remarkable Precision in the Midst of Extraordinary Complexity. *Neuron*, *85*(2), 238–256. https://doi.org/10.1016/j.neuron.2014.12.042

Tsien, R. W., Lipscombe, D., Madison, D. V., Bley, K. R., & Fox, A. P. (1988). Multiple types of neuronal calcium channels and their selective modulation. *Trends in Neurosciences*, *11*(10), 431–438. https://doi.org/10.1016/0166-2236(88)90194-4

Tu, H., Nelson, O., Bezprozvanny, A., Wang, Z., Lee, S.-F., Hao, Y.-H., Serneels, L., De Strooper, B., Yu, G., & Bezprozvanny, I. (2006). Presenilins Form ER Ca2+ Leak Channels, a Function Disrupted by Familial Alzheimer's Disease-Linked Mutations. *Cell*, *126*(5), 981–993. https://doi.org/10.1016/j.cell.2006.06.059

Ullian, E. M., Harris, B. T., Wu, A., Chan, J. R., & Barres, B. A. (2004). Schwann cells and astrocytes induce synapse formation by spinal motor neurons in culture. *Molecular and Cellular Neuroscience*, *25*(2), 241–251. https://doi.org/10.1016/j.mcn.2003.10.011

Urnov, F. D., Rebar, E. J., Holmes, M. C., Zhang, H. S., & Gregory, P. D. (2010). Genome editing with engineered zinc finger nucleases. *Nature Reviews Genetics*, *11*(9), 636–646. https://doi.org/10.1038/nrg2842

Valenzuela, D., Economides, A., Rojas, E., Lamb, T., Nunez, L., Jones, P., Lp, N., Espinosa, R., Brannan, C., & Gilbert, D. (1995). Identification of mammalian noggin and its expression in the adult nervous system. *The Journal of Neuroscience*, *15*(9), 6077–6084. https://doi.org/10.1523/JNEUROSCI.15-09-06077.1995

Vasudevan, S. (2012). Posttranscriptional Upregulation by MicroRNAs. *Wiley Interdisciplinary Reviews: RNA*, *3*(3), 311–330. https://doi.org/10.1002/wrna.121

Ventola, C. L. (2014). Epilepsy management: newer agents, unmet needs, and future treatment strategies. *P & T : A Peer-Reviewed Journal for Formulary Management*, *39*(11), 776–792.

Vezzani, A., Fujinami, R. S., White, H. S., Preux, P.-M., Blümcke, I., Sander, J. W., & Löscher, W. (2016). Infections, inflammation and epilepsy. *Acta Neuropathologica*, *131*(2), 211–234. https://doi.org/10.1007/s00401-015-1481-5

Volpato, V., & Webber, C. (2020). Addressing variability in iPSC-derived models of human disease: Guidelines to promote reproducibility. In *DMM Disease Models and*

Mechanisms (Vol. 13, Issue 1). Company of Biologists Ltd. https://doi.org/10.1242/dmm.042317

Wagnon, J. L., & Meisler, M. H. (2015). Recurrent and Non-Recurrent Mutations of SCN8A in Epileptic Encephalopathy. *Frontiers in Neurology*, *6*. https://doi.org/10.3389/fneur.2015.00104

Wang, H. (1998). KCNQ2 and KCNQ3 Potassium Channel Subunits: Molecular Correlates of the M-Channel. *Science*, *282*(5395), 1890–1893. https://doi.org/10.1126/science.282.5395.1890

Wang, J., Lin, Z. J., Liu, L., Xu, H. Q., Shi, Y. W., Yi, Y. H., He, N., & Liao, W. P. (2017). Epilepsy-associated genes. In *Seizure* (Vol. 44, pp. 11–20). W.B. Saunders Ltd. https://doi.org/10.1016/j.seizure.2016.11.030

Wang, J., Ou, S.-W., & Wang, Y.-J. (2017). Distribution and function of voltage-gated sodium channels in the nervous system. *Channels*, *11*(6), 534–554. https://doi.org/10.1080/19336950.2017.1380758

Wang, J., & Zhao, J. (2021). MicroRNA Dysregulation in Epilepsy: From Pathogenetic Involvement to Diagnostic Biomarker and Therapeutic Agent Development. *Frontiers in Molecular Neuroscience*, *14*. https://doi.org/10.3389/fnmol.2021.650372

Wang, K., Xue, T., Tsang, S., Van Huizen, R., Wong, C. W., Lai, K. W., Ye, Z., Cheng, L., Au, K. W., Zhang, J., Li, G., Lau, C., Tse, H., & Li, R. A. (2005). Electrophysiological Properties of Pluripotent Human and Mouse Embryonic Stem Cells. *STEM CELLS*, *23*(10), 1526–1534. https://doi.org/10.1634/stemcells.2004-0299

Wang, S., Hesen, R., Mossink, B., Nadif Kasri, N., & Schubert, D. (2023). Generation of glutamatergic/GABAergic neuronal co-cultures derived from human induced pluripotent stem cells for characterizing E/I balance in vitro. *STAR Protocols*, *4*(1), 101967. https://doi.org/10.1016/j.xpro.2022.101967

Wang, W., Wang, X., Chen, L., Zhang, Y., Xu, Z., Liu, J., Jiang, G., Li, J., Zhang, X., Wang, K., Wang, J., Chen, G., & Luo, J. (2016). The microRNA miR-124 suppresses seizure activity and regulates CREB1 activity. *Expert Reviews in Molecular Medicine*, *18*, e4. https://doi.org/10.1017/erm.2016.3

Warmflash, A., Sorre, B., Etoc, F., Siggia, E. D., & Brivanlou, A. H. (2014). A method to recapitulate early embryonic spatial patterning in human embryonic stem cells. *Nature Methods*, *11*(8), 847–854. https://doi.org/10.1038/nMeth.3016

Weckhuysen, S., & George, Jr, A. L. (Eds.). (2022). *<i>KCNQ2</i>- and <i>KCNQ3</i>-Associated Epilepsy*. Cambridge University Press. https://doi.org/10.1017/9781009278270

Weckhuysen, S., Ivanovic, V., Hendrickx, R., Van Coster, R., Hjalgrim, H., Moller, R. S., Gronborg, S., Schoonjans, A.-S., Ceulemans, B., Heavin, S. B., Eltze, C., Horvath, R., Casara, G., Pisano, T., Giordano, L., Rostasy, K., Haberlandt, E., Albrecht, B., Bevot, A., … De Jonghe, P. (2013). Extending the KCNQ2 encephalopathy spectrum: Clinical and neuroimaging findings in 17 patients. *Neurology*, *81*(19), 1697–1703. https://doi.org/10.1212/01.wnl.0000435296.72400.a1

Weckhuysen, S., Mandelstam, S., Suls, A., Audenaert, D., Deconinck, T., Claes, L. R. F., Deprez, L., Smets, K., Hristova, D., Yordanova, I., Jordanova, A., Ceulemans, B., Jansen, A., Hasaerts, D., Roelens, F., Lagae, L., Yendle, S., Stanley, T., Heron, S. E., … De Jonghe, P. (2012). KCNQ2 encephalopathy: Emerging phenotype of a neonatal epileptic encephalopathy. *Annals of Neurology*, *71*(1), 15–25. https://doi.org/10.1002/ana.22644

Weise, S. C., Villarreal, A., Heidrich, S., Dehghanian, F., Schachtrup, C., Nestel, S., Schwarz, J., Thedieck, K., & Vogel, T. (2018). TGFβ-Signaling and FOXG1-Expression Are a Hallmark of Astrocyte Lineage Diversity in the Murine Ventral and Dorsal Forebrain. *Frontiers in Cellular Neuroscience*, *12*. https://doi.org/10.3389/fncel.2018.00448

Weissbein, U., Benvenisty, N., & Ben-David, U. (2014). Genome maintenance in pluripotent stem cells. In *Journal of Cell Biology* (Vol. 204, Issue 2, pp. 153–163). https://doi.org/10.1083/jcb.201310135

Wen, H., & Levitan, I. B. (2002). Calmodulin Is an Auxiliary Subunit of KCNQ2/3 Potassium Channels. *The Journal of Neuroscience*, *22*(18), 7991–8001. https://doi.org/10.1523/JNEUROSCI.22-18-07991.2002

Whelan, C. D., Altmann, A., Botía, J. A., Jahanshad, N., Hibar, D. P., Absil, J., Alhusaini, S., Alvim, M. K. M., Auvinen, P., Bartolini, E., Bergo, F. P. G., Bernardes, T., Blackmon, K., Braga, B., Caligiuri, M. E., Calvo, A., Carr, S. J., Chen, J., Chen, S., … Sisodiya, S. M. (2018). Structural brain abnormalities in the common epilepsies assessed in a worldwide ENIGMA study. *Brain*, *141*(2), 391–408. https://doi.org/10.1093/brain/awx341

WHITE, H. S., SMITH-YOCKMAN, M., SRIVASTAVA, A., & WILCOX, K. S. (2006). Therapeutic Assays for the Identification and Characterization of Antiepileptic and Antiepileptogenic Drugs. In *Models of Seizures and Epilepsy* (pp. 539–549). Elsevier. https://doi.org/10.1016/B978-012088554-1/50046-3

Wickenden, A. D., Yu, W., Zou, A., Jegla, T., & Wagoner, P. K. (2000). Retigabine, A Novel Anti-Convulsant, Enhances Activation of KCNQ2/Q3 Potassium Channels. *Molecular Pharmacology*, *58*(3), 591–600. https://doi.org/10.1124/mol.58.3.591

Wilmut, I., Schnieke, A. E., McWhir, J., Kind, A. J., & Campbell, K. H. S. (1997). Viable offspring derived from fetal and adult mammalian cells. *Nature*, *385*(6619), 810–813. https://doi.org/10.1038/385810a0

Wolf, N. I., Bast, T., & Surtees, R. (2005). Epilepsy in inborn errors of metabolism. *Epileptic Disorders : International Epilepsy Journal with Videotape*, *7*(2), 67–81.

Wu, S., Wu, Y., Zhang, X., & Capecchi, M. R. (2014). Efficient germ-line transmission obtained with transgene-free induced pluripotent stem cells. *Proceedings of the National Academy of Sciences of the United States of America*, *111*(29), 10678–10683. https://doi.org/10.1073/pnas.1409933111

Wyner, N., Barash, M., & McNevin, D. (2020). Forensic Autosomal Short Tandem Repeats and Their Potential Association With Phenotype. In *Frontiers in Genetics* (Vol. 11). Frontiers Media S.A. https://doi.org/10.3389/fgene.2020.00884

Xiang, Y., Tanaka, Y., Patterson, B., Kang, Y.-J., Govindaiah, G., Roselaar, N., Cakir, B., Kim, K.-Y., Lombroso, A. P., Hwang, S.-M., Zhong, M., Stanley, E. G., Elefanty, A. G., Naegele, J. R., Lee, S.-H., Weissman, S. M., & Park, I.-H. (2017). Fusion of Regionally Specified hPSC-Derived Organoids Models Human Brain Development and Interneuron Migration. *Cell Stem Cell*, *21*(3), 383-398.e7. https://doi.org/10.1016/j.stem.2017.07.007

Xu, H., Kita, Y., Bang, U., Gee, P., & Hotta, A. (2021). Optimized electroporation of CRISPR-Cas9/gRNA ribonucleoprotein complex for selection-free homologous recombination in human pluripotent stem cells. *STAR Protocols*, *2*(4), 100965. https://doi.org/10.1016/j.xpro.2021.100965

Xu, J.-H., & Tang, F.-R. (2018a). Voltage-Dependent Calcium Channels, Calcium Binding Proteins, and Their Interaction in the Pathological Process of Epilepsy. *International Journal of Molecular Sciences*, *19*(9), 2735. https://doi.org/10.3390/ijms19092735

Xu, X., Gao, D., Wang, P., Chen, J., Ruan, J., Xu, J., & Xia, X. (2018). Efficient homology-directed gene editing by CRISPR/Cas9 in human stem and primary cells using tube electroporation. *Scientific Reports*, *8*(1), 11649. https://doi.org/10.1038/s41598-018-30227-w

Xu, X., Zhan, M., Duan, W., Prabhu, V., Brenneman, R., Wood, W., Firman, J., Li, H., Zhang, P., Ibe, C., Zonderman, A. B., Longo, D. L., Poosala, S., Becker, K. G., & Mattson, M. P. (2007). Gene expression atlas of the mouse central nervous system: impact and interactions of age, energy intake and gender. *Genome Biology*, *8*(11), R234. https://doi.org/10.1186/gb-2007-8-11-r234

Xu, X., & Zhong, Z. (2013). Disease modeling and drug screening for neurological diseases using human induced pluripotent stem cells. *Acta Pharmacologica Sinica*, *34*(6), 755–764. https://doi.org/10.1038/aps.2013.63

Yamanaka, S. (2012). Induced Pluripotent Stem Cells: Past, Present, and Future. *Cell Stem Cell*, *10*(6), 678–684. https://doi.org/10.1016/j.stem.2012.05.005

Yamashita, S., Chiyonobu, T., Yoshida, M., Maeda, H., Zuiki, M., Kidowaki, S., Isoda, K., Morimoto, M., Kato, M., Saitsu, H., Matsumoto, N., Nakahata, T., Saito, M. K., & Hosoi, H. (2016). Mislocalization of syntaxin-1 and impaired neurite growth observed in a human iPSC model for *STXBP1* -related epileptic encephalopathy. *Epilepsia*, *57*(4), e81–e86. https://doi.org/10.1111/epi.13338

Yang, G., Tian, F., Shen, Y., Yang, C., Yuan, H., Li, P., & Gao, Z. (2023a). Functional characterization and in vitro pharmacological rescue of KCNQ2 pore mutations associated with epileptic encephalopathy. *Acta Pharmacologica Sinica*. https://doi.org/10.1038/s41401-023-01073-y

Yang, H., Zhang, G., & Cui, J. (2015). BK channels: multiple sensors, one activation gate. *Frontiers in Physiology*, *6*. https://doi.org/10.3389/fphys.2015.00029

Yang, J., Li, S., He, X. B., Cheng, C., & Le, W. (2016). Induced pluripotent stem cells in Alzheimer's disease: Applications for disease modeling and cell-replacement therapy. In *Molecular Neurodegeneration* (Vol. 11, Issue 1). BioMed Central Ltd. https://doi.org/10.1186/s13024-016-0106-3

Yi, B. A., Minor, D. L., Lin, Y.-F., Jan, Y. N., & Jan, L. Y. (2001). Controlling potassium channel activities: Interplay between the membrane and intracellular factors. *Proceedings of the National Academy of Sciences*, *98*(20), 11016–11023. https://doi.org/10.1073/pnas.191351798

Yin, P., Liu, Y., Xiao, L., & Zhang, C. (2021). Advanced Metallic and Polymeric Coatings for Neural Interfacing: Structures, Properties and Tissue Responses. *Polymers*, *13*(16), 2834. https://doi.org/10.3390/polym13162834

Yu, F. H., & Catterall, W. A. (2003). Overview of the voltage-gated sodium channel family. *Genome Biology*, *4*(3), 207. https://doi.org/10.1186/gb-2003-4-3-207

Yu, J., Vodyanik, M. A., Smuga-Otto, K., Antosiewicz-Bourget, J., Frane, J. L., Tian, S., Nie, J., Jonsdottir, G. A., Ruotti, V., Stewart, R., Slukvin, I. I., & Thomson, J. A. (2007a). Induced Pluripotent Stem Cell Lines Derived from Human Somatic Cells. *Science*, *318*(5858), 1917–1920. https://doi.org/10.1126/science.1151526

Zaken, N., Motro, U., Berdugo, R., Sapir, L. E., & Zamir, A. (2013). Can brothers share the same STR profile? *Forensic Science International: Genetics*, *7*(5), 494–498. https://doi.org/10.1016/j.fsigen.2013.04.011

Zeng, H., Guo, M., Martins-Taylor, K., Wang, X., Zhang, Z., Park, J. W., Zhan, S., Kronenberg, M. S., Lichtler, A., Liu, H.-X., Chen, F.-P., Yue, L., Li, X.-J., & Xu, R.-H. (2010). Specification of Region-Specific Neurons Including Forebrain Glutamatergic Neurons from Human Induced Pluripotent Stem Cells. *PLoS ONE*, *5*(7), e11853. https://doi.org/10.1371/journal.pone.0011853

Zeng, Q., Yang, Y., Duan, J., Niu, X., Chen, Y., Wang, D., Zhang, J., Chen, J., Yang, X., Li, J., Yang, Z., Jiang, Y., Liao, J., & Zhang, Y. (2022). SCN2A-Related Epilepsy: The Phenotypic Spectrum, Treatment and Prognosis. *Frontiers in Molecular Neuroscience*, *15*. https://doi.org/10.3389/fnmol.2022.809951

Zhang, J., Kim, E. C., Chen, C., Procko, E., Pant, S., Lam, K., Patel, J., Choi, R., Hong, M., Joshi, D., Bolton, E., Tajkhorshid, E., & Chung, H. J. (2020a). Identifying mutation hotspots reveals pathogenetic mechanisms of KCNQ2 epileptic encephalopathy. *Scientific Reports*, *10*(1). https://doi.org/10.1038/s41598-020-61697-6

Zhang, X., Huang, C. T., Chen, J., Pankratz, M. T., Xi, J., Li, J., Yang, Y., LaVaute, T. M., Li, X.-J., Ayala, M., Bondarenko, G. I., Du, Z.-W., Jin, Y., Golos, T. G., & Zhang, S.-C. (2010). Pax6 Is a Human Neuroectoderm Cell Fate Determinant. *Cell Stem Cell*, *7*(1), 90–100. https://doi.org/10.1016/j.stem.2010.04.017

Zhang, Y., Mori, M., Burgess, D. L., & Noebels, J. L. (2002). Mutations in High-Voltage-Activated Calcium Channel Genes Stimulate Low-Voltage-Activated Currents in Mouse Thalamic Relay Neurons. *The Journal of Neuroscience*, *22*(15), 6362–6371. https://doi.org/10.1523/JNEUROSCI.22-15-06362.2002

Zhang, Y., Pak, C., Han, Y., Ahlenius, H., Zhang, Z., Chanda, S., Marro, S., Patzke, C., Acuna, C., Covy, J., Xu, W., Yang, N., Danko, T., Chen, L., Wernig, M., & Südhof, T. C. (2013). Rapid Single-Step Induction of Functional Neurons from Human Pluripotent Stem Cells. *Neuron*, *78*(5), 785–798. https://doi.org/10.1016/j.neuron.2013.05.029

Zhang, Y. S., Aleman, J., Shin, S. R., Kilic, T., Kim, D., Mousavi Shaegh, S. A., Massa, S., Riahi, R., Chae, S., Hu, N., Avci, H., Zhang, W., Silvestri, A., Sanati Nezhad, A., Manbohi, A., De Ferrari, F., Polini, A., Calzone, G., Shaikh, N., … Khademhosseini, A. (2017). Multisensor-integrated organs-on-chips platform for automated and continual in situ monitoring of organoid behaviors. *Proceedings of the National Academy of Sciences*, *114*(12). https://doi.org/10.1073/pnas.1612906114

Zhang, Y., Sloan, S. A., Clarke, L. E., Caneda, C., Plaza, C. A., Blumenthal, P. D., Vogel, H., Steinberg, G. K., Edwards, M. S. B., Li, G., Duncan, J. A., Cheshier, S. H., Shuer, L. M., Chang, E. F., Grant, G. A., Gephart, M. G. H., & Barres, B. A. (2016). Purification and Characterization of Progenitor and Mature Human Astrocytes Reveals Transcriptional and Functional Differences with Mouse. *Neuron*, *89*(1), 37–53. https://doi.org/10.1016/j.neuron.2015.11.013

Zhao, X., Xu, Z., Xiao, L., Shi, T., Xiao, H., Wang, Y., Li, Y., Xue, F., & Zeng, W. (2021). Review on the Vascularization of Organoids and Organoids-on-a-Chip. *Frontiers in Bioengineering and Biotechnology*, *9*. https://doi.org/10.3389/fbioe.2021.637048

Zhou, T., Benda, C., Dunzinger, S., Huang, Y., Ho, J. C., Yang, J., Wang, Y., Zhang, Y., Zhuang, Q., Li, Y., Bao, X., Tse, H. F., Grillari, J., Grillari-Voglauer, R., Pei, D., & Esteban, M. A. (2012). Generation of human induced pluripotent stem cells from urine samples. *Nature Protocols*, *7*(12), 2080–2089. https://doi.org/10.1038/nprot.2012.115

Zhou, X., Chen, Z., Xiao, L., Zhong, Y., Liu, Y., Wu, J., & Tao, H. (2022). Intracellular calcium homeostasis and its dysregulation underlying epileptic seizures. *Seizure*, *103*, 126–136. https://doi.org/10.1016/j.seizure.2022.11.007

Zhou, X., Zhuang, F., Li, H., Zheng, K., Hong, Z., Feng, W., Zhou, W., & Chen, J. (2016). Calmodulin regulates KCNQ2 function in epilepsy. *American Journal of Translational Research*, *8*(12), 5610–5618.

Zhu, Y., Sheng, Z.-F., Yao, H., & Li, D.-P. (2022). Emerging mechanisms involving brain Kv7 channel in the pathogenesis of hypertension. *Biochemical Pharmacology*, *206*, 115318. https://doi.org/10.1016/j.bcp.2022.115318

Zuberi, S. M., Wirrell, E., Yozawitz, E., Wilmshurst, J. M., Specchio, N., Riney, K., Pressler, R., Auvin, S., Samia, P., Hirsch, E., Galicchio, S., Triki, C., Snead, O. C., Wiebe, S., Cross, J. H., Tinuper, P., Scheffer, I. E., Perucca, E., Moshé, S. L., & Nabbout, R. (2022). ILAE classification and definition of epilepsy syndromes with onset in neonates and infants: Position statement by the ILAE Task Force on Nosology and Definitions. *Epilepsia*, *63*(6), 1349–1397. https://doi.org/10.1111/epi.17239